frontiers | Research Topics

Examining genetic and epigenetic regulation in cardiovascular development, regeneration and disease

Edited by
Eltyeb Abdelwahid and Katherine Athayde Teixeira de Carvalho

Published in
Frontiers in Cardiovascular Medicine

ISSN 1664-8714
ISBN 978-2-8325-3840-1
DOI 10.3389/978-2-8325-3840-1

About Frontiers

Frontiers is more than just an open access publisher of scholarly articles: it is a pioneering approach to the world of academia, radically improving the way scholarly research is managed. The grand vision of Frontiers is a world where all people have an equal opportunity to seek, share and generate knowledge. Frontiers provides immediate and permanent online open access to all its publications, but this alone is not enough to realize our grand goals.

Frontiers journal series

The Frontiers journal series is a multi-tier and interdisciplinary set of open-access, online journals, promising a paradigm shift from the current review, selection and dissemination processes in academic publishing. All Frontiers journals are driven by researchers for researchers; therefore, they constitute a service to the scholarly community. At the same time, the *Frontiers journal series* operates on a revolutionary invention, the tiered publishing system, initially addressing specific communities of scholars, and gradually climbing up to broader public understanding, thus serving the interests of the lay society, too.

Dedication to quality

Each Frontiers article is a landmark of the highest quality, thanks to genuinely collaborative interactions between authors and review editors, who include some of the world's best academicians. Research must be certified by peers before entering a stream of knowledge that may eventually reach the public - and shape society; therefore, Frontiers only applies the most rigorous and unbiased reviews. Frontiers revolutionizes research publishing by freely delivering the most outstanding research, evaluated with no bias from both the academic and social point of view. By applying the most advanced information technologies, Frontiers is catapulting scholarly publishing into a new generation.

What are Frontiers Research Topics?

Frontiers Research Topics are very popular trademarks of the *Frontiers journals series*: they are collections of at least ten articles, all centered on a particular subject. With their unique mix of varied contributions from Original Research to Review Articles, Frontiers Research Topics unify the most influential researchers, the latest key findings and historical advances in a hot research area.

Find out more on how to host your own Frontiers Research Topic or contribute to one as an author by contacting the Frontiers editorial office: frontiersin.org/about/contact

Examining genetic and epigenetic regulation in cardiovascular development, regeneration and disease

Topic editors

Eltyeb Abdelwahid — Northwestern Medicine, United States

Katherine Athayde Teixeira de Carvalho — Pelé Pequeno Príncipe Research Institute, Brazil

Citation

Abdelwahid, E., Athayde Teixeira de Carvalho, K., eds. (2023). *Examining genetic and epigenetic regulation in cardiovascular development, regeneration and disease*. Lausanne: Frontiers Media SA. doi: 10.3389/978-2-8325-3840-1

Table of contents

frontiers | Frontiers in Cardiovascular Medicine

TYPE Editorial
PUBLISHED 18 October 2023
DOI 10.3389/fcvm.2023.1306263

OPEN ACCESS

EDITED AND REVIEWED BY
Paolo Madeddu,
University of Bristol, United Kingdom

*CORRESPONDENCE
Eltyeb Abdelwahid
✉ eawd123@gmail.com;
✉ eltyeba@uic.edu
Katherine Athayde Teixeira de Carvalho
✉ katherinecarv@gmail.com

RECEIVED 03 October 2023
ACCEPTED 10 October 2023
PUBLISHED 18 October 2023

CITATION
Abdelwahid E and Athayde Teixeira de Carvalho K (2023) Editorial: Examining genetic and epigenetic regulation in cardiovascular development, regeneration and disease. Front. Cardiovasc. Med. 10:1306263. doi: 10.3389/fcvm.2023.1306263

Editorial: Examining genetic and epigenetic regulation in cardiovascular development, regeneration and disease

Eltyeb Abdelwahid[1]* and Katherine Athayde Teixeira de Carvalho[2]*

[1]Feinberg Cardiovascular Research Institute, Feinberg School of Medicine, Northwestern University, Chicago, IL, United States, [2]Department of Medicine, University of Illinois at Chicago, Chicago, IL, United States, [3]Advanced Therapy and Cellular Biotechnology in Regenerative Medicine Department, The Pelé Pequeno Príncipe Research Institute, Child and Adolescent Health Research and Pequeno Príncipe Faculties, Curitiba, Brazil

KEYWORDS

genetic, epigenetic, cardiovascular, disease, therapy

Editorial on the Research Topic
Examining genetic and epigenetic regulation in cardiovascular development, regeneration and disease

Heart disease is the leading cause of death worldwide and is associated with significant socio-economic problems. Examining genetic and epigenetic regulation in cardiovascular development, regeneration and disease can explain multifaceted mechanisms responsible for cardiac dysfunction. Targeting these mechanisms is hoped to ameliorate heart diseases by offering appropriate therapeutic solutions. This special issue comprises 9 articles, including 5 original papers and 4 reviews, which cover pivotal areas including atherosclerosis, atrial fibrillation, fibrosis, cardiac remodeling, therapeutic vaccination, non-coding RNA, thrombosis, and hypertrophic cardiomyopathy. Thus, multiple questions are addressed to draw attention to the current knowledge in this field and to open the door for possible future research advancing molecular genetics and epigenetics of cardiac pathologies and related interventions.

As reviewed by Zhao et al. FGF21, a promising cardioprotective factor, has been shown by recent studies to improve cardiac function by playing regulatory roles targeting different heart tissue components, including cardiac myocytes, immune cells, and fibroblasts. These effects occur via modulation of distinct biological mechanisms, including cell death, metabolism, oxidative stress, fibrosis, and inflammatory processes. Thus, FGF21 appears to be a potential protective molecule in the heart. Xue et al. updated the readers on works addressing the roles of non-coding RNA in atrial fibrillation. They discussed the concept of ncRNAs as strong regulators of the occurrence and progression of AF. Iversen et al. described AtheroVax as a peptide vaccine targeting sTNFR2 to inhibit the progression of atherosclerosis. The authors expect this novel vaccine to have a longer duration of action compared to current therapies which require chronic treatment that encounters problems associated with lack of patient compliance. Matta et al. explored potential differences in cardiovascular outcomes in heterozygous familial hypercholesterolemia (HFH) population under medical care with vs. without a causative variant and assessed the association between different gene variants and atherosclerotic cardiovascular disease (ASCVD). It

appears that the presence of a causative variant may not represent an independent predictor of adverse cardiovascular outcomes in heterozygous familial hypercholesterolemia (HFH) patients. The elevation of LDL-c level is suggested to remain the strongest independent predictor of ASCVD. Doh et al. discussed various existing and emerging strategies to improve technologies concerning variants of uncertain significance (VUS) and their possible involvement in the pathogenicity of VUS in hypertrophic cardiomyopathy (HCM). The classification of a genetic variant leads to ambiguity in explanation, risk stratification, and clinical setting. Therefore, this review offered information on some basic science methods to help the characterization of VUS in HCM. Kukida et al. manipulated components of the renin angiotensin system in renal proximal tubules to understand if this can alter atherosclerosis in hypercholesterolemic mice. This study found that while whole-body AT1R inhibition reduced atherosclerosis equivalently in the studied male and female mice; PTC-specific manipulation of the RAS pathway did not change hypercholesterolemia-induced atherosclerosis. Wu et al. performed LC–MS/MS analysis to identify proteins with altered ubiquitination in AF tissues. The authors identified significant alterations in ubiquitination between the SR and AF groups. The results characterized alterations that are suggested to modulate the development of AF and may thus provide an effective therapeutic strategy against AF. The study by Nguyen et al. showed a novel mechanism regulating the suppressive effects of L-flow on endothelial cell inflammation, migration, proliferation, apoptosis, and fibrosis via increasing CHK1-induced SENP2 S344 phosphorylation. The findings are considered a good basis for further studies aiming to characterize the potential impact of this mechanism on the cardiovascular system. The study by Natae et al. revealed that the five strongly associated SNPs combined with non-genetic factors may allow the prediction of individual Venous thrombosis (VT) risk susceptibility. These novel findings shed new light on the determinants of VT as one of the three leading problems associated with cardiovascular pathology.

Elucidation of the genetic and epigenetic basis of cardiac disease should pave the way for the identification of new targets and the development of new drugs (1–3). Papers included in this special issue address recent discoveries of mechanisms controlling cardiovascular diseases and discuss their potential to be used in preventive, diagnostic and therapeutic technologies for managing heart dysfunction. Future studies would benefit from using various genetic models and cutting edge molecular and cellular technologies to advance current discoveries by clarifying genetic hubs governing cardiac pathophysiology. We are delighted to have been able to put together in this issue some of the important works reflecting the advances in this field, with much more to come.

Author contributions

EA: Conceptualization, Writing – original draft, Writing – review & editing. KA: Conceptualization, Writing – original draft, Writing – review & editing.

Conflict of interest

The authors declare that the research was conducted in the absence of any commercial or financial relationships that could be construed as a potential conflict of interest.

Publisher's note

References

1. Wang M, Tu X. The Genetics and Epigenetics of Ventricular Arrhythmias in Patients Without Structural Heart Disease. *Front Cardiovasc Med.* (2022) 9:891399.

2. Abdelwahid E, de Carvalho KAT. Editorial: MicroRNAs in Heart Regeneration: Regulatory Mechanisms and Therapeutic Applications. *Front Cardiovasc Med.* (2022) 9:863332.

3. Abdelwahid E, Kalvelyte A, Stulpinas A, de Carvalho KA, Guarita-Souza LC, Foldes G. Stem cell death and survival in heart regeneration and repair. *Apoptosis.* (2016) 21(3):252–68. doi: 10.1007/s10495-015-1203-4

frontiers | Frontiers in Cardiovascular Medicine

TYPE Review
PUBLISHED 21 June 2023
DOI 10.3389/fcvm.2023.1202730

OPEN ACCESS

EDITED BY
Yoshiyuki Ikeda,
Kagoshima University, Japan

REVIEWED BY
Hiroya Ohta,
Tokushima Bunri University, Japan
Anna Planavila,
University of Barcelona, Spain

*CORRESPONDENCE
Zhangping Liao
✉ liaozp1980@163.com

RECEIVED 09 April 2023
ACCEPTED 07 June 2023
PUBLISHED 21 June 2023

CITATION
Zhao Z, Cui X and Liao Z (2023) Mechanism of fibroblast growth factor 21 in cardiac remodeling.
Front. Cardiovasc. Med. 10:1202730.
doi: 10.3389/fcvm.2023.1202730

Mechanism of fibroblast growth factor 21 in cardiac remodeling

Zeyu Zhao[1], Xuemei Cui[2] and Zhangping Liao[3]*

[1]Queen Mary College, Nanchang University, Nanchang, China, [2]Fourth Clinical Medical College, Nanchang University, Nanchang, China, [3]Jiangxi Provincial Key Laboratory of Basic Pharmacology School of Pharmaceutical Science, Nanchang University, Nanchang, China

Cardiac remodeling is a basic pathological process that enables the progression of multiple cardiac diseases to heart failure. Fibroblast growth factor 21 is considered a regulator in maintaining energy homeostasis and shows a positive role in preventing damage caused by cardiac diseases. This review mainly summarizes the effects and related mechanisms of fibroblast growth factor 21 on pathological processes associated with cardiac remodeling, based on a variety of cells of myocardial tissue. The possibility of Fibroblast growth factor 21 as a promising treatment for the cardiac remodeling process will also be discussed.

KEYWORDS

fibroblast growth factor 21 (FGF21), heart remodeling, energy metabolism, oxidation, inflammation, autophagy

Introduction

Cardiac remodeling refers to a series of changes in the heart that lead to increased ventricular dilation, cardiac dysfunction, and molecular changes which can be caused by a diminished variety of factors (1), such as myocardial infarction (MI), hypertension, obesity, and valvular heart diseases (2). Numerous kinds of cells, including endothelial cells, immune cells, and fibroblasts, are involved in the remodeling process, which aims to cope with risk factors, reduce myocardial damage and initiate repair processes to fill the damaged area (3). However, cardiac remodeling can also lead to diminishing cardiac contractility and a restricted supply of energy substrates and oxygen, resulting in elevated levels of cardiac fibrosis and hypertrophy (4, 5). Although cardiac remodeling is initially considered an adaptation to restore cardiac function after damage. The unlimited pathological change results in cardiomyocyte disarrangement and dysfunction (6), eventually leading to heart failure (HF), the outcome of cardiac adverse events (7). Accordingly, the use of interventions in the early stages to preserve the structure and cardiac function is necessary to delay the progression and improve patients' quality of life (8).

One potential intervention for cardiac remodeling is the use of fibroblast growth factor 21 (FGF21). FGF21 is initially identified in the liver and subsequently is also found to be expressed in brown adipose tissue, skeletal muscle, and pancreas, where it shows its effects mainly through a paracrine manner (9). While the heart is traditionally viewed as an effector organ of FGF21, studies have also shown that it can produce FGF21 in response to damage. By binding to the receptor fibroblast growth factor receptor (FGFR)1 and cofactors β-klotho, FGF21 activated the downstream genes to play a crucial role in cardioprotection (10). However, a recent study has pointed out that FGF21-FGFR4 signaling promoted cardiac hypertrophy (11).

After damage occurs, cardiomyocytes secrete FGF21 in an autocrine manner and reduced myocardial injury (12). Besides, FGF21 originating from other tissues has been shown to contribute to the limitation of cardiac damage and the reversal of cardiac

remodeling. Following MI, the liver played a significant role as a major source of circulating FGF21 levels (13). Additionally, FGF21 derived from brown adipose tissue was found to attenuate adverse cardiac remodeling in mice with hypertension (14). Studies have shown that FGF21 resists cardiac remodeling and the following damage through ways such as promoting autophagy, alleviating inflammation, oxidative stress, and regulating energy metabolism (12, 15–17).

FGF21 has been shown to play a protective role in various cardiovascular diseases including MI, atherosclerosis, and diabetic cardiomyopathy in different studies (18–20), and FGF21 knockout mice tend to present pathological phenotypes (21). Moreover, FGF21 levels predict the prognosis of many heart diseases such as hypertension, dilated cardiomyopathy, and MI (22–24).

Recent studies report that FGF21 is involved in the prevention of cardiac damage. The review examines the mechanisms of FGF21 against cardiac remodeling, providing potential survival benefits through a range of pathways including autophagy, metabolic stability, oxidation, inflammation, and fibrosis. The mechanism by which FGF21 exerts protective effects on the heart are listed in **Figure 1**. Additionally, this review discusses the potential implications for clinical research on FGF21-related drugs.

FGF21 in autophagy

Cellular autophagy is a process that makes cellular energy reuse by degrading autophagic vesicles containing cytoplasmic material. It is a positive implication for cardiomyocytes in resisting stress (25, 26). Recycling misfolded proteins back as energy substrates reduces the demand of cells for external nutrients, removing mitochondria residuals, toxic metabolic substrates, and reactive oxygen species (ROS) in mitochondrial dysfunction (27).

The activation of autophagy helps to maintain cardiac homeostasis and prevent myocardium hypertrophy. The energy provided by autophagy supports cell survival, helping to maintain the number of cardiomyocytes and preserve cardiac function after stress (28). A study has reported that after MI, autophagy limited cardiac damage by reducing the scar size and holding cardiac function (29). The inhibition of autophagy would lead to pronounced signs of cellular hypertrophy in the myocardium (28). Angiogenesis is beneficial for improving postinfarction collateral perfusion, reducing infarct size, and attenuating the negative effect on contractility of the infarcted area, and autophagy plays a role in initiating angiogenesis (30).

Both mTORC1 and Beclin1 are autophagy-associated molecules, playing key roles in cardiac plasticity (31). As a

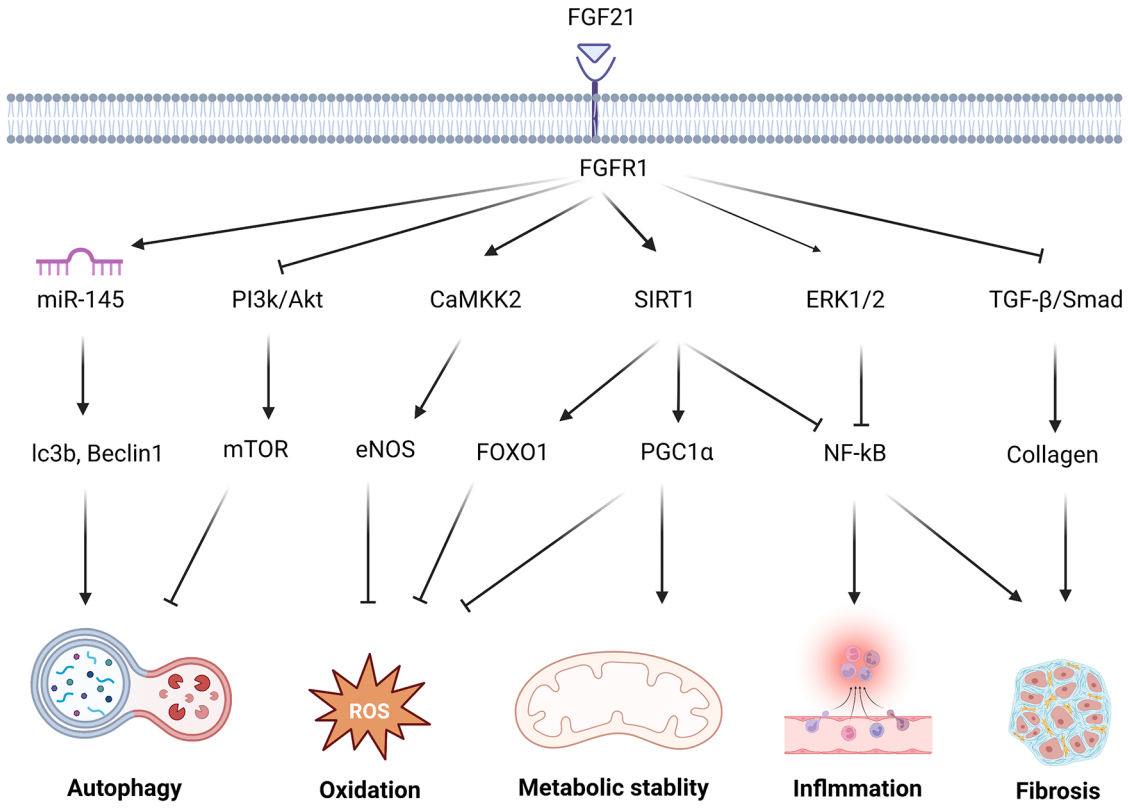

FIGURE 1
The molecular mechanism and effect of FGF21 in protecting against cardiac remodeling. FGF21 regulates multiple signaling pathways to protect against cardiac remodeling. FGF21 inhibited PI3K/Akt/mTOR pathway and upgraded the miR-145 level to enhance the autophagy level. FGF21 promotes CAMKK2-eNOS to elevate the vasomotor capacity and alleviate oxidative stress injury. via activation of FOXO1 and PGC1 α, SIRT1 results in multiple antioxidant proteins and transcription factors associated with oxidative stress levels. NF-kB, as a key transcription factor related to inflammation, under the action of FGF21, is inhibited by SIRT1, ERK1/2. FGF21 attenuates this adverse alteration. Reducing TGF-β/Smad signaling also helps avoid the secretion of large amounts of collagen by fibroblasts which may cause collagen deposition and fibrosis.

serine/threonine kinase, mTORC1 acts to inhibit autophagy activity at various levels. By inhibiting the transport of nuclear transcription factor EB(TFEB), mTORC1 reduced the transcription of autophagy related (Atg) genes (32). The phosphorylation of DCP2 induced by mTORC1 made specific Atg mRNA degradation (33). The autophagosome formation discontinued after the phosphorylation of unc-51-like autophagy activating kinase 1 (Ulk1) at Ser757 (34). Beclin1 is another well-known protein in autophagy initiating, regarded as a marker of autophagy activity. By protein interaction, Beclin1 was one of the vital components of the Class III phosphatidylinositol 3-kinase (PI3K)-III complex, which acted as a platform to recruit multiple proteins to form mature autophagosomes (35).

FGF21 in cellular autophagy can be beneficial for attenuating cardiomyocyte damage after stress. As a peroxisome-proliferator-activated receptor agonist, the protective effect of Fenofibrate in the diabetes-induced cardiac remodeling was depended on FGF21- Sirtuin-1 (SIRT1) activated autophagy (17). The lack of FGF21 led to the impairment of autophagy and accumulation of fatty acid, making high-fat-diet mice cardiomyocytes hypertrophy (36).

FGF21 regulated autophagy through different pathways. By increasing TFEB transcriptional activity, FGF21 administration enhanced the autophagy effect and relieved the ischemia-reperfusion (I/R) injury in vascular endothelial cells (37). FGF21 protected against I/R injury, enhancing cell autophagy and reducing inflammation through regulating miR-145, with the upregulation of lc3b (lc3b I/II) and Beclin1 (38). Through KEGG pathway analysis, the PI3K-Akt-mTOR pathway was thought to be associated with FGF21. FGF21 promoted autophagy by inhibiting PI3K-Akt-mTOR transduction (39). Another study proved that FGF21 inhibited atherogenesis by up-regulating autophagy, enabling cholesterol efflux and reducing lipid accumulation in foam cells, this effect was related to the activated rack-1 pathway (18).

FGF21 in energy metabolism

The alteration in energy supply is closely associated with pathological cardiac hypertrophy. They can even precede the appearance of a detectable cardiac hypertrophic result. The shift of substrate metabolism was viewed as an important feature of cardiac hypertrophy (40). Physiologically, cardiac energy was supplied by fatty acids, and approximately 70% ATP was provided by lipid substrates (41). However, cardiac tissue still preserved the ability to use various types of energy substrates including ketone bodies under different conditions, which was known as metabolic flexibility (42). Since deviating in metabolic pathways simultaneously led to cardiac hypofunction and maladaptive hypertrophy, the inhibition of related pathways might restore regular metabolic capacity while attenuating cardiac remodeling.

Cardiac diseases can exhibit diverse metabolic preference profiles. Heart failure relied on glycolysis and lactate for energy, whereas diabetes-induced cardiomyopathy was typically characterized by a dominance of lipid metabolism (43–45). For late-stage patients, the instability of the energy supply directly affected contractile function, and the limited metabolic pathways further interfered with ATP generation, ultimately causing HF (40, 46). Based on a proteomic study, FGF21 was found to restore the levels of pyruvate kinase isozymes M1/M2, which improved the energy supply after I/R injury (47).

FGF21 acted on upstream signals to regulate AMPK(Adenosine 5′-monophosphate -activated protein kinase)/SIRT1/PGC (peroxisome proliferators-activated receptor γ coactivator)-1α pathways. AMPK/SIRT1/PGC-1a was considered a target pathway involved in the regulation of metabolic stability, with its effects including the coordination of ATP levels, modulation of mitochondria function, and lipid metabolism (48–51). CD36 was a fatty acid translocase that can activate the AMPK pathway to accelerate lipid metabolism under fatty acid mediation (52). In FGF21 knockout mice's hearts, there was severe lipid accumulation and CD36 levels upregulation, accompanied by a decrease in phosphorylation levels of AMPK protein and PGC-1α expression, showing that CD36 cannot activate AMPK/SIRT1/PGC-1α pathway without FGF21 presence and thus led to metabolic dysregulation (16, 53). LKB1 was essential for AMPK activation. The inhibition of LKB1 weakened FGF21 promoting effect of mitochondrial function, demonstrating that the benefits of FGF21 promoting mitochondrial synthesis and mitochondrial oxidative capacity required the AMPK/SIRT1/PGC-1α pathways (54).

A study using angiopoietin 2-induced cardiac hypertrophy mice noted that FGF21 treatment increased SIRT1 deacetylation activity, promoted AMPK phosphorylation, and reduced cardiac hypertrophy in a SIRT1-dependent pathway (55). In brown adipose tissue, upon adenosine binding to the surface receptor A_2AR, released FGF21 can be upregulated by phosphorylating AMPK and PGC-1 α against cardiac hypertrophy (14). In MI model mice with the activated AMPK/SIRT1/PGC-1α pathway, circulating FGF21 levels were greatly higher even at the early onset and lasted up to a week (56). The ability of the FGF21-AMPK pathway to rapidly respond to early ischemic injury suggested that it may serve as a key to reducing MI injury.

FGF21 in oxidation

ROS-mediated oxidative stress injury contributed to the progression of cardiac remodeling and HF. The balance between various oxidant and antioxidant enzymes, including catalases, glutathione peroxidases, xanthine oxidases, and NADPH oxidase (NOX), generally maintains ROS levels at low levels. In situations of overloading or insufficient blood supply, mitochondrial dysfunction made hearts generate insufficient ATP, increased oxidative stress (57), overproduction of hydrogen peroxide, which ultimately led to cardiomyocyte necrosis, left ventricular dysfunction, and eventually HF (58). The experiment proved that cardiomyocyte apoptosis induced by oxidative stress was one of the reasons for myocardial decompensation (59).

ROS promoted the imbalanced growth of cardiomyocytes through multiple pathways, ultimately causing cardiac

hypertrophy and remodeling (60). By directly activating the transcription factor NF-kB, ROS induced the transcription of more pro-hypertrophic genes (61). NADPH oxidase was a major source of superoxide in the cardiovascular system (62). The reaction between excessive superoxide anion and Nitric Oxide (NO) formed the peroxynitrite (ONOO-), decreasing NO bioavailability, causing vasoconstriction, and leading to the early formation of atherosclerotic plaques (63). Animal studies have shown a positive relationship between increased levels of oxidative stress and disease progression in multiple animal models of HF (64–66). Similarly, FGF21 levels were also specifically elevated in patients with poor prognosis HF (67), a coincidence that has led to thoughts about a possible relationship between FGF21 and the effects of oxidative stress.

In cardiomyocytes, FGF21 production was regulated by ROS level in an autocrine manner. High levels of ROS, which were stimulated by calcium ions released from endoplasmic reticulum, triggered a signal transduction pathway known as the unfolding protein response (UPR) which activated several transmembrane sensors, ultimately resulting in elevated FGF21 expression levels (68).

FGF21 treatment improved resistance to oxidative stress by elevating the expression levels of oxidative enzymes such as superoxide dismutase (SOD) and glutathione (69). It also activates nitric oxide synthase (eNOS) to increase NO production and reduce oxidation, guaranteeing the normal contractile function of blood vessels and reducing the adverse effects of peroxides on cells (70).

Studies have shown that FGF21 induced the expression of antioxidant genes. Through the Sirt1-FOXO1 pathway, FGF21 enhanced catalases, SOD2 levels, and the pro-apoptotic protein BIM lessened (55). In the absence of FGF21, SIRT1 effects that induced the levels of uncoupling protein (UCP)3, peroxiredoxin5, glutathione peroxidase1, catalase, and sequestosome1 were abolished (71).

Another study illustrated that recombinant FGF21 activated CaMKK2/AMPKα signaling, enhancing eNOS phosphorylation and reducing oxidative stress responses to ameliorate diabetes-induced aortic endothelial disorders (72).

Via AMPK/PGC1α/SIRT1 signaling, FGF21 led to a rise of nuclear factor erythroid 2–related factor 2 (Nrf2) and downstream antioxidative enzymes activity such as NOX4, UCP2 (73).

For atrial remodeling induced by oxidative stress, FGF21 functioned by regulating the degradation of myofibrils and levels of calpain, a calcium-dependent protease, which helped to maintain cardiac function, improved arrhythmia symptoms, and preserved electrophysiological function (74).

FGF21 in inflammation

The main reason for acute inflammatory responses is cardiomyocyte necrosis in response to various adverse factors. After damage happened, innate immune cells localized in the heart were activated, recognizing endogenous damage-associated molecular patterns, clearing necrotic cells, and releasing proinflammatory factors. Circulating immune cells were then recruited, further infiltrating the damaged area (75). This early inflammatory response was necessary to initiate the repair process, protecting the heart from further damage. However, an uncontrolled chronic inflammatory response can further aggravate cardiac adaption (76).

Chronic inflammation was one of the most important stages in the progression process of cardiac remodeling. Patients with HF have shown significantly elevated levels of proinflammatory cells and chemokines. Inhibition a series of pro-inflammatory chemokines including IL-1 and TNF-α was beneficial for attenuating adverse cardiac remodeling, maintaining cardiac function, and reducing fibrotic area (77, 78).

Proinflammatory cell activation potentiated inflammatory responses through different pathways, and their phenotypic heterogeneity dictated that they played distinct roles in cardiac inflammation.

Despite comprising only 6%–8% of noncardiomyocytes in normal cardiac tissue, cardiac macrophages massively migrated and proliferated in the remote area during the chronic healing process of MI to mediate the onset of distant myocardial remodeling, and high levels of blood-derived macrophages had a strong link to heart failure with reduced ejection fraction (HFrEF), whereas heart confined macrophages might be more involved in post-MI repair (79).

Plasma FGF21 levels were significantly elevated in patients with HFrEF, regardless of the presence of cardiac cachexia. This elevation was independently associated with the inflammatory marker IL-6, suggesting that the inflammatory response was a contributing factor to elevated FGF21 levels (80).

Among peripheral blood leukocytes, FGF21 was highly expressed in monocytes and neutrophils (81). By increasing the expression of GLUT-1, FGF21 upregulated the ability to uptake glucose in activated monocytes, which can be beneficial in immune activation (82). FGF21 played a crucial role in aiding in clearing damaged cell remnants in phagosomes, resulting from the upregulation of NOX2 transcription and expression (81).

In addition to reducing infiltration of circulating immune cells, FGF21 shifted innate macrophages towards the anti-inflammatory M2 subtype rather than pro-inflammatory (83). FGF21 negatively regulated the early formation of atherosclerotic plaques by preventing the transformation of macrophages into foam cells and reducing macrophage migration by inhibiting the NF-kB signaling pathway (84).

CD4 + Th17 cells were thought to be directly involved in the progression of adverse remodeling from hypertrophy to HF in the situation of pressure overload (85). FGF21 regulated STAT3/RORγ phosphorylation and pro-T-cell expansion IL-23 levels, reducing splenic Th17 cell differentiation and proliferation, and ultimately downregulating the levels of pro-inflammatory factor IL-17, thereby alleviating arthritis in mice (86). This suggests that FGF21 can induce inflammation by downregulating T cells through the regulation of the Th17-IL-17 axis.

Multiple studies have demonstrated hemagglutination propensity, platelet activation, and levels of associated adhesion molecules all increase in HF patients (87). After activation and adhesion to the capillary wall, platelets secreted a variety of pro-

inflammatory factors, promoted macrophage infiltration, and regulated precursor cell to foam cell transformation, ultimately leading to small vessel endothelial thickening and sclerotic plaque formation of large vessels. Agglutination of platelets following an acute cardiac event further enhanced microvascular obstruction and potentiated the inflammatory response (88).

To reduce reperfusion injury after MI, antiplatelet and antithrombotic drugs are routinely used in the clinic (89). FGF21 reduced factor VII expression which was a hallmark of the extrinsic coagulation pathway. Variations in the fluorescence intensity levels of platelet surface markers proved that FGF21 inhibited platelet activation, reducing hemagglutination. By regulating the ERK1/2 and TGF(Transforming Growth Factor)-β/Smad2 pathway, FGF21 promoted the expression of tPA and suppressed the expression of PAI, so that fibrinolysis was activated without bleeding risk (90).

FGF21 presented anti-inflammatory properties by modulating the balance between pro-inflammation and anti-inflammation factors. The administration of FGF21 led to a downregulation of several pro-inflammatory factors and increased the expression of anti-inflammatory cytokines over a long period (83). Another *in vitro* experiment pointed out that this kind of action of FGF21 was related to IL-10 in the ERK1/2 pathway (15). Additionally, FGF21 alleviated inflammation in vascular endothelial cells through SIRT1-mediated NF-kB deacetylation (91). **Figure 2** summarizes the roles of FGF21 in different cells of myocardial tissue.

FGF21 in cardiac fibrosis

Fibrosis is considered as a crucial process in heart remodeling. After encountering pressure, fibroblasts secreted a large number of collagen fibers to the interstitium, and this excessive fiber deposition triggered the disarrangement of cardiomyocytes (92). The hypertension phenotype presented an increased wall/lumen ratio in resistance arteries, which was related to the activation and decomposition of collagens and other extracellular matrix components (ECM) components (93). After MI, fibroblast activation resulted in the deposition of collagen to form a scar, which helped to ensure the intactness of residual myocardial tissue and avoided serious consequences such as cardiac rupture (4, 94). During the post-infarction repair period, the distal area of the myocardium without infarction had massive fibrin deposition, leading to interstitial remodeling, reducing cardiac compliance, and promoting ventricular diastolic dysfunction development (95).

By using an efficient carrier, FGF21 administration attenuated cardiac fibrosis, resulting in decreased mRNA levels of cardiac hypertrophy and fibrosis markers in diabetic cardiomyopathy mice (96). FGF21 released from brown adipose tissue ameliorated cardiac fibrosis and hypertension-induced myocardial remodeling (14). In vitro experiments showed that FGF21 significantly decreased myofibroblast markers α-SMA and ACTA2 mRNA levels, suggesting that FGF21 was related to attenuating cardiac fibrosis (14, 97). The administration of the homolog of FGF21, LY2405319 in mice with liver fibrosis, reduced the levels of type

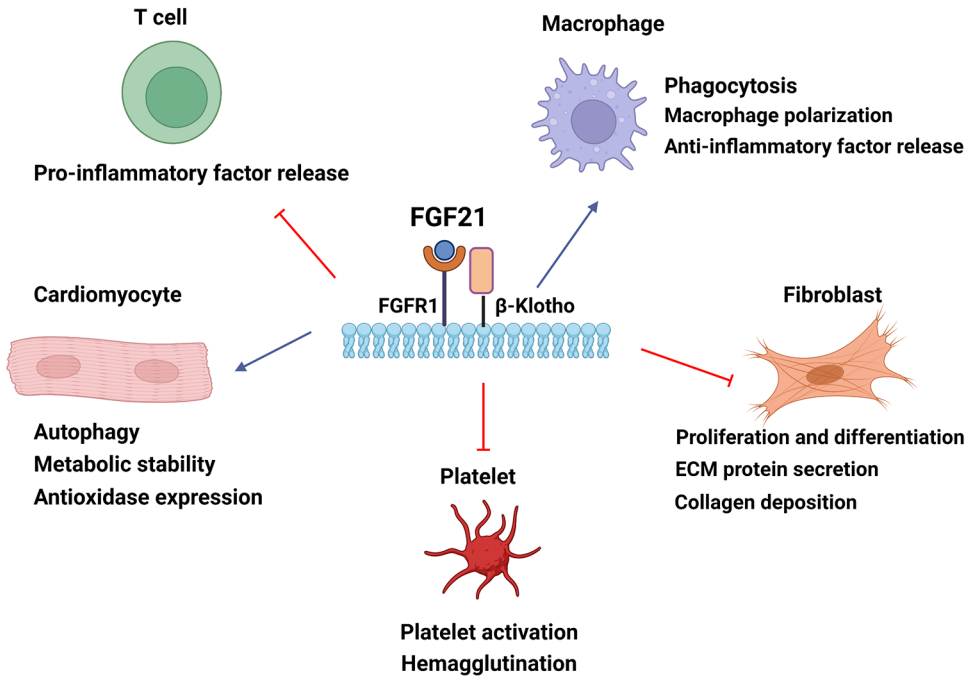

FIGURE 2
The cellular mechanisms by which FGF21 confers cardioprotection in cardiac tissue. FGF21 modulates cardiomyocyte energy metabolism and autophagy and improves oxidative stress damage. FGF21 can mediate macrophage polarization to the anti-inflammatory subtype and regulate cytokine levels to alleviate inflammatory responses. FGF21 upregulates phagocytosis to eliminate damaged remnants. The inhibition of fibroblast reduces collagen deposition of the extracellular matrix and ameliorates cardiac fibrosis by FGF21. FGF21 also downregulates hemagglutination by reducing platelet activation. Blue arrow, upregulation; red arrow, downregulation. ECM, extracellular matrix.

1 collagen and α-SMA in tissue, resulting from inhibiting the succinate- G-protein coupled receptor 91 pathway (98).

TGFβ is one of the key factors leading to cardiac remodeling, accelerating fibroblast proliferation, and inducing accumulation of ECM components, which led to impaired cardiac function (99). FGF21 treatment attenuated the fibrotic phenotype by upregulating the transcription factor EGR1 (100). FGF21 also decreased collagen synthesis in MI mice through TGF-β1/Smad2/3-MMP (metalloproteinase)2/9 signaling (101). FGF21 downregulated MMP9 levels through NF-kB [Z.-C (102)]. Through the FGFR1/Syk/NLRP3 inflammasome pathway, FGF21 restrained the proliferation and migration of vascular smooth muscle cells and neointimal hyperplasia, marked by increasing in PCNA, cyclin D1 and MMP9 (103).

Galectin(Gal)-3 is mainly secreted by macrophages in the heart, released into the cytoplasmic matrix in association with collagen receptor action. It can promote macrophage migration, cardiac fibroblast proliferation, and collagen deposition in the matrix, leading to reduced ejection fraction (104). FGF21 regulated Gal-3 levels in H9c2 cells in a dose-dependent manner and ECM-related proteins (fibronectin, collagen I) levels were also decreased under FGF21 treatment (105). This suggested that FGF21 may play a protective role in the heart by reducing the level of cardiac fibrosis through downregulating Gal-3 levels. However, due to the inadequacy of the available evidence, more studies are still needed to further determine the relationship between FGF21 and Gal-3.

Clinical application and prospects

FGF21, as a metabolically associated protective factor, has been shown to have potential clinical applications in various diseases. Elevated serum levels of FGF21 have been observed in response to stress stimuli and have been associated with a higher risk of morbidity and poor prognosis in multiple diseases. One analysis indicated that FGF21 levels were useful in predicting the severity and prognostic risk in patients with community-acquired pneumonia (106). Clinical studies have also shown that FGF21 is useful in predicting HF (107–110). Serum FGF21 levels were higher under acute insufficient sleep conditions when adipose tissue FGF21 promoter region was methylated (111).

Due to the short half-life and susceptibility to plasma proteases, FGF21 was difficult to use in clinical practice. Therefore, diverse chemical modifications have been used to increase its stability and applicability (112). Current clinical studies targeting FGF21 mainly focus on its ameliorative effects on metabolic diseases. The use of fibroblast activation protein inhibitors, BR103354, successfully elevates FGF21 levels in cynomolgus monkeys (113). Treatment of nonalcoholic fatty liver disease using bms-986036, a PEGylated FGF21 analog, resulting in a considerable decrease in liver fat and fibrosis in patients after 16 weeks of treatment, with very limited adverse effects (114).

Preclinical pharmacological studies have extensively validated the protective effects of FGF21 in damaged hearts. AMPK-FGF21 helped regulate the survival of cardiomyocytes under ischemic conditions after MI (56). FGF21 ameliorated atrial fibrillation and tachycardia by reducing excessive fibrosis (74). FGF21 has been shown to improve post-infarction arrhythmias and preserve electrophysiological function through mediating cardiac sodium current and inward rectifier potassium current (115). By improving FGFR1 phosphorylation, long-term FGF21 administration helped to alleviate high-fat-diet-induced left heart dysfunction and restored FGF21 sensitivity (116). In alcoholic cardiomyopathy, FGF21 improved adverse effects related to dysfunctional mitochondria by mediating autophagic pathways (117). However, a recent study reported that FGF21-FGFR4 signaling upregulated the activity of ERK1/2, enhancing diabetes mouse concentric cardiac hypertrophy and adverse cardiac remodeling (11). The FGF21 analog shows promise as a candidate for the diagnosis and therapy of cardiac diseases, but further investigation is needed to support its use in the future.

Conclusion

The review mainly expounds on the possibility that FGF21, as a promising cardioprotective factor, improves cardiac function and ultimately retarding the progress of cardiac diseases. The actions of FGF21 for the heart are extensive. On the one hand, FGF21 has a regulatory effect targeted to different populations of cardiac tissue, including cardiomyocytes, immune cells, and fibroblasts. On the other hand, by acting on AMPK/SIRT1/PGC-1α, PI3K-Akt, ERK1/2, and TGF-β/Smad2 to mediate vital mechanisms, including autophagy, energy metabolism, oxidative stress, inflammation, and fibrosis, it is verified that FGF21 acts as a possible cardiac protective molecule. Therefore, the next steps in the development of relevant studies on targeted therapy of FGF21 in cardiac remodeling will be promising directions.

Author contributions

ZZ conceptualized and wrote the manuscript. XC drew the figures and revised the manuscipt. ZL revised the manuscript. All authors contributed to the article and approved the submitted version.

Acknowledgments

This study was supported by the National Natural Science Foundation of China (82060657). Figures were created with Biorender.com

Conflict of interest

The authors declare that the research was conducted in the absence of any commercial or financial relationships that could be construed as a potential conflict of interest.

Publisher's note

References

1. Diez J, Ertl G. A translational approach to myocardial remodelling. *Cardiovasc Res.* (2008) 81(3):409–11. doi: 10.1093/cvr/cvn352

2. Cohn JN, Ferrari R, Sharpe N. Cardiac remodeling—concepts and clinical implications: a consensus paper from an international forum on cardiac remodeling. *J Am Coll Cardiol.* (2000) 35(3):569–82. doi: 10.1016/S0735-1097(99)00630-0

3. Frantz S, Bauersachs J, Ertl G. Post-Infarct remodelling: contribution of wound healing and inflammation. *Cardiovasc Res.* (2008) 81(3):474–81. doi: 10.1093/cvr/cvn292

4. Pfeffer MA, Braunwald E. Ventricular remodeling after myocardial infarction. Experimental observations and clinical implications. *Circulation.* (1990) 81(4):1161–72. doi: 10.1161/01.CIR.81.4.1161

5. Miura T, Miki T. Limitation of myocardial infarct size in the clinical setting: current Status and challenges in translating animal experiments into clinical therapy. *Basic Res Cardiol.* (2008) 103(6):501–13. doi: 10.1007/s00395-008-0743-y

6. Porter KE, Turner NA. Cardiac fibroblasts: at the heart of myocardial remodeling. *Pharmacol Ther.* (2009) 123(2):255–78. doi: 10.1016/j.pharmthera.2009.05.002

7. Ponikowski P, Voors AA, Anker SD, Bueno H, Cleland JGF, Coats AJS, et al. 2016 ESC guidelines for the diagnosis and treatment of acute and chronic heart failure. *Eur Heart J.* (2016) 37(27):2129–200. doi: 10.1093/eurheartj/ehw128

8. Hill JA, Olson EN. Cardiac plasticity. *N Engl J Med.* (2008) 358(13):1370–80. doi: 10.1056/NEJMra072139

9. Zhang Y, Liu D, Long X-X, Fang Q-C, Jia W-P, Li H-T. The role of FGF21 in the pathogenesis of cardiovascular disease. *Chin Med J.* (2021) 134(24):2931–43. doi: 10.1097/CM9.0000000000001890

10. Lü Y, Liu J-H, Zhang L-K, Jie DU, Zeng X-J, Hao G, et al. Fibroblast growth factor 21 as a possible endogenous factor inhibits apoptosis in cardiac endothelial cells. *Chin Med J.* (2010) 123(23):3417–21. doi: 10.3760/cma.j.issn.0366-6999.2010.23.008

11. Yanucil C, Kentrup D, Li X, Grabner A, Schramm K, Martinez EC, et al. FGF21-FGFR4 Signaling in cardiac myocytes promotes concentric cardiac hypertrophy in mouse models of diabetes. *Sci Rep.* (2022) 12(1):7326. doi: 10.1038/s41598-022-11033-x

12. Planavila A, Redondo I, Hondares E, Vinciguerra M, Munts C, Iglesias R, et al. Fibroblast growth factor 21 protects against cardiac hypertrophy in mice. *Nat Commun.* (2013) 4(1):2019. doi: 10.1038/ncomms3019

13. Sun J-Y, Du L-J, Shi X-R, Zhang Y-Y, Liu Y, Wang Y-L, et al. An IL-6/STAT3/MR/FGF21 axis mediates heart-liver cross-talk after myocardial infarction. *Sci Adv.* (2023) 9(14):eade4110. doi: 10.1126/sciadv.ade4110

14. Ruan C-C, Kong L-R, Chen X-H, Ma Y, Pan X-X, Zhang Z-B, et al. A2a receptor activation attenuates hypertensive cardiac remodeling via promoting brown adipose tissue-derived FGF21. *Cell Metab.* (2018) 28(3):476–89. e5. doi: 10.1016/j.cmet.2018.06.013

15. Li J-y, Wang N, Khoso MH, Shen C-b, Guo M-z, Pang X-x, et al. FGF-21 elevated IL-10 production to correct LPS-induced inflammation. *Inflammation.* (2018a) 41(3):751–59. doi: 10.1007/s10753-018-0729-3

16. Yan X, Chen J, Zhang C, Zhou S, Zhang Z, Chen J, et al. FGF21 deletion exacerbates diabetic cardiomyopathy by aggravating cardiac lipid accumulation. *J Cell Mol Med.* (2015) 19(7):1557–68. doi: 10.1111/jcmm.12530

17. Zhang J, Cheng Y, Gu J, Wang S, Zhou S, Wang Y, et al. Fenofibrate increases cardiac autophagy via FGF21/SIRT1 and prevents fibrosis and inflammation in the hearts of type 1 diabetic mice. *Clin Sci.* (2016) 130(8):625–41. doi: 10.1042/CS20150623

18. Xiaolong L, Dongmin G, Liu M, Zuo W, Huijun H, Qiufen T, et al. FGF21 Induces autophagy-mediated cholesterol efflux to inhibit atherogenesis via RACK1 up-regulation. *J Cell Mol Med.* (2020) 24(9):4992–5006. doi: 10.1111/jcmm.15118

19. Xu Z, Sun J, Tong Q, Lin Q, Qian L, Park Y, et al. The role of ERK1/2 in the development of diabetic cardiomyopathy. *Int J Mol Sci.* (2016) 17(12):2001. doi: 10.3390/ijms17122001

20. Liu SQ, Roberts D, Kharitonenkov A, Zhang B, Hanson SM, Li YC, et al. Endocrine protection of ischemic myocardium by FGF21 from the liver and adipose tissue. *Sci Rep.* (2013) 3(1):2767. doi: 10.1038/srep02767

21. Pan X, Shao Y, Wu F, Wang Y, Xiong R, Zheng J, et al. FGF21 prevents angiotensin II-induced hypertension and vascular dysfunction by activation of ACE2/angiotensin-(1–7) axis in mice. *Cell Metab.* (2018) 27(6):1323–37. e5. doi: 10.1016/j.cmet.2018.04.002

22. Zhang W, Chu S, Ding W, Wang F. Serum level of fibroblast growth factor 21 is independently associated with acute myocardial infarction. *PLOS ONE.* (2015) 10(6):e0129791. doi: 10.1371/journal.pone.0129791

23. Semba RD, Crasto C, Strait J, Sun K, Schaumberg DA, Ferrucci L. Elevated serum fibroblast growth factor 21 is associated with hypertension in community-dwelling adults. *J Hum Hypertens.* (2013) 27(6):397–99. doi: 10.1038/jhh.2012.52

24. Gu L, Jiang W, Zheng R, Yao Y, Ma G. Fibroblast growth factor 21 correlates with the prognosis of dilated cardiomyopathy. *Cardiology.* (2021) 146(1):27–33. doi: 10.1159/000509239

25. Sciarretta S, Maejima Y, Zablocki D, Sadoshima J. The role of autophagy in the heart. *Annu Rev Physiol.* (2018) 80(1):1–26. doi: 10.1146/annurev-physiol-021317-121427

26. Levine B, Klionsky DJ. Development by self-digestion. *Dev Cell.* (2004) 6(4):463–77. doi: 10.1016/S1534-5807(04)00099-1

27. Green DR, Galluzzi L, Kroemer G. Mitochondria and the autophagy–inflammation–cell death axis in organismal aging. *Science.* (2011) 333(6046):1109–12. doi: 10.1126/science.1201940

28. Nakai A, Yamaguchi O, Takeda T, Higuchi Y, Hikoso S, Taniike M, et al. The role of autophagy in cardiomyocytes in the basal state and in response to hemodynamic stress. *Nat Med.* (2007a) 13(5):619–24. doi: 10.1038/nm1574

29. Maejima Y, Kyoi S, Zhai P, Liu T, Li H, Ivessa A, et al. Mst1 inhibits autophagy by promoting the interaction between Beclin1 and bcl-2. *Nat Med.* (2013) 19(11):1478–88. doi: 10.1038/nm.3322

30. Lu Q, Yao Y, Hu Z, Hu C, Song Q, Ye J, et al. Angiogenic factor AGGF1 activates autophagy with an essential role in therapeutic angiogenesis for heart disease. *PLoS Biol.* (2016) 14(8):e1002529. doi: 10.1371/journal.pbio.1002529

31. Shi B, Ma M, Zheng Y, Pan Y, Lin X. MTOR and Beclin1: two key autophagy-related molecules and their roles in myocardial ischemia/reperfusion injury. *J Cell Physiol.* (2019) 234(8):12562–68. doi: 10.1002/jcp.28125

32. Noda T. Regulation of autophagy through TORC1 and MTORC1. *Biomolecules.* (2017) 7(4):52. doi: 10.3390/biom7030052

33. Hu G, McQuiston T, Bernard A, Park Y-D, Qiu J, Vural A, et al. A conserved mechanism of TOR-dependent RCK-mediated MRNA degradation regulates autophagy. *Nat Cell Biol.* (2015) 17(7):930–42. doi: 10.1038/ncb3189

34. Rabanal-Ruiz Y, Otten EG, Korolchuk VI. MTORC1 as the main gateway to autophagy. *Essays Biochem.* (2017) 61(6):565–84. doi: 10.1042/EBC20170027

35. McKnight NC, Yue Z. Beclin 1, an essential component and master regulator of PI3K-III in health and disease. *Curr Pathobiol Rep.* (2013) 1(4):231–38. doi: 10.1007/s40139-013-0028-5

36. Rupérez C, Lerin C, Ferrer-Curriu G, Cairo M, Mas-Stachurska A, Sitges M, et al. Autophagic control of cardiac steatosis through FGF21 in obesity-associated cardiomyopathy. *Int J Cardiol.* (2018) 260:163–70. doi: 10.1016/j.ijcard.2018.02.109

37. Chen F, Zhan J, Yan X, al Mamun A, Zhang Y, Xu Y, et al. FGF21 alleviates microvascular damage following limb ischemia/reperfusion injury by TFEB-mediated autophagy enhancement and anti-oxidative response. *Signal Transduct Targeted Ther.* (2022) 7(1):349. doi: 10.1038/s41392-022-01172-y

38. Hu S, Cao S, Tong Z, Liu J. FGF21 Protects myocardial ischemia-reperfusion injury through reduction of MiR-145-mediated autophagy. *Am J Transl Res.* (2018) 10(11):3677–88. PMID: 30662618 PMCID: PMC6291727.

39. Dai H, Hu W, Zhang L, Jiang F, Mao X, Yang G, et al. FGF21 Facilitates autophagy in prostate cancer cells by inhibiting the PI3K–Akt–MTOR signaling pathway. *Cell Death Dis.* (2021) 12(4):303. doi: 10.1038/s41419-021-03588-w

40. Bertero E, Maack C. Metabolic remodelling in heart failure. *Nat Rev Cardiol.* (2018) 15(8):457–70. doi: 10.1038/s41569-018-0044-6

41. Stanley W. Regulation of myocardial carbohydrate metabolism under normal and ischaemic conditions potential for pharmacological interventions. *Cardiovasc Res.* (1997) 33(2):243–57. doi: 10.1016/S0008-6363(96)00245-3

42. Kim TT, Dyck JRB. Is AMPK the savior of the failing heart? *Trends Endocrinol Metab.* (2015) 26(1):40–8. doi: 10.1016/j.tem.2014.11.001

43. Rijzewijk LJ, van der Meer RW, Lamb HJ, de Jong HWAM, Lubberink M, Romijn JA, et al. Altered myocardial substrate metabolism and decreased diastolic

function in nonischemic human diabetic cardiomyopathy. *J Am Coll Cardiol*. (2009) 54(16):1524–32. doi: 10.1016/j.jacc.2009.04.074

44. Choi YS, de Mattos ABM, Shao D, Li T, Nabben M, Kim M, et al. Preservation of myocardial fatty acid oxidation prevents diastolic dysfunction in mice subjected to angiotensin II infusion. *J Mol Cell Cardiol*. (2016) 100:64–71. doi: 10.1016/j.yjmcc.2016.09.001

45. Kolwicz SC, Olson DP, Marney LC, Garcia-Menendez L, Synovec RE, Tian R. Cardiac-Specific deletion of acetyl CoA carboxylase 2 prevents metabolic remodeling during pressure-overload hypertrophy. *Circ Res*. (2012) 111(6):728–38. doi: 10.1161/CIRCRESAHA.112.268128

46. Neubauer S. The failing heart — an engine out of fuel. *N Engl J Med*. (2007) 356 (11):1140–51. doi: 10.1056/NEJMra063052

47. Cong W-T, Ling J, Tian H-S, Ling R, Wang Y, Huang B-B, et al. Proteomic study on the protective mechanism of fibroblast growth factor 21 to ischemia–reperfusion injury. *Can J Physiol Pharmacol*. (2013) 91(11):973–84. doi: 10.1139/cjpp-2012-0441

48. Cantó C, Gerhart-Hines Z, Feige JN, Lagouge M, Noriega L, Milne JC, et al. AMPK Regulates energy expenditure by modulating NAD+ metabolism and SIRT1 activity. *Nature*. (2009) 458(7241):1056–60. doi: 10.1038/nature07813

49. Matsushima S, Sadoshima J. The role of sirtuins in cardiac disease. *Am J PhysiolHeart Circ Physiol*. (2015) 309(9):H1375–89. doi: 10.1152/ajpheart.00053.2015

50. Cantó C, Auwerx J. PGC-1α, SIRT1 and AMPK, an energy sensing network that controls energy expenditure. *Curr Opin Lipidol*. (2009) 20(2):98–105. doi: 10.1097/MOL.0b013e328328d0a4

51. Hardie DG. AMP-Activated/SNF1 protein kinases: conserved guardians of cellular energy. *Nat Rev Mol Cell Biol*. (2007) 8(10):774–85. doi: 10.1038/nrm2249

52. Samovski D, Sun J, Pietka T, Gross RW, Eckel RH, Su X, et al. Regulation of AMPK activation by CD36 links fatty acid uptake to β-oxidation. *Diabetes*. (2015) 64(2):353–59. doi: 10.2337/db14-0582

53. Chen C, Meng Z, Zheng Y, Hu B, Shen E. Fibroblast growth factor 21 inhibition aggravates cardiac dysfunction in diabetic cardiomyopathy by improving lipid accumulation. *Exp Ther Med*. (2018) 15(1):75–84. doi: 10.3892/etm.2017.5375

54. Chau MDL, Gao J, Yang Q, Wu Z, Gromada J. Fibroblast growth factor 21 regulates energy metabolism by activating the AMPK–SIRT1–PGC-1α pathway. *Proc Natl Acad Sci USA*. (2010) 107(28):12553–58. doi: 10.1073/pnas.1006962107

55. Li S, Zhu Z, Xue M, Yi X, Liang J, Niu C, et al. Fibroblast growth factor 21 protects the heart from angiotensin II-induced cardiac hypertrophy and dysfunction via SIRT1. *Biochim Biophys Acta (BBA)*. (2019) 1865(6):1241–52. doi: 10.1016/j.bbadis.2019.01.019

56. Sunaga H, Koitabashi N, Iso T, Matsui H, Obokata M, Kawakami R, et al. Activation of cardiac AMPK-FGF21 feed-forward loop in acute myocardial infarction: role of adrenergic overdrive and lipolysis byproducts. *Sci Rep*. (2019) 9 (1):11841. doi: 10.1038/s41598-019-48356-1

57. Chistiakov DA, Shkurat TP, Melnichenko AA, Grechko Av, Orekhov AN. The role of mitochondrial dysfunction in cardiovascular disease: a brief review. *Ann Med*. (2018) 50(2):121–27. doi: 10.1080/07853890.2017.1417631

58. Nickel AG, von Hardenberg A, Hohl M, Löffler JR, Kohlhaas M, Becker J, et al. Reversal of mitochondrial transhydrogenase causes oxidative stress in heart failure. *Cell Metab*. (2015) 22(3):472–84. doi: 10.1016/j.cmet.2015.07.008

59. Cesselli D, Jakoniuk I, Barlucchi L, Beltrami AP, Hintze TH, Nadal-Ginard B, et al. Oxidative stress–mediated cardiac cell death is a Major determinant of ventricular dysfunction and failure in dog dilated cardiomyopathy. *Circ Res*. (2001) 89(3):279–86. doi: 10.1161/hh1501.094115

60. Tsutsui H, Kinugawa S, Matsushima S. Oxidative stress and heart failure. *Am J Physiol Heart Circ Physiol*. (2011) 301(6):H2181–90. doi: 10.1152/ajpheart.00554.2011

61. Kumar S, Seqqat R, Chigurupati S, Kumar R, Baker KM, Young D, et al. Inhibition of nuclear factor *K*B regresses cardiac hypertrophy by modulating the expression of extracellular matrix and adhesion molecules. *Free Radic BiolMed*. (2011) 50(1):206–15. doi: 10.1016/j.freeradbiomed.2010.10.711

62. Ago T, Kuroda J, Pain J, Fu C, Li H, Sadoshima J. Upregulation of Nox4 by hypertrophic stimuli promotes apoptosis and mitochondrial dysfunction in cardiac myocytes. *Circ Res*. (2010) 106(7):1253–64. doi: 10.1161/CIRCRESAHA.109.213116

63. Violi F, Basili S, Nigro C, Pignatelli P. Role of NADPH oxidase in atherosclerosis. *Future Cardiol*. (2009) 5(1):83–92. doi: 10.2217/14796678.5.1.83

64. Dai D-F, Johnson SC, Villarin JJ, Chin MT, Nieves-Cintrón M, Chen T, et al. Mitochondrial oxidative stress mediates angiotensin II–induced cardiac hypertrophy and gαq overexpression–induced heart failure. *Circ Res*. (2011) 108(7):837–46. doi: 10.1161/CIRCRESAHA.110.232306

65. Dai D-F, Hsieh EJ, Liu Y, Chen T, Beyer RP, Chin MT, et al. Mitochondrial proteome remodelling in pressure overload-induced heart failure: the role of mitochondrial oxidative stress. *Cardiovasc Res*. (2012) 93(1):79–88. doi: 10.1093/cvr/cvr274

66. Mollnau H, Oelze M, August M, Wendt M, Daiber A, Schulz E, et al. Mechanisms of increased vascular superoxide production in an experimental model of idiopathic dilated cardiomyopathy. *Arterioscler, Thromb, Vasc Biol*. (2005) 25 (12):2554–59. doi: 10.1161/01.ATV.0000190673.41925.9B

67. Fan L, Gu L, Yao Y, Ma G. Elevated Serum fibroblast growth factor 21 is relevant to heart failure patients with reduced ejection fraction. *Comput Math Methods Med*. (2022) 2022:1–6. doi: 10.1155/2022/7138776

68. Tabari FS, Karimian A, Parsian H, Rameshknia V, Mahmoodpour A, Majidinia M, et al. The roles of FGF21 in atherosclerosis pathogenesis. *Rev Endocr Metab Disord*. (2019) 20(1):103–14. doi: 10.1007/s11154-019-09488-x

69. Zhang S, Yu D, Wang M, Huang T, Wu H, Zhang Y, et al. FGF21 Attenuates pulmonary fibrogenesis through ameliorating oxidative stress in vivo and in vitro. *Biomed Pharmacother*. (2018) 103:1516–25. doi: 10.1016/j.biopha.2018.03.100

70. Wang X-M, Song S-S, Xiao H, Gao P, Li X-J, Si L-Y. Fibroblast growth factor 21 protects against high glucose induced cellular damage and dysfunction of endothelial nitric-oxide synthase in endothelial cells. *Cell Physiol Biochem*. (2014) 34(3):658–71. doi: 10.1159/000363031

71. Planavila A, Redondo-Angulo I, Ribas F, Garrabou G, Casademont J, Giralt M, et al. Fibroblast growth factor 21 protects the heart from oxidative stress. *Cardiovasc Res*. (2015) 106(1):19–31. doi: 10.1093/cvr/cvu263

72. Ying L, Li N, He Z, Zeng X, Nan Y, Chen J, et al. Fibroblast growth factor 21 ameliorates diabetes-induced endothelial dysfunction in mouse aorta via activation of the CaMKK2/AMPKα signaling pathway. *Cell Death Dis*. (2019) 10(9):665. doi: 10.1038/s41419-019-1893-6

73. Kawakami R, Sunaga H, Iso T, Kaneko R, Koitabashi N, Obokata M, et al. Ketone body and FGF21 coordinately regulate fasting-induced oxidative stress response in the heart. *Sci Rep*. (2022) 12(1):7338. doi: 10.1038/s41598-022-10993-4

74. Chen M, Zhong J, Wang Z, Xu H, Chen H, Sun X, et al. Fibroblast growth factor 21 protects against atrial remodeling via reducing oxidative stress. *Front Cardiovasc Med*. (2021) 8:720581. doi: 10.3389/fcvm.2021.720581

75. Peet C, Ivetic A, Bromage DI, Shah AM. Cardiac monocytes and macrophages after myocardial infarction. *Cardiovasc Res*. (2020) 116(6):1101–12. doi: 10.1093/cvr/cvz336

76. Dick SA, Epelman S. Chronic heart failure and inflammation. *Circ Res*. (2016) 119(1):159–76. doi: 10.1161/CIRCRESAHA.116.308030

77. Sun M, Chen M, Dawood F, Zurawska U, Li JY, Parker T, et al. Tumor necrosis factor-α mediates cardiac remodeling and ventricular dysfunction after pressure overload state. *Circulation*. (2007) 115(11):1398–407. doi: 10.1161/CIRCULATIONAHA.106.643585

78. Bujak M, Dobaczewski M, Chatila K, Mendoza LH, Li N, Reddy A, et al. Interleukin-1 receptor type I signaling critically regulates infarct healing and cardiac remodeling. *Am J Pathol*. (2008) 173(1):57–67. doi: 10.2353/ajpath.2008.070974

79. Sager HB, Hulsmans M, Lavine KJ, Moreira MB, Heidt T, Courties G, et al. Proliferation and recruitment contribute to myocardial macrophage expansion in chronic heart failure. *Circ Res*. (2016) 119(7):853–64. doi: 10.1161/CIRCRESAHA.116.309001

80. Refsgaard Holm M, Christensen H, Rasmussen J, Johansen ML, Schou M, Faber J, et al. Fibroblast growth factor 21 in patients with cardiac cachexia: a possible role of chronic inflammation. *ESC Heart Fail*. (2019) 6(5):983–91. doi: 10.1002/ehf2.12502

81. Wang W-f, Ma L, Liu M-y, Zhao T-t, Zhang T, Yang Y-b, et al. A novel function for fibroblast growth factor 21: stimulation of NADPH oxidase-dependent ROS generation. *Endocrine*. (2015) 49(2):385–95. doi: 10.1007/s12020-014-0502-9

82. Wang N, Li J-y, Li S, Guo X-c, Wu T, Wang W-f, et al. Fibroblast growth factor 21 regulates foam cells formation and inflammatory response in ox-LDL-induced THP-1 macrophages. *Biomed Pharmacother*. (2018a) 108:1825–34. doi: 10.1016/j.biopha.2018.09.143

83. Wang D, Liu F, Zhu L, Lin P, Han F, Wang X, et al. FGF21 Alleviates neuroinflammation following ischemic stroke by modulating the temporal and spatial dynamics of microglia/macrophages. *J Neuroinflammation*. (2020) 17(1):257. doi: 10.1186/s12974-020-01921-2

84. Wang N, Li J-Y, Zhao T-t, Li S-m, Shen C-B, Li D-S, et al. FGF-21 Plays a crucial role in the glucose uptake of activated monocytes. *Inflammation*. (2018b) 41(1):73–80. doi: 10.1007/s10753-017-0665-7

85. Gröschel C, Sasse A, Röhrborn C, Monecke S, Didié M, Elsner L, et al. T helper cells with specificity for an antigen in cardiomyocytes promote pressure overload-induced progression from hypertrophy to heart failure. *Sci Rep*. (2017) 7(1):15998. doi: 10.1038/s41598-017-16147-1

86. Li S-m, Yu Y-h, Li L, Wang W-f, Li D-s. Treatment of CIA mice with FGF21 down-regulates TH17-IL-17 axis. *Inflammation*. (2016) 39(1):309–19. doi: 10.1007/s10753-015-0251-9

87. Chung I, Lip GYH. Platelets and heart failure. *Eur Heart J*. (2006) 27 (22):2623–31. doi: 10.1093/eurheartj/ehl305

88. Badimon L, Padró T, Vilahur G. Atherosclerosis, platelets and thrombosis in acute ischaemic heart disease. *Eur Heart J*. (2012) 1(1):60–74. doi: 10.1177/2048872612441582

89. Bienvenu LA, Maluenda A, McFadyen JD, Searle AK, Yu E, Haller C, et al. Combined antiplatelet/anticoagulant drug for cardiac ischemia/reperfusion injury. *Circ Res*. (2020) 127(9):1211–13. doi: 10.1161/CIRCRESAHA.120.317450

90. Li S, Jia H, Liu Z, Wang N, Guo X, Cao M, et al. Fibroblast growth factor-21 as a novel metabolic factor for regulating thrombotic homeostasis. *Sci Rep*. (2022) 12 (1):400. doi: 10.1038/s41598-021-00906-2

91. Zhou X, Wang X, Lu L, Deng M, Shi X. Fibroblast growth factor 21 improves lipopolysaccharide-induced pulmonary microvascular endothelial cell dysfunction and inflammatory response through SIRT1-mediated NF-*K*B deacetylation. *Can J Physiol Pharmacol*. (2022) 100(6):492–99. doi: 10.1139/cjpp-2021-0454

92. Volders PGA, Willems IEMG, Cleutjens JPM, Aren J-W, Havenith MG, Daemen MJAP. Interstitial collagen is increased in the non-infarcted human myocardium after myocardial infarction. *J Mol Cell Cardiol*. (1993) 25(11):1317–23. doi: 10.1006/jmcc.1993.1144

93. Intengan HD, Schiffrin EL. Vascular remodeling in hypertension. *Hypertension*. (2001) 38(3):581–87. doi: 10.1161/hy09t1.096249

94. Prabhu SD, Frangogiannis NG. The biological basis for cardiac repair after myocardial infarction. *Circ Res*. (2016) 119(1):91–112. doi: 10.1161/CIRCRESAHA.116.303577

95. Talman V, Ruskoaho H. Cardiac fibrosis in myocardial infarction—from repair and remodeling to regeneration. *Cell Tissue Res*. (2016) 365(3):563–81. doi: 10.1007/s00441-016-2431-9

96. Gao J, Liu J, Meng Z, Li Y, Hong Y, Wang L, et al. Ultrasound-Assisted C3F8-filled PLGA nanobubbles for enhanced FGF21 delivery and improved prophylactic treatment of diabetic cardiomyopathy. *Acta Biomater*. (2021) 130:395–408. doi: 10.1016/j.actbio.2021.06.015

97. Ferrer-Curriu G, Redondo-Angulo I, Guitart-Mampel M, Ruperez C, Mas-Stachurska A, Sitges M, et al. Fibroblast growth factor-21 protects against fibrosis in hypertensive heart disease. *J Pathol*. (2019) 248(1):30–40. doi: 10.1002/path.5226

98. Le CT, Nguyen G, Park SY, Choi DH, Cho E-H. LY2405319, An analog of fibroblast growth factor 21 ameliorates α-smooth muscle actin production through inhibition of the succinate—g-protein couple receptor 91 (GPR91) pathway in mice. *PLOS ONE*. (2018) 13(2):e0192146. doi: 10.1371/journal.pone.0192146

99. Dobaczewski M, Chen W, Frangogiannis NG. Transforming growth factor (TGF)-β signaling in cardiac remodeling. *J Mol Cell Cardiol*. (2011) 51(4):600–6. doi: 10.1016/j.yjmcc.2010.10.033

100. Li J, Gong L, Zhang R, Li S, Yu H, Liu Y, et al. Fibroblast growth factor 21 inhibited inflammation and fibrosis after myocardial infarction via EGR1. *Eur J Pharmacol*. (2021a) 910:174470. doi: 10.1016/j.ejphar.2021.174470

101. Ma Y, Kuang Y, Bo W, Liang Q, Zhu W, Cai M, et al. Exercise training alleviates cardiac fibrosis through increasing fibroblast growth factor 21 and regulating TGF-*B*1-Smad2/3-MMP2/9 signaling in mice with myocardial infarction. *Int J Mol Sci*. (2021) 22(22):12341. doi: 10.3390/ijms222212341

102. Pan Z-C, Wang S-P, Ou T-T, Liu H, Ma J-W, Wang W-X, et al. A study on the expression of FGF-21 and NF-*K*B pathway in the tissues of atherosclerotic mice. *Eur Rev Med Pharmacol Sci*. (2017) 21(3 Suppl):102–7. PMID: 28745781.

103. Wei W, Li X-X, Xu M. Inhibition of vascular neointima hyperplasia by FGF21 associated with FGFR1/syk/NLRP3 inflammasome pathway in diabetic mice. *Atherosclerosis*. (2019) 289:132–42. doi: 10.1016/j.atherosclerosis.2019.08.017

104. Lin Y-H, Lin L-Y, Wu Y-W, Chien K-L, Lee C-M, Hsu R-B, et al. The relationship between Serum galectin-3 and Serum markers of cardiac extracellular matrix turnover in heart failure patients. *Clin Chim Acta*. (2009) 409(1–2):96–9. doi: 10.1016/j.cca.2009.09.001

105. Sun M, Jin L, Bai Y, Wang L, Zhao S, Ma C, et al. Fibroblast growth factor 21 protects against pathological cardiac remodeling by modulating galectin-3 expression. *J Cell Biochem*. (2019) 120(12):19529–40. doi: 10.1002/jcb.29260

106. Ebrahimi F, Wolffenbuttel C, Blum CA, Baumgartner C, Mueller B, Schuetz P, et al. Fibroblast growth factor 21 predicts outcome in community-acquired pneumonia: secondary analysis of two randomised controlled trials. *Eur Respir J*. (2019) 53(2):1800973. doi: 10.1183/13993003.00973-2018

107. Gan F, Huang J, Dai T, Li M, Liu J. Serum level of fibroblast growth factor 21 predicts long-term prognosis in patients with both diabetes Mellitus and coronary artery calcification. *Ann Palliat Med*. (2020) 9(2):368–74. doi: 10.21037/apm.2020.03.28

108. Sommakia S, Almaw NH, Lee SH, Ramadurai DKA, Taleb I, Kyriakopoulos CP, et al. FGF21 (fibroblast growth factor 21) defines a potential cardiohepatic signaling circuit in End-stage heart failure. *Circulation*. (2022) 15(3):e008910. doi: 10.1161/CIRCHEARTFAILURE.121.008910

109. Ianoș RD, Pop C, Iancu M, Rahaian R, Cozma A, Procopciuc LM. Diagnostic performance of Serum biomarkers fibroblast growth factor 21, galectin-3 and copeptin for heart failure with preserved ejection fraction in a sample of patients with type 2 diabetes Mellitus. *Diagnostics*. (2021) 11(9):1577. doi: 10.3390/diagnostics11091577

110. Chou R-H, Huang P-H, Hsu C-Y, Chang C-C, Leu H-B, Huang C-C, et al. Circulating fibroblast growth factor 21 is associated with diastolic dysfunction in heart failure patients with preserved ejection fraction. *Sci Rep*. (2016) 6(1):33953. doi: 10.1038/srep33953

111. Brandão M, Eduardo L, Espes D, Westholm JO, Martikainen T, Westerlund N, et al. Acute sleep loss alters circulating fibroblast growth factor 21 levels in humans: a randomised crossover trial. *J Sleep Res*. (2022) 31(2):e13472. doi: 10.1111/jsr.13472

112. Geng L, Lam KSL, Xu A. The therapeutic potential of FGF21 in metabolic diseases: from bench to clinic. *Nat Rev Endocrinol*. (2020) 16(11):654–67. doi: 10.1038/s41574-020-0386-0

113. Cho JM, Yang EH, Quan W, Nam EH, Cheon HG. Discovery of a novel fibroblast activation protein (FAP) inhibitor, BR103354, with anti-diabetic and anti-steatotic effects. *Sci Rep*. (2020) 10(1):21280. doi: 10.1038/s41598-020-77978-z

114. Sanyal A, Charles ED, Neuschwander-Tetri BA, Loomba R, Harrison SA, Abdelmalek MF, et al. Pegbelfermin (BMS-986036), a PEGylated fibroblast growth factor 21 analogue, in patients with non-alcoholic steatohepatitis: a randomised, double-blind, placebo-controlled, phase 2a trial. *Lancet*. (2018) 392(10165):2705–17. doi: 10.1016/S0140-6736(18)31785-9

115. Li J, Li Y, Liu Y, Yu H, Xu N, Huang D, et al. Fibroblast growth factor 21 ameliorates NaV1.5 and Kir2.1 channel dysregulation in human AC16 cardiomyocytes. *Front Pharmacol*. (2021b) 12:715466. doi: 10.3389/fphar.2021.715466

116. Tanajak P, Sa-nguanmoo P, Wang X, Liang G, Li X, Jiang C, et al. Fibroblast growth factor 21 (FGF21) therapy attenuates left ventricular dysfunction and metabolic disturbance by improving FGF21 sensitivity, cardiac mitochondrial redox homoeostasis and structural changes in Pre-diabetic rats. *Acta Physiol*. (2016) 217 (4):287–99. doi: 10.1111/apha.12698

117. Romanello V. FGF21: a promising therapeutic agent for alcoholic cardiomyopathy? *J Pathol*. (2021) 254(3):213–15. doi: 10.1002/path.5654

frontiers | Frontiers in Cardiovascular Medicine

TYPE Mini Review
PUBLISHED 14 July 2023
DOI 10.3389/fcvm.2023.1210762

OPEN ACCESS

EDITED BY
Daniel M. Johnson,
The Open University, United Kingdom

REVIEWED BY
Miron Sopic,
University of Belgrade, Serbia

*CORRESPONDENCE
Jijun Ding
✉ 732388316@qq.com

RECEIVED 28 April 2023
ACCEPTED 27 June 2023
PUBLISHED 14 July 2023

CITATION
Xue Z, Zhu J, Liu J, Wang L and Ding J (2023) Research progress of non-coding RNA in atrial fibrillation.
Front. Cardiovasc. Med. 10:1210762.
doi: 10.3389/fcvm.2023.1210762

Research progress of non-coding RNA in atrial fibrillation

Zongqian Xue, Jinbiao Zhu, Juan Liu, Lingli Wang and Jijun Ding*

Department of Cardiology, Aoyang Hospital Affiliated to Jiangsu University, Zhangjiagang, China

Atrial fibrillation (AF) is a common arrhythmia in clinic, and its incidence is increasing year by year. In today's increasingly prevalent society, ageing poses a huge challenge to global healthcare systems. AF not only affects patients' quality of life, but also causes thrombosis, heart failure and other complications in severe cases. Although there are some measures for the diagnosis and treatment of AF, specific serum markers and targeted therapy are still lacking. In recent years, ncRNAs have become a hot topic in cardiovascular disease research. These ncRNAs are not only involved in the occurrence and development of AF, but also in pathophysiological processes such as myocardial infarction and atherosclerosis, and are potential biomarkers of cardiovascular diseases. We believe that the understanding of the pathophysiological mechanism of AF and the study of diagnosis and treatment targets can form a more systematic diagnosis and treatment framework of AF and provide convenience for individuals with AF and the society.

KEYWORDS

atrial fibrillation, ncRNAs, biomarker, diagnosis, exosome

1. Introduction

Atrial fibrillation (AF) is a common arrhythmias in clinic, with a high risk of death, stroke, and peripheral embolism, and its incidence has been increasing year by year. Risk factors for AF are closely related to cardiovascular disease, with organic or functional heart problems being more common. In addition, age, gender and genetic factors are also important factors leading to the occurrence of AF (1, 2). AF not only affects life quality of the patients, but also has complications such as thrombosis and heart failure in severe cases. Atrial remodeling is considered to be the basis of the occurrence and development of AF, including structural remodeling, electrical remodeling, neural remodeling, etc (3–5). The diagnosis of AF mainly depends on electrocardiogram findings, which are often found after complications occur, and there is a certain lag (6). Therefore, biomarkers have potential value in the early diagnosis of AF. Currently, drug therapy for AF patients has poor efficacy and side effects. Radiofrequency ablation is more effective than drug therapy, but the patients are yet able to avoid the operational risks, postoperative recurrence, and high healthcare cost (7–9). Actively searching for new diagnosis and treatment strategies and exploring the molecular mechanism of AF have great clinical significance and translational prospects.

In recent years, non-coding RNA (ncRNA) has become a research hotspot in cardiovascular diseases. ncRNA mainly includes miRNA, LncRNA and CircRNA. These ncRNAs can not only participate in the occurrence and development of AF, but also play a part in the pathophysiological processes such as myocardial infarction and atherosclerosis, which are potential biomarkers for cardiovascular diseases (10). This article reviews the pathophysiological mechanism of AF, introduces the mechanism and potential value of ncRNAs in AF, and provides a theoretical basis for the diagnosis, treatment and prognosis monitoring of AF (**Figure 1**, **Tables 1**, **2**).

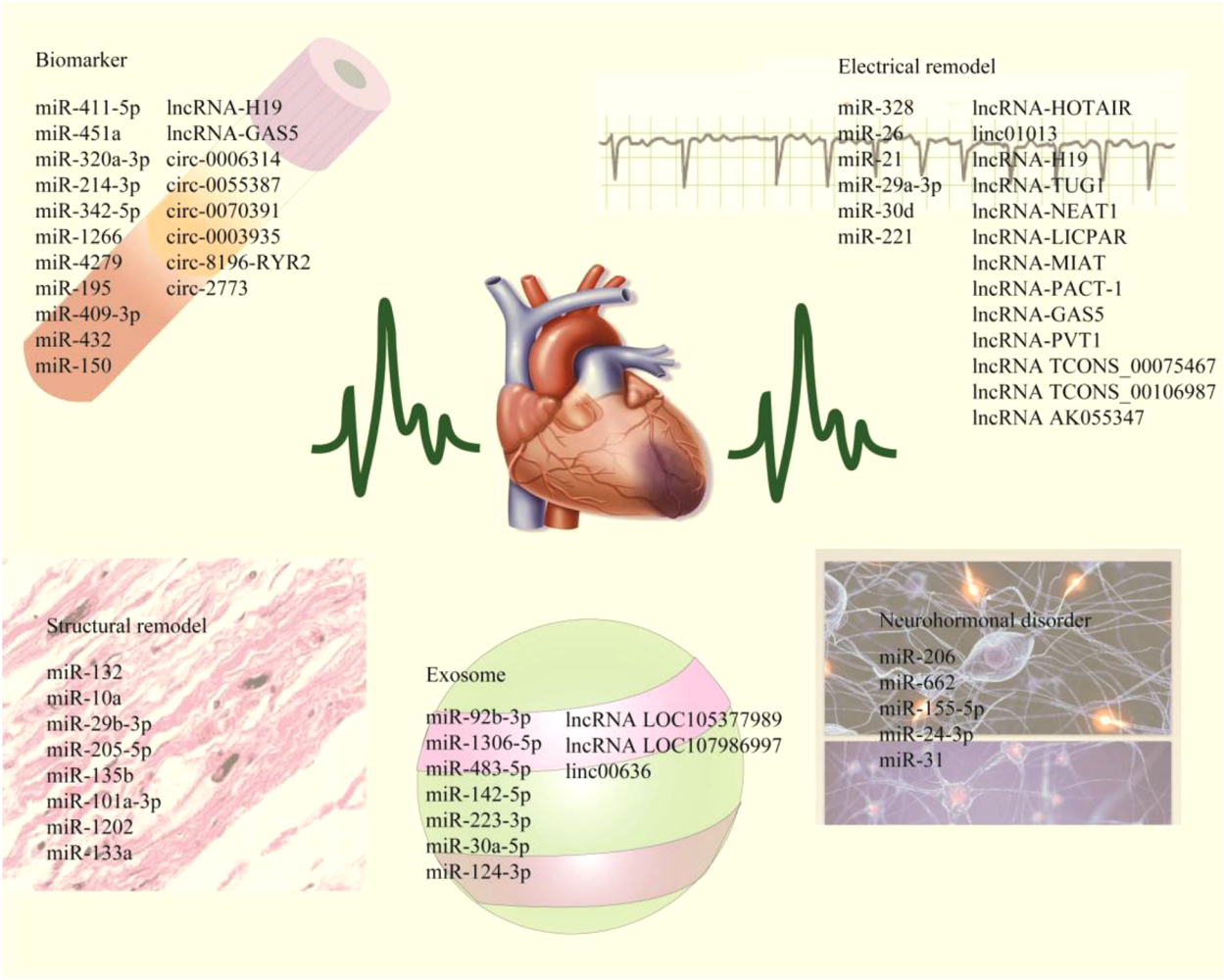

FIGURE 1
The schematic highlights ncRNAs associated with myocardial electrical remodeling, fibrosis, neurohormone disorders, and exosomes, while including plasma markers associated with AF diagnosis and prognotic monitoring.

2. Pathophysiology of AF

AF can be classified as paroxysmal, persistent and permanent according to the duration of the attack. The pathogenesis of AF involves a variety of factors, mainly including electrical remodeling, structural remodeling, and neurohormonal disorders. These mechanisms lead to the development and maintenance of AF (83, 84). Although the pathogenesis of AF is complex, it is mainly related to electrical remodeling and structural remodeling. Existing studies suggest that ncRNAs play an important role in its occurrence and development (**Table 1**) (85–87).

3. miRNAs involved in the diagnosis and prognostic monitoring of AF

The early symptoms of AF are not obvious, the main clinical manifestations are palpitation, dyspnea and dizziness, which are easy to be ignored by patients, and routine electrocardiogram is difficult to monitor, so the diagnosis is often missed (88, 89). At present, BNP and troponin are the main clinical biomarkers for the diagnosis of cardiovascular diseases, but they are mainly used for the diagnosis of heart failure and myocardial infarction, and have no significant significance for the diagnosis of AF. In recent years, the research on ncRNA has become increasingly in-depth. The differential expression of ncRNAs in cardiac tissue and blood of patients with AF may become auxiliary diagnostic biomarkers for AF (**Table 2**) (90, 91).

Risk stratification of subsequent cardiovascular events in patients with AF helps guide prevention strategies. Nossent AY et al. analyzed differentially expressed miRNAs in 26 patients using sequencing technology, and screened out one miR-411-5p in combination with clinical prognosis as a potential valuable prognostic biomarker for patients with AF (69). Recurrent AF after catheter ablation seriously affected the prognosis of patients. Therefore, Garcia-Seara J et al. recruited 42 patients with AF for catheter ablation. The analysis measured the expression of 84

TABLE 1 ncRNAs involved in the pathophysiology of AF.

ncRNAs	Expression	Remodeling	Targets	Ref.
miR-205-5p	Downregulation	Structural remodeling	EHMT2/ IGFBP3	(11)
miR-181b	Upregulation	Structural remodeling	Sema3A	(12)
miR-423	Downregulation	Electrical remodeling	Calcium handling protein	(13)
miR-29b	Downregulation	Structural remodeling	TGFβR1	(14)
miR-34a	Upregulation	Electrical remodeling	TASK1	(15)
miR-21	Upregulation	Structural remodeling	IL-18 FGFR1	(16)
miR-662	Upregulation	Electrical remodeling Neurohormonal disorders	CREB1	(17)
miR-425-5p	Upregulation	Structural remodeling	CREB1	(18)
miR-135b	Downregulation	Structural remodeling	TGFβR1	(19)
miR-146b-5p	Upregulation	Structural remodeling	TIMP4	(20)
miR-199a-5p	Upregulation	Electrical remodeling	NCX	(21)
miR-22-5p	Upregulation	Electrical remodeling	NCX	(21)
miR-101a-3p	Downregulation	Structural remodeling	EZH2	(22)
miR-1202	Upregulation	Structural remodeling	nNOS TGFβ1	(23)
miR-133a	Downregulation	Structural remodeling	CTGF	(24)
miR-205	Upregulation	Structural remodeling	P4HA3	(11, 25)
miR-4443	Upregulation	Structural remodeling	THBS1	(26)
miR-155	Upregulation	Electrical remodeling	CACNA1C	(27)
miR-29b-3p	Downregulation	Structural remodeling	PDGFB	(28, 29)
miR-324-3p	Downregulation	Structural remodeling	TGFβ1	(30)
miR-210	Upregulation	Structural remodeling	Foxp3	(31)
miR-27b-3p	Downregulation	Structural remodeling	CX43	(32)
miR-23	Upregulation	Structural remodeling	TGFβ1	(33)
miR-133	Downregulation	Structural remodeling	ZFHX3	(34)
miR-10a	Upregulation	Structural remodeling	TGFβ1 Smads	(35)
miR-155-5p	Upregulation	Neurohormonal disorders	eNOS	(36)
miR-24-3p	Upregulation	Neurohormonal disorders	eNOS	(36)
miR-138-5p	Downregulation	Structural remodeling	CYP11B2	(37)
miR-27b	Downregulation	Structural remodeling	ALK5	(32, 38)
miR-30c	Downregulation	Structural remodeling	TGFβRII	(39)
miR-208b	Upregulation	Electrical remodeling	CACNA1C CACNB2 SERCA2	(40)
miR-29a	Upregulation	Electrical remodeling	CACNA1C	(41)
miR-31	Upregulation	Neurohormonal disorders	nNOS	(42)
miR-30d	Upregulation	Electrical remodeling	IK.ACh	(43)
miR-30a	Upregulation	Structural remodeling	Snail 1	(44)
miR-206	Upregulation	Neurohormonal disorders	SOD1	(45)
miR-146b-5p	Upregulation	Structural remodeling	TIMP4	(20)
miR-132	Downregulation	Structural remodeling	CTGF	(46)
miR-106b-25	Downregulation	Electrical remodeling	RyR2	(47)
miR-21	Upregulation	Electrical remodeling	CACNA1C CACNB2	(16, 48)
miR-26	Downregulation	Electrical remodeling	KCNJ2	(49)
miR-221	Upregulation	Electrical remodeling	KCNJ5	(50)
miR-499	Upregulation	Electrical remodeling	SK3	(51, 52)
miR-328	Upregulation	Electrical remodeling	CACNA1C CACNB2	(51)
HOTAIR	Upregulation	Structural remodeling	PTBP1 Wnt5a	(9)
H19	Upregulation	Structural remodeling	VEGFA TGFβ	(53)
NEAT1	Upregulation	Structural remodeling	NPAS2	(54)
LICPAR	Upregulation	Structural remodeling	Smad2/3	(55)
LINC01013	Upregulation	Structural remodeling	TGF-β1	(56)
TUG1	Upregulation	Structural remodeling	miR-29b-3p	(57)
PCAT-1	Upregulation	Structural remodeling	TGF-β1	(58)
TCONS00106987	Upregulation	Electrical remodeling	KCNJ2	(59)
GAS5	Upregulation	Structural remodeling	ALK5	(60)
MIAT	Upregulation	Structural remodeling	TGFβ1	(61)
PVT1	Upregulation	Structural remodeling	TGFβ1	(62)
KCNQ1OT1	Upregulation	Electrical remodeling	CACNA1C	(63)
AK055347	Upregulation	Neurohormonal disorders	MSS51	(64)
CAMTA1	Upregulation	Structural remodeling	TGFBR1	(65)
circ_0004104	Upregulation	Structural remodeling	TGFβ	(66)
circ_0000672	Upregulation	Structural remodeling	TRAF6	(67)
circ_0005019	Upregulation	Electrical remodeling	Kcnn3	(68)

(*Continued*)

TABLE 1 Continued

TABLE 2 Potential biomarker of ncRNAs for AF.

ncRNAs	Expression	Biological fluid	Function	Ref
miR-411-5p	Upregulation	Blood	Auxiliary diagnostic	(69)
miR-451a	Downregulation	Blood	Prognostic monitor	(70)
miR-320a-3p	Upregulation	Plasma	Prognostic monitor	(28)
miR-214-3p	Upregulation	Serum	Auxiliary diagnostic	(71)
miR-342-5p	Upregulation	Serum	Auxiliary diagnostic	(71)
miR-1266	Upregulation	Bloo	Auxiliary diagnostic	(72)
miR-4279	Upregulation	Blood	Auxiliary diagnostic	(72)
miR-4666a-3p	Upregulation	Blood	Auxiliary diagnostic	(72)
miR-208a	Downregulation	Serum	Auxiliary diagnostic	(73)
miR-483-5p	Upregulation	Serum	Prognostic monitor	(73)
miR-199a	Downregulation	Blood	Prognostic monitor	(74)
miR-409-3p	Downregulation	Plasma	Prognostic monitor	(75)
miR-432	Downregulation	Plasma	Prognostic monitor	(75)
miRNA-150	Downregulation	Plasma	Auxiliary diagnostic	(76)
lncRNA H19	Upregulation	Plasma	Prognostic monitor	(77)
LncRNA GAS5	Downregulation	Plasma	Auxiliary diagnostic Prognostic monitor	(78)
has_circ_0006314	Upregulation	Blood	Prognostic monitor	(79)
hsa_circ_0055387	Upregulation	Blood	Prognostic monitor	(79)
hsa_circ_0070391	Upregulation	Plasma	Auxiliary diagnostic	(80)
hsa_circ_0003935	Downregulation	Plasma	Auxiliary diagnostic	(80)
circ 8196-RYR2	Upregulation	Blood	Prognostic monitor	(81)
circRNA_2773	Upregulation	PBMC	Auxiliary diagnostic	(82)

miRNAs in both non-relapsed and relapsed groups, the results showed that miRNA-451a was down-regulated in relapsed patients, and the recurrence of AF was positively correlated with an increased percentage of scars. It is suggested that low expression of miR-451a may play an important role in the recurrence of AF by controlling fibrosis and progression (70). Akselrod AS et al. found that plasma miR-320a-3p level in patients with AF was higher than that in healthy controls, and the expression level was positively correlated with CHADS-VASc score (28). Sasano T et al. identified 11 candidate miRNAs using high-throughput sequencing and clinical sample validation, and found that miR-214-3p and miR-342-5p had high accuracy in the diagnosis of patients with AF combined with clinicpathological parameter analysis (71). Yang et al. observed genome-wide differential expression profiles of miRNAs in 180 peripheral blood samples and found 14 miRNAs with significant differential expression, among which miR-1266, miR-4279 and miR-4666a-3p were significantly increased in expression, which are potential targets for future diagnosis and treatment of AF (72). About one-third of patients undergoing coronary artery bypass grafting will develop postoperative AF, which seriously affects the prognosis of patients. In order to monitor the occurrence of postoperative AF, Athanasiou et al. prospectively recruited 34 patients after surgery, and compared the myocardial tissue with normal sinus rhythm after surgery, and found 16 differentially expressed miRNAs. The expression of miR-208a was significantly decreased, and the expression of miR-483-5p was significantly increased. It is suggested that these differentially expressed miRNAs can be used to predict the recurrence of AF after coronary artery bypass grafting (73). Kilic et al. recruited 63 patients after coronary artery bypass grafting and monitored their heart rate until discharge. Among them, 20 patients developed postoperative AF, and PCR detected the expression of miR-199a and miR-195. The results showed that the expression of miR-199a significantly decreased in the postoperative AF group, demonstrate its effectiveness as a biomarker for cardiac surgery management (74). By Solexa sequencing 100 patients with AF who underwent catheter ablation and 100 healthy individuals, Wu et al. found that miR-409-3p and miR-432 were significantly reduced in the plasma of patients with AF and are potential markers of AF (75). Xia et al. showed for the first time that plasma miRNA-150 levels in patients with atrial fibrillation are significantly lower than those in healthy individuals, which is a potential biomarker to aid in the diagnosis of atrial fibrillation (76). These studies indicate that miRNAs differentially expressed in plasma of patients with AF and postoperative patients can play an important indicator role in the diagnosis and prognosis monitoring of AF.

4. miRNAs involved in the regulation of electrical remodeling

Electrical remodeling of atrial muscle is closely related to the occurrence of AF. Electrical remodeling refers to recurrent episodes of AF or continuous atrial stimulation, which leads to progressive shortening of the effective refractory period of the atrium, and the decrease, reversal or disappearance of the physiological frequency adaptation of the atrial refractory period, making AF more likely to be induced and sustained (87, 92). AF is caused by abnormal electrical activity of atrial myocardium. During the occurrence of AF, many ion channels also have significant changes, mainly including: L-type Ca^{2+} channel, transient outward K^+ channel, strong inward rectification K^+ channel (IK1), acetylcholine-activated K^+ channel (IK, ACh), and ultra-fast delayed rectification K^+ channel (IKur) (93, 94).

Yang et al. found that the expression of miR-328 was increased in the atrial tissue of AF mouse models, and the high expression of miR-328 could reduce the L-type Ca^{2+} current and shorten the duration of atrial action potential. Mechanism studies have confirmed that CACNA1C and CACNB1 are the target genes of miR-328, and miR-328 can interact with L-type Ca^{2+} channel protein subunits to participate in atrial electroremodeling in AF (51). Nattel et al. found that the expression of miR-26 was down-regulated in the atrial tissues of AF patients, and low-expressed miR-26 was a potential regulatory gene for the electrophysiological effects of Ca^{2+} dependent nuclear factor of activated T cells (NFAT) signaling pathway, and an important participant in the persistence of AF (49). Ricardo et al. found that the high expression of miR-21 in cardiomyocytes of patients with AF was negatively correlated with the expression of CACNA1C and the density of I (Ca, L), suggesting that miR-21 may be involved in the downregulation of L-type Ca^{2+} I (Ca, L) induced by chronic AF, and is the key to the persistence of AF (95). Similarly, Qiu et al. found that CACNA1C is a direct target gene of miR-29a-3p, and miR-29a-3p negatively regulates

CACNA1C. miR-29a-3p may be a potential target for AF treatment (41). Lee et al. found that miR-499 was significantly upregulated in AF, resulting in downregulation of small conductance calcium-activated potassium channel 3 (SK3), which may contribute to electrical remodeling of AF and is a novel site associated with the onset of AF (52). Katsushige et al. used high-throughput sequencing analysis to find that miR-30d was significantly up-regulated in myocardial cells of AF patients, and functional enrichment analysis found that miR-30d was a candidate gene for ion channel remodeling. Interference with miR-30d down-regulated the expression of kcnj3/Kir3.1, accompanied by a decrease in the acetylcholine-sensitive internal rectification K^+ current (IK.ACh) (43). Barbara et al. found that miR-221 reduced the abundance and function of L-type Ca^{2+} channels and Kcnj5 channels. MiR-221 can regulate L-type Ca^{2+} channels and Kcnj5 channels, thus potentially contributing to the generation and propagation of cardiac excitation (50).

5. miRNAs involved in the regulation of structural remodeling

Electrical remodeling is the pathological change in the initial stage of AF, while structural remodeling is the material basis for the long-term maintenance of AF, and it is also the most obvious change of atrium (96, 97). Atrial dilatation and fibrosis are the main features of structural remodeling in AF. Atrial fibrosis may lead to slowing of conduction velocity, conduction block to promote reentry and increase susceptibility to AF (98).

Studies have shown that connective tissue growth factor (CTGF) plays an important role in the process of fibrosis. Zhang et al. found that the expression of miR-132 decreased in AF cardiomyocytes. Luciferase assay confirmed that miR-132 could bind to the 3 ‘-untranslated region of CTGF, thereby inhibiting the expression of CTGF and regulating the fibrosis of cardiac fibroblasts (46). Yang et al. found that overexpression of miR-10a significantly prolonged the duration of AF and decreased Smad7 protein expression. TGF-β1 reversed the inhibitory effect of miR-10a on Smad7, alleviated atrial remodeling, and ultimately inhibited cardiac fibrosis (35). Similarly, Xu et al. found that miR-29b-3p could reduce the degree of atrial fibrosis, and high expression of miR-29b-3p could reduce the expression of fibrosis markers collagen- I and a-SMA, and increase the protein expression of Cx43, thus reversing atrial remodeling (29). Studies have shown that the expression of miR-205-5p is decreased in atrial tissues of patients with AF, and overexpression of miR-205-5p can reduce the expression of TGF-β1, α-SMA, Col III and other fibrosis-related proteins. Mechanism studies have shown that miR-205-5p regulates H3 histone methylation by targeting EHMT2, promotes IGFBP3 expression, and further affects atrial myocyte fibrosis (11). The study found that the expression of miR-29b was low in the atrial tissue of AF rats, overexpression miR-29b can reduce atrial fibrosis, reduce the expression of COL1A1, COL3A1 and TGFβ1, and shorten the duration of AF in rats (14). In addition, the expression of miR-135b was down-regulated in AF tissues, while the expression of miR-135b target genes TGFBR1 and TGFBR2 was up-regulated in myocardial fibroblasts. Quercetin can promote miR-135b expression, inhibit TGF-β/Smads pathway, reduce atrial tissue fibrosis and collagen deposition, and thus relieve AF (19). Xu et al. found that miR-101a-3p may prevent AF in rats by targeting EZH2 to inhibit collagen synthesis and atrial fibrosis, which provides a potential target for the prevention of AF (22). miR-1202 was found to negatively regulate atrial fibrosis by targeting nNOS by reducing cell differentiation, collagen deposition, and TGF-β1/Smad2/3 pathway activity (23). Overexpression of miR-133a can inhibit the proliferation and migration of atrial cells, reduce the expression of fibrosis markers and CTGF protein, and improve myocardial fibrosis (24).

6. miRNAs involved in the regulation of neurohormonal disorders

Autonomic dysfunction is a type of dysfunction that occurs when the balance between sympathetic and parasympathetic nerves is disrupted. cardiac autonomic nerve remodeling (ANR) refers to the changes in the distribution density and spatial arrangement of the autonomic nerve caused by some diseases of the heart (99–102).

Studies have shown that the contents of tetrahydrobioterin (BH4) and NO are related to nerve regeneration. GCH1 is the rate-limiting enzyme of BH4 synthesis. Hou et al. found that the expression of miR-206 was increased in atrial fibrillation myocarde. High expression of miR-206 could inhibit GCH1, thus affecting the content of BH4 and NO in myocarde (103). In a similar study, miR-206 expression was increased in the the left superior ganglionated plexus (SLGPs). High expression of miR-206 inhibited the expression of superoxide dismutase 1 (SOD1) and increased the levels of reactive oxygen species (ROS) *in vitro* and *in vivo*, further exacerbating ANR (45). miR-662 can also regulate the expression of neuropeptides and participate in the occurrence and development of AF after myocardial infarction (17). It was found that the levels of miR-155-5p and miR-24-3p were significantly decreased and the levels of eNOS and NO were increased in patients with AF after ablation compared with those who did not receive ablation therapy (36). Casadei B et al. found that atrial specific upregulation of miR-31 in AF resulted in inhibition of muscular dystrophin (DYS) translation and accelerated degradation of nNOS mRNA, leading to significant reductions in atrial DYS and nNOS protein content and nitric oxide availability. Inhibition of miR-31 restores DYS and nNOS in human AF and normalizes APD and rate dependence of APD (42).

7. ncRNAs and AF-beyond miRNAs

With the increase of studies on ncRNAs in AF, lncRNAs and circRNAs play an increasingly significant role in AF. Therefore, in addition to miRNAs, this manuscript also discussed the current research content of other ncRNAs in AF.

CHA 2 ds2-VASc score was originally used to stratify stroke risk in patients with AF, in order to study whether lncRNAs could improve the predictive ability of CHA 2 ds2-VASc score for stroke. Li et al. added the ability of lncRNA expression level to predict stroke in CHA 2 ds2-VASc scoring model. The results showed that lncRNA H19 plasma expression level was correlated with the risk of stroke in patients with AF, which could significantly improve the ability to predict the risk of stroke in patients with AF, and was a potential prognostic monitoring marker (77). LncRNA GAS5 is significantly down-regulated in the plasma of patients with AF, which is a potential biomarker for the diagnosis and prognosis monitoring of AF (78). Similar studies have found that has_circ_0006314 and hsa_circ_0055387 also have potential predictive value for postoperative AF (79). Fan et al. used GEO database to screen out two different circRNAs. The expression of hsa_circ_0070391 in plasma was up-regulated and hsa_circ_0003935 down-regulated. The area under ROC curve indicated that both of them had high diagnostic efficiency (80). Wang et al. examined plasma circ 8196-RYR2 levels in 136 patients following ablation of AF, suggesting that circ 8196-RYR2 could be used as a new predictor of late recurrence after surgical ablation (81). Another study also show that low expression of circRNA_2773 is a potential diagnostic marker for AF (82).

AF is often accompanied by excessive proliferation of cardiac fibroblasts (CFs). It was found that the expression of HOTAIR was increased in the myocardium of patients with AF, and Ang II significantly increased the activity of atrial fibroblasts. HOTAIR knockdown can significantly inhibit AF cardiac tissue fibrosis by regulating Wnt signaling pathway (9). Knocking down LINC01013 reduced baseline expression of fibrosis markers and their response to TGF-β1. TGF-β1 stimulated atrial fibroblasts to induce the expression of LINC01013, and its knockdown reduced the activation of fibroblasts (56). Plasma H19 levels were significantly higher in patients with AF compared with healthy volunteers. Upregulation of H19 expression contributes to the proliferation and synthesis of extracellular matrix (ECM) related proteins, thereby promoting myocardial fibrosis (53). It was found that the serum TUG1 level was elevated and the expression of miR-29b-3p was low in patients with AF. Pearson correlation analysis showed that TUG1 was negatively correlated with miR-29b-3p expression in AF patients. TUG1 knockdown inhibits vascular endothelium-induced cardiomyocyte proliferation (57). NEAT1 expression was up-regulated in atrial tissues of patients with AF, and was positively correlated with the expression of type I collagen (coll I) and type III collagen (coll III). In addition, the loss of NEAT1 attenuates angiotensin II (Ang II), leading to atrial fibroblast proliferation, migration, and collagen production. These findings suggest that NEAT1 plays an important role in atrial fibrosis and is a new potential molecular target for the treatment of AF (54). In AF patients, LICPAR and TGF-β1 expression were up-regulated and positively correlated. Further analysis showed that Ang II increased LIPCAR, Smad2/3 phosphorylation, and α-smooth muscle actin (α-SMA) levels. Up-regulation of LIPCAR could further promote the promoting effects of Ang II on the phosphorylation levels of LIPCAR, Collagen I, Collagen II, α-SMA and Smad2/3, cell viability and proliferation of atrial fibroblasts. These studies suggest that lncRNA LICPAR regulates atrial fibrosis primarily by regulating the TGF-β/Smad pathway (55). Studies found that down-regulation of lncRNA MIAT could significantly relieve AF, increase atrial effective refractory period (AERP), inhibit the expression of fibrosis-related genes coll I, coll III, CTGF, TGF-β1, and effectively reduce AF induced atrial fibrosis (61). PCAT-1 expression was increased in AF patients. PCAT-1 knockdown inhibited the proliferation of AC16 cells. Mechanism studies showed that TGF-β1 was the target of PCAT-1, and its expression in AF tissues was positively correlated with that of PCAT-1. PCAT-1 can promote the proliferation of AF cells by promoting TGF-β1 (58). The expression of GAS5 in myocardium of AF patients was significantly decreased. Overexpression of GAS5 can inhibit the growth of AC16 cells. In addition, further experiments showed that ALK5 was the target of GAS5, and its expression in AF tissue was negatively correlated with that of GAS5. lncRNA GAS5 may inhibit AF cell fibrosis by inhibiting ALK5 (60). The expression of PVT1 in AF patients was increased and positive for coll I and coll III. Overexpression of PVT1 promoted Ang-II-induced atrial fibroblast proliferation, collagen generation, and TGF-β1/Smad signaling activation, while PVT1 knockdown did the opposite. Mechanically, PVT1 acts as a sponge for miR-128-3p and promotes Sp1 expression, thereby activating the TGF-β1/Smad signaling pathway (62).

Hou et al. found that lncRNA TCONS_00075467 may also participate in atrial myocardial electrical remodeling. Interference with TCONS_00075467 can shorten the effective refractory period of the atria *in vivo* and reduce the duration of L-type calcium current and action potential *in vitro* (104). Similarly, lncRNA TCONS-00106987 is up-regulated in atrial tissue of patients with AF. Mechanism studies have shown that TCONS_00106987 induces the transcription of its target gene KCNJ2 through miR-26, and increases the inward rectification K^+ current (IK1). Thus facilitating electrical reconfiguration (59). Studies have shown that interference with lncRNA AK055347 can inhibit the activity of cardiomyocytes, accompanied by the downregulation of Cyp450 and ATP synthase. Mechanism studies have confirmed that AK055347 may regulate the mitochondrial energy production by regulating Cyp450, ATP synthase and MSS51, thus participating in the pathogenesis of AF (64).

8. Exosome-associated ncRNAs involved in the regulation of AF

In recent years, it has been found that exosome-derived ncRNAs have different expression profiles in various diseases and are a potential non-invasive diagnostic biomarker, which has been widely studied in the medical field. Similarly, exosomes can also be detected in body fluids of patients with atrial fibrillation, and the non-coding RNA carried by them is of great significance for auxiliary diagnosis and prognostic monitoring of AF (105, 106).

Wei et al. demonstrated differences in the expression of miRNAs in plasma exosomes in patients with AF. Among them,

miR-92b-3p, miR-1306-5p and miR-let-7b-3p had significant differences, and gene enrichment analysis showed that these miRNAs and target genes were mainly involved in the occurrence of AF through affecting biological processes such as energy metabolism, lipid metabolism, inflammation and enzyme activity (107). Similar studies have found that miR-483-5p, miR-142-5p and miR-223-3p are also involved in the occurrence and development of AF (108). Joung et al. found that exosomes in the peripheral blood of patients with atrial fibrillation can reduce cardiomyocyte viability, lead to abnormal Ca^{2+} channel and induce reactive oxygen species (ROS) production. High-throughput sequencing found that miR-30a-5p expression was decreased in peripheral blood exosomes of patients with AF, and exosomes with high expression of miR-30a-5p could attenuate pacemaker induced Ca^{2+} channel abnormalities (109). Hou et al. screened the differential miRNAs of peripheral blood and exosomes in 40 patients with AF, and found that miR-124-3p was significantly up-regulated, and the high expression of miR-124-3p could improve the viability and proliferation ability of myocardial fibroblasts. Mechanism studies have shown that miR-124-3p can promote the activation and proliferation of fibroblasts through AXIN1 by regulating the WNT/β-catenin signaling pathway (110). Similarly, Exosomal lncRNAs are also potential biomarkers for AF. Joung et al. identified 26 differentially expressed lncrnas in serum exosomes from patients with persistent AF. lncRNAs LOC105377989 and LOC107986997 continued to increase, has significant diagnostic effectiveness for AF, and is a potential biomarker for the diagnosis of AF (106). Lei et al. using GEO database, LINC00636 was found to be an antifibrotic molecule with decreased expression in peripheral blood exosomes of patients with AF. Mechanism studies have shown that LINC00636 can promote the expression of miR-450a-2-3p, thereby inhibiting the expression of MAPK1, and thereby improve cardiac fibrosis in patients with AF (111).

9. Conclusions

In recent years, with the deepening of research, ncRNAs play an important role in the occurrence and development of AF. Differential expression of ncRNAs in peripheral blood of patients with AF provides a new theoretical basis for auxiliary diagnosis of AF. At the same time, ncRNAs are involved in myocardial cell remodeling and ion channel remodeling, providing a new scheme for the treatment of AF.

This manuscript reviews the research progress of ncRNAs in the occurrence, treatment and potential biomarkers of AF. According to the existing studies, we can find that ncRNAs are closely related to AF and involved in the occurrence and progression of AF, which is worthy of further study and has great clinical significance.

Author contributions

ZX and JZ drafted the manuscript; JL and LW reviewed and edited the manuscript. JD provided ideas. All authors contributed to the article and approved the submitted version.

Funding

This work was supported by the Science and Technology Project of Zhangjiagang City (ZKS2043), Zhangjiagang City Health Youth Science and Technology Project (ZJGQNKJ202113) and Suzhou Science and Technology Development Plan (SKJYD2021006).

Conflict of interest

The authors declare that the research was conducted in the absence of any commercial or financial relationships that could be construed as a potential conflict of interest.

Publisher's note

References

1. Lau DH, Nattel S, Kalman JM, Sanders P. Modifiable risk factors and atrial fibrillation. *Circulation*. (2017) 136:583–96. doi: 10.1161/CIRCULATIONAHA.116.023163

2. Staerk L, Sherer JA, Ko D, Benjamin EJ, Helm RH. Atrial fibrillation: epidemiology, pathophysiology, and clinical outcomes. *Circ Res*. (2017) 120:1501–17. doi: 10.1161/CIRCRESAHA.117.309732

3. Abed HS, Wittert GA, Leong DP, Shirazi MG, Bahrami B, Middeldorp ME, et al. Effect of weight reduction and cardiometabolic risk factor management on symptom burden and severity in patients with atrial fibrillation: a randomized clinical trial. *Jama*. (2013) 310:2050–60. doi: 10.1001/jama.2013.280521

4. Lau DH, Linz D, Sanders P. New findings in atrial fibrillation mechanisms. *Card Electrophysiol Clin*. (2019) 11:563–71. doi: 10.1016/j.ccep.2019.08.007

5. Voskoboinik A, Kalman JM, De Silva A, Nicholls T, Costello B, Nanayakkara S, et al. Alcohol abstinence in drinkers with atrial fibrillation. *N Engl J Med*. (2020) 382:20–8. doi: 10.1001/jama.2013.280521

6. Antman EM, Leopold JA, Sauer WH, Zei PC. Atrial fibrillation—what is it and how is it treated? *N Engl J Med*. (2022) 387:e38. doi: 10.1056/NEJMp2212939

7. Dawson K, Wakili R, Ordög B, Clauss S, Chen Y, Iwasaki Y, et al. MicroRNA29: a mechanistic contributor and potential biomarker in atrial fibrillation. *Circulation*. (2013) 127:1466–75. 1475e1461–1428. doi: 10.1161/CIRCULATIONAHA.112.001207

8. Hijazi Z, Oldgren J, Lindbäck J, Alexander JH, Connolly SJ, Eikelboom JW, et al. The novel biomarker-based ABC (age, biomarkers, clinical history)-bleeding risk score for patients with atrial fibrillation: a derivation and validation study. *Lancet*. (2016) 387:2302–11. doi: 10.1016/S0140-6736(16)00741-8

9. Tan W, Wang K, Yang X, Wang K, Wang N, Jiang TB. LncRNA HOTAIR promotes myocardial fibrosis in atrial fibrillation through binding with PTBP1 to increase the stability of Wnt5a. *Int J Cardiol.* (2022) 369:21–8. doi: 10.1016/j.ijcard.2022.06.073

10. Halushka PV, Goodwin AJ, Halushka MK. Opportunities for microRNAs in the crowded field of cardiovascular biomarkers. *Annu Rev Pathol.* (2019) 14:211–38. doi: 10.1146/annurev-pathmechdis-012418-012827

11. Xiao Z, Xie Y, Huang F, Yang J, Liu X, Lin X, et al. MicroRNA-205-5p plays a suppressive role in the high-fat diet-induced atrial fibrosis through regulation of the EHMT2/IGFBP3 axis. *Genes Nutr.* (2022) 17:11. doi: 10.1186/s12263-022-00712-z

12. Lai YJ, Tsai FC, Chang GJ, Chang SH, Huang CC, Chen WJ, et al. miR-181b targets semaphorin 3A to mediate TGF-β-induced endothelial-mesenchymal transition related to atrial fibrillation. *J Clin Invest.* (2021) 23(1):6. doi: 10.3390/ijms23010006

13. Park H, Park H, Park J. Circulating microRNA-423 attenuates the phosphorylation of calcium handling proteins in atrial fibrillation. *Mol Med Rep.* (2015) 66(1):1–11.

14. Han X, Wang S, Yong Z, Zhang X, Wang X. miR-29b ameliorates atrial fibrosis in rats with atrial fibrillation by targeting TGFβRI and inhibiting the activation of smad-2/3 pathway. *J Bioenerg Biomembr.* (2022) 54:81–91. doi: 10.1007/s10863-022-09934-7

15. Wiedmann F, Kraft M, Kallenberger S, Büscher A, Paasche A. MicroRNAs regulate TASK-1 and are linked to myocardial dilatation in atrial fibrillation. *J Am Heart Assoc.* (2022) 11:e023472. doi: 10.1161/JAHA.121.023472

16. Pradhan K, Niehues P, Neupane B, Maleck C, Sharif-Yakan A, Emrani M, et al. MicroRNA-21 mediated cross-talk between cardiomyocytes and fibroblasts in patients with atrial fibrillation. *Front Cardiovasc Med.* (2023) 10:1056134. doi: 10.3389/fcvm.2023.1056134

17. Zhang P, Liu B. Integrative bioinformatics analysis reveals that infarct-mediated overexpression of potential miR-662/CREB1 pathway-induced neuropeptide VIP is associated with the risk of atrial fibrillation: a correlation analysis between myocardial electrophysiology and neuroendocrine. *Dis Markers.* (2022) 132(13): e142548. doi: 10.1155/2021/8116633

18. Wei F, Ren W, Zhang X, Wu P, Fan J. miR-425-5p is negatively associated with atrial fibrosis and promotes atrial remodeling by targeting CREB1 in atrial fibrillation. *J Cardiol.* (2022a) 79:202–10. doi: 10.1016/j.jjcc.2021.09.012

19. Wang H, Jiang W, Hu Y, Wan Z, Bai H, Yang Q, et al. Quercetin improves atrial fibrillation through inhibiting TGF-β/smads pathway via promoting MiR-135b expression. *Phytomedicine.* (2021a) 93:153774. doi: 10.1016/j.phymed.2021.153774

20. Ye Q, Liu Q, Ma X, Bai S, Chen P, Zhao Y, et al. MicroRNA-146b-5p promotes atrial fibrosis in atrial fibrillation by repressing TIMP4. *J Cell Mol Med.* (2021) 25:10543–53. doi: 10.1111/jcmm.16985

21. Garcia-Elias A, Tajes M, Yañez-Bisbe L, Enjuanes C, Comín-Colet J, Serra SA, et al. Atrial fibrillation in heart failure is associated with high levels of circulating microRNA-199a-5p and 22-5p and a defective regulation of intracellular calcium and cell-to-cell communication. *Int J Mol Sci.* (2023) 10:1056134. doi: 10.3390/ijms221910377

22. Zhu J, Zhu N, Xu J. Mir-101a-3p overexpression prevents acetylcholine-CaCl(2)-induced atrial fibrillation in rats via reduction of atrial tissue fibrosis, involving inhibition of EZH2. *Mol Med Rep.* (2021) 2021:8116633.

23. Xiao J, Zhang Y, Tang Y, Dai H, Ouyang Y, Li C, et al. MiRNA-1202 promotes the TGF-β1-induced proliferation, differentiation and collagen production of cardiac fibroblasts by targeting nNOS. *PLoS One.* (2021a) 16:e0256066.

24. Su H, Su H, Liu CH, Hu HJ, Zhao JB, Zou T, et al. H(2)S inhibits atrial fibrillation-induced atrial fibrosis through miR-133a/CTGF axis. *Cytokine.* (2021) 146:155557. doi: 10.1016/j.cyto.2021.155557

25. Xiao Z, Reddy DPK, Xue C, Liu X, Chen X, Li J, et al. Profiling of miR-205/P4HA3 following angiotensin II-induced atrial fibrosis: implications for atrial fibrillation. *Front Cardiovasc Med.* (2021b) 8:609300. doi: 10.3389/fcvm.2021.609300

26. Xiao J, Zhang Y. hsa-miR-4443 inhibits myocardial fibroblast proliferation by targeting THBS1 to regulate TGF-β1/α-SMA/collagen signaling in atrial fibrillation. *Braz J Med Biol Res.* (2021) 54:e10692. doi: 10.1590/1414-431X202010692

27. Wang J, Ye Q, Bai S, Chen P, Zhao Y, Ma X, et al. Inhibiting microRNA-155 attenuates atrial fibrillation by targeting CACNA1C. *J Mol Cell Cardiol.* (2021b) 155:58–65. doi: 10.1016/j.yjmcc.2021.02.008

28. Zhelankin AV, Vasiliev SV, Stonogina DA, Babalyan KA, Sharova EI, Doludin YV, et al. Elevated plasma levels of circulating extracellular miR-320a-3p in patients with paroxysmal atrial fibrillation. *Int J Mol Sci.* (2021) 16(8):e0256066. doi: 10.3390/ijms21103485

29. Lv X, Lu P, Hu Y, Xu T. Overexpression of MiR-29b-3p inhibits atrial remodeling in rats by targeting PDGF-B signaling pathway. *Oxid Med Cell Longev.* (2021) 146:155557. doi: 10.1155/2021/3763529

30. Xu J, Lei S, Sun S, Zhang W, Zhu F, Yang H, et al. MiR-324-3p regulates fibroblast proliferation via targeting TGF-β1 in atrial fibrillation. *Int Heart J.* (2020) 61:1270–8. doi: 10.1536/ihj.20-423

31. Chen Y, Chang G. IL-6-miR-210 suppresses regulatory T cell function and promotes atrial fibrosis by targeting Foxp3. *Mol Cells.* (2020) 43:438–47. doi: 10.14348/molcells.2019.2275

32. Lv X, Li J, Hu Y, Wang S, Yang C, Li C, et al. Overexpression of miR-27b-3p targeting Wnt3a regulates the signaling pathway of wnt/β-catenin and attenuates atrial fibrosis in rats with atrial fibrillation. *Oxid Med Cell Longev.* (2021) 155:58–65. doi: 10.1155/2019/5703764

33. Yu RB, Li K, Wang G, Gao GM, Du JX. MiR-23 enhances cardiac fibroblast proliferation and suppresses fibroblast apoptosis via targeting TGF-β1 in atrial fibrillation. *Eur Rev Med Pharmacol Sci.* (2019) 23:4419–24.

34. Cheng WL, Kao YH. MicroRNA-133 suppresses ZFHX3-dependent atrial remodelling and arrhythmia. *Acta Physiol (Oxf).* (2019) 227:e13322. doi: 10.1111/apha.13322

35. Li PF, He RH, Shi SB, Li R, Wang QT, Rao GT, et al. Modulation of miR-10a-mediated TGF-β1/smads signaling affects atrial fibrillation-induced cardiac fibrosis and cardiac fibroblast proliferation. *Biosci Rep.* (2020) 61(6):1270–8. doi: 10.1042/BSR20181931

36. Wang M, Sun L. Ablation alleviates atrial fibrillation by regulating the signaling pathways of endothelial nitric oxide synthase/nitric oxide via miR-155-5p and miR-24-3p. *J Cell Biochem.* (2019) 120:4451–62. doi: 10.1002/jcb.27733

37. Xie H, Fu JL, Xie C. MiR-138-5p is downregulated in patients with atrial fibrillation and reverses cardiac fibrotic remodeling via repressing CYP11B2. *Eur Rev Med Pharmacol Sci.* (2018) 22:4642–7.

38. Wang Y, Cai H, Li H, Gao Z, Song K. Atrial overexpression of microRNA-27b attenuates angiotensin II-induced atrial fibrosis and fibrillation by targeting ALK5. *Hum Cell.* (2018) 31:251–60. doi: 10.1007/s13577-018-0208-z

39. Xu J, Wu H, Chen S, Qi B, Zhou G, Cai L, et al. MicroRNA-3°c suppresses the pro-fibrogenic effects of cardiac fibroblasts induced by TGF-β1 and prevents atrial fibrosis by targeting TGFβRII. *J Cell Mol Med.* (2018) 22:3045–57. doi: 10.1111/jcmm.13548

40. Cañón S, Caballero R, Herraiz-Martínez A, Pérez-Hernández M, López B, Atienza F, et al. miR-208b upregulation interferes with calcium handling in HL-1 atrial myocytes: implications in human chronic atrial fibrillation. *J Mol Cell Cardiol.* (2016) 99:162–73. doi: 10.1016/j.yjmcc.2016.08.012

41. Zhao Y, Yuan Y, Qiu C. Underexpression of CACNA1C caused by overexpression of microRNA-29a underlies the pathogenesis of atrial fibrillation. *Med Sci Monit.* (2016) 22:2175–81. doi: 10.12659/MSM.896191

42. Reilly S, Liu X, Carnicer R, Rajakumar T, Sayeed R, Krasopoulos G, et al. Evaluation of the role of miR-31-dependent reduction in dystrophin and nNOS on atrial-fibrillation-induced electrical remodelling in man. *Lancet.* (2015) 385(Suppl 1):S82. doi: 10.1016/S0140-6736(15)60397-X

43. Morishima M, Iwata E, Nakada C, Tsukamoto Y, Takanari H, Miyamoto S, et al. Atrial fibrillation-mediated upregulation of miR-30d regulates myocardial electrical remodeling of the G-protein-gated K(+) channel. *IK ACh Circ J.* (2016) 80:1346–55. doi: 10.1253/circj.CJ-15-1276

44. Yuan CT, Li XX, Cheng QJ, Wang YH, Wang JH, Liu CL. MiR-30a regulates the atrial fibrillation-induced myocardial fibrosis by targeting snail 1. *Int J Clin Exp Pathol.* (2015) 8:15527–36.

45. Zhang Y, Zheng S, Geng Y, Xue J, Wang Z, Xie X, et al. MicroRNA profiling of atrial fibrillation in canines: miR-206 modulates intrinsic cardiac autonomic nerve remodeling by regulating SOD1. *PLoS One.* (2015) 10:e0122674.

46. Qiao G, Xia D, Cheng Z, Zhang G. Mir-132 in atrial fibrillation directly targets connective tissue growth factor. *Mol Med Rep.* (2017) 16:4143–50. doi: 10.3892/mmr.2017.7045

47. Zhu H, Xue H, Jin QH, Guo J, Chen YD. Increased expression of ryanodine receptor type-2 during atrial fibrillation by miR-106-25 cluster independent mechanism. *Exp Cell Res.* (2019) 375:113–7. doi: 10.1016/j.yexcr.2018.11.025

48. Adam O, Löhfelm B, Thum T, Gupta SK, Puhl SL, Schäfers HJ, et al. Role of miR-21 in the pathogenesis of atrial fibrosis. *Basic Res Cardiol.* (2012) 107:278. doi: 10.1007/s00395-012-0278-0

49. Luo X, Pan Z, Shan H, Xiao J, Sun X, Wang N, et al. MicroRNA-26 governs profibrillatory inward-rectifier potassium current changes in atrial fibrillation. *J Clin Invest.* (2013) 123:1939–51. doi: 10.1172/JCI62185

50. Binas S, Knyrim M, Hupfeld J, Kloeckner U, Rabe S, Mildenberger S, et al. miR-221 and −222 target CACNA1C and KCNJ5 leading to altered cardiac ion channel expression and current density. *Cell Mol Life Sci.* (2020) 77:903–18. doi: 10.1007/s00018-019-03217-y

51. Lu Y, Zhang Y, Wang N, Pan Z, Gao X, Zhang F, et al. MicroRNA-328 contributes to adverse electrical remodeling in atrial fibrillation. *Circulation.* (2010) 122:2378–87. doi: 10.1161/CIRCULATIONAHA.110.958967

52. Ling TY, Wang XL, Chai Q, Lau TW, Koestler CM, Park SJ, et al. Regulation of the SK3 channel by microRNA-499–potential role in atrial fibrillation. *Heart Rhythm.* (2013) 10:1001–9. doi: 10.1016/j.hrthm.2013.03.005

53. Guo F, Tang C. LncRNA H19 drives proliferation of cardiac fibroblasts and collagen production via suppression of the miR-29a-3p/miR-29b-3p-VEGFA/TGF-β axis. *Mol Cells.* (2022) 45:122–33. doi: 10.14348/molcells

54. Dai H, Zhao N, Liu H, Zheng Y, Zhao L. LncRNA nuclear-enriched abundant transcript 1 regulates atrial fibrosis via the miR-320/NPAS2 axis in atrial fibrillation. *Front Pharmacol.* (2021) 12:647124. doi: 10.3389/fphar.2021.647124

55. Wang H, Song T, Zhao Y, Zhao J, Wang X, Fu X. Long non-coding RNA LICPAR regulates atrial fibrosis via TGF-β/smad pathway in atrial fibrillation. *Tissue Cell.* (2020) 67:101440. doi: 10.1016/j.tice.2020.101440

56. Quaife NM, Chothani S, Schulz JF, Lindberg EL, Vanezis K, Adami E, et al. LINC01013 Is a determinant of fibroblast activation and encodes a novel fibroblast-activating micropeptide. *J Cardiovasc Transl Res.* (2023) 16:77–85. doi: 10.1007/s12265-022-10288-z

57. Guo Y, Sun Z, Chen M, Lun J. LncRNA TUG1 regulates proliferation of cardiac fibroblast via the miR-29b-3p/TGF-β1 axis. *Front Cardiovasc Med.* (2021) 8:646806. doi: 10.3389/fcvm.2021.646806

58. Chen Q, Feng C, Liu Y, Li QF, Qiu FY, Wang MH, et al. Long non-coding RNA PCAT-1 promotes cardiac fibroblast proliferation via upregulating TGF-β1. *Eur Rev Med Pharmacol Sci.* (2019) 23:10517–22.

59. Du J, Li Z, Wang X, Li J, Liu D, Wang X, et al. Long noncoding RNA TCONS-00106987 promotes atrial electrical remodelling during atrial fibrillation by sponging miR-26 to regulate KCNJ2. *J Cell Mol Med.* (2020) 24:12777–88. doi: 10.1111/jcmm.15869

60. Lu J, Xu FQ, Guo JJ, Lin PL, Meng Z, Hu LG, et al. Long noncoding RNA GAS5 attenuates cardiac fibroblast proliferation in atrial fibrillation via repressing ALK5. *Eur Rev Med Pharmacol Sci.* (2019) 23:7605–10.

61. Yao L, Zhou B, You L, Hu H, Xie R. LncRNA MIAT/miR-133a-3p axis regulates atrial fibrillation and atrial fibrillation-induced myocardial fibrosis. *Mol Biol Rep.* (2020) 47:2605–17. doi: 10.1007/s11033-020-05347-0

62. Cao F, Li Z, Ding WM, Yan L, Zhao QY. LncRNA PVT1 regulates atrial fibrosis via miR-128-3p-SP1-TGF-β1-smad axis in atrial fibrillation. *Mol Med.* (2019) 25:7. doi: 10.1186/s10020-019-0074-5

63. Shen C, Kong B, Liu Y, Xiong L, Shuai W, Wang G, et al. YY1-induced Upregulation of lncRNA KCNQ1OT1 regulates angiotensin II-induced atrial fibrillation by modulating miR-384b/CACNA1C axis. *Biochem Biophys Res Commun.* (2018) 505:134–40. doi: 10.1016/j.bbrc.2018.09.064

64. Chen G, Guo H, Song Y, Chang H, Wang S, Zhang M, et al. Long non-coding RNA AK055347 is upregulated in patients with atrial fibrillation and regulates mitochondrial energy production in myocardiocytes. *Mol Med Rep.* (2016) 14:5311–7. doi: 10.3892/mmr.2016.5893

65. Zhang L, Lou Q, Zhang W, Yang W, Li L, Zhao H, et al. CircCAMTA1 facilitates atrial fibrosis by regulating the miR-214-3p/TGFBR1 axis in atrial fibrillation. *J Mol Histol.* (2023) 54:55–65. doi: 10.1007/s10735-022-10110-9

66. Gao Y, Liu Y, Fu Y, Wang Q, Liu Z, Hu R, et al. The potential regulatory role of hsa_circ_0004104 in the persistency of atrial fibrillation by promoting cardiac fibrosis via TGF-β pathway. *BMC Cardiovasc Disord.* (2021) 21:25. doi: 10.1186/s12872-021-01847-4

67. Liu X, Wu M, He Y, Gui C, Wen W, Jiang Z, et al. Construction and integrated analysis of the ceRNA network hsa_circ_0000672/miR-516a-5p/TRAF6 and its potential function in atrial fibrillation. *Sci Rep.* (2023) 13:7701. doi: 10.1038/s41598-023-34851-z

68. Wu N, Li C, Xu B, Xiang Y, Jia X, Yuan Z, et al. Circular RNA mmu_circ_0005019 inhibits fibrosis of cardiac fibroblasts and reverses electrical remodeling of cardiomyocytes. *BMC Cardiovasc Disord.* (2021) 21:308. doi: 10.1186/s12872-021-02128-w

69. Nopp S, Van Der Bent ML, Kraemmer D. Circulatory miR-411-5p as a novel prognostic biomarker for Major adverse cardiovascular events in patients with atrial fibrillation. *Int J Mol Sci.* (2016) 14(6):5311–7. doi: 10.3390/ijms24043861

70. Lage R, Cebro-Márquez M. Circulating miR-451a expression may predict recurrence in atrial fibrillation patients after catheter pulmonary vein ablation. *Cells.* (2023) 54(1):55–65. doi: 10.3390/cells12040638

71. Natsume Y, Oaku K, Takahashi K, Nakamura W, Oono A, Hamada S, et al. Combined analysis of human and experimental murine samples identified novel circulating MicroRNAs as biomarkers for atrial fibrillation. *Circ J.* (2018) 82:965–73. doi: 10.1253/circj.CJ-17-1194

72. Xu G, Cui Y, Jia Z, Yue Y, Yang S. The values of coronary circulating miRNAs in patients with atrial fibrillation. *PLoS One.* (2016) 11:e0166235.

73. Harling L, Lambert J, Ashrafian H, Darzi A, Gooderham NJ, Athanasiou T. Elevated serum microRNA 483-5p levels may predict patients at risk of post-operative atrial fibrillation. *Eur J Cardiothorac Surg.* (2017) 51:73–8. doi: 10.1093/ejcts/ezw245

74. Yamac AH, Kucukbuzcu S, Ozansoy M, Gok O, Oz K, Erturk M, et al. Altered expression of micro-RNA 199a and increased levels of cardiac SIRT1 protein are associated with the occurrence of atrial fibrillation after coronary artery bypass graft surgery. *Cardiovasc Pathol.* (2016) 25:232–6. doi: 10.1016/j.carpath.2016.02.002

75. Liu T, Zhong S, Rao F, Xue Y, Qi Z, Wu S. Catheter ablation restores decreased plasma miR-409-3p and miR-432 in atrial fibrillation patients. *Europace.* (2016) 18:92–9. doi: 10.1093/europace/euu366

76. Liu Z, Zhou C, Liu Y, Wang S, Ye P, Miao X, et al. The expression levels of plasma micoRNAs in atrial fibrillation patients. *PLoS One.* (2012) 7:e44906. doi: 10.1371/journal.pone.0044906

77. Zhang Y, Wang D, Wu N, Chen X, Yuan Z, Jia X, et al. Role of circulating long non-coding RNA for the improvement of the predictive ability of the CHA 2 DS 2 -VASc score in patients with atrial fibrillation. *Chin Med J (Engl).* (2022) 135:1451–8. doi: 10.1097/CM9.0000000000002213

78. Shi J, Chen L, Chen S, Wu B, Yang K, Hu X. Circulating long noncoding RNA, GAS5, as a novel biomarker for patients with atrial fibrillation. *J Clin Lab Anal.* (2021) 35:e23572. doi: 10.1002/jcla.23572

79. Chen Y, Ouyang T, Yin Y, Fang C, Tang CE, Luo J, et al. Analysis of infiltrated immune cells in left atriums from patients with atrial fibrillation and identification of circRNA biomarkers for postoperative atrial fibrillation. *Front Genet.* (2022) 13:1003366. doi: 10.3389/fgene.2022.1003366

80. Wei F, Zhang X, Kuang X, Gao X, Wang J, Fan J. Integrated analysis of circRNA-miRNA-mRNA-mediated network and its potential function in atrial fibrillation. *Front Cardiovasc Med.* (2022b) 9:883205. doi: 10.3389/fcvm.2022.883205

81. Zhu X, Wang Y, Mo R, Chong H, Cao C, Fan F, et al. Left atrial appendage circular RNAs are new predictors of atrial fibrillation recurrence after surgical ablation in valvular atrial fibrillation patients. *Heart Surg Forum.* (2021b) 24:E968–e976. doi: 10.1532/hsf.4125

82. Wen JL, Ruan ZB, Wang F, Chen GC, Zhu JG, Ren Y, et al. Construction of atrial fibrillation-related circRNA/lncRNA-miRNA-mRNA regulatory network and analysis of potential biomarkers. *J Clin Lab Anal.* (2023) 37:e24833.

83. Sagris M, Vardas EP. Atrial fibrillation: pathogenesis. *Predisposing Factors, and Genetics.* (2016) 25(3):232–6.

84. Brundel B, Ai X. Atrial fibrillation. *Nat Rev Dis Primers.* (2022) 8:21. doi: 10.1038/s41572-022-00347-9

85. Nattel S, Harada M. Atrial remodeling and atrial fibrillation: recent advances and translational perspectives. *J Am Coll Cardiol.* (2014) 63:2335–45. doi: 10.1016/j.jacc.2014.02.555

86. Mahajan R, Lau DH, Brooks AG, Shipp NJ, Manavis J, Wood JP, et al. Electrophysiological, electroanatomical, and structural remodeling of the atria as consequences of sustained obesity. *J Am Coll Cardiol.* (2015) 66:1–11. doi: 10.1016/j.jacc.2015.04.058

87. Takemoto Y, Ramirez RJ, Kaur K, Salvador-Montañés O, Ponce-Balbuena D, Ramos-Mondragón R, et al. Eplerenone reduces atrial fibrillation burden without preventing atrial electrical remodeling. *J Am Coll Cardiol.* (2017) 70:2893–905. doi: 10.1016/j.jacc.2017.10.014

88. Davidson KW, Barry MJ, Mangione CM, Cabana M, Caughey AB, Davis EM, et al. Screening for atrial fibrillation: uS preventive services task force recommendation statement. *Jama.* (2022) 327:360–7. doi: 10.1001/jama.2022.5207

89. Lee C. Screening for atrial fibrillation in asymptomatic older adults. *N Engl J Med.* (2022) 387:565–7. doi: 10.1056/NEJMclde2203726

90. Roberts E, Ludman AJ, Dworzynski K, Al-Mohammad A, Cowie MR, Mcmurray JJ, et al. The diagnostic accuracy of the natriuretic peptides in heart failure: systematic review and diagnostic meta-analysis in the acute care setting. *Br Med J.* (2015) 350:h910. doi: 10.1136/bmj.h910

91. Honda Y, Mok Y, Ishigami J, Ashley KE, Hoogeveen RC, Ballantyne CM, et al. The fifth-generation cardiac troponin T and cardiovascular disease in the community. *J Am Coll Cardiol.* (2021) 78:2019–21. doi: 10.1016/j.jacc.2021.08.066

92. Yoo S, Pfenniger A, Hoffman J, Zhang W, Ng J, Burrell A, et al. Attenuation of oxidative injury with targeted expression of NADPH oxidase 2 short hairpin RNA prevents onset and maintenance of electrical remodeling in the canine atrium: a novel gene therapy approach to atrial fibrillation. *Circulation.* (2020) 142:1261–78. doi: 10.1161/CIRCULATIONAHA.119.044127

93. Harada M, Tadevosyan A, Qi X, Xiao J, Liu T, Voigt N, et al. Atrial fibrillation activates AMP-dependent protein kinase and its regulation of cellular calcium handling: potential role in metabolic adaptation and prevention of progression. *J Am Coll Cardiol.* (2015) 66:47–58. doi: 10.1016/j.jacc.2015.04.056

94. Schmidt C, Wiedmann F, Zhou XB, Heijman J, Voigt N, Ratte A, et al. Inverse remodelling of K2P3.1K+ channel expression and action potential duration in left ventricular dysfunction and atrial fibrillation: implications for patient-specific antiarrhythmic drug therapy. *Eur Heart J.* (2017) 38:1764–74.

95. Barana A, Matamoros M, Dolz-Gaitón P, Pérez-Hernández M, Amorós I, Núñez M, et al. Chronic atrial fibrillation increases microRNA-21 in human atrial myocytes decreasing L-type calcium current. *Circ Arrhythm Electrophysiol.* (2014) 7:861–8. doi: 10.1161/CIRCEP.114.001709

96. Beyer C, Tokarska L, Stühlinger M, Feuchtner G, Hintringer F, Honold S, et al. Structural cardiac remodeling in atrial fibrillation. *JACC Cardiovasc Imaging.* (2021) 14:2199–208. doi: 10.1016/j.jcmg.2021.04.027

97. Yamaguchi N, Xiao J, Narke D, Shaheen D, Lin X, Offerman E, et al. Cardiac pressure overload decreases ETV1 expression in the left atrium, contributing to atrial electrical and structural remodeling. *Circulation.* (2021) 143:805–20. doi: 10.1161/CIRCULATIONAHA.120.048121

98. Narducci ML, Volpe M. Atrial fibrosis detected by cardiac magnetic resonance in persistent atrial fibrillation: a useful risk stratifier but not ideal electrophysiological endpoint for catheter ablation. *Eur Heart J.* (2022) 43:3196–7. doi: 10.1093/eurheartj/ehac424

99. Wang W, Wang X, Zhang Y, Li Z, Xie X, Wang J, et al. Transcriptome analysis of canine cardiac fat pads: involvement of two novel long non-coding RNAs in atrial fibrillation neural remodeling. *J Cell Biochem.* (2015) 116:809–21. doi: 10.1002/jcb.25037

100. Oliveira M, Silva Júnior ELD, Martins YO, Rocha HaL. Cardiac autonomic nervous system remodeling may play a role in atrial fibrillation: a study of the autonomic nervous system and myocardial receptors. *Arq Bras Cardiol.* (2021) 117:999–1007. doi: 10.36660/abc.20200725

101. Jiang W, Xu M, Qin M, Zhang D, Wu S, Liu X, et al. Role and mechanism of lncRNA under magnetic nanoparticles in atrial autonomic nerve remodeling during radiofrequency ablation of recurrent atrial fibrillation. *Bioengineered.* (2022) 13:4173–84. doi: 10.1080/21655979.2021.2024324

102. Zhao J, Zhang Y, Yin Z, Zhu Y, Xin F, Zhang H, et al. Impact of proinflammatory epicardial adipose tissue and differentially enhanced autonomic remodeling on human atrial fibrillation. *J Thorac Cardiovasc Surg.* (2023) 165:e158–74. doi: 10.1016/j.jtcvs.2022.03.013

103. Wei J, Zhang Y, Li Z, Wang X, Chen L, Du J, et al. GCH1 Attenuates cardiac autonomic nervous remodeling in canines with atrial-tachypacing via tetrahydrobiopterin pathway regulated by microRNA-206. *Pacing Clin Electrophysiol.* (2018) 41:459–71. doi: 10.1111/pace.13289

104. Li Z, Wang X, Wang W, Du J, Wei J, Zhang Y, et al. Altered long non-coding RNA expression profile in rabbit atria with atrial fibrillation: tCONS_00075467 modulates atrial electrical remodeling by sponging miR-328 to regulate CACNA1C. *J Mol Cell Cardiol.* (2017) 108:73–85. doi: 10.1016/j.yjmcc.2017.05.009

105. Hao H, Dai C, Han X, Li Y. A novel therapeutic strategy for alleviating atrial remodeling by targeting exosomal miRNAs in atrial fibrillation. *Biochim Biophys Acta Mol Cell Res.* (2022) 1869:119365. doi: 10.1016/j.bbamcr.2022.119365

106. Kang JY, Mun D, Kim H, Yun N, Joung B. Serum exosomal long noncoding RNAs as a diagnostic biomarker for atrial fibrillation. *Heart Rhythm.* (2022) 19:1450–8. doi: 10.1016/j.hrthm.2022.05.033

107. Wei Z, Bing Z, Shaohuan Q, Yanran W, Shuo S, Bi T, et al. Expression of miRNAs in plasma exosomes derived from patients with atrial fibrillation. *Clin Cardiol.* (2020) 43:1450–9. doi: 10.1002/clc.23461

108. Wang S, Min J, Yu Y, Yin L, Wang Q, Shen H, et al. Differentially expressed miRNAs in circulating exosomes between atrial fibrillation and sinus rhythm. *J Thorac Dis.* (2019) 11:4337–48. doi: 10.21037/jtd.2019.09.50

109. Mun D, Kim H, Kang JY, Yun N, Youn YN, Joung B. Small extracellular vesicles derived from patients with persistent atrial fibrillation exacerbate arrhythmogenesis via miR-30a-5p. *Clin Sci (Lond).* (2022) 136:621–37. doi: 10.1042/CS20211141

110. Zhu P, Li H, Zhang A, Li Z, Zhang Y, Ren M, et al. MicroRNAs sequencing of plasma exosomes derived from patients with atrial fibrillation: miR-124-3p promotes cardiac fibroblast activation and proliferation by regulating AXIN1. *J Physiol Biochem.* (2022) 78:85–98. doi: 10.1007/s13105-021-00842-9

111. Liu L, Luo F, Lei K. Exosomes containing LINC00636 inhibit MAPK1 through the miR-450a-2-3p overexpression in human pericardial fluid and improve cardiac fibrosis in patients with atrial fibrillation. *Mediators Inflamm.* (2021) 2021:9960241. doi: 10.1155/2021/9960241

frontiers | Frontiers in Cardiovascular Medicine

TYPE Review
PUBLISHED 18 July 2023
DOI 10.3389/fcvm.2023.1206541

OPEN ACCESS

EDITED BY
Jun-Jun Yeh,
Ditmanson Medical Foundation Chia-Yi Christian Hospital, Taiwan

REVIEWED BY
Vanesa Esteban,
Health Research Institute Foundation Jimenez Diaz (IIS-FJD), Spain
David John Vigerust,
Vanderbilt University, United States

*CORRESPONDENCE
Patrick L. Iversen
patmanphd@gmail.com

RECEIVED 15 April 2023
ACCEPTED 03 July 2023
PUBLISHED 18 July 2023

CITATION
Iversen PL, Kipshidze N, Kipshidze N, Dangas G, Ramacciotti E, Kakabadze Z and Fareed J (2023) A novel therapeutic vaccine targeting the soluble TNFα receptor II to limit the progression of cardiovascular disease: AtheroVax™. Front. Cardiovasc. Med. 10:1206541. doi: 10.3389/fcvm.2023.1206541

A novel therapeutic vaccine targeting the soluble TNFα receptor II to limit the progression of cardiovascular disease: AtheroVax™

Patrick L. Iversen[1]*, Nicholas Kipshidze[2], Nodar Kipshidze[3], George Dangas[4], Eduardo Ramacciotti[5], Zurab Kakabadze[6] and Jawed Fareed[7]

[1]Department of Environmental and Molecular Toxicology, Oregon State University, Corvallis, OR, United States, [2]New York Cardiovascular Research, New York, NY, United States, [3]Mailman School of Public Health, Columbia University, New York, NY, United States, [4]Department of Cardiology, Icahn School of Medicine at Mount Sinai, New York, NY, United States, [5]Science Valley Research Institute, Sao Paulo, Brazil, [6]Head Department of Clinical Anatomy, Tbilisi State Medical University, Tbilisi, Georgia, [7]Department of Molecular Pharmacology and Neuroscience, Loyola University Medical Center, Maywood, IL, United States

The burden of atherosclerotic cardiovascular disease contributes to a large proportion of morbidity and mortality, globally. Vaccination against atherosclerosis has been proposed for over 20 years targeting different mediators of atherothrombosis; however, these have not been adequately evaluated in human clinical trials to assess safety and efficacy. Inflammation is a driver of atherosclerosis, but inflammatory mediators are essential components of the immune response. Only pathogenic forms of sTNFR2 are acted upon while preserving the membrane-bound (wild-type) TNFR2 contributions to a non-pathogenic immune response. We hypothesize that the inhibition of sTNRF2 will be more specific and offer long-term treatment options. Here we describe pre-clinical findings of an sTNFR2-targeting peptide vaccine (AtheroVax™) in a mouse model. The multiple pathways to synthesis of the soluble TNFRII receptor (sTNFRII) were identified as sTNFRII(PC), sTNFRII(Δ7), and sTNFRII(Δ7,9). The sTNFRII(Δ7) peptide, NH2-DFALPVEKPLCLQR-COOH is specific to sTNFR2 based on an mRNA splice-variant in which exon 6 is joined to exon 8. The role of sTNFRII(Δ7) as a mediator of prolonged TNFα activity by preventing degradation and clearance was investigated. Inflammation is a critical driver of onset, progression and expansion of atherosclerosis. The TNFα ligand represents a driver of inflammation that is mediated by a splice variant of TNFR2, referred to as sTNFRII(Δ7). The multiple forms of TNFRII, both membrane bound and soluble, are associated with distinctly different phenotypes. sTNFRII(PC) and sTNFRII(Δ7) are not equivalent to etanercept because they lack a clearance mechanism. The unique peptide associated with sTNFRII(Δ7) contains a linear B-cell epitope with amino acids from both exon 6 and exon 8 supporting the vaccine design. Animal studies to evaluate the vaccine are ongoing, and results will be forthcoming. We describe a peptide vaccine targeting sTNFR2 in limiting the progression of atherosclerosis. A therapeutic vaccine limiting the progression of atherosclerosis will greatly contribute to the reduction in morbidity and mortality from cardiovascular disease. It is likely the vaccine will be used in combination with the current standards of care and lifestyle modifications.

KEYWORDS

atherosclerotic cardiovascular disease, tumor necrosis factor alpha, TNFRII, soluble TNFRII, therapeutic vaccine, peptide vaccine

1. Introduction

A therapeutic atherosclerosis vaccine with the objective to prevent or reduce development and progression of atherosclerosis has the potential to reduce incidence of heart attack and stroke. Atherosclerosis is characterized by lipid-rich plaques in large and medium-sized arteries that appear to originate from a chronic inflammatory response. The progressive plaque growth, plaque rupture or erosion with subsequent thrombus formation can lead to arterial occlusion and cardiovascular disease (CVD). The approach to a therapeutic atherosclerosis vaccine is to target are reduce levels of molecules that contribute to the development and progression of atherosclerosis.

Current measures to prevent and treat CVD include cholesterol-lowering, antiarrhythmic, and antihypertensive drugs which coupled with bypass surgery and percutaneous interventions have significantly reduced CVD mortality. Emerging vaccines offer a new dimension in the treatment of CVD. Promising preclinical studies with vaccines targeting PCSK9 (1) and oxidized LDL (2) reveal reduced atherosclerotic plaque formation in animal models. The results support the need for broader research and evaluation of vaccine safety and efficacy in humans. Finally, even if a therapeutic atherosclerosis vaccine is developed, it will likely be used in combination with the current standards of care.

Patients with myocardial infarction or high-risk heart disease that received influenza vaccine within 72 h of an invasive coronary procedure had a lower risk of all-cause death, MI, or stent thrombosis, and cardiovascular death 1 year after vaccination (3). The influenza vaccine is associated with lowering proinflammatory cytokines (4) and may exert anti-inflammatory and plaque stabilizing effects (5). The association of influenza vaccine with CVD supports the role of chronic inflammation as a central driver of CVD. Control of chronic inflammatory mediators is likely to be key to reducing CVD (6).

Cardiac inflammatory signaling is complex and multifaceted including triggers from viral infections and biochemical stresses. Numerous anti-inflammatory agents are available but have so far had limited success in the treatment of CVD (**Table 1**).

2. Tumor necrosis factor-α (TNF-α)

The tumor necrosis factor (TNF) super-family is composed of 19 different ligands and 29 receptors. This super-family is a pivotal component in cellular signaling cellular differentiation, survival and death (7). Immune responses are downstream to TNF signals involving both innate and adaptive immune cells. The interplay of ligand and receptors is complex and when dysregulated, inflammatory and autoimmune consequences can result.

Tumor necrosis factor-α (TNF-α) expression is triggered by the immune system response to pathogens and their associated toxins. TNFα is synthesized as a transmembrane precursor protein (mTNF-α) as a 26 kDa (233 amino acids, a 76 amino acid leader and 157 amino acid body). The mTNF-α is then proteolytically cleaved by the TNF-α converting enzyme (TACE or ADAM17) to create a free soluble homotrimer sTNF-α as 17 kDa monomers. TNF-α interacts with two receptors: TNFR1 known as CD120a and p55 and TNFR2 known as CD120b and p75. These receptors also bind lymphotoxin alpha (LT-α). The extracellular domain of TNFR2 is composed of 4 cysteine rich domains (CRD) identified as CRD1, CRD2, CRD3, and CRD4. TNFR2 is in a trimeric form as it sits on the cell membrane. Binding TNF-α activates the TNFR2 cytoplasmic domain. This TNFR2' signals through TRAF2 and induces JNK and NF-kB activation. TNFR1 may mediate bacterial and viral challenges but TNFR2 is primarily involved in response to viral challenges.

TNF-α is one of the most potent pro-inflammatory cytokines. Biosynthesis is controlled at a post-transcriptional stage through the competitive binding of tristetraprolin (TTP) to an AU-rich untranslated region in the 3'-region of the mRNA. Dephosphorylated TTP binds the mRNA and promotes degradation and phosphorylation weakens TTP affinity for mRNA. Stimuli such as lipopolysaccharide (LPS), interleukin 1β (IL-1β), IL-6, interferon gamma (IFN-γ), tissue trauma or hypoxia regulate translocation of TTP from the nucleus to the cytoplasm resulting in enhanced TNF-α biosynthesis. Mitogen-activated protein kinases (MAPK) is involved in control of numerous genes including nuclear factor kappa B (NF-κB) which positively regulates the promoter of TTP.

TABLE 1 Current anti-inflammatory therapy for atherosclerotic cardiovascular disease.

Class	Examples	Comments
Cyclooxygenase (COX) inhibitors	Aspirin, ibuprofen, naproxen	Other than aspirin may increase risk of heart attack and stroke
Arachidonate 5-llipoxygenase	Licofelone	
Immune selective (ImSAIDs)		
TNFα inhibitors	Remicade and Humera	Arthritis; Antidrug antibodies limit use
TNFα receptor Fc fusion	Etanercept (Enbrel)	Used in psoriasis
IL-6 MAb	Toculizumab	Used in Juvenile arthritis and COVID-19
IL-12/23 MAb	Ustekinumab	Used in Crohn's and psoriasis
IL-1/IL-1 receptor	Anakinra/Rilonacept	Autoimmune disease
Immunosuppressants	Glucocorticoids Calcineurin Inhibitors- tacrolimus mTOR inhibitors-sirolimus Methotrexate	Short term regimens
Immune signal transduction modulators	Tyrosine kinase inhibitors-Gleevec Janus kinase inh.- Barcitinib PPAR agonists- troglitazone	
Anti-gout agents	Colchicine	Acute treatment regimens

TNF-α promotes insulin resistance leading to obesity and type 2 diabetes. It is used by the immune system as a signal released by macrophages to coordinate an inflammatory response. However, TNF-α is also produced by mast cells, endothelial cells, cardiac myocytes, adipose tissue, fibroblasts, and neurons. Resulting immune responses include fever, apoptotic cell death, cachexia (wasting syndrome), and inflammation (heat, swelling, redness, and pain) while inhibiting tumorigenesis and infections.

2.1. TNF-α agonist

Initially, a cytotoxic factor produced by lymphocytes, lymphotoxin, was reported by two independent groups in 1964 (8). The name tumor necrosis factor was reported for a cytotoxic factor produced by macrophages in 1974. These cytotoxic factors were identified based on their ability to kill mouse fibrosarcoma cells (9). Excessive production of TNF was associated with the cause of malaria disease and endotoxin poisoning (10). Subsequent studies have identified production in cell types beyond the macrophage to include lymphoid cells, mast cells, endothelial cells, cardiac myocytes, adipose tissue, fibroblasts, and neurons.

TNF-α is used as an immunostimulant drug, Tasonermin, in the treatment of certain cancers with modest effectiveness. The soluble sTNF-α is also administered therapeutically from recombinant (rhTNF-α; amino acids 77-233) production methods. The inhibition of PBMCs by rhTNF-α, IC_{50}, is 1,728 ± 11 ng/ml and the effective concentration, EC_{50}, is 250 ± 1 ng/ml. The IC_{50} in Caco-2 cells was 297 ng/ml, HepG-2 cells was 197 ng/ml, and MCF-7 cells was 374 ng/ml (11).

TNF-α mRNA half-life was 75.3 ± 16.7 min (**Table 2**) in keratinocytes treated with UVB alone and 56.0 ± 4.5 min following UVB plus IL-1-α (not significantly different). No TNF-α mRNA was detected in keratinocytes following sham treatment (12). The half-life of TNF-α mRNA is 140 min in primary alveolar macrophages in control media. The mRNA is stabilized by cigarette smoke extract, the half-life is prolonged to well over 300 min (13). An immediate-early response gene, tristetraprolin (TTP), can destabilize the TNF-α mRNA.

Administration of 2 μg/kg/0.5 h in rats resulted in a plasma half-life of 5–8 min. Administration of doses between 10 and 500 μg/kg/0.5 h by intravenous infusion in rats resulted in dose independent plasma half-life of about 0.5 h (14). The half-life for rhTNF-α in rhesus macaques was between 1.2 and 2.1 h with doses of 10, 20, 30, and 120 μg/kg/0.5 h. The NHP studies suggested two different elimination mechanisms for TNF-α clearance, a nonspecific non-saturable process, and a specific saturable process (15).

TABLE 2 TNFα half-life observations.

Measure	Half-life (hours)	Comments
TNFα mRNA	0.9–2.3	Can be reduced post transcriptionally by tristetraprolin (TTP)
sTNFα protein	1.2–2.1	Clearance by multiple mechanisms

The sTNF binds TNFR1 with $Kd = 1.9 \times 10^{-11}$ M but TNFR2 with $Kd = 4.2 \times 10^{-10}$ M and the sTNF/TNFR1 complex depends on stabilization while the sTNF/TNFR2 complexes are short lived and may not be signaling competent (16). TNFR2 signaling is best activated by mTNF/TNFR2 complexes.

TNF-α appears to have contradictory effects on almost every type of cancer. Pro-tumorigenic effects include proliferation, promotion through TNFR1 and IL-17, immunosuppression, progression cell survival from reverse signaling, and metastasis through p38 MAPK, Erk1/2 and β-catenin. Anti-tumorigenic effects include tumor cell apoptosis, inhibition of proliferation, and generation of specific cytotoxic CD8 + lymphocytes (17).

2.2. TNF receptors

Binding TNFR1 leads to assembly of a complex of TNF receptor 1 associated protein with death domain (TRADD), the receptor associated factor 2 (TRAF2), the receptor interacting protein kinase (RIP1), and the cellular inhibitor of apoptosis proteins (cIAPs) 1 and 2. The selection of intracellular binding partners is influenced by the cIAP in the complex. Adapter signaling can produce several different signals: (1) a death inducing signaling complex (DISC) composed of TRADD/fas associated death domain (FADD)/procaspase 8 complex resulting in apoptosis, (2) phosphorylation of IKKβ leading to nuclear localization of nuclear factor kappa B (NFκB) free dimers and transcriptional activation of the NFκB pathway, and (3) recruitment of the necrosome complex leading to membrane permeabilization and necroptosis.

The TNFR2 signaling complex lacks the death domain but does include cIAP1/cIAP2 and signal through non-canonical activation of NFκB, the c-jun N-terminal kinase (JNK), p38 MAPK, and lipid phosphatidylinositol-4,5-bisphosphonate (PIP2) to produce proliferation of regulatory T cells (Treg) and activation of PKB/Akt in promoting cell survival and proliferation. Broadly, the actions of TNFR1 and TNFR2 have opposing effects on the immune system.

2.3. TNF-α inhibitors

TNF-α inhibitors include a spectrum of monoclonal antibodies: (a) Infliximab (Remicade) is a mouse Fv domain fused to a human Fcγ1 IgG1, (b) adalimumab and golimumab are human Fv domains with human Fcγ1 IgG1, (c) etanercept (Enbrel) is the four cysteine-rich domains (CRD) domains of TNFR2 fused to human Fcγ1 IgG1, and (d) certolizumab pegol is a humanized Fv (from murine) Fab' with the hinge region cross-linked to two 20 kDa molecules of polyethylene glycol. The current indications for anti-TNF-α include immune-mediated inflammatory diseases (IMID) such as rheumatoid arthritis, Crohn's disease, juvenile idiopathic arthritis, plaque psoriasis, ankylosing spondylitis, ulcerative colitis, and non-infectious uveitis (**Table 3**).

Remicade (infliximab) a chimeric monoclonal antibody binding TNF-α is administered in combination with

TABLE 3 Comparison of approved TNF-α inhibitors.

Agent	Half-life (D)	ADA (%)	Nab (%)	Regimen	Cost/QALY
Remicade (infliximab)	9.0–20	51.2	85.6	IV Q 8 weeks	$79,518/12.34 (18)
Humera (adalimumab)	9.6	93.4	41.4	SQ Q- 2 weeks	91,695/13.25
Enbrel (etanercept)	2.4–3.9	0–7	0	SQ 2x/week	$87,441/11.79
Cimzia (vertolizumab)	14	51.2	>60	SQ/IV Q-2 weeks	

methotrexate (MTX 10–25 mg/wk PO) at a dose of 3–5 mg/kg IV every 8 weeks. Important limitations include antidrug antibodies (ADA) which are observed in 51.2 percent of patients in a 30-week treatment period and neutralizing antibodies (Nab) are observed in 85.6 percent of patients in a 30-week treatment period (19). A meta-analysis of the half-life of Remicade was observed to range from 9.0 to 20.3 days but clearance is enhanced by 48 percent in patients with ankylosing spondylitis compared to rheumatoid arthritis. Clearance is also enhanced in individuals with ADA (20).

Humera (adalimumab) is a recombinant human monoclonal antibody that binds TNF-α administered as a 40 mg dose SQ. The elimination half-life was 231.9 h in adult male healthy volunteers with a 71 percent coefficient of variation (21). This study identified 93.4 percent of patients with ADA by day 70 and 41.4 percent of patients with Nabs by day 70.

Etanercept is a 75 kDa fusion protein capable of binding TNF-α 50- to 100-fold more potent than the endogenous TNFR1/R2. Enbrel was evaluated in clinical trials beginning in 1993 with approval for RA in 1998. A human dose of Enbrel (Etanercept) is 50 mg in 1 ml administered subcutaneously once a week. The dose results in a Cmax of 3,151 ± 1,261 ng/ml and a half-life 94.6 ± 19.2 h in healthy adults (22). A dose ranging study in patients with rheumatoid arthritis (RA) observed an elimination half-life of 57.8 ± 26.1 h at 50 mg SQ twice-weekly to 68.2 ± 27.4 h at 10 mg SQ once weekly. The observed EC_{50} was between 465 and 573 ng/ml and a steady state concentration of 1,170 ng/ml was observed in patients receiving 50 mg once-weekly (23). A 3 year follow-up study reveals 4.1 percent of patients fail to adhere to etanercept therapy due to medical reasons (24). Patients treated with Enbrel are at increased risk for developing serious infections leading to hospitalization and death.

Cimzia (Certolizumab Pegol) is a humanized monoclonal antibody conjugated to polyethylene glycol Fab fragment. The dose of 200 mg every other week (up to 800 mg) SQ and 10 mg/kg IV are administered with an elimination half-life of approximately 14 days and clearance is enhanced in patients with inflammatory conditions such as RA (25). Incidence of ADA was about 65 percent and over 97 percent of the response led to Nabs (26).

Some patients taking TNF-α inhibitors develop aggravation of disease and new onset of autoimmunity. This contradictory action suggests an immunosuppressive action of TNF-α which some ascribe to enhancement of regulatory T-cells (Tregs) due to binding TNFR2. One of the key limitations with inhibitors is the increased risk of infection such as tuberculosis (TB), development of autoimmune diseases and lymphomas (27). In addition, current inhibitor therapies often induce production of ADAs and specific NAbs leading to diminish inhibitor efficacy.

3. TNF-α and atherosclerosis

Animal models provide insights into the association between TNF-α and heart specific inflammation. Mice fed an atherogenic diet are protected from atherosclerotic lesion formation in *Tnfa*$^{-/-}$ mice and exclusive expression of mTNF-α reduces the inflammatory response (28). *Apoe*$^{-/-}$ mice fed an atherogenic diet show reduced plaque growth in *Tnfa*$^{-/-}$ mice (29). In the ischemia reperfusion model, mice show lower infarct area and improved cardiac functions in *Tnfa*$^{-/-}$ mice (30). Mice infected with coxsackievirus B3 to induce myocarditis have reduced myocarditis but no changes in virus titer in *Tnfa*$^{-/-}$ mice (31). The animal model data reveal a dual role of TNF-α and opposing effects of TNFR1 and TNFR2. These experimental data address the clinical failure of TNF-α inhibitors in heart failure patients and further suggest targeting TNFR2 over TNF-α.

TNFR1 and TNFR2 have opposing effects in the heart. TNFR1 exacerbates hypertrophy, inflammation, and cell death in heart failure but TNFR2 limits these events (32). TNFR1 aggravates ventricular remodeling but TNFR2 improves the action after myocardial infarction.

TNF-α is associated with increased risk of coronary heart disease development (33). IMID patients have increased risk of atherosclerotic cardiovascular events. Chronic inflammation leads to acceleration of atherosclerosis (34). Myocardial infarction rates are reduced in rheumatoid arthritis patients taking anti-TNF-α therapies (35, 36). However, enthusiasm for use of TNF-α inhibitors for treatment of patients with cardiovascular risk remains controversial as a few large multi-center comparative studies fail to demonstrate benefit for cardiovascular-related events, heart failure, death risk and improved cardiovascular outcomes (37–39).

The apparent disconnect between animal models of coronary heart disease and outcomes from human studies using TNF-α inhibitors may be due to limited target specificity of TNF-α inhibitors. However, use of TNF-α inhibitors is associated with multiple limitations.

4. Soluble TNFR2

Levels of sTNFRs are associated with increased mortality and morbidity in a diverse range of human diseases (**Figure 1**). The membrane bound TNFRs may be derived by proteolytic cleavage by TNF-α converting enzyme (TACE). They retain ligand binding activity as soluble receptors. T676G SNP (M196R) in exon 6 of the TNFR2 gene is associated with enhanced sTNFRs released by T cells in RA. The SNP was not associated with radiographic or functional severity of RA. This variant shows

10.3389/fcvm.2023.1206541

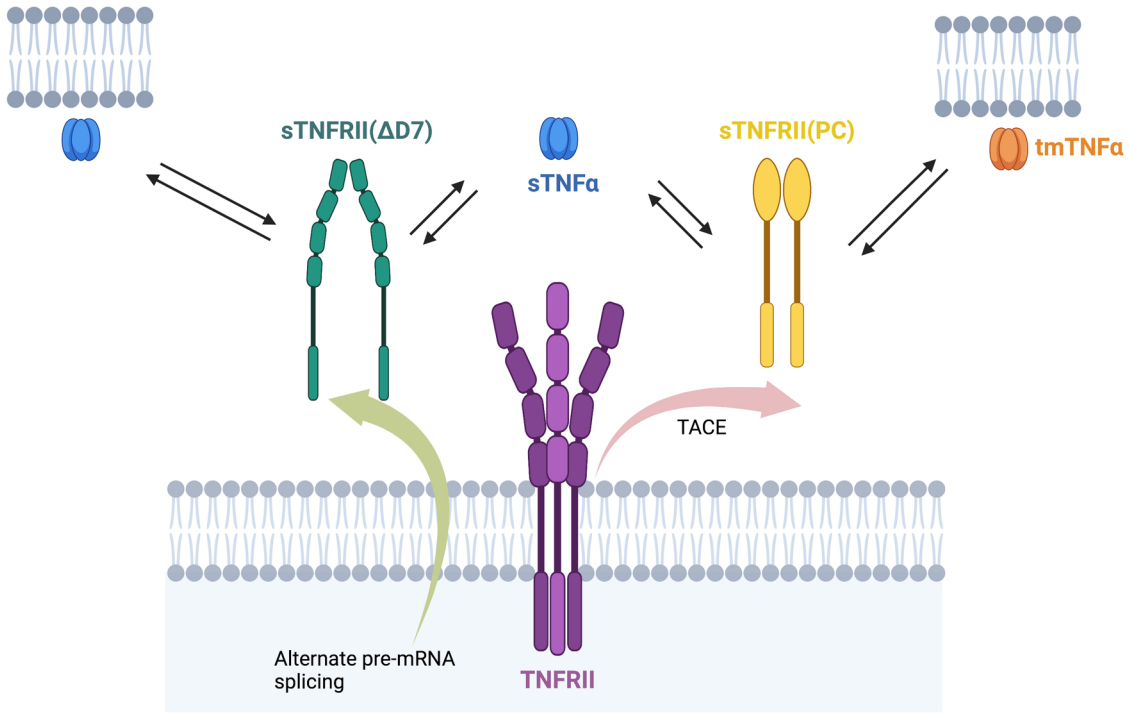

FIGURE 1
sTNFRII(PC), sTNFRII (Δ7), and sTNFRII(Δ7,8) bind sTNFα and tmTNFα. The multiple forms of the TNFRII, both membrane bound and soluble, can all bind either a membrane bound or soluble form of TNFα. This diversity of binding proteins leads to complexity in TNFα stability and signaling.

significantly lower induction of NF-κB and enhanced TNFR1 signaling of apoptosis (40).

sTNFRs are associated with sites of inflammation such as arthritis in Bechet's disease (41). sTNFR2 is a marker of cardiovascular disease in people with diabetes (42). sTNFR2 levels were associated with DNA methylation (epigenetic regulation) in circulating lymphocytes from participants in the Framingham Heart Study (43). A study of 48 patients with ST-elevation myocardial infarction (STEMI). In STEMI patients, circulating levels of sTNFR1 and sTNFR2 are associated with infarct size and LV dysfunction. It appears they play a role in apoptosis in ischemia-reperfusion injury (44). A study of 131 patients with chronic kidney disease (CKD) were evaluated. They conclude sTNFR1 (HR 1.51) and sTNFR2 (HR 1.13) are independently associated to all-cause mortality or an increased risk for cardiovascular events in advanced CKD irrespective of the cause of kidney disease (45). Increased concentrations of circulating TNFR1 and TNFR2 (sTNFR1 and sTNFR2) were associated with increased risks of cardiovascular events and mortality in patients with stable coronary heart disease (46).

Psoriasis patients treated with TNFα inhibitors produce more sTNFα and sTNFR2 and patients not responding produce higher levels of both sTNFα and sTNFR2 (47).

A soluble TNFR2 is also synthesized by alternate splicing of pre-mRNA (**Figure 2**) in response to inflammation (48). The splice variant lacks exon 7 and 8 that encode the transmembrane domain of TNFR2. An antisense strategy has been evaluated to induce skipping of exon 7 of TNFR2. The exon skipping strategy demonstrated amelioration of symptoms in a collagen-induced arthritis mouse model and promoted survival in a TNF-α induced hepatitis mouse model (49). A few key limitations with the antisense study include the oligonucleotide signaling through Tol-receptors leading to NFκB signaling, inability to discriminate between TACE and antisense induced sTNFR2, and limited quantities of Δ7-TNFR2 protein produced. While therapeutically challenging, an antisense oligonucleotide can be utilized as a control to produce the target sTNFR2 antigen in animal models.

4.1. sTNFRII(Δ7) role in inflammation

TNF-α is a central regulator of the inflammatory response. Therapeutic interventions include both agonists and antagonists. As an agonist, both the mRNA encoding TNF-α and the translated protein have short half-lives so chronic effects such as rheumatoid arthritis or atherosclerosis require chronic gene expression. TNF-α can produce contradictory and opposite effects in multiple circumstances. The diversity of TNF-α effects appears to be associated with the two receptors, TNFR1 and TNFR2 with therapeutic intervention focus on TNFR2.

The association of TNFR2 with pathogenesis in humans and animal models is complicated by limitations in measures of the soluble TNFR2 in the context of membrane TNFR2. The appearance of a soluble TNFR2 in blood may lead to two

10.3389/fcvm.2023.1206541

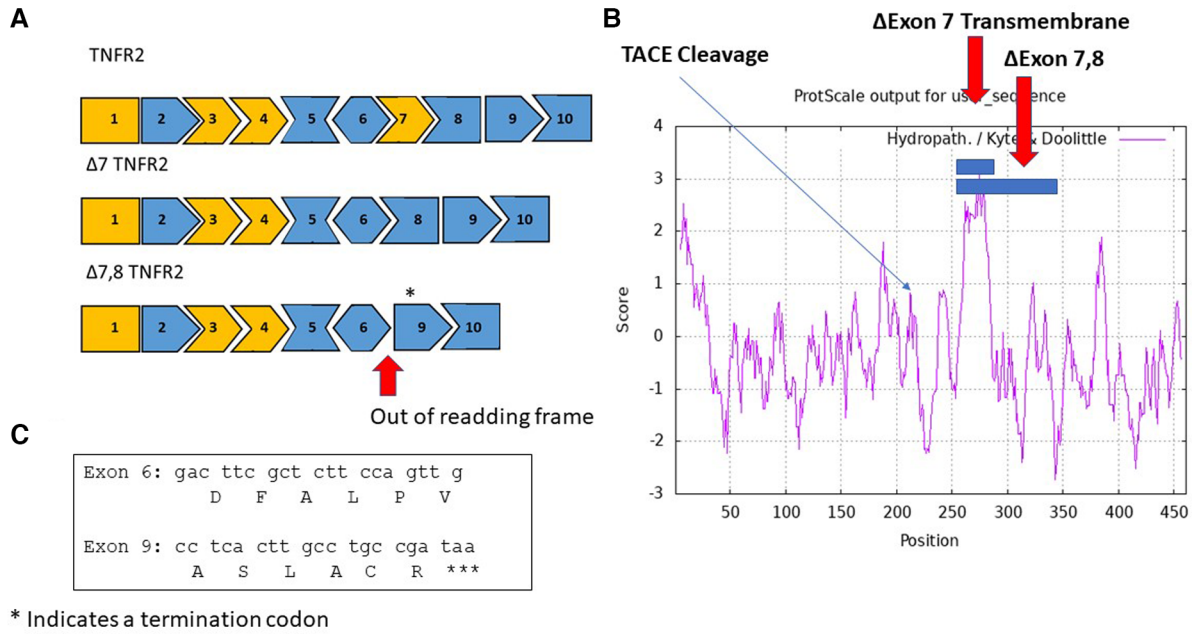

FIGURE 2
Alternate splice variants of TNFR2 include sTNFRII (Δ7), and sTNFRII(Δ7,8). (**A**) An exon map of the TNFRII displays the 10 exons in the gene with cassette exons indicated in orange. Two splice variants are shown, an in-frame variant in which exon 7 is skipped resulting in the sTNFRII(Δ7) variant and an out of frame variant sTNFRII(Δ7,8). The asterisk above exon 9 indicates the location of a termination codon TAA. (**B**) A hydropathy map of TNFRII with blue bars indicating amino acids exclude associated with exons 7 and 7 plus 8 are located in the transmembrane domain. An arrow indicates the location of the TACE cleavage site responsible for releasing the extracellular domain of sTNFRII(PC). (**C**) The nucleic acid and amino acid sequences joined in the sTNFRII (Δ7,8) splice variant.

opposing interpretations (**Figure 3**). First, the most frequently reported action is to bind TNFα as a "decoy" receptor, an endogenous TNFα inhibitor, resulting in lower free sTNFα levels and reduced inflammation. The opposing interpretation also involves binding free sTNFα but the outcome is stabilization of sTNFα by protecting it from clearance and degradation leading to prolonged inflammation. The second interpretation proposes the free sTNFα plus sTNFR2 bound sTNFα are physiologically relevant. Reference TNFα levels in healthy individuals were 0.083 ± 0.14 pg/ml which is approximately 1,000 times lower than levels of sTNFR1 (942 ± 32 ng/ml) and sTNFR2 (2,587 ± 76 ng/ml). The sTNFR2 is then a high capacity, low affinity receptor for TNF-α that has no known signal transduction activity. The sTNFR2 does not include a clearance mechanism as is observed in etanercept which is composed of both TNFR2 ligand binding domain but also an Fc domain providing for clearance. Even with the Fc domain fused to the TNFR CRD, TNFα levels are higher in psoriasis patients taking etanercept compared to adalimumab and infliximab. The second interpretation is consistent with clinical observations of poor outcomes and treatment failures associated with elevated sTNFR2.

5. Vaccine strategies for chronic inflammation

Vaccines for management of infectious diseases have historically used large antigens such attenuated (yellow fever, measles, mumps, and rubella), inactivated (polio, rabies, influenza, and hepatitis A) or subunit (Hepatitis B, human papillomavirus, and influenza) pathogens. The large antigens are preferred because their multiple epitopes offer a hedge against variation in pathogens and limit immune evasion. However, use of pathogens as large antigens in vaccines can be associated with significant adverse events. Reactivation of an attenuated tuberculosis vaccine (BCG) was administered to 251 neonates were given three oral doses in Lubeck Germany in 1930. 173 infants developed signs of TB and 72 died (50). A diphtheria vaccine unknowingly contaminated with *Staphylococcus aureus* was administered to 21 children in Bundaberg Australia in 1928. 12 of the children died within 2 days of vaccination (51). Large antigens may also increase the potential for autoimmune host reactions. The US FDA prohibited (21 CFR 610.19) Group A streptococcus organisms or their derivatives from vaccines because they may induce dangerous tissue reactions in humans. The action was based on administration of an M protein vaccine to 21 healthy siblings of patients with rheumatic fever. Two of the individuals developed rheumatic fever and another developed possible rheumatic fever (52). The FDA revoked the specific requirements for *S. pyogenes* vaccine in 2006 and now peptide-based vaccines utilize segments of the M-protein as well as non-M protein antigens (53). Vaccines designed to target self-protein targets do not share the need for large antigens as there is minimal opportunity for immune evasion.

Large antigens present numerous epitopes to the immune system and can result in "immune confusion." Some surface-

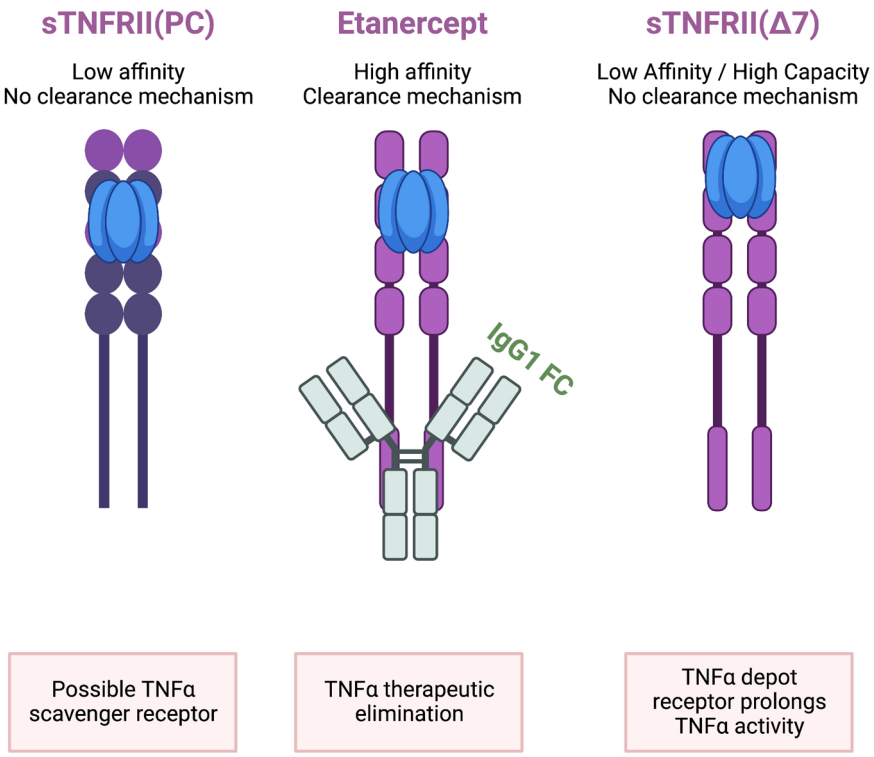

FIGURE 3
sTNFRII (Δ7) is not equivalent to etanercept or sTNFRII(PC). All three molecules contain the four extracellular CRD regions and can bind TNFα. Only Etanercept has a clearance mechanism provided by the fusion with a human IgG1 Fc region capable of removing bound TNFα from circulation. The relative abundance of sTNFRII(Δ7) is on the order of 2,500 ng/ml which is in excess of TNFα in healthy individuals which is on the order of 0.08 pg/ml. The low affinity but high-capacity binding is proposed to bind TNFα and protect it from rapid degradation based on the 1–2 h half-live of TNFα. The net effect is that the sTNFRII(Δ7) is a depot reservoir for TNFα extending the proinflammatory activity.

exposed regions of the antigen are associated with subdominant or weak antibody responses in contrast to immunodominant epitopes (54). For example, Dengue virus interacts with host cell receptors with a fusion loop (FL) of the M protein. While the FL domain is an immunodominant region, it leads to poorly neutralizing antibodies while other sites in the M protein are subdominant but elicit protective antibodies (55). Dengue vaccine development has been hampered by this situation. Another example involves the hemagglutinin (HA) of influenza A virus (IAV). The highly conserved HA stem region is associated with protective antibodies, but this site is subdominant (56). This explains why IAV vaccines need to be updated for each season's infection. Vaccines with large antigens present both immunodominant and subdominant regions and apparent immune confusion with respect to efficacy.

Current trends utilize smaller peptides to avoid the complexity of reactions to large antigens. Peptide vaccines are synthetically prepared so the antigen can be fully characterized. The production is highly reproducible, fast, and cost-effective. The vaccines are generally water soluble and may be stored without refrigeration. The small size limits potential for allergic or autoimmune responses.

Peptide-based anticancer vaccines targeting human papilloma virus (HPV) utilize 7–14 amino acid epitope sequences targeting the E5, E6, and E7 proteins of HPV-16. The linear B-cell epitopes effectively activate CD8 + cell responses but lack Th epitopes. The small peptides are not promptly recognized by antigen presenting cells (APC) so immunostimulatory adjuvants and vaccine formulations are necessary to ensure vaccine efficacy. A universal T helper epitope that covers a broad range of HLA alleles called PADRE (AKFVAAQTLKAAA) is more stimulatory that natural Th epitopes (57). Immunostimulant peptides can be added including influenza hemagglutinin CD4 + peptide ($HA_{307–319}$; PKYVKQNTLKLAT) or tetanus toxoid peptide ($TT_{830–844}$; CG-QYIKANSKFIGITEL) (58).

5.1. Epitope-peptide based vaccines

Active immunization with vaccines targeting TNF-α are being developed to address the cost and antidrug antibody (ADA) limitations of current TNF-α inhibitors including infliximab, adalimumab and etanercept. Initial attempts employed the sTNF-α molecule as the immunogen including TNF-K and TNF AutoVaccine. These approaches are effective in animal model studies (59) but were not successful in human clinical trials (60).

An epitope-based vaccine pursues design for optimal target specificity (61). The result is a vaccine with fewer allergenic and reactogenic effects (62). The key limitation is small peptides are inherently poor in immunogenicity imposing requirements for an

appropriate scaffold and adjuvant. A TNF epitope vaccine, CRM197, has been described which employs the epitope peptide (AA 80–97) (63) from monoclonal antibody binding and a transmembrane domain of the diphtheria toxoid as adjuvant (64).

Alternative splicing describes how multiple transcripts can be created from a single pre-mRNA, which are then translated into a family of protein isoforms. The splicing process is controlled by spliceosomes, splice sites, and splicing elements for splicing factors. Alternative splicing is associated with many cardiac diseases including hypertrophic cardiomyopathy (alternate splicing of myomesin and troponin), myotonic dystrophy type 1 (DM1; alternate splicing of dystrophia myotonica protein kinase), Brugada syndrome (abnormal splicing of SCN5A), dilated cardiomyopathy, ischemic cardiomyopathy, and atherosclerosis (65). Alternative splicing of apoptotic pathways plays a central role in development of cardiovascular disease with alternate splice forms of TNF-α. The alternate spliced protein isoforms may represent neoantigens that may be exploited by vaccines.

Vaccination against atherosclerosis as a potential effective approach has been under investigation for more than 20 years. Different antigens have been tested in animals with a great success. Lipid-related antigens like Ox- LDL, PCSK9, non-lipid related antigens like interleukins, HSPs β2GPI, DNA vaccination and whole cell vaccination are some examples of successful examinations in animals (66). Plant-based vaccination which has some advantages over traditional methods has recently attracted the attention of the scientific community.

AtheroVax is a therapeutic vaccine for individuals with ongoing coronary artery disease. The vaccine antigen is an alternately spliced variants of the tumor necrosis factor alpha receptor 2 (TNFR2). The TNF-alpha inflammation pathway is an important driver of atherosclerosis and formation of vascular plaque. Targeting the disease associated neoantigen, sTNFR2, that exploits the novel pre-mRNA joining of exon 6 to exons 8 and/or 9 thus sparing the membrane bound, wild-type, TNFR2 (**Table 4**). The vaccine is expected to have a long duration of action that can replace current therapies that while effective, require chronic treatment resulting in frequent failures due to lack of patient compliance.

The sTNFR2 is a soluble extracellular protein observed in blood plasma. A vaccine producing humoral responses (antibodies) more prominently than cellular (cytotoxic T-cell) responses is desired. Aluminum-based adjuvants such as aluminum hydroxide (Alum) are poor stimulators of cellular immune responses.

TABLE 4 Rationale for targeting sTNFRII.

Observation	References
TNFα has a very short half-life, 1.2–2 h	(15)
Relationship between [TNFα] and sTNFRII is not inverse	(47)
Associated with sites of inflammation, arthritis in Bechet's disease.	(41)
Associated with cardiovascular disease in diabetics	(42)
Associated with increased risks of cardiovascular events and mortality in patients with stable coronary heart disease	(46)
Psoriasis patients treated with TNFα inhibitors produce more sTNFα and sTNFR2 and patients not responding produce higher levels of both sTNFα and sTNFR2	(47)
Associated with all-cause mortality or an increased risk for cardiovascular events in advanced CKD	(45)
sTNFR2 levels were linked to epigenetic regulation associated with proinflammatory gene expression in lymphocytes from participants in the Framingham Heart Study	(43)

6. Conclusions

A therapeutic vaccine for the treatment of atherosclerotic CVD targeting chronic inflammation supported by expression of the sTNFRII(Δ7) splice variant is described. The approach to the vaccine is based on the premise that chronic inflammation is a key driver of CVD. TNFα and the associated signal transduction pathway is central to the maintenance of chronic inflammation. While numerous anti-TNFα therapeutics are currently available, they have limitations for use in treating CVD including variable responses and emergence of antidrug antibodies (ADA). An understanding of the diverse forms of the TNF receptors may explain the variable responses to TNFα ultimately focusing attention to the TNFRII. The TNFRII receptor is further complicated by the expression of both membrane bound and at least two soluble forms. The proteolytically cleaved soluble form sTNFRII(PC) is distinct in structure and function from the alternate splice form sTNFRII(Δ7). The small peptide vaccine, AtheroVax, is a linear B-cell epitope created by joining exons 6–8 which is unique to the sTNFRII(Δ7) and is not expected to cross react with the membrane bound (mTNFRII) or sTNFRII(PC). The resulting therapeutic vaccine specificity supports chronic use in limiting the development and progression of atherosclerosis.

AtheroVax is a unique vaccine for atherosclerotic CVD by targeting chronic inflammation and not the process of cholesterol synthesis, transport, and states of oxidation. The

TABLE 5 Target product profile (TPP).

Product properties	Minimum acceptable	Ideal
Primary indication	Prevention of atherosclerosis progression	Prevention of atherosclerosis
Patient population	Adults with atherosclerosis who are at risk for progression to MACE	Adults at risk for atherosclerosis
Treatment duration	Chronic	Chronic
Delivery mode	Injection (IM, SC, ID)	Subcutaneous injection
Dosage form	Sterile liquid with adjuvant	Sterile dry powder for rehydration in isotonic saline
Regimen	Once/6 months	Once/year
Efficacy	Equal to current SOC	Better outcomes than SOC
Risks/side effects		Local injection site reactions treated with NSAIDs

proposed benefit is summarized in a target product profile (Table 5). The treatment regimen is expected to be once to twice a year which is expected to limit cost and support compliance to the treatment regimen. The expectation of low cast and anticipated product stability may even support acceptance as a global therapy for CVD.

The potential successful development of AtheroVax is likely to be used in conjunction with other treatments such as standard of care medications and lifestyle modifications.

Author contributions

PI, NiK and NoK all contributed to the development of the manuscript and preparation of the figures. GD, ER, ZK, and JF all contributed to the improvement of the manuscript and critical review of the subject matter. All authors contributed to the article and approved the submitted version.

Conflict of interest

The authors PI, NiK, and NoK all are co-inventors of the AtheroVax vaccine and share interest in commercial development of the vaccine.

The remaining authors declare that the research was conducted in the absence of any commercial or financial relationships that could be construed as a potential conflict of interest.

Publisher's note

References

1. Zeitlinger M, Bauer M, Reindl-Schwaighofer R, Stoekenbroek RM, Lambert G, Berger-Sieczkowski E, et al. A phase I study assessing the safety, tolerability, immunogenicity, and low-density lipoprotein cholesterol-lowering activity of immunotherapeutics targeting PCKS9. *Eur J Cliin Pharmacol.* (2021) 77:1473–84. doi: 10.1007/s00228-021-03149-2

2. Zhu L, He Z, Wu F, Ding R, Jiang Q, Zhang J, et al. Immunization with advanced glycation end products modified low density lipoprotein inhibits atherosclerosis progression in diabetic apoE an LDLR null mice. *Cardiovasc Diabetol.* (2014) 13:151. doi: 10.1186/s12933-014-0151-6

3. Fröbert O, Götberg M, Erlinge D, Akhtar Z, Christiansen EH, MacIntyre CR, et al. Influenza vaccination after myocardial infarction. *Circulation.* (2021) 144:1476–84. doi: 10.1161/CIRCULATIONAHA.121.057042

4. Atoui R, Ebrahim F, Saroka K, Mireau J, et al. Influenza vaccination blunts the inflammatory response in patients undergoing cardiopulmonary bypass. *Ann Thorac Surg.* (2021) 111:1923–30. doi: 10.1016/j.athoracsur.2020.07.052

5. Bermudez-Fajardo A, Oviedo-Orta E. Influenza vaccination promotes stable atherosclerotic plaques in apoE knockout mice. *Atherosclerosis.* (2011) 217:97–105. doi: 10.1016/j.atherosclerosis.2011.03.019

6. Tsoupras A, Lordan R, Zabetakis I. Inflammation, not cholesterol, is a cause of chronic disease. *Nutrients.* (2018) 10:604. doi: 10.3390/nu10050604

7. Locksley RM, Killeen N, Lenardo MJ. The TNF and TNF receptor superfamilies: integrating mammalian biology. *Cell.* (2001) 104:487–501. doi: 10.1016/S0092-8674(01)00237-9

8. Ruddle NH, Waksman BH. Cytotoxicity mediated by soluble antigen and lymphocytes in delayed hypersensitivity. 3. Analysis of mechanism. *J Exp Med.* (1968) 128(6):1267–79. doi: 10.1084/jem.128.6.1267

9. Carswell EA, Old LJ, Kassel RL, Green S, Fiore N, Williamson B, et al. An endotoxin-induced serum factor that causes necrosis of tumors. *Proc Natl Acad Sci.* (1975) 72(9):3666–70. doi: 10.1073/pnas.72.9.3666

10. Clark IA, Virelizier JL, Carswell EA, Wood PR. Possible importance of macrophage-derived mediators in acute malaria. *Infect Immun.* (1981) 32(3):1058–66. doi: 10.1128/iai.32.3.1058-1066.1981

11. El-Baky NA, El-Fakharany EM, Sabry SA, El-Helow ER, Redwan EM, Sabry A, et al. De novo optimized cell-free system for expression of soluble and active human tumor necrosis factor-alpha. *Biology.* (2022) 11:157. doi: 10.3390/biology11020157

12. Bashir MM, Sharma MR, Werth VP. UVB and pro-inflammatory cytokines synergistically activate TNF-α production in keratinocytes throughenhanced gene transcription. *J Invest Dermatol.* (2009) 129(4):994–1001. doi: 10.1038/jid.2008.332

13. Zhao XK, Che P, Cheng ML, Zhang Q, Mu M, Li H, et al. Tristetraprolin down-regulation contributes to persistent TNF-alpha expression induced by cigarette smoke extract through a post-transcriptional mechanism. *PLoS One.* (2016) 11(12):e0167451. doi: 10.1371/journal.pone.0167451

14. Zahn G, Greischel A. Pharmacokinetics of tumor necrosis factor alpha after intravenous administration in rats. Dose dependence and influence of tumor necrosis factor beta. *Arzneimittelforschung.* (1989) 39(9):1180–2.

15. Greischel A, Zahn G. Pharmacokinetics of recombinant human tumor necrosis factor alpha in rhesus monkeys after intravenous administration. *J Pharmacol Exp Ther.* (1989) 251(1):358–61.

16. Grell M, Wajant H, Zimmermann G, Scheurich P. The type I receptor (CD120a) is the high-affinity receptor for soluble tumor necrosis factor. *Proc Natl Acad Sci USA.* (1998) 95:570–5. doi: 10.1073/pnas.95.2.570

17. Mefcogliano MF, Bruni S, Mauro F, Elizalde PV, Schillaci R. Harnessing tumor necrosis factor alpha to achieve effective cancer immunotherapy. *Cancers.* (2021) 13:564. doi: 10.3390/cancers13030564

18. Gholame A, Azizpoor J, Aflaki E, Rezaee M, Keshavarz K. Cost-effectiveness analysis of biopharmaceuticals for treating rheumatoid arthritis: infliximab, adalimumab, and etanercept. *BioMed Res International.* (2021) 2021:4450162. doi: 10.1155/2021/4450162

19. Cohen SB, Alten R, Kameda H, Hala T, Radominski SC, Rehman MI, et al. A randomized controlled trial comparing PF-06438179/GP1111 (an infliximab biosimilar) and infliximab reference product for treatment of moderate to severe active rheumatoid arthritis despite methotrexate therapy. *Arthritis Res Ther.* (2018) 20:155. doi: 10.1186/s13075-018-1646-4

20. Passot C, Mulleman D, Bejan-Angoulvant T, Aubourg A, Willot S, Lecomte T, et al. The underlying inflammatory chronic disease influences infliximab pharmacokinetics. *MAbs.* (2016) 8(7):1407–16. doi: 10.1080/19420862.2016.1216741

21. Zhang H, Wu M, Sun J, Zhu X, Li C, Ding Y, et al. Pharmacokinetics, safety, and immunogenicity of HLX03, an adalimumab biosimilar, compared with reference biologic in healthy Chinese male volunteers: results of a randomized, double-blind, parallel controlled, phase I study. *Pharmacol Res Perspect.* (2021) 9:e00733. doi: 10.1002/prp2.733

22. Shennak M, Al-Jaouni R, Kshirasagar S, Kasibhatta RS, Godse N, Al-Ghazawi A, et al. An open-label, randomized, single-dose, ccrossover, comparative pharmacokinetics study of YLB113 and the entanercept reference product in healthy adult malesubjects. *Eur J Drug Met Pharmacokinet.* (2020) 45:467–75. doi: 10.1007/s13318-020-00613-9

23. Breedveld F, Jones HE, Peifer K, Korth-Bradley J. A pilot dose-finding study of etanercept in rheumatoid arthritis. *Clin Transl Sci.* (2018) 11:38–45. doi: 10.1111/cts.12502

24. Vogelzang EH, Hebing RCF, Nurmohamed MT, van Kuijk AWR, Kruijff JWF, l'Ami J, et al. Adherence to etanercept therapy in rheumatoid arthritis patients during 3 years of follow-up. *PLoS One.* (2018) 13(10):e0205125. doi: 10.1371/journal.pone.0205125

25. Patel AM, Moreland LW. Certolizumab pegol: a new biologic targeting rheumatoid arthritis. *Expert Rev Clin Immunol.* (2010) 6(6):855–66. doi: 10.1586/eci.10.69

26. Wang Z, Huang J, Xie D, He D, Lu A, Liang C. Toward overcoming treatment failure in rheumatoid arthritis. *Front Immunol*. (2021) 12:755844. doi: 10.3389/fimmu.2021.755844

27. Monaco C, Nanchahal J, Taylor P, Feldmann M. Anti-TNF therapy: past, present and future. *Int Immunol*. (2015) 27:55–62. doi: 10.1093/intimm/dxu102

28. Canault M, Peiretti F, Mueller C, Kopp F, Morange P, Rihs S, et al. Exclusive expression of transmembrane TNF-α in mice reduces the inflammatory response in early lipid lesions of aortic stenosis. *Atherosclerosis*. (2004) 172:211–8. doi: 10.1016/j.atherosclerosis.2003.10.004

29. Xiao N, Yin M, Zhang L, Qu X, Du H, Sun X, et al. Tumor necrosis factor-alpha deficieny retards fatty-streak lesion by influencing expression of inflammatory factors in apoE-null mice. *Mol Gener Metab*. (2009) 96:239–44. doi: 10.1016/j.ymgme.2008.11.166

30. Maekawa N, Wada H, Kanda T, Niwa T, Yamada Y, Saito K, et al. Improved myocardial ischemia/reperfusion injury in mice lacking tumor necrosis factor-α. *J Amm Coll Cardiol*. (2002) 39:1229–35. doi: 10.1016/S0735-1097(02)01738-2

31. Huber SA, Sartini D. Roles of tumor necrosis factor alpha (TNF-α) and the p55 TNF receptor in CD1d induction and coxsackievirus B3-induced myocarditis. *J Virol*. (2005) 79:2659–65. doi: 10.1128/JVI.79.5.2659-2665.2005

32. Hamid T, Gu Y, Ortines RV, Bhattacharya C, Wang G, Xuan YT, et al. Divergent tumor necrosis factor-related remodeling responses in heart failure: role of nuclear factor-kappa B and inflammatory activation. *Circulation*. (2009) 119:1386–97. doi: 10.1161/CIRCULATIONAHA.108.802918

33. Pulido-Gomez K, Hernandez-Diaz Y, Tovilla-Zarate CA, Juarez-Rojop IE, Gonzalez-Castro TB, Lopez-Narvaez ML, et al. Association of G308A and G238A polymorphisms on the TNF-α gene and risk of coronary heart disease: systemic review and meta-analysis. *Arch Med Res*. (2016) 47:557–72. doi: 10.1016/j.arcmed.2016.11.006

34. Arida A, Protogerou AD, Kitas GD, Sfikakis PP. Systemic inflammatory response and atherosclerosis: the paradigm of chronic inflammatory rheumatic diseases. *Int J Mol Sci*. (2018) 19(7):1890. doi: 10.3390/ijms19071890

35. Low AS, Symmons DP, Lunt M, Mercer LK, Gale CP, Watson KD, et al. Relationship between exposure to tumor necrosis factor inhibitor therapy and incidence and severity of myocardial infarction in patients with rheumatoid arthritis. *Ann Rheum Dis*. (2017) 76:654–60. doi: 10.1136/annrheumdis-2016-209784

36. Ntusi NAB, Francis JM, Sever E, Liu A, Piechnik SK, Ferreira VM, et al. Anti-TNF modulation reduces myocardial inflammation and improves cardiovascular function in systemic rheumatoid diseases. *Int J Cardioll*. (2018) 270:253–9. doi: 10.1016/j.ijcard.2018.06.099

37. Al-Aly Z, Pan H, Zeringue A, Xian H, McDonald JR, El-Achkar TM, et al. Tumor necrosis factor-α blockade, cardiovascular outcomes, and survival in rheumatoid arthritis. *Ann Rheum Dis*. (2007) 66:670–5. doi: 10.1136/ard.2006.062497

38. Setoguchi S, Schneeweiss S, Avorn J, Katz JN, Weinblatt ME, Levin R, et al. Tumor necrosis factor-α antagonist use and heart failure in elderly patients with rheumatoid arthritis. *Am Heart J*. (2008) 156:336–41. doi: 10.1016/j.ahj.2008.02.025

39. Solomon DH, Rassen JA, Kuriya B, Chen L, Harrold LR, Graham DJ, et al. Heart failure risk among patients with rheumatoid arthritis starting a TNF antagonist. *Ann Rheum Dis*. (2013) 72:1813–8. doi: 10.1136/annrheumdis-2012-202136

40. Glossop JR, Dawes PT, Nixon NB, Mattey DL. Polymorphism in the tumor necrosis factor receptor II gene is associated with circulating levels of soluble tumor necrosis factor receptors in rheumatoid arthritis. *Arthritis Res Ther*. (2005) 7:R1227–34. doi: 10.1186/ar1816

41. Turan B, Pfister K, Diener PA, Helll M, Moller B, Boyvat A, et al. Soluble tumor necrosis factor receptors sTNFR1 and sTNFR2 are produced at sites of inflammation and are markers of arthritis activity in Behcet's disease. *Scand J Rheumatol*. (2008) 37:135–41. doi: 10.1080/03009740701747137

42. Shai I, Schulze MB, Manson JE, Rexrode KM, Stampfer MJ, Mantzoros C, et al. A prospective study of soluble tumor necrosis factor-alpha receptor II (sTNFRII) and risk of coronary heart disease among women with type 2 diabetes. *Diabetes Care*. (2005) 28:1376–82. doi: 10.2337/diacare.28.6.1376

43. Mendelson MM, Johannes R, Liu C, Huan T, Yao C, Miao X, et al. Epigenome-wide association study of soluble tumor necrosis factor receptor 2 levels in the framingham heart study. *Front Pharmacol*. (2018) 9:207. doi: 10.3389/fphar.2018.00207

44. Nilsson L, Szymanowski A, Swahn E, Jonasson L. Soluble TNF receptors are associated with infact size and ventricular dysfunction in ST-elevation myocardial infarction. *PLoS One*. (2013) 8(2):e55477. doi: 10.1371/journal.pone.0055477

45. Neirynck N, Glorieux G, Schepers E, Verbeke F, Venholder R. Soluble tumor necrosis factor receptor 1 and 2 predict outcomes in advanced chronic kidney disease: a prospective cohort study. *PLoS One*. (2015) 10(3):e0122073. doi: 10.1371/journal.pone.0122073

46. Carlsson AC, Ruge T, Kjoller E, Hidden J, Kolmos HJ, Sajadieh A. 10-Year associations between tumor necrosis factor receptors 1 and 2 and cardiovascular events in patients with stable coronary heart disease: a CLARICOR (effect of clarithromycin on mortality and morbidity in patients with ischemic heart disease) trial substudy. *J Am Heart Assoc*. (2018) 7:e008299. doi: 10.1161/JAHA.117.008299

47. Gibellini L, DeBiasi S, Bianchini E, Bartolomeo R, Fabiano A, Manfredini M, et al. Anti-TNF-α drugs differentially affect the TNF-α-s TNFR system and monocyte subsets in patients with psoriasis. *PLoS One*. (2016) 11(12):e0167757. doi: 10.1371/journal.pone.0167757

48. Lainez B, Fernandez-Real JM, Romero X, Esplugues E, Canete JD, Ricart W, et al. Identification and characterization of a novel spliced variant that encodes human soluble tumor necrosis factor receptor 2. *Int Immunol*. (2004) 16:169–77. doi: 10.1093/intimm/dxh014

49. Graziewicz MA, Tarrant TK, Buckley B, Orum H, Kole R, Sazani P, et al. An endogenous TNF-α antagonist induced by splice-switching oligonucleotides reduces inflammation in hepatitis and arthritis mouse models. *Mol Ther*. (2008) 16(7):1316–22. doi: 10.1038/mt.2008.85

50. Fox GJ, Orlova M, Schurr E. Tuberculosis in newborns: lessons of the "lubeck disaster" (1929-1933). *PLoS Pathog*. (2016) 12(1):e1005271. doi: 10.1371/journal.ppat.1005271

51. Akers H, Porter S. Bundaberg's gethsemane: the tragedy of the inoculated children. *Royal Historical Society Queensland J*. (2008) 20(7):261–78.

52. Massell BF, Honikman LH, Amezcua J. Rheumatic fever following streptococcal vaccination. Report of three cases. *J Am Med Assoc*. (1969) 207:1115–9. doi: 10.1001/jama.1969.03150190037007

53. Walkinshaw DR, Wright MEE, Mullin AE, Excler JL, Kim JH, Steer AC, et al. The Streptococcus pyogenes vaccine landscape. *Npj Vaccines*. (2023) 8:16. doi: 10.1038/s41541-023-00609-x

54. Lindahl G. Subdominance in antibody responses: implications for vaccine development. *Microbiol Mol Biol Rev*. (2021) 85:e00078–20. doi: 10.1128/MMBR.00078-20

55. Slon Campos JL, Mongkolsapaya J, Screaton GR. The immune responses against flaviviruses. *Nat Immunol*. (2018) 19:1189–98. doi: 10.1038/s41590-018-0210-3

56. Okuno Y, Isegawa Y, Sasao F, Ueda S. A commin neutralizing epitope conserved between the hemagglutinins of influenza A virus H1 and H2 strains. *J Virol*. (1993) 67:2552–8. doi: 10.1128/jvi.67.5.2552-2558.1993

57. Alexander J, Sidney J, Southwood S, Kubo RT, Sette A, Grey HM, et al. Development of high potency universal DR-restricted helper epitopes by modification of high affinity DR-blocking peptides. *Immunity*. (1994) 1(9):751–61. doi: 10.1016/S1074-7613(94)80017-0

58. Zhang J, Fan J, Skwarczynski M, Stephenson RJ, Toth I, Hussein WM. Peptide-based nanovaccines in the treatment of cervical cancer: a review of recent advances. *Int J Nanomed*. (2022) 17:869–900. doi: 10.2147/IJN.S269986

59. Le Buanec H, Delavallee L, Bessis N, Paturance S, Bizzini B, Gallo R, et al. TNFalpha kinoid vaccination-induced neutralizing antibodies to TNFalpha protect mice from autologous TNFalph-driven chronic and acute inflammation. *Proc Natl Acad Sci USA*. (2006) 103(51):19442–7. doi: 10.1073/pnas.0604827103

60. Durez P, Vandepapeliere P, Miranda P, Toncheva A, Berman A, Kehler T, et al. Therapeutic vaccination with TNF-kinoid in TNF antagonist-resistant rheumatoid arthritis: a phase II randomized, controlled clinical trial. *PLoS One*. (2014) 9(12):e113465. doi: 10.1371/journal.pone.0113465

61. Skwarczynski M, Toth I. Peptide-based synthetic vaccines. *Chem Sci*. (2016) 7(2):842–54. doi: 10.1039/C5SC03892H

62. Jones LH. Recent advances in the molecular design of synthetic vaccines. *Nat Chem*. (2015) 7(12):952–60. doi: 10.1038/nchem.2396

63. Nagahira K, Fukuda Y, Terakawa M, Hashino J, Nasu T, Nakazato H, et al. Epitope mapping of monoclonal antibodies to tumor necrosis factor-α. *Immunol Lett*. (1995) 46(1-2):135–41. doi: 10.1016/0165-2478(95)00031-Y

64. Zhang L, Wang J, Xu A, Zhong C, Lu W, Deng L. Rationally designed TNF-α epitope-scaffold immunogen induces sustained antibody response and alleviates collagen induced arthritis in mice. *PLoS One*. (2016) 11(9):e0163080. doi: 10.1371/journal.pone.0163080

65. Dlamini Z, Tshidino SC, Hull R. Abnormalities in alternative splicing of apoptotic genes and cardiovascular diseases. *Int J Mol Sci*. (2015) 16:27171–90. doi: 10.3390/ijms161126017

66. Amirfakhryan H. Vaccination against atherosclerosis: a brief review and update. *J Cardiol Cardiovasc Sci*. (2020) 4(1):35–40. doi: 10.29245/2578-3025/2020/1.1190

frontiers | Frontiers in Cardiovascular Medicine

TYPE Original Research
PUBLISHED 19 July 2023
DOI 10.3389/fcvm.2023.1182554

OPEN ACCESS

EDITED BY
Eltyeb Abdelwahid,
Northwestern Medicine, United States

REVIEWED BY
Antonina Giammanco,
University of Palermo, Italy
David M. Diamond,
University of South Florida, United States

*CORRESPONDENCE
Jean Ferrières
✉ jean.ferrieres@univ-tlse3.fr

RECEIVED 08 March 2023
ACCEPTED 28 June 2023
PUBLISHED 19 July 2023

CITATION
Matta A, Rabès JP, Taraszkiewicz D, Carrié D, Roncalli J and Ferrières J (2023) Effect of causative genetic variants on atherosclerotic cardiovascular disease in heterozygous familial hypercholesterolemia patients.
Front. Cardiovasc. Med. 10:1182554.
doi: 10.3389/fcvm.2023.1182554

Effect of causative genetic variants on atherosclerotic cardiovascular disease in heterozygous familial hypercholesterolemia patients

Anthony Matta[1,2,3], Jean Pierre Rabès[4,5], Dorota Taraszkiewicz[6], Didier Carrié[6], Jérôme Roncalli[6] and Jean Ferrières[6,7]*

[1]Department of Cardiology, Civilians Hospital of Colmar, Colmar, France, [2]Department of Cardiology, Notre Dame des Secours University Hospital Center, Byblos, Lebanon, [3]School of Medicine and Medical Sciences, Holy Spirit University of Kaslik, Jounieh, Lebanon, [4]Department of Biochemistry and Molecular Genetics, Ambroise Paré University Hospital (APHP), Université Paris-Saclay, Paris, France, [5]UFR (Unité de Formation et de Recherche) Simone Veil-Santé, Versailles-Saint-Quentin-en-Yvelines University, Paris, France, [6]Department of Cardiology, Toulouse University Hospital, Rangueil, France, [7]Department of Epidemiology, Health Economics and Public Health, UMR INSERM 1295, Toulouse-Rangueil University Hospital, Toulouse University School of Medicine, Toulouse, France

Background: Heterozygous familial hypercholesterolemia (HFH) is an autosomal dominant genetic disorder leading to a lifetime exposure to high low-density lipoprotein cholesterol (LDL-c) level and an increased risk of premature atherosclerotic cardiovascular disease (ASCVD). We evaluate the effect of a causative genetic variant to predict ASCVD in HFH patients undergoing treatment.
Materials and methods: A retrospective cohort was conducted on 289 patients with possible, probable, and definite diagnosis of HFH according to Dutch Lipid Clinic Network Score and in whom DNA analyses were performed and mean LDL-c level was above 155 mg/dl. The study population was divided into groups based on the presence or not of a causative variant (pathogenic or likely pathogenic). We observed each of the study's participants for the occurrence of ASCVD.
Results: A causative variant was detected in 42.2% of study participants, and ASCVD has occurred in 21.5% of HFH patients. The incidence of ASCVD (27% vs. 17.4%, $p = 0.048$) and the mean of LDL-c under an optimal medical treatment (226 ± 59 mg/dl vs. 203 ± 37 mg/dl, $p = 0.001$) were higher in HFH-causative variant carriers than others. After adjusting on confounders, ASCVD was positively associated with LDL-c level [OR = 2.347; 95% (1.305–4.221), $p = 0.004$] and tends toward a negative association with HDL-c level [OR = 0.140; 95% (0.017–1.166), $p = 0.059$]. There is no more association between the detection of a causative variant and the occurrence of ASCVD [OR = 1.708; 95% (0.899–3.242), $p = 0.102$]. Kaplan Meier and log rank test showed no significant differences in event-free survival analysis between study groups ($p = 0.523$).
Conclusion: In this study population under medical care, it seems that the presence of a causative variant did not represent an independent predictor of adverse cardiovascular outcomes in HFH patients, and LDL-c level played an undisputable causal role.

KEYWORDS

heterozygous familial hypercholesterolemia, genetic variant, cardiovascular disease, LDL-c, atherosclerosis

Introduction

Heterozygous familial hypercholesterolemia (HFH) is an autosomal dominant genetic disorder leading to a lifetime exposure to high low-density lipoprotein cholesterol (LDL-c) level and an increased risk of premature atherosclerotic cardiovascular disease (ASCVD). In most countries, the heterozygous form of familial hypercholesterolemia (FH) usually affects 1 in 313 to 120 individuals (1–3). The Dutch Lipid Clinic Network Score (DLCNS) is a valid diagnostic score for FH. It includes a set of criteria: patient's family history of early-onset cardiovascular disease in his first-degree relatives, personal history of cardiovascular disease, physical signs of hypercholesterolemia (tendinous xanthoma and/or arcus cornealis prior to age 45 years), circulating level of LDL-c, and positive DNA analysis for a genetic variant in *LDLR* (low-density lipoprotein cholesterol receptor), *APOB* (apolipoprotein B), or *PCSK9* (proprotein convertase subtilisin/kexin type-9) gene (4). DLCNS stratifies the diagnosis of FH into four categories: unlikely (<3 points), possible (3–5 points), probable (6–8 points), and definite (>8 points). Thus, DNA testing is recommended in FH patients by several international and scientific societies. It ensures a precise molecular diagnosis, a screening cascade identifying unknown and asymptomatic FH patients among closed family members, an early initiation of optimal medical therapy, and a prognostic stratification (5, 6). Apart from the traditional HFH-causing variants in *LDLR*, *APOB*, and *PCSK9* genes, the detection of mutant *APOE* gene in HFH patients is recently considered as a cause or an exacerbating factor of HFH phenotype (6–8). It seems that patients with digenic causality, combined *LDLR* and *PCSK9* gene variants, experienced poor cardiovascular outcomes marked by a high frequency of non-fatal myocardial infarction (9). It is noteworthy that the risk of obstructive coronary artery disease in HFH patients with pathogenic variant and LDL-c level of ≥190 mg/dl was 22 times higher than that of general population with LDL-c level of ≤ 130 mg/dl (10). It was also six times higher in HFH patients without pathogenic variant compared with the reference group (10). In the setting of HFH, clinical trials evaluating the risk of atherosclerosis depending on DNA analysis are scarce in literature. Most published ones assess the difference in risk between FH patients and the general population. The present study compares cardiovascular outcomes in HFH population under medical care with versus without a causative variant and evaluates the association between different gene variants and ASCVD.

Materials and methods

Study design and population

A retrospective cohort was conducted on 854 patients who were referred to the Department of Preventive Cardiology at Toulouse University Hospital, Rangueil, France, and for whom the results of DNA analysis test are available. We collected the available controls of lipid panel during the follow-up period while receiving the maximum tolerated medical therapy. The follow-up period extended from the date of the first lipid panel till the occurrence of ASCVD or the last available follow-up. The DLCNS and means of collected LDL-c levels in the course of time were calculated for each of the study's participants. Patients aged above 18 years old and who fulfilled the diagnostic criteria of possible, probable, and definite HFH according to DLCNS were included in this study (289 patients). Patients with incomplete data (lack of follow-up information), younger than 18 years old, with mean LDL-c of <155 mg/dl, and unlikely for HFH diagnosis (DLCNS of <3) were excluded from this study (558 patients). One patient with homozygous FH was also excluded. Six patients with genetic variant of unknown significance were excluded. Then, we observed study participants till the occurrence of a significant atherosclerotic cardiovascular event or the last available follow-up. The study population was divided into two groups: first, according to the development or not of ASCVD and, second, according to the detection or not of a causative variant. We evaluate the differences in the incidence of ASCVD and means of total cholesterol, LDL-c, HDL-c, triglycerides, lipoprotein(a) [Lp(a)], apolipoprotein A1 (Apo A1), and apolipoprotein B (Apo B) levels among the study groups.

Data collection and end point

Baseline characteristics of study population, results of DNA analysis, and full lipid panel tests [total cholesterol, LDL-c, HDL-c, triglycerides, Lp(a), Apo A1, and Apo B] under an optimal tolerated lipid-lowering therapy were collected throughout the follow-up period. The DLCNS and means of cholesterol, LDL-c, HDL-c, triglycerides, Lp(a), Apo A1, and Apo B levels were calculated for each of study's participants, respectively. ASCVD was defined by a more than 50% reduction in the diameter of peripheral arteries or carotids on Doppler ultrasound, an ischemic stroke was revealed on cerebral imaging, and more than 50% reduction in the coronary artery lumen was detected on a coro scanner or coronary angiography. DNA sequencing of the *LDLR*, *PCSK9*, *APOB*, and *APOE* genes were performed. All genetic variants and their causal effects were verified by "RJP" and subsequently classified as pathogenic, likely pathogenic, variant of unknown significance, likely benign, or benign. Considering their consequences, pathogenic and likely pathogenic causative genetic variants were segregated into two subtypes: moderate or severe. Severe variants encompass large rearrangements and point mutations accounting for non-sense, frameshifts, splicing, and initiation codon loss mutations. Moderate variants include missense, in-frame deletion, or duplication and 5′ regulatory mutations. The HFH-causative variant carriers group includes pathogenic and likely pathogenic variants, whereas HFH-no causative variant group includes variants of unknown significance, benign and likely benign variants, and patients with undetected genetic variant. We aim to evaluate if HFH with a causative variant patient undergoing medical care was more associated with ASCVD compared with HFH-no causative variant carrier. Patients were informed at hospital admissions that their clinical data could be used for research purposes in anonymous form, and non-opposition consent forms were obtained. The cohort was

registered by the Ministry of Research and the Regional Health Agency Occitanie (no. DC-2017-298).

Statistical analysis

Statistical analyses were performed using SPSS version 20.0. Qualitative variables were expressed by frequency and percentages, while quantitative variables were summarized as means and standard deviations. Categorical variables were compared with the use of χ^2 test or Fisher's exact test as appropriate, while continuous variables were studied with the use of *t*-test. Normality and variance homogeneity for continuous variables were checked. Kaplan–Meier curve and log rank test were used for survival analysis. Multivariable logistic regression analysis was used to test the association of ASCVD with HFH-causative variants. A two-sided *p*-value of ≤0.05 was considered to be of statistical significance.

Results

Out of 854 screened patients, a total of 289 patients were included in this study. The mean age of study population was 49 ± 13 years old, and 37% of study participants were males. Based on DLCNS, the diagnosis of HFH was definite (>8 points) in 48.8%, probable (6–8) in 4.2%, and possible (3–5) in 47.1%. The DNA analysis detected a genetic causative variant in 42.2% of study participants. The causative variants were found on *LDLR* gene in 33.6%, *APOB* gene in 7.6%, *PCSK9* in 0.3%, and *APOE* in 0.7% (**Figure 1**). Over a mean follow-up period of 5.97 ± 5.97 years, ASCVD has occurred in 21.5% of study participants. The observed cardiovascular events were coronary artery disease (1.4%), ischemic stroke (1.4%), and peripheral artery disease (1.4%). Compared with no ASCVD group, HFH patients who developed ASCVD were commonly males (48.4% vs. 33.9%, $p = 0.037$), were older (52 ± 12 vs. 48 ± 13, $p = 0.027$), and had higher means of total cholesterol (310 ± 74 vs. 288 ± 46, $p = 0.029$) and LDL-c (233 ± 66 vs. 207 ± 41, $p = 0.004$) levels. In addition, causative variants were significantly more expressed in study participants with versus without ASCVD (53.2% vs. 39.2%, $p = 0.048$) (**Table 1**). On the other hand, HFH-causative variant carriers were younger (45 ± 14 vs. 52 ± 11, $p = 0.001$) with higher mean LDL-c level (226 ± 59 vs. 203 ± 37, $p = 0.001$). Also, HFH patients with pathogenic and likely pathogenic variant were at greater risk of ASCVD (27% vs. 17.4%, $p = 0.048$) (**Table 2**). After adjusting on confounders (age, sex, HDL-c and LDL-c levels), the multivariable logistic regression showed a positive association of LDL-c level [OR = 2.658; 95% (1.495–4.729), $p = 0.001$] and age [OR = 1.034; 95% (1.009–1.060), $p = 0.008$] with ASCVD, respectively. The HDL-c level tends toward a negative association with ASCVD [OR = 0.132; 95% (0.016–1.073), $p = 0.058$], whereas male sex tends toward a positive association [OR = 1.823; 95% (1.974–3.413), $p = 0.061$]] (**Table 3**—model 1). Unlike the results of bivariate analyses, the detection of a causative variant becomes no more significantly associated with ASCVD [OR = 1.713; 95% (0.902–3.256), $p = 0.100$] (**Table 3**—model 2). Only after excluding LDL-c from the statistical model, the association between the presence of causative genetic variant and ASCVD was statistically significant [OR = 2.149; 95% (1.170–3.948), $p = 0.014$] (**Table 3**—model 3). Similar results were found after a second revision of genetic analyses stratifying study participants into three categories: severe, moderate, and no causative genetic variant (**Supplementary Tables S1** and **S2**). Note that the means of LDL-c differed significantly among study sub-groups (**Table 4**) and this difference was mainly observed between *LDLR* variant carriers and those with no causative variant ($p = 0.003$) (**Table 5**). Lastly, the Kaplan–Meier curve and log rank test failed to detect a significant difference in survival analysis for freedom of ASCVD between study groups (no causative variant vs. causative variant carriers, $p = 0.547$) (**Figure 2**).

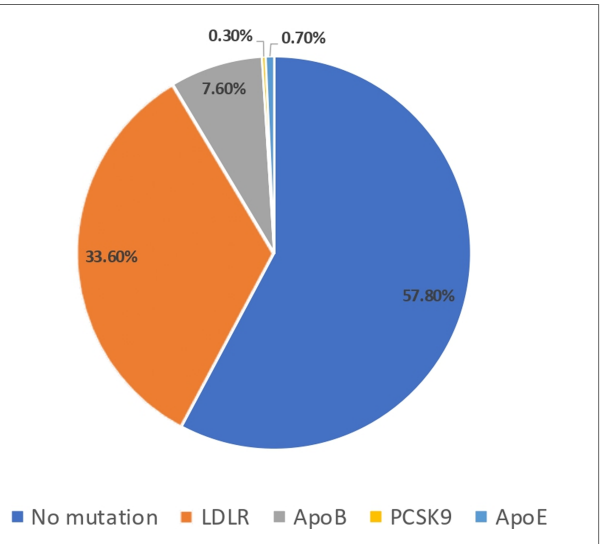

FIGURE 1
Pie chart representing the prevalence of no mutation, *LDLR*, Apo B, PCSK9, and Apo E mutations in the study population.

Discussion

The present study is one of the few available studies to report on the prediction of HFH-causative variants including *APOE* variant type. It showed that HFH-causative variant carriers are more likely exposed to cardiovascular events and expressed a higher level of LDL-c, especially those with *LDLR* variant type. However, the detection of HFH-causative variant *per se* was not significantly associated with the occurrence of ASCVD in the course of time. Thus, the increased level of LDL-c remains the strongest independent predictor of ASCVD.

To date, available evidence on the effect of genetic variants on cardiovascular risk in HFH patients is controversial. For example, in Dutch HFH patients, the effect of *LDLR* variant type on survival analysis for freedom of cardiovascular event was only observed in the statistical models after excluding LDL-c level (11). Like us, authors conclude to a greater role of LDL-c level

TABLE 1 Characteristics of study population with versus without atherosclerotic cardiovascular disease (ASCVD).

	Study population ($N = 289$)	ASCVD group ($N = 62$)	No ASCVD group ($N = 227$)	*p*-Value
Age (year)	49 ± 13	52 ± 12	48 ± 13	0.027
Males (*N*, %)	107 (37%)	30 (48.4%)	77 (33.9%)	0.037
BMI (kg/m^2)	24.3 ± 4.5	24.6 ± 3.9	24.2 ± 4.6	0.554
Smoker (*N*, %)	53 (18.3%)	11 (17.7%)	42 (18.5%)	0.891
Systemic hypertension (*N*, %)	44 (15.2%)	11 (17.7%)	33 (14.5%)	0.534
Diabetes mellitus (*N*, %)	8 (2.8%)	4 (6.5%)	4 (1.8%)	0.068
Causative mutation (*N*, %)	122 (42.2%)	33 (53.2%)	89 (39.2%)	0.048
Mutated gene (*N*, %)				0.163
LDLR	97 (33.6%)	25 (40.3%)	72 (31.7%)	
Apo B	22 (7.6%)	7 (11.3%)	15 (6.6%)	
PCSK9	1 (0.3%)	0	1 (0.4%)	
Apo E	2 (0.7%)	1 (1.6%)	1 (0.4%)	
DLNCS (*N*, %)				0.001
3–5 points (possible)	136 (47.1%)	13 (21.0%)	123 (54.2%)	
6–8 points (probable)	12 (4.2%)	11 (17.7%)	1 (0.4%)	
>8 points (definite)	141 (48.8%)	38 (61.3%)	103 (45.4%)	
Mean total cholesterol (mg/dl)	292 ± 54	310 ± 74	288 ± 46	0.029
Mean LDL-c (mg/dl)	213 ± 49	233 ± 66	207 ± 41	0.004
Mean HDL-c (mg/dl)	60 ± 25	56 ± 16	62 ± 27	0.162
Mean triglyceride (mg/dl)	125 ± 55	133 ± 58	123 ± 54	0.146
Mean Lp(a) (mg/dl)	44 ± 49	49 ± 43	43 ± 48	0.446
<10 mg/dl (%)	33%	26.3%	34.4%	0.589
10–50 mg/dl (%)	33%	34.2%	32.8%	
>50 mg/dl (%)	34%	39.5%	32.8%	
Mean Apo A1 (mg/dl)	156 ± 25	151 ± 22	157 ± 25	0.168
Mean Apo B (mg/dl)	150 ± 33	152 ± 39	149 ± 34	0.667
Follow-up (year)	5.97 ± 5.97	5.10 ± 6.36	6.20 ± 5.85	0.197

BMI, body mass index; *LDLR*, low-density lipoprotein cholesterol receptor; PCSK9, proprotein convertase subtilisin/kexin type-9; Apo, apolipoprotein; DLNCS, Dutch Lipid Network Clinic Score; LDL-c, low-density lipoprotein cholesterol; HDL-c, high-density lipoprotein cholesterol; Lp(a), lipoprotein (a).

TABLE 2 Characteristics of study population with versus without causative mutation.

	Study population ($N = 289$)	Causative mutation group ($N = 122$)	No causative mutation group ($N = 167$)	*p*-Value
Age (year)	49 ± 13	45 ± 14	52 ± 11	0.001
Males (*N*, %)	107 (37%)	46 (37.7%)	61 (36.5%)	0.838
BMI (kg/m^2)	24.32 ± 4.46	24.09 ± 5.09	24.48 ± 3.97	0.470
Smoker (*N*, %)	53 (18.3%)	24 (19.7%)	29 (17.4%)	0.617
Systemic hypertension (*N*, %)	44 (15.2%)	14 (11.5%)	30 (18%)	0.129
Diabetes mellitus (*N*, %)	8 (2.8%)	4 (3.3%)	4 (2.4%)	0.725
Mean total cholesterol (mg/dl)	292 ± 54	299 ± 66	288 ± 42	0.087
Mean LDL-c (mg/dl)	213 ± 49	226 ± 59	203 ± 37	0.001
Mean HDL-c (mg/dl)	60 ± 25	57 ± 15	63 ± 30	0.032
Mean triglyceride (mg/dl)	125 ± 55	110 ± 41	137 ± 61	0.001
Mean Lpa (mg/dl)	44 ± 49	41 ± 44	46 ± 52	0.405
<10 mg/dl (%)	33%	32.6%	33.3%	0.532
10–50 mg/dl (%)	33%	36.8%	30.4%	
>50 mg/dl (%)	34%	30.5%	36.3%	
Mean Apo A1 (mg/dl)	156 ± 25	152 ± 27	159 ± 23	0.033
Mean Apo B (mg/dl)	150 ± 35	156 ± 41	145 ± 29	0.030
ASCVD (*N*, %)	62 (21.5%)	33 (27%)	29 (17.4%)	0.048
Follow-up (year)	5.97 ± 5.97	7.31 ± 6.54	4.98 ± 5.32	0.001

BMI, body mass index; LDL-c, low-density lipoprotein cholesterol; HDL-c, high-density lipoprotein cholesterol; Lp(a), lipoprotein (a); Apo, apolipoprotein; ASCVD, atherosclerotic cardiovascular disease.

than causative variant *per se* on predicting cardiovascular risk. This shared conclusion ensues from the similarity between both study's findings, in particular multivariable analysis results. Also, a recently published large French cohort has indirectly illustrated the same finding. This cohort has showed almost similar all-cause mortality rate in HFH patients with clinical versus genetic

TABLE 3 Statistical models of multivariable logistic regression investigating the association between the presence of causative mutation and development of atherosclerotic cardiovascular disease adjusted on confounders.

Model 1			
	OR	95% CI	*p*-Value
Sex	1.823	(1.974–3.413)	0.061
Age	1.034	(1.009–1.060)	0.008
Mean LDL-c	2.658	(1.495–4.729)	0.001
Mean HDL-c	0.132	(0.016–1.073)	0.058
Model 2			
	OR	95% CI	*p*-Value
Sex	1.880	(1.000–3.532)	0.050
Age	1.040	(1.014–1.067)	0.003
Causative mutation	1.713	(0.902–3.256)	0.100
Mean LDL-c	2.336	(1.298–4.205)	0.005
Mean HDL-c	0.148	(0.018–1.223)	0.076
Model 3			
	OR	95% CI	*p*-Value
Sex	2.003	(1.076–3.728)	0.028
Age	1.044	(1.018–1.070)	0.001
Causative mutation	2.149	(1.170–3.948)	0.014
Mean HDL-c	0.236	(0.033–1.697)	0.151

OR, odds ratio; CI, confidence interval; LDL-c, low-density lipoprotein cholesterol; HDL-c, high-density lipoprotein cholesterol.

TABLE 4 Kruskal–Wallis test comparing the means of lipid panel components between study population sub-groups.

	No causative mutation ($N = 167$)	*LDLR* ($N = 97$)	Apo B ($N = 22$)	PCSK9/ Apo E ($N = 3$)	*p*-Value
Total cholesterol (mg/dl)	287 ± 42	297 ± 68	309 ± 55	289 ± 77	0.551
LDL-c (mg/dl)	203 ± 37	225 ± 61	231 ± 52	218 ± 51	0.014
HDL-c (mg/dl)	63 ± 30	55 ± 14	63 ± 15	64 ± 14	0.017
Lpa (mg/dl)	46 ± 52	42 ± 46	37 ± 38	36 ± 34	0.986
Apo A1 (mg/dl)	159 ± 23	149 ± 26	159 ± 26	174 ± 41	0.033
Apo B (mg/dl)	146 ± 29	153 ± 42	162 ± 30	194 ± 81	0.150

LDL-R, low-density lipoprotein cholesterol receptor; PCSK9, proprotein convertase subtilisin/kexin type-9; Apo, apolipoprotein; LDL-c, low-density lipoprotein cholesterol; HDL-c, high-density lipoprotein cholesterol; Lpa, lipoprotein a.

TABLE 5 Bonferroni test comparing the mean difference of low-density lipoprotein cholesterol between study sub-groups.

		95% CI	*p*-Value
	LDLR	(−0.3733; −0.0506)	0.003
No mutation	PCSK9/Apo E	(−0.8827; 0.5895)	1
	Apo B	(−0.5645; 0.0086)	0.063
	No mutation	(0.0506; 0.3733)	0.003
LDLR	PCSK9/Apo E	(−0.6753; 0.8062)	1
	Apo B	(−0.3643; 0.2324)	1
	No mutation	(−0.5895; 0.8,827)	1
PCSK9/Apo E	*LDLR*	(−0.8062; 0.6753)	1
	Apo B	(−0.9091; 0.6463)	1
	No mutation	(−0.0086; 0.5645)	0.063
Apo B	*LDLR*	(−0.2324; 0.3643)	1
	PCSK9/Apo E	(−0.6463; 0.9091)	1

LDLR, low-density lipoprotein cholesterol receptor; PCSK9, proprotein convertase subtilisin/kexin type-9; Apo, apolipoprotein.

diagnosis (5.54 vs. 4.66 per 1,000 persons). Therefore, the rates of coronary events (24.66 vs. 15.89 per 1,000), cerebral events (3.44 vs. 2.47 per 1,000), and peripheral artery disease (3.63 vs. 2.66 per 1,000) were slightly higher in those with clinical diagnosis (12). In Copenhagen general population, no significant differences in coronary artery disease and myocardial infarction-free survival were observed between *APOB* variant carriers versus non-carriers (13). A significant difference in LDL-c level was mainly observed in patients expressing *LDLR* variant type (13,14). In opposition, some studies found that HFH patients with genetic variant are at elevated risk for adverse cardiovascular outcomes compared with no-variant group (15–18). Benn M. et al. reported a risk of coronary artery disease in LDL-c receptor gene mutation carriers 3.3 times higher than that in non-carriers (13). Khera and co-workers reported that being aware of FH mutation provides additional benefits on cardiovascular risk prediction than LDL-c level alone (17). Data from Japan suggest that genetic diagnosis may identify individuals at high risk by reflecting a lifetime exposure to the increased level of LDL-c (18). In France, we observed that one-third of patients carrying a severe mutation experienced a cardiovascular event with an average of 2.5 events per patient, while one-fourth of patients carrying a moderate mutation experienced a cardiovascular event with an average of two events per patient (19). A 2- to 3-fold increase in the risk of coronary artery disease has also been reported in HFH variant carriers (16). Indeed, the baseline LDL-c before initiating a medical treatment has been only used (16). In the present study, we were interested in LDL-c profile under optimal medical therapy as it may reflect more precisely the atherosclerotic impact of a causative variant in the real-world practice. Other studies have identified an association between *LDLR* variant type and ASCVD by revealing a link with carotid plaque formation (14) and obstructive coronary artery disease (13, 14, 17, 20). This augmentation in cardiovascular risk was not observed with the remaining genetic variants, *PCSK9* and *APOB*. In line with previously published studies, we do not reveal a significant difference in cardiovascular risk related to gender in HFH patients. However, it seems likely that males could be at higher risk and HDL-c level could be inversely associated with ASCVD in such HFH-treated population (21–23). Also, it is worth highlighting the potential role of non-LDL genetic factors that result in hypercoagulation and hypofibrinolysis as causal components of ASCVD in HFH patients, independent of elevated LDL-c (24, 25). For example, Kastelein's group has shown an association between coagulation gene polymorphisms, e.g., G20210A, and ASCVD in FH patients (26). These investigators showed that FH individuals had increased factor VIII compared with non-FH (27). A literature review of these findings has been provided by Ravnskov et al. (28, 29). These findings may partially explain the beneficial effects of statins in FH due to their pleiotropic and anticoagulant effects (30–32). Thus, the discrepancy between the study's results on

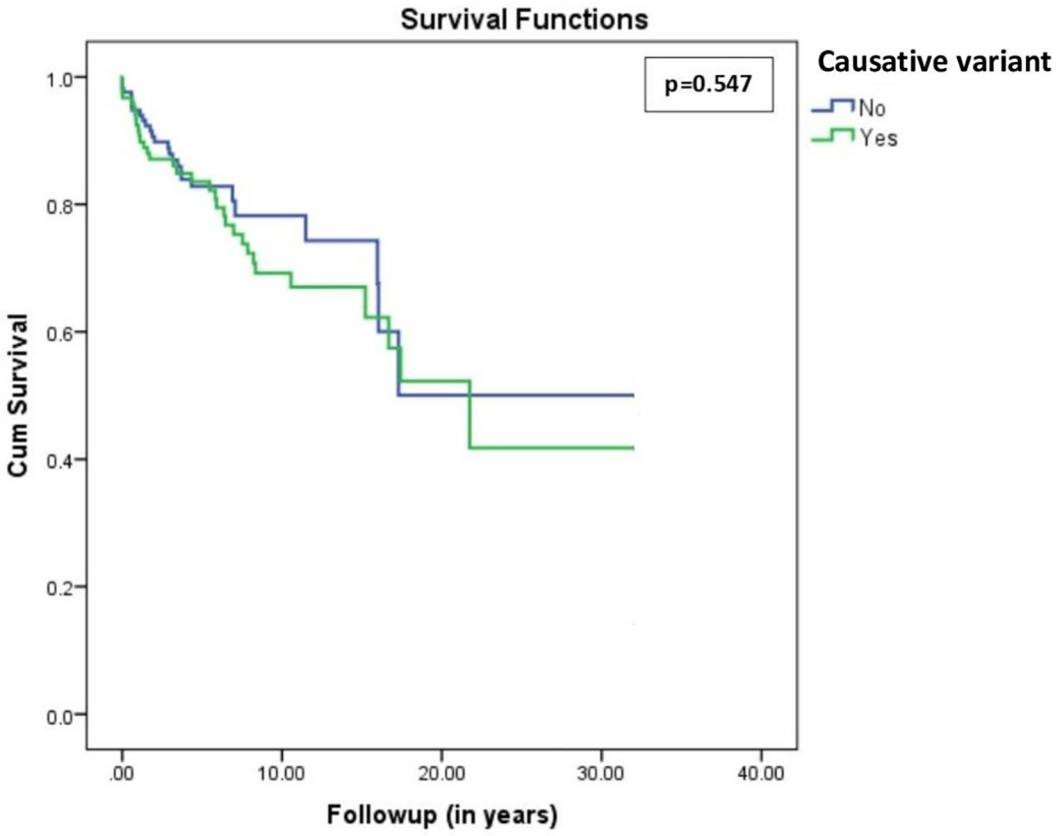

FIGURE 2
Kaplan–Meier survival analysis for freedom of atherosclerotic cardiovascular disease in FH patients with versus without causative mutation ($p = 0.547$).

atherosclerosis risk prediction of causative variant in HFH patients may be related to differences in non-LDL genetic factors' expression among the study's populations.

To summarize, it seems that the effect of a causative variant on atherosclerosis in HFH patients solely passes via the LDL-c level. Then, DNA analysis mainly plays a key role in the diagnosis and screening cascade. It provides an early diagnosis among family members and may reduce the lifelong exposure to high LDL-c level, whereas its usefulness for risk stratification remains uncertain (33, 34). A recently published paper highlights that the risk of incident cardiovascular disease event depends on a cumulative exposure to LDL-c (35). Otherwise, the cost–benefit analysis of genetic analysis tests is another concern even in the developed countries like Europe and Australia (36–38). Lastly, non-LDL genetic factors that result in hypercoagulation and hypofibrinolysis play a potential role as causal components of ASCVD in HFH patients, independent of elevated LDL-c.

Limitations

The study design may predispose to selection bias. This study was carried out in a single large tertiary center, but this also promotes the homogeneity of the patient's management and follow-up approach. The differences in lipid-lowering therapy and dose changes over time were not discussed. A large proportion of study participants were statin-intolerant patients. Statin intolerance is defined as the inability to tolerate at least two statins, one at the lowest starting dose. However, we assessed the last medical treatment of each of the study's participants. We observed that 60.9% of study participants were treated with PCSK9i alone; 26.6% with PCSK9i and statins; 9.7% with PCSK9i, statins, and ezetimibe; and 2.8% with PCSK9i and ezetimibe. The number of collected lipid panel tests varies between study participants. In addition, we mention the small sample size and limited number of study participants in *PCSK9* and *APOE* sub-groups reducing the ability to make conclusion about differences among study sub-groups. The polygenic risk score in HFH-no causative variant carriers was not evaluated noticing that it is not yet widely performed due to a less robust evidence base for utility (39).

Conclusion

The present study emphasizes the undisputable causal role of LDL-c for the occurrence of ischemic cardiovascular events in HFH patients with and without the causative genetic variant. While the incidence of ASCVD and level of LDL-c were higher

in HFH pathogenic or likely pathogenic variant carriers, the detection of a causative variant did not represent *per se* an independent predictor of adverse cardiovascular outcomes. Thus, the usefulness of DNA analysis on top of LDL-c level for prognostic classification is uncertain. Additional larger prospective studies are warranted to examine this question.

Data availability statement

The raw data supporting the conclusions of this article will be made available by the authors, without undue reservation.

Ethics statement

Ethical review and approval were not required for the study on human participants in accordance with the local legislation and institutional requirements. Written informed consent from the patients/participants or patients'/participants' legal guardian/next of kin was not required for participation in this study in accordance with the national legislation and the institutional requirements.

Author contributions

All authors contributed to the article and approved the submitted version.

Funding

Rangueil Hospital, CHU-Toulouse, provided the article processing fee.

Conflict of interest

The authors declare that the research was conducted in the absence of any commercial or financial relationships that could be construed as a potential conflict of interest.

Publisher's note

Supplementary material

The Supplementary Material for this article can be found online at: https://www.frontiersin.org/articles/10.3389/fcvm.2023.1182554/full#supplementary-material

References

1. Beheshti SO, Madsen CM, Varbo A, Nordestgaard BG. Worldwide prevalence of familial hypercholesterolemia: meta-analyses of 11 million subjects. *J Am Coll Cardiol.* (2020) 75:2553–66. doi: 10.1016/j.jacc.2020.03.057

2. Pang J, Sullivan DR, Brett T, Kostner KM, Hare DL, Watts GF. Familial hypercholesterolaemia in 2020: a leading tier 1 genomic application. *Heart Lung Circul.* (2020) 29:619–33. doi: 10.1016/j.hlc.2019.12.002

3. Bérard E, Bongard V, Haas B, Dallongeville J, Moitry M, Cottel D, et al. Prevalence and treatment of familial hypercholesterolemia in France. *Can J Cardiol.* (2019) 35:744–52. doi: 10.1016/j.cjca.2019.02.013

4. Nordestgaard BG, Chapman MJ, Humphries SE, Ginsberg HN, Masana L, Descamps OS, et al. Familial hypercholesterolemia is underdiagnosed and undertreated in the general population: guidance for clinicians to prevent coronary heart disease: consensus statement of the European atherosclerosis society. *Eur Heart J.* (2013) 34:3478–90. doi: 10.1093/eurheartj/eht273

5. Sturm AC, Knowles JW, Gidding SS, Ahmad ZS, Ahmed CD, Ballantyne CM, et al. Clinical genetic testing for familial hypercholesterolemia: JACC scientific expert panel. *J Am Coll Cardiol.* (2018) 72:662–80. doi: 10.1016/j.jacc.2018.05.044

6. Abifadel MS, Rabès JP, Boileau CR. Genetic testing in familial hypercholesterolemia. *JACC Basic Trans Sci.* (2021) 6:831–3. doi: 10.1016/j.jacbts.2021.10.004

7. Tada H, Yamagami K, Kojima N, Shibayama J, Nishikawa T, Okada H, et al. Prevalence and impact of apolipoprotein E7 on LDL cholesterol among patients with familial hypercholesterolemia. *Front Cardiovasc Med.* (2021) 8:625852. doi: 10.3389/fcvm.2021.625852

8. Abou Khalil Y, Marmontel O, Ferrières J, Paillard F, Yelnik C, Carreau V, et al. APOE Molecular spectrum in a French cohort with primary dyslipidemia. *Int J Mol Sci.* (2022) 23:5792. doi: 10.3390/ijms23105792

9. Doi T, Hori M, Harada-Shiba M, Kataoka Y, Onozuka D, Nishimura K, et al. Patients with LDLR and PCSK9 gene variants experienced higher incidence of cardiovascular outcomes in heterozygous familial hypercholesterolemia. *J Am Heart Assoc.* (2021) 10:e018263. doi: 10.1161/JAHA.120.018263

10. McGowan MP, Dehkordi SHH, Moriarty PM, Duell PB. Diagnosis and treatment of heterozygous familial hypercholesterolemia. *J Am Heart Assoc.* (2019) 8:e013225. doi: 10.1161/JAHA.119.013225

11. Souverein OW, Defesche JC, Zwinderman AH, Kastelein JJP, Tanck MWT. Influence of LDL-receptor mutation type on age at first cardiovascular event in patients with familial hypercholesterolaemia. *Eur Heart J.* (2007) 28:299–304. doi: 10.1093/eurheartj/ehl366

12. Ferrières J, Farnier M, Bruckert E, Vimont A, Durlach V, Ferrari E, et al. Burden of cardiovascular disease in a large comtemporary cohort of patients with heterozygous familial hypercholesterolemia. *Atherosclerosis Plus.* (2022) 50:17–24. doi: 10.1016/j.athplu.2022.08.001

13. Benn M, Watts GF, Tybjaerg-Hansen A, Nordestgaard BG. Mutations causative of familial hypercholesterolaemia: screening of 98098 individuals from the Copenhagen general population study estimated a prevalence of 1 in 217. *Eur Heart J.* (2016) 37:1384–94. doi: 10.1093/eurheartj/ehw028

14. Rubba P, Gentile M, Marotta G, Iannuzzi A, Sodano M, De Simone B, et al. Causative mutations and premature cardiovascular disease in patients with heterozygous familial hypercholesterolaemia. *Eur J Prev Cardiol.* (2017) 24:1051–9. doi: 10.1177/2047487317702040

15. Sharifi M, Futema M, Nair D, Humphries SE. Polygenic hypercholesterolemia and cardiovascular disease risk. *Curr Cardiol Rep.* (2019) 21:43. doi: 10.1007/s11886-019-1130-z

16. Séguro F, Rabès JP, Taraszkiewicz D, Ruidavets JB, Bongard V, Ferrieres J. Genetic diagnosis of familial hypercholesterolemia is associated with premature and high coronary heart disease. *Clin Cardiol.* (2018) 41:385–91. doi: 10.1002/clc.22881

17. Khera AV, Won HH, Peloso GM, Lawson KS, Bartz TM, Deng X, et al. Diagnostic yield and clinical utility of sequencing familial hypercholesterolemia

genes in patients with severe hypercholesterolemia. *J Am Coll Cardiol*. (2016) 67:2578–89. doi: 10.1016/j.jacc.2016.03.520

18. Tada H, Kawashiri M, Nohara A, Inazu A, Mabuchi H, Yamagishi M. Impact of clinical signs and genetic diagnosis of familial hypercholesterolaemia on the prevalence of coronary artery disease in patients with severe hypercholesterolaemia. *Eur Heart J*. (2017) 38:1573–9. doi: 10.1093/eurheartj/ehx004

19. Rabès JP, Beliard S, Carrie A. Familial hypercholesterolemia: experience from France. *Curr Opin Lipidol*. (2018) 29:65–71. doi: 10.1097/MOL.0000000000000496

20. Paquette M, Dufour R, Baass A. The montreal-FH-SCORE: a new score to predict cardiovascular events in familial hypercholesterolemia. *J Clin Lipidol*. (2017) 11:80–6. doi: 10.1016/j.jacl.2016.10.004

21. Benn M, Watts GF, Tybjaerg-Hansen A, Nordestgaard BG. Familial hypercholesterolemia in the danish general population: prevalence, coronary artery disease, and cholesterol-lowering medication. *J Clin Endocrinol Metab*. (2012) 97:3956–64. doi: 10.1210/jc.2012-1563

22. Real JT, Chaves FJ, Martinez-Uso I, Garcia-Garcia AB, Ascaso JF, Carmena R. Importance of HDL cholesterol levels and the total/HDL cholesterol ratio as a risk factor for coronary heart disease in molecularly defined heterozygous familial hypercholesterolemia. *Eur Heart J*. (2001) 22:465–71. doi: 10.1053/euhj.2000.2408

23. Bianconi V, Banach M, Pirro M. Why patients with familial hypercholesterolemia are at high cardiovascular risk? Beyond LDL-c levels. *Trends Cardiovasc Med*. (2021) 31:205–15. doi: 10.1016/j.tcm.2020.03.004

24. Nordoy A, Brox JH, Holme S, Killie JE, Lenner RA. Platelets and coagulation in patients with familial hypercholesterolemia (Type-IIA). *Acta Med Scand*. (1983) 213:129–35. doi: 10.1111/j.0954-6820.1983.tb03704.x

25. Saxon DJ. Adenosine diphosphate-induced platelet-aggregation and hypercholesterolemia. *Faseb J*. (1991) 5:A900–A900.

26. Jansen AC, Aalst-Cohen ES, Tanck MW, Cheng S, Fontecha MR, Li J, et al. Genetic determinants of cardiovascular disease risk in familial hypercholesterolemia. *Arterioscler Thromb Vasc Biol*. (2005) 25:1475–81. doi: 10.1161/01.ATV.0000168909.44877.a7

27. Huijgen R, Kastelein JJP, Meijers JCM. Increased coagulation factor VIII activity in patients with familial hypercholesterolemia. *Blood*. (2011) 118:6990. doi: 10.1182/blood-2011-10-386227

28. Ravnskov U, de Lorgeril M, Kendrick M, Diamond DM. Importance of coagulation factors as critical components of premature cardiovascular disease in familial hypercholesterolemia. *Int J Mol Sci*. (2022) 23:23. doi: 10.3390/ijms23169146

29. Ravnskov U, de Lorgeril M, Kendrick M, Diamond DM. Inborn coagulation factors are more important cardiovascular risk factors than high LDL-cholesterol in familial hypercholesterolemia. *Med Hypotheses*. (2018) 121:60–3. doi: 10.1016/j.mehy.2018.09.019

30. Undas A, Brummel-Ziedins KE, Mann KG. Anticoagulant effects of statins and their clinical implications. *Thromb Haemostasis*. (2014) 111:392–400. doi: 10.1160/Th13-08-0720

31. Barale C, Frascaroli C, Senkeev R, Cavalot F. Russo I: simvastatin effects on inflammation and platelet activation markers in hypercholesterolemia. *Biomed Res Int*. (2018) 2018. doi: 10.1155/2018/6508709

32. Harmaki N, Ikeda H, Takenada K, Katoh A, Sugano R, Yamagishi Si, et al. Fluvastatin alters platelet aggregability in patients with hypercholesterolemia: possible improvement of intraplatelet redox imbalance via HMG-Co A reductase. *Arterioscler Thromb Vasc Biol*. (2007) 27:1471–7. doi: 10.1161/ATVBAHA.106.128793

33. Ferrières J, Lambert J, Lussier-Cacan S, Davignon J. Coronary artery disease in heterozygous familial hypercholesterolemia patients with the same LDL receptor gene mutation. *Circulation*. (1995) 92:290–5. doi: 10.1161/01.CIR.92.3.290

34. Séguro F, Bongard V, Bérard E, Taraszkiewicz D, Ruidavets JB, Ferrières J. Dutch lipid clinic network low-density lipoprotein cholesterol criteria are associated with long-term mortality in the general population. *Arch Cardiovasc Dis*. (2015) 108 (10):511–8. doi: 10.1016/j.acvd.2015.04.003

35. Domanski MJ, Tian X, Wu CO, Reis JP, Dey AK, Gu Y, et al. Time course of LDL cholesterol exposure and cardiovascular disease event risk. *J Am Coll Cardiol*. (2020) 76:1507–16. doi: 10.1016/j.jacc.2020.07.059

36. Ademi Z, Watts GF, Pang J, Sijbrands EJ, Van Bockxmeer FM, O'Learly P, et al. Cascade screening based on genetic testing is cost-effective: evidence for the implementation of models of care for familial hypercholesterolemia. *J Clin Lipidol*. (2014) 8:390–400. doi: 10.1016/j.jacl.2014.05.008

37. Lazaro P, de Isla LP, Watts GF, Alonso R, Norman R, Muniz O, et al. Cost-effectiveness of a cascade screening program for the early detection of familial hypercholesterolemia. *J Clin Lipidol*. (2017) 11:260–71. doi: 10.1016/j.jacl.2017.01.002

38. Marks D, Wonderling D, Thorogood M, Lambert H, Humphries SE, Neil HA. Cost effectiveness analysis of different approaches of screening for familial hypercholesterolemia. *Br Med J*. (2002) 324:1303. doi: 10.1136/bmj.324.7349.1303

39. Sarraju A, Knowles JW. Genetic testing and risk scores: impact on familial hypercholesterolemia. *Front Cardiovasc Med*. (2019) 6:5. doi: 10.3389/fcvm.2019.00005

frontiers | Frontiers in Cardiovascular Medicine

TYPE Mini Review
PUBLISHED 01 August 2023
DOI 10.3389/fcvm.2023.1238515

OPEN ACCESS

EDITED BY
Speranza Rubattu,
Sapienza University of Rome, Italy

REVIEWED BY
Andreas Brodehl,
Heart and Diabetes Center North Rhine-Westphalia, Germany

*CORRESPONDENCE
Julian E. Stelzer
✉ julian.stelzer@case.edu

RECEIVED 11 June 2023
ACCEPTED 20 July 2023
PUBLISHED 01 August 2023

CITATION
Doh CY, Kampourakis T, Campbell KS and Stelzer JE (2023) Basic science methods for the characterization of variants of uncertain significance in hypertrophic cardiomyopathy. Front. Cardiovasc. Med. 10:1238515. doi: 10.3389/fcvm.2023.1238515

Basic science methods for the characterization of variants of uncertain significance in hypertrophic cardiomyopathy

Chang Yoon Doh[1], Thomas Kampourakis[2], Kenneth S. Campbell[3] and Julian E. Stelzer[4]*

[1]School of Medicine, Case Western Reserve University, Cleveland, OH, United States, [2]Randall Centre for Cell and Molecular Biophysics, and British Heart Foundation Centre of Research Excellence, King's College London, London, United Kingdom, [3]Division of Cardiovascular Medicine, University of Kentucky, Lexington, KY, United States, [4]Department of Physiology and Biophysics, School of Medicine, Case Western Reserve University, Cleveland, OH, United States

With the advent of next-generation whole genome sequencing, many variants of uncertain significance (VUS) have been identified in individuals suffering from inheritable hypertrophic cardiomyopathy (HCM). Unfortunately, this classification of a genetic variant results in ambiguity in interpretation, risk stratification, and clinical practice. Here, we aim to review some basic science methods to gain a more accurate characterization of VUS in HCM. Currently, many genomic data-based computational methods have been developed and validated against each other to provide a robust set of resources for researchers. With the continual improvement in computing speed and accuracy, in silico molecular dynamic simulations can also be applied in mutational studies and provide valuable mechanistic insights. In addition, high throughput *in vitro* screening can provide more biologically meaningful insights into the structural and functional effects of VUS. Lastly, multi-level mathematical modeling can predict how the mutations could cause clinically significant organ-level dysfunction. We discuss emerging technologies that will aid in better VUS characterization and offer a possible basic science workflow for exploring the pathogenicity of VUS in HCM. Although the focus of this mini review was on HCM, these basic science methods can be applied to research in dilated cardiomyopathy (DCM), restrictive cardiomyopathy (RCM), arrhythmogenic cardiomyopathy (ACM), or other genetic cardiomyopathies.

KEYWORDS

hypertrophic cardiomyopathy (HCM), dilated cardiomyopathy (DCM), variants of uncertain clinical significance (VUS), restrictive cardiomyopathy (RCM), high throughput screen (HTS), mathematical modeling & simulation, arrhythmogenic cardiomyopathy, cardiac myosin binding protein C (cMyBP-C)

Introduction

Hypertrophic cardiomyopathy (HCM) is a common heart condition with a prevalence of 1:200–500 (1, 2). It is characterized by an increase in left ventricular wall thickness in the absence of abnormal loading conditions and without an identifiable secondary cause such as hypertension or aortic stenosis (3). It is thought to be a result of heterogeneous sets of mutations in sarcomere proteins (4, 5). Since HCM is highly variable in both expressivity and penetrance with many modifying factors (6, 7), the precise genetic determination is important for diagnosis, treatment, and prognosis.

About 40%–60% of people suffering from HCM have one or more mutations in sarcomere proteins (3, 5, 8). Of the genes with established pathogenicity for HCM (9), the vast majority (35%–60%) are found in the genes encoding for cardiac myosin binding protein C (*MYBPC3*) and myosin heavy chain (*MYH7*) (8, 10, 11) (**Figure 1A**). Of those, a significant proportion is thought to be due to missense mutations (4%–19% in *MYBPC3%* and 93% in *MYH7*), underlying its substantial contribution to HCM (11–13). Other genes that contribute a smaller proportion of HCM cases include *TNNT2* (5%–10%), *TNNI3* (5%–7%), *MYL2* (2%–4%), *MYL3* (1%–2%), *TPM1* (<1%), and *ACTC1* (<1%) (14). Interestingly, pathogenic substitutions seem to cluster in certain regions of the mutated protein (12, 15–17). For example, HCM-linked missense variants in MYBPC3 have been shown to cluster in specific regions, i.e., domains C3, C6 and C10, suggesting that those domains might be mutational "hot-spots" (12). Similarly, HCM-linked variants in MYH7 cluster in specific regions commonly associated with stabilizing the cardiac myosin head OFF state (i.e., interacting heads motif), in good agreement with the myofilament hypercontractile phenotype of HCM variants (18).

A variety of techniques are used to identify genetic variants, such as whole genome sequencing or targeted HCM multigene panels. The variants are then classified based on criteria developed by the American College of Medical Genetics and Genomics (19, 20). Although whole genome techniques yielded larger numbers of pathogenic variants helping confirm the diagnosis for many (21, 22), it also resulted in an exponential increase in "variants with uncertain significance" (VUS) (23). As a result, there is ambiguity and difficulty in clinical interpretation.

Due to these limitations, VUS are typically disregarded in the clinical decision-making process because there is insufficient information (5, 24). However, prior research showed that sarcomere mutations of uncertain significance or multiple VUS variants in an individual with HCM are associated with earlier disease onset and worse outcomes, thus, improved VUS characterization is critical for clinical management and improved outcomes (23, 25).

Here, we provide a roadmap of validated basic science methods and emerging concepts to help reclassify VUS and address the current limitations of VUS interpretation. These methods can improve characterization of HCM-associated VUS by obtaining molecular, mechanistic, and functional information, thereby, aid in risk stratification, improved medical management and prognostication. Finally, characterization of the pathogenicity or mechanisms of VUS will facilitate development of targeted disease-modifying therapies. These methods can be applied to research in dilated cardiomyopathy (DCM), restrictive cardiomyopathy (RCM), arrhythmogenic cardiomyopathy (ACM), or other genetic cardiomyopathies.

Computational and genomic methods used in identification of VUS

The classification of mutations in people with HCM starts with pooling data from population, disease and sequence databases and *de novo*, allelic, computational, predictive, or segregation data (19, 26). Gene-level experimental tools for high throughput screening of identified HCM mutations for pathogenicity, are reviewed elsewhere (27–29). Although large databases like the ClinVar database (https://www.ncbi.nlm.nih.gov/clinvar/), SHaRe registry https://www.theshareregistry.org/), and HGMD database (https://www.hgmd.cf.ac.uk/ac/index.php) have been created and curated by the above-mentioned computational methods, large numbers of HCM mutations are still classified as VUS and require re-classification (9, 25, 30).

Many computational tools were developed to improve the prediction of the pathogenicity of genetic variants in recent years (31–33). CardioBoost utilizes an algorithm called "disease-specific variant classifier" to predict the pathogenicity of missense variants of inherited cardiomyopathies and arrhythmias (34). The authors showed a high level of accuracy for variants classified with >90% confidence, which were associated with disease status and clinical severity (34). In fact, disease-specific classifiers have been shown to perform better than methods not trained specifically on features specific to the genes involved in HCM (35). A similar machine learning algorithm using the etiological fraction showed that 4%–20% of cases could be reclassified into pathogenic variants and be used for clinical applications and predictive testing in probands' relatives (36).

Other tools utilize high-resolution structural data of proteins and the effect that mutations have on protein folding and stability to predict their pathogenicity (37). A study of people with *MYBPC3* VUS using the STRUM tool (evaluating the change in free energy of domain folding upon introduction of a mutation) showed that mutations that produced misfolding were associated with lower event-free survival (38).

Developments in neural networks and artificial intelligence also allow identification of pathogenicity in cardiac sarcomere protein mutations. For example, the disease mutation, phenotype, and pathogenicity in cardiac myosin and myosin binding protein C (MyBPC) mutations were combined to predict global disease mechanism using a neural/Bayes network (39). Although there are limitations in AI technology, work has been done to overcome those challenges and aid in a robust characterization of the functional consequences of VUS and the interpretation of variant classification (40).

Because many computational algorithms have not been validated, the relative performance in identifying potential pathogenicity of variants were assessed in a recent study (11). The authors developed a method to perform variant prediction benchmarks and quantified which algorithms were better in discriminating HCM variant pathogenicity than others (11). They reported that utilizing a combination of the best performing tools can help to narrow down the most important VUS to screen (11).

As there are many different computational tools (11, 32), it may be beneficial to create a consolidated platform of all available algorithms to streamline the in-silico re-classification process, and potentially produce a combined score of pathogenicity scaled by the tested accuracy of each tool. The combine use of these rapid computational algorithms may improve accuracy of prediction and help guide clinical practice.

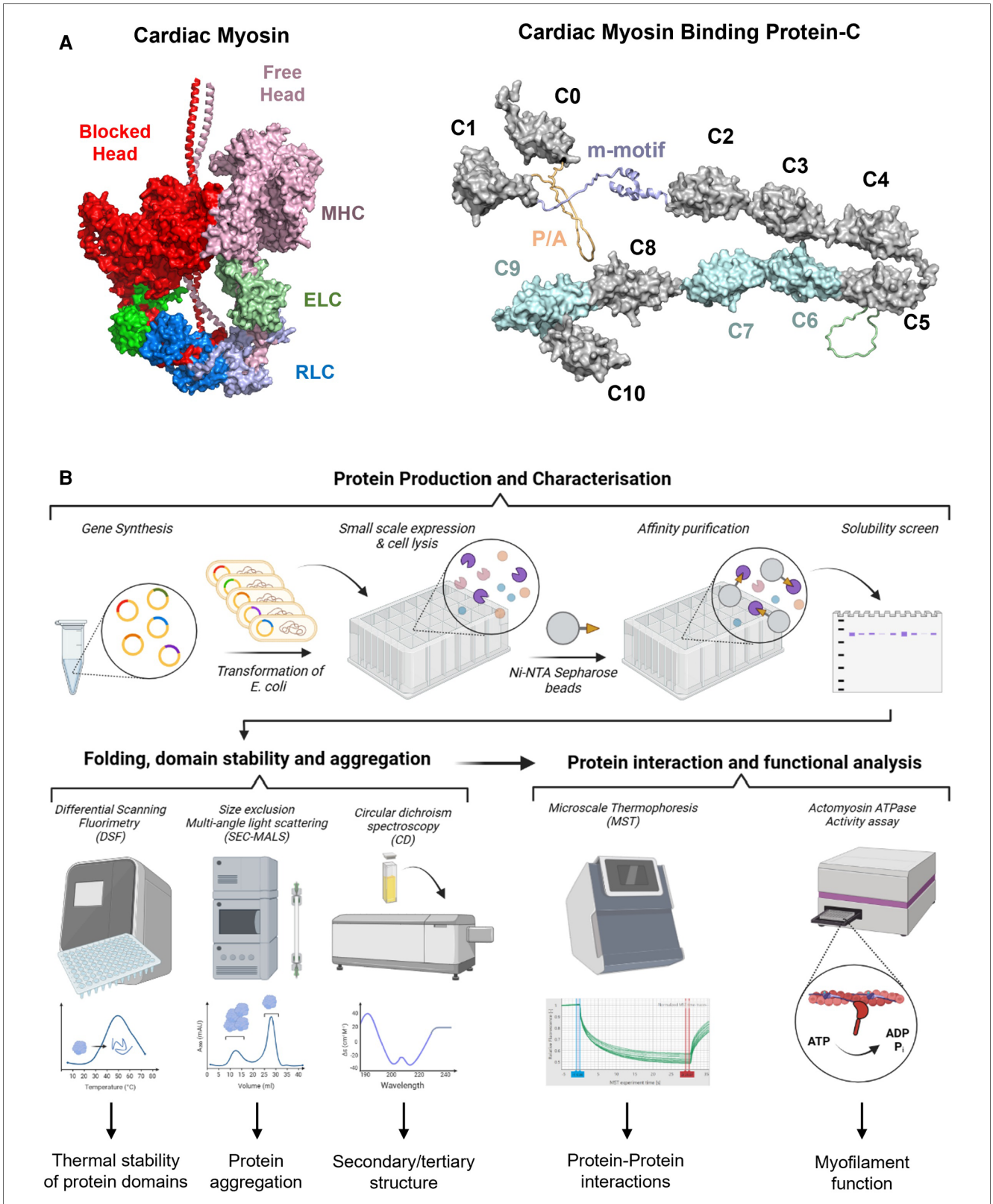

FIGURE 1
(A) Structural models of cardiac myosin folded into the interacting heads motif (left) and cardiac myosin binding protein-C (right). Individual domains are labelled accordingly. RLC, regulatory light chain; ELC, essential light chain; MHC, myosin heavy chain; P/A, proline/alanine-rich linker. (B) High throughput *in vitro* screening process for VUS in genes associated with HCM. Gene synthesis and expression allows an initial screen for protein folding and production of purified proteins for characterization. A variety of biophysical techniques such as differential scanning fluorimetry, circular dichroism spectroscopy, and size exclusion multi-angle scattering can aid in characterizing the folding pathway, protein stability, and aggregation potential. More advanced techniques such as microscale thermophoresis or NADH-coupled ATPase assays can also be performed in high throughput micro-well formats. By utilizing this high throughput *in vitro* screening pipeline, it will be possible to obtain mechanistically and clinically meaningful information for VUS in HCM.

Rapid protein modeling and molecular dynamics simulations

With improvements in various aspects of molecular dynamics simulations (MDS) such as modeling software, high performance computing, or advanced sampling techniques, MDS can be readily applied to mutational analyses of VUS in HCM (41–44) (**Figure 1A**). In the protein simulation workflow, one of the most time-consuming processes is model creation and validation. A recently developed tool ("Ensembler") may enable a high throughput method to produce simulation-ready ensembles of protein models with and without VUS mutations (45). It can accomplish the series of tasks necessary to build a validated model by combining various tools and libraries including homology modeling, refinement, protonation, solvation, and simulation using open-source Python codes that can also be customized (45).

Following the modeling process, many techniques can be applied to study HCM VUS pathogenicity. One method is simply to simulate two models, one with and without the VUS of interest, and to compare the results of protein structure, dynamics, or interactions. However, this method can be time consuming and require much user input. Thus, many automated or semiautomated servers and tools have been developed to accelerate the process. In the Galaxy server, one can rapidly assess hydrogen bond interactions and principal components (transforming higher dimensional data to a set of orthogonal axes) to determine how intra- and inter-molecular structure and dynamics are affected by the VUS (46). In the tool HTMD, more detailed parameters such as relaxation or equilibrium time scales, folding/unfolding pathways, standard free energy, protein conformation, and secondary structure changes can be screened (47). Other high throughput MDS methods and algorithms assess the mechanism or kinetics of protein-ligand association and modulation by amino acid substitutions (48).

The automation process provides valuable information about a HCM VUS rapidly, but it will still require further study for "hits" or mutations that seem to alter structure or function. For example, a confirmatory MDS study for an HCM-causing substitution in cMyBPC (p.Y235S) showed that this pathogenic variant altered specific intramolecular interactions that explained the hypercontractile cross bridge behavior (41). Another study showed that protein MDS combined with experimental correlation was helpful in reclassification of VUS (49). They used the averaged structural changes resulting from various thin filament protein variants together with differential scanning calorimetry (DSC) experiments to propose the reclassification of nine VUS mutations as benign, likely benign, likely pathogenic, and pathogenic (49). Such combinatorial workflow can provide an additional method to reaffirm disease mechanisms.

Simulations can be time consuming and resource heavy; however, with the continual improvement in the speed of computation, and streamlining processes of simulations, we foresee that in silico modeling and simulation will be a valuable tool in assessing pathogenicity of many HCM VUS.

High throughput *in vitro* screening tools for rapid characterization of VUS

Although in silico methods for predicting variant pathogenicity have significantly improved over the last decade (50), the output scores or results do not inform about potential molecular etiologies. More biologically meaningful insights into the structural and functional effects of VUS can be gained by utilizing high throughput pipelines for the production, and biophysical and biochemical characterization of a large number of protein constructs (**Figure 1B**).

Gene synthesis has become an affordable tool for the design and creation of large libraries of protein expression constructs. Subsequent small-scale expression of these constructs in micro-well format not only allows an initial screen for protein folding by measuring the distribution of protein variants in the soluble and insoluble cellular fractions(51), but also generates sufficient material (usually in the low milligram scale) for initial biophysical characterization (52). Hexahistidine-tagged single or multi-domain constructs of sarcomere proteins can be produced in high yields and purified to >90% homogeneity using a single optimized purification step (53), suggesting that the production of large number of protein constructs carrying individual VUS is highly feasible. Recombinant proteins produced from bacterial sources usually do not carry any post-translational modifications (PTMs) identified in the mammalian heart *in vivo* (i.e., serine or threonine phosphorylation). However, known PTMs can be readily introduced into purified protein constructs using *in vitro* biochemical assays (53–55) and incorporated into the analysis pipeline.

Misfolded proteins can derail proteostasis by aggregate-formation, local cleavage or accelerated protein turnover (56). Stability of solubly expressed protein domains can be directly assessed in a high throughput manner via differential scanning fluorimetry (DSF) in either 96- or 384-well format, which allows for the identification of variants that likely alter domain folding by changes in the observable melting temperature (57–60). Initial "hits" in DSF screen can subsequently be confirmed using orthogonal methods such as circular dichroism (CD) spectroscopy, which can give additional information of changes in protein secondary and tertiary structure. More recently, a high-throughput label-free chemical denaturation workflow has been developed that allows the determination of protein thermodynamic stability using a semi-automated plate reader system (52). Lastly, size exclusion-multi angle light scattering (SEC-MALS) in combination with an auto-sampler allows the rapid assessment of the aggregation behavior of large number of protein variants. The combined workflow of solubility screens, and various techniques to assess domain stability and folding will allow the rapid identification of potential pathogenic variants that cause HCM via changes in proteostasis.

Previous studies showed that about a third of investigated VUS in *MYBPC3* do not affect either mRNA or protein stability (61, 62), adding an additional layer of complexity and difficulty to the classification of those variants into either benign or pathogenic.

Variants that do not affect mRNA/protein stability are likely to alter protein-protein interactions (39). However, traditional techniques such as isothermal titration calorimetry or surface plasmon resonance spectroscopy severely limit the number of variants that can be examined because they are too time consuming.

This limitation can be overcome by incorporating new biophysical interaction techniques into the *in vitro* screening pipeline. Microscale thermophoresis (MST) is a rapid and sensitive method to quantify biomolecular interactions, which in contrast to classical methods is highly material-, time-, and cost-efficient (63, 64). MST measures the movement of biomolecules along temperature gradients which is determined by the molecule's size and shape, hydration shell and surface charge distribution. Previous studies have successfully used MST to characterize the binding of sarcomere protein domains to both thin and thick filament components (53, 65, 66). Moreover, recent developments in plate reader technologies accelerated the measurement of myofilament protein function by utilizing Foerster Resonance Energy Transfer (FRET)-based technologies to probe protein-protein interactions (67, 68). FRET is based on the radiation-free transfer of energy from a donor to an acceptor fluorophore when they are in sufficient proximity to each other (<15 nm). It can therefore be employed to determine both the structural dynamics and interactions of proteins. Recent studies have successfully employed FRET to test for the effects of HCM-associated mutations on cMyBPC structural dynamics and its interaction with both actin and myosin (68, 69).

Additionally, myofilament function can readily be measured in a high throughput micro-well format using NADH-coupled ATPase assays (70). Previous studies used this assay system to measure the effects of cMyBPC fragments on thin filament activation (71), and protocols can be readily adopted to test for the functional effects of a plethora of VUS in other proteins. Lastly, induced pluripotent stem cells (iPSCs) have diverse applications and are extensively used in genetic studies, but are the topic of other focused reviews and are not reviewed here (72–82).

In summary, high throughput *in vitro* screening pipelines have the potential to not only discriminate between pathogenic and benign variants, but also help to understand the molecular etiologies associated with individual variants (**Figure 1**). Integration of experimental results into meaningful matrices to assess pathogenicity, and bridging between the structural and functional consequences observed in isolated proteins to cell and organ level function are areas of focus for future improvements.

Mathematical modeling and simulation to explore effects of VUS on higher level function

Computer modeling may be able to complement the experimental techniques described above and eventually be scaled to test a large number of VUS in short time. The primary goal would be to develop a framework that can predict whether a variant will lead to clinically significant organ-level dysfunction. Once that is accomplished, it might be possible to extend the framework to test potential therapeutic interventions.

Both sarcomere (83–85) and organ-level (85, 86) modeling have rich histories but screening cMyBPC VUS is particularly challenging. In particular, the computer model will need to span from molecular events that occur with timescales of milliseconds to organ-level growth that takes place over weeks and months (87). Numerous challenges will need to be overcome.

We will take cMyBPC as an example. At the sarcomere level, the computer model will need to reproduce the effects of cMyBPC VUS on myofilament level function. At present, cMyBPC is thought to modulate contractile function in two ways: by stabilizing myosin heads in their functional OFF or super-relaxed state, and by extending towards and subsequently binding to thin filaments, which can alter its regulatory state. These competing effects are further complicated by the fact that cMyBPC is localized to distinct regions of thick filaments so that some myosin heads are likely to be directly impacted by cMyBPC while others are left unaffected. Recent structural data suggests that even within the C-zone, each of the three crowns within the thick filament's 43 nm repeat could interact with cMyBPC in a different way (88, 89). Different strategies for simulating these interactions exist (90) but spatially-explicit models that track the location and status of individual molecules in the filament lattice arguably provide the most direct approach (91–93). This area of work remains relatively underdeveloped, but there are published simulations performed using the FiberSim framework that predict how different modes of cMyBPC function will impact myofilament contractile function (94).

Scaling towards the organ level provides additional challenges because of the heart's complex shape and motion during the cardiac cycle. The most common approach is to use finite element modeling, but this technique is very computationally demanding. As a result, most organ-level models are based on very simple contraction modules that are unable to capture the complexity of cMyBPC effects. One approach would be to embed a spatially explicit system like FiberSim (94) inside each element of a complex 3D model, but these calculations will have to be optimized for wide-spread deployment. A simpler alternative is to drive an organ-level model like CircAdapt (95) with a sarcomere-level system that can capture cMyBPC's effects.

One of the remaining challenges is how to simulate growth. By definition, individuals with HCM have abnormally thick ventricular walls. Ideally, the modeling framework would be able to capture that thickening so that benign variants of cMyBPC lead to hearts of normal size while pathogenic mutations produce walls that thicken over time. This is another area of cutting-edge research, and the technology is advancing rapidly (96). Most models to date have used macroscopic variables, such as stress or strain, to drive growth but recent studies (97) suggest that intrinsic sarcomere-level contractility may be a better predictor of wall thickening. Whether eccentric growth (changes in chamber diameter) is paired directly to concentric growth (changes in wall thickness) remains unclear.

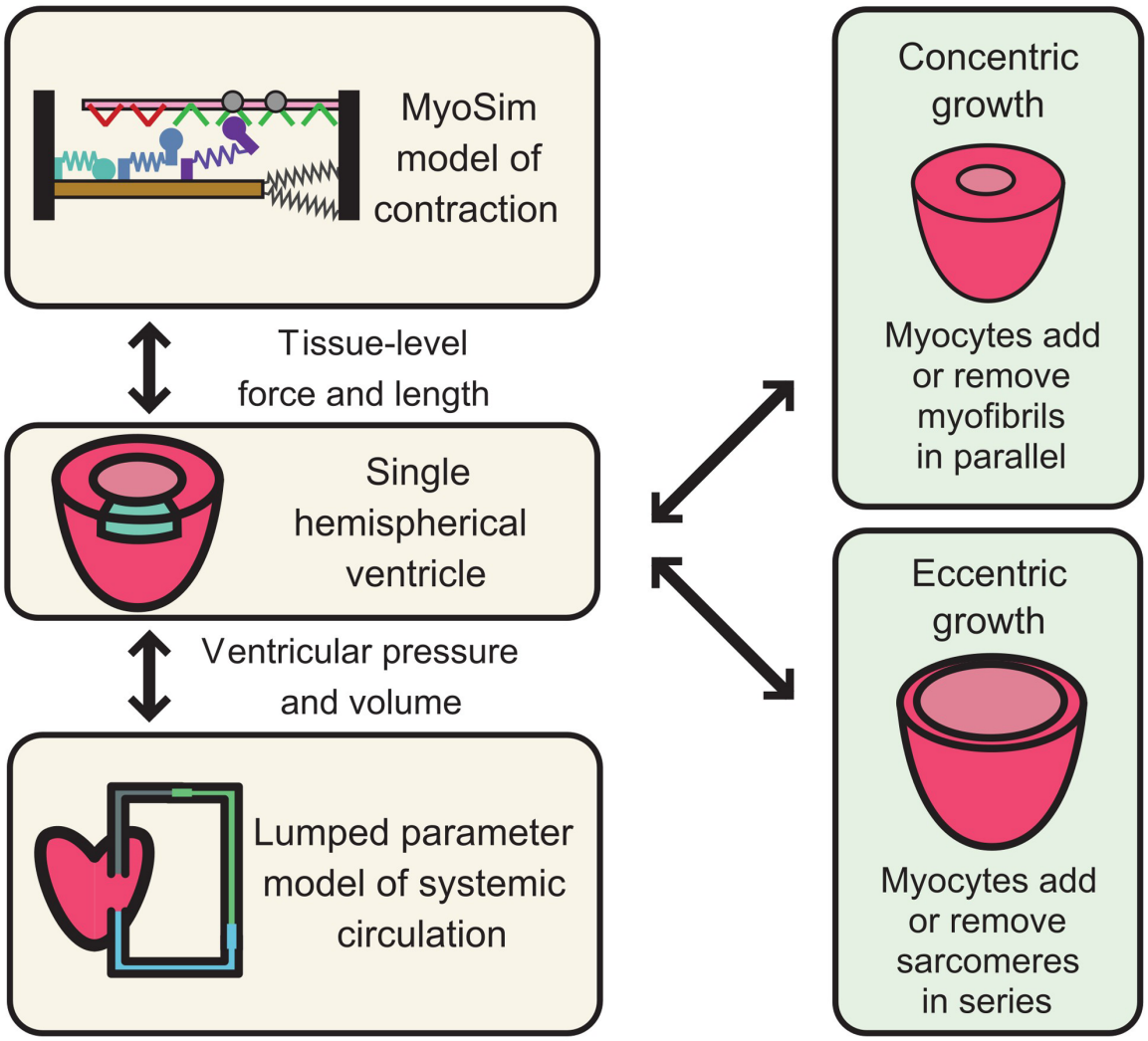

FIGURE 2
Mathematical modeling and simulation framework for HCM-associated VUS in cardiac MyBPC. The left-hand panels illustrate a multiscale system in which a sarcomere-level model of myofilament function is embedded inside a ventricle and pumps blood around a closed circulation. Growth can be added to this framework by allowing myocytes to add myofibrils in parallel (concentric growth, wall thickening) or to add sarcomeres in series (eccentric growth, chamber dilation). If the approach is to be useful for testing the potential impact of VUS, the sarcomere-level model must reproduce the different potential biophysical actions of cardiac MyBPC.

In summary, computer modeling has the potential to help bridge the gap between genetic variants and predictions of clinically important phenotypes (**Figure 2**). This will require bridging multiple structural and temporal scales, but important components of the framework already exist at each level. The main challenge will be developing a system that links the disparate scales together.

Discussion and perspectives

The key issues regarding variants of uncertain significance are the huge numbers of variants identified with genome sequencing technology, difficulty in interpretation, and lack of use in clinical decision making. We reviewed various existing basic science tools and emerging frameworks to address some of these limitations facing VUS interpretation, and how these technologies can be applied to characterize or reclassify HCM-causing VUS. Although there are still many limitations of various algorithms and techniques mentioned, it may provide a conceptual workflow to guide future work in elucidating the functional role of a VUS in HCM. There are other basic science methods not reviewed here that may be applicable as well (e.g., rapid animal model generation and testing) (98–100). By utilizing advanced computational techniques and simulation, high throughput *in vitro* methods, and multi-level mathematical modeling, the improved characterization of HCM VUS will facilitate better medical decision making, improve risk stratification, and allow personalized treatment options. The exploration of VUS

causing HCM may also lay the foundation for further detailed *in vivo* functional experiments or clinical trials to evaluate evidence-based therapies.

Author contributions

All authors contributed to the article and approved the submitted version.

Funding

This work was supported by grants awarded by the NIH National Heart, Lung, and Blood Institute (NHLBI) grants R01 HL146676 and R01 HL114770.

Conflict of interest

The authors declare that the research was conducted in the absence of any commercial or financial relationships that could be construed as a potential conflict of interest.

Publisher's note

References

1. Baudhuin LM, Kotzer KE, Kluge ML, Maleszewski JJ. What is the true prevalence of hypertrophic cardiomyopathy? *J Am Coll Cardiol*. (2015) 66:1845–6. doi: 10.1016/j.jacc.2015.07.074

2. Amberger JS, Bocchini CA, Schiettecatte F, Scott AF, Hamosh A. OMIM.Org: online mendelian inheritance in man (OMIM®), an online catalog of human genes and genetic disorders. *Nucleic Acids Res*. (2015) 43:D789–98. doi: 10.1093/nar/gku1205

3. Marian AJ, Braunwald E. Hypertrophic cardiomyopathy. *Circ Res*. (2017) 121:749–70. doi: 10.1161/CIRCRESAHA.117.311059

4. Ho CY, Charron P, Richard P, Girolami F, Van Spaendonck-Zwarts KY, Pinto Y. Genetic advances in sarcomeric cardiomyopathies: state of the art. *Cardiovasc Res*. (2015) 105:397–408. doi: 10.1093/cvr/cvv025

5. Elliott PM, Anastasakis A, Borger MA, Borggrefe M, Cecchi F, Charron P, et al. ESC guidelines on diagnosis and management of hypertrophic cardiomyopathy: the Task Force for the Diagnosis and Management of Hypertrophic Cardiomyopathy of the European Society of Cardiology (ESC). *Eur Heart J*. (2014) 35(39):2733–79. doi: 10.1093/eurheartj/ehu284

6. Roma-Rodrigues C, Fernandes AR. Genetics of hypertrophic cardiomyopathy: advances and pitfalls in molecular diagnosis and therapy. *Appl Clin Genet*. (2014) 7:195–208. PMID: 25328416; PMCID: PMC4199654. doi: 10.2147/TACG.S49126.

7. Semsarian C, Semsarian CR. Variable penetrance in hypertrophic cardiomyopathy. *J Am Coll Cardiol*. (2020) 76:560–2. doi: 10.1016/j.jacc.2020.06.023

8. Cheng Z, Fang T, Huang J, Guo Y, Alam M, Qian H. Hypertrophic cardiomyopathy: from phenotype and pathogenesis to treatment. *Front Cardiovasc Med*. (2021) 8:722340. PMID: 34760939; PMCID: PMC8572854. doi: 10.3389/fcvm.2021.722340.

9. Landrum MJ, Lee JM, Benson M, Brown GR, Chao C, Chitipiralla S, et al. Clinvar: improving access to variant interpretations and supporting evidence. *Nucleic Acids Res*. (2018) 46:D1062–7. doi: 10.1093/nar/gkx1153

10. Bourfiss M, van Vugt M, Alasiri AI, Ruijsink B, van Setten J, Schmidt AF, et al. Prevalence and disease expression of pathogenic and likely pathogenic variants associated with inherited cardiomyopathies in the general population. *Circ Genom Precis Med*. (2022) 15(6):e003704. Epub 2022 Oct 20. PMID: 36264615; PMCID: PMC9770140. doi: 10.1161/CIRCGEN.122.003704.

11. Barbosa P, Ribeiro M, Carmo-Fonseca M, Fonseca A. Clinical significance of genetic variation in hypertrophic cardiomyopathy: comparison of computational tools to prioritize missense variants. *Front Cardiovasc Med*. (2022) 9:975478. PMID: 36061567; PMCID: PMC9433717. doi: 10.3389/fcvm.2022.975478.

12. Helms AS, Thompson AD, Glazier AA, Hafeez N, Kabani S, Rodriguez J, et al. Spatial and functional distribution of *MYBPC3* pathogenic variants and clinical outcomes in patients with hypertrophic cardiomyopathy. *Circ Genom Precis Med*. (2020) 13:396–405. doi: 10.1161/CIRCGEN.120.002929

13. Carrier L. Targeting the population for gene therapy with MYBPC3. *J Mol Cell Cardiol*. (2021) 150:101–8. doi: 10.1016/j.yjmcc.2020.10.003

14. Gerull B, Klaassen S, Brodehl A. The genetic landscape of cardiomyopathies. In: Erdmann J, Moretti A, editors. *Genetic causes of cardiac disease. Cardiac and vascular biology*. Cham: Springer (2019). Vol. 7. Issue 45–91. https://doi.org/10.1007/978-3-030-27371-2_2

15. Harris SP, Lyons RG, Bezold KL. In the thick of it. *Circ Res*. (2011) 108:751–64. doi: 10.1161/CIRCRESAHA.110.231670

16. Homburger JR, Green EM, Caleshu C, Sunitha MS, Taylor RE, Ruppel KM, et al. Multidimensional structure-function relationships in human β-cardiac myosin from population-scale genetic variation. *Proc Natl Acad Sci USA*. (2016) 113:6701–6. doi: 10.1073/pnas.1606950113

17. Waring A, Harper A, Salatino S, Kramer C, Neubauer S, Thomson K, et al. Data-driven modelling of mutational hotspots and in silico predictors in hypertrophic cardiomyopathy. *J Med Genet*. (2021) 58:556–64. doi: 10.1136/jmedgenet-2020-106922

18. Alamo L, Ware JS, Pinto A, Gillilan RE, Seidman JG, Seidman CE, et al. Effects of myosin variants on interacting-heads motif explain distinct hypertrophic and dilated cardiomyopathy phenotypes. *Elife*. (2017) 6:e24634. PMID: 28606303; PMCID: PMC5469618. doi: 10.7554/eLife.24634.

19. Richards S, Aziz N, Bale S, Bick D, Das S, Gastier-Foster J, et al. Standards and guidelines for the interpretation of sequence variants: a joint consensus recommendation of the American college of medical genetics and genomics and the association for molecular pathology. *Genet Med*. (2015) 17:405–24. doi: 10.1038/gim.2015.30

20. Arbustini E, Behr ER, Carrier L, van Duijn C, Evans P, Favalli V, et al. Interpretation and actionability of genetic variants in cardiomyopathies: a position statement from the European society of cardiology council on cardiovascular genomics. *Eur Heart J*. (2022) 43:1901–16. doi: 10.1093/eurheartj/ehab895

21. Richard P, Charron P, Carrier L, Ledeuil C, Cheav T, Pichereau C, et al. Hypertrophic Cardiomyopathy. *Circulation*. (2003) 107:2227–32. doi: 10.1161/01.CIR.0000066323.15244.54

22. Van Driest SL, Ellsworth EG, Ommen SR, Tajik AJ, Gersh BJ, Ackerman MJ. Prevalence and Spectrum of thin filament mutations in an outpatient referral population with hypertrophic cardiomyopathy. *Circulation*. (2003) 108:445–51. doi: 10.1161/01.CIR.0000080896.52003.DF

23. Burns C, Bagnall RD, Lam L, Semsarian C, Ingles J. Multiple gene variants in hypertrophic cardiomyopathy in the era of next-generation sequencing. *Circ Cardiovasc Genet*. (2017) 10(4):e001666. PMID: 28790153. doi: 10.1161/CIRCGENETICS.116.001666.

24. Charron P, Arad M, Arbustini E, Basso C, Bilinska Z, Elliott P, et al. Genetic counselling and testing in cardiomyopathies: a position statement of the European society of cardiology working group on myocardial and pericardial diseases. *Eur Heart J*. (2010) 31:2715–26. doi: 10.1093/eurheartj/ehq271

25. Ho CY, Day SM, Ashley EA, Michels M, Pereira AC, Jacoby D, et al. Genotype and lifetime burden of disease in hypertrophic cardiomyopathy. *Circulation*. (2018) 138:1387–98. doi: 10.1161/CIRCULATIONAHA.117.033200

26. Bonaventura J, Polakova E, Vejtasova V, Veselka J. Genetic testing in patients with hypertrophic cardiomyopathy. *Int J Mol Sci*. (2021) 22:10401. doi: 10.3390/ijms221910401

27. Oulas A, Minadakis G, Zachariou M, Spyrou GM. Selecting variants of unknown significance through network-based gene-association significantly improves risk prediction for disease-control cohorts. *Sci Rep*. (2019) 9:3266. doi: 10.1038/s41598-019-39796-w

28. Spielmann M, Kircher M. Computational and experimental methods for classifying variants of unknown clinical significance. *Cold Spring Harb Mol Case Stud*. (2022) 8(3):a006196. PMID: 35483875; PMCID: PMC9059783. doi: 10.1101/mcs.a006196.

29. Ipe J, Swart M, Burgess K, Skaar T. High-throughput assays to assess the functional impact of genetic variants: a road towards genomic-driven medicine. *Clin Transl Sci*. (2017) 10:67–77. doi: 10.1111/cts.12440

30. Stenson PD, Ball E V, Mort M, Phillips AD, Shiel JA, Thomas NST, et al. Human gene mutation database (HGMD ®): 2003 update. *Hum Mutat*. (2003) 21:577–81. doi: 10.1002/humu.10212

31. Liu Y, Yeung WSB, Chiu PCN, Cao D. Computational approaches for predicting variant impact: an overview from resources, principles to applications. *Front Genet*. (2022) 13:981005. PMID: 36246661; PMCID: PMC9559863. doi: 10.3389/fgene.2022.981005.

32. Livesey BJ, Marsh JA. Interpreting protein variant effects with computational predictors and deep mutational scanning. *Dis Model Mech*. (2022) 15(6): dmm049510. Epub 2022 Jun 23. PMID: 35736673; PMCID: doi: PMC9235876. doi: 10.1242/dmm.049510.

33. Li G, Panday SK, Alexov E. SAAFEC-SEQ: a sequence-based method for predicting the effect of single point mutations on protein thermodynamic stability. *Int J Mol Sci*. (2021) 22:606. doi: 10.3390/ijms22020606

34. Zhang X, Walsh R, Whiffin N, Buchan R, Midwinter W, Wilk A, et al. Disease-specific variant pathogenicity prediction significantly improves variant interpretation in inherited cardiac conditions. *Genet Med*. (2021) 23:69–79. doi: 10.1038/s41436-020-00972-3

35. Jordan DM, Kiezun A, Baxter SM, Agarwala V, Green RC, Murray MF, et al. Development and validation of a computational method for assessment of missense variants in hypertrophic cardiomyopathy. *Am J Hum Genet*. (2011) 88:183–92. doi: 10.1016/j.ajhg.2011.01.011

36. Walsh R, Mazzarotto F, Whiffin N, Buchan R, Midwinter W, Wilk A, et al. Quantitative approaches to variant classification increase the yield and precision of genetic testing in Mendelian diseases: the case of hypertrophic cardiomyopathy. *Genome Med*. (2019) 11:5. doi: 10.1186/s13073-019-0616-z

37. Quan L, Lv Q, Zhang Y. STRUM: structure-based prediction of protein stability changes upon single-point mutation. *Bioinformatics*. (2016) 32:2936–46. doi: 10.1093/bioinformatics/btw361

38. Thompson AD, Helms AS, Kannan A, Yob J, Lakdawala NK, Wittekind SG, et al. Computational prediction of protein subdomain stability in MYBPC3 enables clinical risk stratification in hypertrophic cardiomyopathy and enhances variant interpretation. *Genet Med*. (2021) 23:1281–7. doi: 10.1038/s41436-021-01134-9

39. Burghardt TP, Ajtai K. Neural/Bayes network predictor for inheritable cardiac disease pathogenicity and phenotype. *J Mol Cell Cardiol*. (2018) 119:19–27. doi: 10.1016/j.yjmcc.2018.04.006

40. Krittanawong C, Johnson KW, Choi E, Kaplin S, Venner E, Murugan M, et al. Artificial intelligence and cardiovascular genetics. *Life*. (2022) 12:279. doi: 10.3390/life12020279

41. Doh CY, Li J, Mamidi R, Stelzer JE. The HCM-causing Y235S cMyBPC mutation accelerates contractile function by altering C1 domain structure. *Biochim Biophys Acta Mol Basis Dis*. (2019) 1865:661–77. doi: 10.1016/j.bbadis.2019.01.007

42. Krishnamoorthy N, Gajendrarao P, Olivotto I, Yacoub M. Impact of disease-causing mutations on inter-domain interactions in cMyBP-C: a steered molecular dynamics study. *J Biomol Struct Dyn*. (2017) 35:1916–22. doi: 10.1080/07391102.2016.1199329

43. Tsaturyan AK, Zaklyazminskaya E V, Polyak ME, Kopylova G V, Shchepkin D V, Kochurova AM, et al. De Novo Asp219Val mutation in cardiac tropomyosin associated with hypertrophic cardiomyopathy. *Int J Mol Sci*. (2022) 24:18. doi: 10.3390/ijms24010018

44. Halder SS, Rynkiewicz MJ, Creso JG, Sewanan LR, Howland L, Moore JR, et al. Mechanisms of pathogenicity in the hypertrophic cardiomyopathy-associated TPM1 variant S215l. *PNAS Nexus*. (2023) 2(3):pgad011. PMID: 36896133; PMCID: PMC9991458. doi: 10.1093/pnasnexus/pgad011.

45. Parton DL, Grinaway PB, Hanson SM, Beauchamp KA, Chodera JD. Ensembler: enabling high-throughput molecular simulations at the superfamily scale. *PLoS Comput Biol*. (2016) 12:e1004728. doi: 10.1371/journal.pcbi.1004728

46. Bray SA, Senapathi T, Barnett CB, Grüning BA. Intuitive, reproducible high-throughput molecular dynamics in galaxy: a tutorial. *J Cheminform*. (2020) 12:54. doi: 10.1186/s13321-020-00451-6

47. Doerr S, Harvey MJ, Noé F, De Fabritiis G. HTMD: high-throughput molecular dynamics for molecular discovery. *J Chem Theory Comput*. (2016) 12:1845–52. doi: 10.1021/acs.jctc.6b00049

48. Harvey MJ, De Fabritiis G. High-throughput molecular dynamics: the powerful new tool for drug discovery. *Drug Discov Today*. (2012) 17:1059–62. doi: 10.1016/j.drudis.2012.03.017

49. Mason AB, Lynn ML, Baldo AP, Deranek AE, Tardiff JC, Schwartz SD. Computational and biophysical determination of pathogenicity of variants of unknown significance in cardiac thin filament. *JCI Insight*. (2021) 6(23):e154350. PMID: 34699384; PMCID: PMC8675185. doi: 10.1172/jci.insight.154350.

50. de Garcia FAO, de Andrade ES, Palmero EI. Insights on variant analysis in silico tools for pathogenicity prediction. *Front Genet*. (2022) 13:1010327. PMID: 36568376; PMCID: PMC9774026. doi: 10.3389/fgene.2022.1010327.

51. Rees M, Nikoopour R, Fukuzawa A, Kho AL, Fernandez-Garcia MA, Wraige E, et al. Making sense of missense variants in TTN-related congenital myopathies. *Acta Neuropathol*. (2021) 141:431–53. doi: 10.1007/s00401-020-02257-0

52. Perez-Riba A, Itzhaki LS. A method for rapid high-throughput biophysical analysis of proteins. *Sci Rep*. (2017) 7:9071. doi: 10.1038/s41598-017-08664-w

53. Ponnam S, Kampourakis T. Microscale thermophoresis suggests a new model of regulation of cardiac myosin function via interaction with cardiac myosin-binding protein C. *J Biol Chem*. (2022) 298(1):101485. doi: 10.1016/j.jbc.2021.101485

54. Ponnam S, Sevrieva I, Sun Y-B, Irving M, Kampourakis T. Site-specific phosphorylation of myosin binding protein-C coordinates thin and thick filament activation in cardiac muscle. *Proc Natl Acad Sci USA*. (2019) 116:15485–94. doi: 10.1073/pnas.1903033116

55. Patel BG, Wilder T, Solaro RJ. Novel control of cardiac myofilament response to calcium by S-glutathionylation at specific sites of myosin binding protein C. *Front Physiol*. (2013) 4:2–11. doi: 10.3389/fphys.2013.00336

56. McLendon PM, Robbins J. Proteotoxicity and cardiac dysfunction. *Circ Res*. (2015) 116:1863–82. doi: 10.1161/CIRCRESAHA.116.305372

57. Szatkowski L, Lynn ML, Holeman T, Williams MR, Baldo AP, Tardiff JC, et al. Proof of principle that molecular modeling followed by a biophysical experiment can develop small molecules that restore function to the cardiac thin filament in the presence of cardiomyopathic mutations. *ACS Omega*. (2019) 4:6492–501. doi: 10.1021/acsomega.8b03340

58. Doh CY, Bharambe N, Holmes JB, Dominic KL, Swanberg CE, Mamidi R, et al. Molecular characterization of linker and loop-mediated structural modulation and hinge motion in the C4-C5 domains of cMyBPC. *J Struct Biol*. (2022) 214:107856. doi: 10.1016/j.jsb.2022.107856

59. Bunch TA, Guhathakurta P, Lepak VC, Thompson AR, Kanassatega R-S, Wilson A, et al. Cardiac myosin-binding protein C interaction with actin is inhibited by compounds identified in a high-throughput fluorescence lifetime screen. *J Biol Chem*. (2021) 297:100840. doi: 10.1016/j.jbc.2021.100840

60. Smelter DF, de Lange WJ, Cai W, Ge Y, Ralphe JC. The HCM-linked W792R mutation in cardiac myosin-binding protein C reduces C6 FnIII domain stability. *Am J Physiol Heart Circ Physiol*. (2018) 314:H1179–91. doi: 10.1152/ajpheart.00686.2017

61. Pricolo MR, Herrero-Galán E, Mazzaccara C, Losi MA, Alegre-Cebollada J, Frisso G. Protein thermodynamic destabilization in the assessment of pathogenicity of a variant of uncertain significance in cardiac myosin binding protein C. *J Cardiovasc Transl Res*. (2020) 13:867–77. doi: 10.1007/s12265-020-09959-6

62. Suay-Corredera C, Pricolo MR, Herrero-Galán E, Velázquez-Carreras D, Sánchez-Ortiz D, García-Giustiniani D, et al. Protein haploinsufficiency drivers identify MYBPC3 variants that cause hypertrophic cardiomyopathy. *J Biol Chem*. (2021) 297:100854. doi: 10.1016/j.jbc.2021.100854

63. Jerabek-Willemsen M, Wienken CJ, Braun D, Baaske P, Duhr S. Molecular interaction studies using microscale thermophoresis. *Assay Drug Dev Technol*. (2011) 9:342–53. doi: 10.1089/adt.2011.0380

64. El Deeb S, Al-Harrasi A, Khan A, Al-Broumi M, Al-Thani G, Alomairi M, et al. Microscale thermophoresis as a powerful growing analytical technique for the investigation of biomolecular interaction and the determination of binding parameters. *Methods Appl Fluoresc*. (2022) 10:042001. doi: 10.1088/2050-6120/ac82a6

65. Nag S, Trivedi DV, Sarkar SS, Adhikari AS, Sunitha MS, Sutton S, et al. The myosin mesa and the basis of hypercontractility caused by hypertrophic cardiomyopathy mutations. *Nat Struct Mol Biol*. (2017) 24:525–33. doi: 10.1038/nsmb.3408

66. Sarkar SS, Trivedi D V, Morck MM, Adhikari AS, Pasha SN, Ruppel KM, et al. The hypertrophic cardiomyopathy mutations R403Q and R663H increase the number of myosin heads available to interact with actin. *Sci Adv*. (2020) 6(14):eaax0069. PMID: 32284968; PMCID: PMC7124958. doi: 10.1126/sciadv.aax0069.

67. Gunther LK, Rohde JA, Tang W, Cirilo JA, Marang CP, Scott BD, et al. FRET And optical trapping reveal mechanisms of actin activation of the power stroke and phosphate release in myosin V. *J Biol Chem*. (2020) 295:17383–97. doi: 10.1074/jbc.RA120.015632

68. Kanassatega R-S, Bunch TA, Lepak VC, Wang C, Colson BA. Human cardiac myosin-binding protein C phosphorylation- and mutation-dependent structural dynamics monitored by time-resolved FRET. *J Mol Cell Cardiol*. (2022) 166:116–26. doi: 10.1016/j.yjmcc.2022.02.005

69. Bunch TA, Guhathakurta P, Thompson AR, Lepak VC, Carter AL, Thomas JJ, et al. Drug discovery for heart failure targeting myosin-binding protein C. *bioRxiv*. (2023):2023.04.03.535496. doi: 10.1101/2023.04.03.535496

70. Radnai L, Stremel RF, Sellers JR, Rumbaugh G, Miller CA. A semi-high-throughput adaptation of the NADH-coupled ATPase assay for screening small molecule inhibitors. *J Visualized Exp*. (2019) (150):10.3791/60017. doi: 10.3791/60017.

71. Belknap B, Harris SP, White HD. Modulation of thin filament activation of myosin ATP hydrolysis by N-terminal domains of cardiac myosin binding protein-C. *Biochemistry*. (2014) 53:6717–24. doi: 10.1021/bi500787f

72. Ma N, Zhang JZ, Itzhaki I, Zhang SL, Chen H, Haddad F, et al. Determining the pathogenicity of a genomic variant of uncertain significance using CRISPR/Cas9 and human-induced pluripotent stem cells. *Circulation*. (2018) 138:2666–81. doi: 10.1161/CIRCULATIONAHA.117.032273

73. Guo H, Liu L, Nishiga M, Cong L, Wu JC. Deciphering pathogenicity of variants of uncertain significance with CRISPR-edited iPSCs. *Trends Genet*. (2021) 37:1109–23. doi: 10.1016/j.tig.2021.08.009

74. Pham QT, Raad S, Mangahas C-L, M'Callum M-A, Raggi C, Paganelli M. High-throughput assessment of mutations generated by genome editing in induced pluripotent stem cells by high-resolution melting analysis. *Cytotherapy*. (2020) 22:536–42. doi: 10.1016/j.jcyt.2020.06.008

75. Li H, Busquets O, Verma Y, Syed KM, Kutnowski N, Pangilinan GR, et al. Highly efficient generation of isogenic pluripotent stem cell models using prime editing. *Elife*. (2022) 11:e79208. PMID: 36069759; PMCID: PMC9584603. doi: 10.7554/eLife.79208.

76. Tristan CA, Ormanoglu P, Slamecka J, Malley C, Chu P-H, Jovanovic VM, et al. Robotic high-throughput biomanufacturing and functional differentiation of human pluripotent stem cells. *Stem Cell Rep*. (2021) 16:3076–92. doi: 10.1016/j.stemcr.2021.11.004

77. Paull D, Sevilla A, Zhou H, Hahn AK, Kim H, Napolitano C, et al. Automated, high-throughput derivation, characterization and differentiation of induced pluripotent stem cells. *Nat Methods*. (2015) 12:885–92. doi: 10.1038/nmeth.3507

78. Mosqueira D, Mannhardt I, Bhagwan JR, Lis-Slimak K, Katili P, Scott E, et al. CRISPR/Cas9 editing in human pluripotent stem cell-cardiomyocytes highlights arrhythmias, hypocontractility, and energy depletion as potential therapeutic targets for hypertrophic cardiomyopathy. *Eur Heart J*. (2018) 39:3879–92. doi: 10.1093/eurheartj/ehy249

79. Toepfer CN, Sharma A, Cicconet M, Garfinkel AC, Mücke M, Neyazi M, et al. Sarctrack. *Circ Res*. (2019) 124:1172–83. doi: 10.1161/CIRCRESAHA.118.314505

80. Brodehl A, Ebbinghaus H, Deutsch M-A, Gummert J, Gärtner A, Ratnavadivel S, et al. Human induced pluripotent stem-cell-derived cardiomyocytes as models for genetic cardiomyopathies. *Int J Mol Sci*. (2019) 20:4381. doi: 10.3390/ijms20184381

81. Helms AS, Tang VT, O'Leary TS, Friedline S, Wauchope M, Arora A, et al. Effects of MYBPC3 loss-of-function mutations preceding hypertrophic cardiomyopathy. *JCI Insight*. (2020) 5(2):e133782. PMID: 31877118; PMCID: PMC7098724. doi: 10.1172/jci.insight.133782.

82. Lam CK, Wu JC. Disease modelling and drug discovery for hypertrophic cardiomyopathy using pluripotent stem cells: how far have we come? *Eur Heart J*. (2018) 39:3893–5. doi: 10.1093/eurheartj/ehy388

83. Huxley AF. Muscle structure and theories of contraction. *Prog Biophys Biophys Chem*. (1957) 7:255–318. doi: 10.1016/S0096-4174(18)30128-8

84. Landesberg A, Sideman S. Mechanical regulation of cardiac muscle by coupling calcium kinetics with cross-bridge cycling: a dynamic model. *Am J Physiol Heart Circ Physiol*. (1994) 267:H779–95. doi: 10.1152/ajpheart.1994.267.2.H779

85. Niederer SA, Campbell KS, Campbell SG. A short history of the development of mathematical models of cardiac mechanics. *J Mol Cell Cardiol*. (2019) 127:11–9. doi: 10.1016/j.yjmcc.2018.11.015

86. Arts T, Reneman RS, Veenstra PC. A model of the mechanics of the left ventricle. *Ann Biomed Eng*. (1979) 7:299–318. doi: 10.1007/BF02364118

87. Campbell KS, Yengo CM, Lee L-C, Kotter J, Sorrell VL, Guglin M, et al. Closing the therapeutic loop. *Arch Biochem Biophys*. (2019) 663:129–31. doi: 10.1016/j.abb.2019.01.006

88. Tamborrini D, Wang Z, Wagner T, Tacke S, Stabrin M, Grange M, et al. In situ structures from relaxed cardiac myofibrils reveal the organization of the muscle thick filament. *bioRxiv*. (2023):2023.04.11.536387. doi: 10.1101/2023.04.11.536387

89. Dutta D, Nguyen V, Campbell KS, Padrón R, Craig R. Cryo-EM structure of the human cardiac myosin filament. *bioRxiv*. (2023):2023.04.11.536274. doi: 10.1101/2023.04.11.536274

90. Walcott S, Docken S, Harris SP. Effects of cardiac myosin binding protein-C on actin motility are explained with a drag-activation-competition model. *Biophys J*. (2015) 108:10–3. doi: 10.1016/j.bpj.2014.11.1852

91. Daniel TL, Trimble AC, Bryant Chase P. Compliant realignment of binding sites in muscle: transient behavior and mechanical tuning. *Biophys J*. (1998) 74:1611–21. doi: 10.1016/S0006-3495(98)77875-0

92. Smith DA, Geeves MA, Sleep J, Mijailovich SM. Towards a unified theory of muscle contraction. I: foundations. *Ann Biomed Eng*. (2008) 36:1624–40. doi: 10.1007/s10439-008-9536-6

93. Tanner BCW, Daniel TL, Regnier M. Sarcomere lattice geometry influences cooperative myosin binding in muscle. *PLoS Comput Biol*. (2007) 3:e115. doi: 10.1371/journal.pcbi.0030115

94. Kosta S, Colli D, Ye Q, Campbell KS. Fibersim: a flexible open-source model of myofilament-level contraction. *Biophys J*. (2022) 121:175–82. doi: 10.1016/j.bpj.2021.12.021

95. Lumens J, Delhaas T, Kirn B, Arts T. Three-Wall segment (TriSeg) model describing mechanics and hemodynamics of ventricular interaction. *Ann Biomed Eng*. (2009) 37:2234–55. doi: 10.1007/s10439-009-9774-2

96. Sharifi H, Mann CK, Rockward AL, Mehri M, Mojumder J, Lee L-C, et al. Multiscale simulations of left ventricular growth and remodeling. *Biophys Rev*. (2021) 13:729–46. doi: 10.1007/s12551-021-00826-5

97. Davis J, Davis LC, Correll RN, Makarewich CA, Schwanekamp JA, Moussavi-Harami F, et al. A tension-based model distinguishes hypertrophic versus dilated cardiomyopathy. *Cell*. (2016) 165:1147–59. doi: 10.1016/j.cell.2016.04.002

98. Minami Y, Yuan Y, Ueda HR. High-throughput genetically modified animal experiments achieved by next-generation mammalian genetics. *J Biol Rhythms*. (2022) 37:135–51. doi: 10.1177/07487304221075002

99. Maass A, Leinwand LA. Animal models of hypertrophic cardiomyopathy. *Curr Opin Cardiol*. (2000) 15:189–96. doi: 10.1097/00001573-200005000-00012

100. Purevjav E. Animal models of cardiomyopathies. In: Tvrdá E, Chandra Yenisetti S, editors. *Animal models in medicine and biology*. London: IntechOpen (2020). p. 1–21. doi: 10.5772/intechopen.89033

frontiers | Frontiers in Cardiovascular Medicine

TYPE Original Research
PUBLISHED 16 August 2023
DOI 10.3389/fcvm.2023.1250234

OPEN ACCESS

EDITED BY
Jingyan Han,
Boston University, United States

REVIEWED BY
Rongxue Wu,
The University of Chicago, United States
Ming He,
University of Alabama at Birmingham, United States

*CORRESPONDENCE
Alan Daugherty
✉ alan.daugherty@uky.edu
Hong S. Lu
✉ hong.lu@uky.edu

†These authors share first authorship

RECEIVED 29 June 2023
ACCEPTED 03 August 2023
PUBLISHED 16 August 2023

CITATION
Kukida M, Amioka N, Ye D, Chen H, Moorleghen JJ, Liang C-L, Howatt DA, Katsumata Y, Yanagita M, Sawada H, Daugherty A and Lu HS (2023) Manipulation of components of the renin angiotensin system in renal proximal tubules fails to alter atherosclerosis in hypercholesterolemic mice. Front. Cardiovasc. Med. 10:1250234. doi: 10.3389/fcvm.2023.1250234

Manipulation of components of the renin angiotensin system in renal proximal tubules fails to alter atherosclerosis in hypercholesterolemic mice

Masayoshi Kukida[1†], Naofumi Amioka[1†], Dien Ye[1], Hui Chen[1], Jessica J. Moorleghen[1], Ching-Ling Liang[1], Deborah A. Howatt[1], Yuriko Katsumata[2,3], Motoko Yanagita[4,5], Hisashi Sawada[1,6,7], Alan Daugherty[1,6,7]* and Hong S. Lu[1,6,7]*

[1]Saha Cardiovascular Research Center, University of Kentucky, Lexington, KY, United States, [2]Sanders-Brown Center on Aging, University of Kentucky, Lexington, KY, United States, [3]Department of Biostatistics, University of Kentucky, Lexington, KY, United States, [4]Department of Nephrology, Kyoto University Graduate School of Medicine, Kyoto, Japan, [5]Institute for the Advanced Study of Human Biology (WPI-ASHBi), Kyoto University, Kyoto, Japan, [6]Saha Aortic Center, University of Kentucky, Lexington, KY, United States, [7]Department of Physiology, University of Kentucky, Lexington, KY, United States

Background and objective: Whole body manipulation of the renin-angiotensin system (RAS) consistently exerts profound effects on experimental atherosclerosis development. A deficit in the literature has been a lack of attention to the effects of sex. Also, based on data with gene-deleted mice, the site of RAS activity that influences lesion formation is at an unknown distant location. Since angiotensin (AngII) concentrations are high in kidney and the major components of the RAS are present in renal proximal tubule cells (PTCs), this study evaluated the role of the RAS in PTCs in atherosclerosis development.
Methods and results: Mice with an LDL receptor −/− background were fed Western diet to induce hypercholesterolemia and atherosclerosis. We first demonstrated the role of AT1 receptor antagonism on atherosclerosis in both sexes. Losartan, an AngII type 1 (AT1) receptor blocker, had greater blood pressure-lowering effects in females than males, but equivalent effects between sexes in reducing atherosclerotic lesion size. To determine the roles of renal AT1a receptor and angiotensin-converting enzyme (ACE), either component was deleted in PTCs after weaning using a tamoxifen-inducible Cre expressed under the control of an *Ndrg1* promoter. Despite profound deletion of AT1a receptor or ACE in PTCs, the absence of either protein did not influence development of atherosclerosis in either sex. Conversely, mice expressing human angiotensinogen and renin in PTCs or expressing human angiotensinogen in liver but human renin in PTCs did not change atherosclerotic lesion size in male mice.

Abbreviations
AAV, adeno-associated virus; ACE, angiotensin-converting enzyme; AGT, angiotensinogen; AngII, angiotensin II; *Agtr1a*, angiotensin II type 1a receptor (mouse gene); AT1aR, angiotensin II type 1a receptor (mouse protein); AT1bR, angiotensin II type 1b receptor (mouse protein); AT1R, angiotensin II type 1 receptor (human); hAGT, human angiotensinogen; hREN, human renin; LDL, low-density lipoprotein; *Ndrg1*, N-myc downstream-regulated gene 1; PRC, plasma renin concentration; PTC, proximal tubular cells; RAS, renin-angiotensin system; TC, total cholesterol.

Conclusion: Whole-body AT1R inhibition reduced atherosclerosis equivalently in both male and female mice; however, PTC-specific manipulation of the RAS components had no effects on hypercholesterolemia-induced atherosclerosis.

KEYWORDS

angiotensin, angiotensinogen, renin, angiotensin-converting enzyme, AT1 receptor, atherosclerosis, kidney, proximal tubules

Introduction

Angiotensin II (AngII) is the principal bioactive peptide of the renin-angiotensin system (RAS), which is produced from angiotensinogen (AGT) through sequential cleavage by renin and angiotensin-converting enzyme (ACE). AngII is a potent contributor to atherosclerosis through binding to AngII type 1 receptor (AT1R in humans and AT1aR in mice). Sex differences in atherosclerosis have been noted in previous studies (1). However, most mouse studies focus on effects of the RAS components on atherosclerosis in male mice, while there is a paucity of studies that performed simultaneous comparisons of the efficacy of RAS inhibition on atherosclerosis in both male and female mice.

Whole body manipulation of the RAS has generated a highly consistent literature on its role in regulating experimental atherosclerosis (2, 3). However, there has not been a clearly defined location for the production of AngII that influences atherosclerosis or the cellular location for activation of AT1aR to promote the disease. The RAS components are present throughout the body. Classically, the principal location for producing AngII has been liver for AGT, renal juxtaglomerular cells for renin, and lung for ACE (4). Of note, many tissues and cell types have AT1aR and every component to generate AngII. These RAS components are also present in atherosclerotic lesions and resident cell types of the vascular wall (5–9). Although one prevailing hypothesis has been that the RAS in circulating leukocytes and/or resident cell types of the vessel wall exerts an important role in atherosclerosis (5–9), deletion of AT1aR on macrophages (a major cell type in atherosclerosis) or resident cell types of the arterial wall does not affect atherosclerosis (9–11), indicating that AngII-AT1aR stimulation may not act directly on the vascular wall to promote atherosclerosis.

Our studies have demonstrated that either whole-body or liver-specific inhibition of AGT synthesis decreases atherosclerosis and reduces renal, but not plasma, AngII concentrations (12–14). Further, inhibition of megalin, an endocytic receptor for many molecules including AGT and renin on renal proximal tubules, results in profound reductions of renal AngII concentrations and atherosclerosis (12). Although these findings implicate that the renal RAS contributes to atherosclerosis, there has no direct evidence to support this hypothesis. Since AT1aR and ACE are abundant in renal proximal tubule cells (PTCs), the present study used an inducible PTC-specific genetic mouse strain to delete either AT1aR or ACE in PTCs and determined whether deleting either component affects hypercholesterolemia-induced atherosclerosis in LDL receptor −/− mice. In addition to genetic deletion of AT1aR or ACE, we manipulated AGT and renin by implementing human AGT and renin transgenes in PTCs (15) or human AGT in liver with human renin in PTCs of LDL receptor −/− mice.

Materials and methods

Detailed Materials and Methods are available in the manuscript or the online-only Data Supplement. The data that support the findings reported in this manuscript are available in the **Supplementary Excel File**.

Animals

LDL receptor −/− (Stock # 002207), ROSA26R^{LacZ} (Stock # 003474), and ROSA26R$^{mT/mG}$ (Stock # 007676) mice were purchased from The Jackson Laboratory (Bar Harbor, ME, USA). *Agtr1a* (Angiotensin II type 1a receptor) floxed (*Agtr1a* f/f) mice (10, 16) and *Ace* (angiotensin-converting enzyme) floxed (*Ace* f/f) mice (17, 18) were developed by the authors and maintained for in house breeding. *Ndrg1*-CreERT2 breeding pairs were provided by Dr. Motoko Yanagita at Kyoto University in Japan (19). Transgenic mice expressing human AGT or human renin in PTCs driven by a kidney androgen-related protein promoter (*Kap*-hAGT and *Kap*-hREN, respectively) were provided by Dr. Curt Sigmund (15, 20).

The breeding strategy for generating PTC-specific AT1aR or ACE deficient mice are shown in **Table 1**.

To validate *Ndrg1*-Cre specificity, male *Ndrg1*-CreERT2 mice were bred with either female ROSA26R^{LacZ} or ROSA26R$^{mT/mG}$ mice to generate ROSA26R^{LacZ} × *Ndrg1*-CreERT2 or mT/mG × *Ndrg1*-CreERT2 mice. To induce Cre activity, mice at 4–6 weeks of age were injected intraperitoneally with tamoxifen (150 mg/kg/day)

TABLE 1 Breeding strategy for *Agtr1a* f/f or *Ace* f/f × *Ndrg1*-CreERT2 mice.

	Female parent	Male parent	Offspring for breeding or experiments
F0	f/f	*Ndrg1*-CreERT2$^{+/0}$	Female f/+ × *Ndrg1*-CreERT2$^{0/0}$ Male f/+ × *Ndrg1*-CreERT2$^{+/0}$
F1	f/+ × *Ndrg1*-CreERT2$^{0/0}$	f/+ × *Ndrg1*-CreERT2$^{+/0}$	Female f/f × *Ndrg1*-CreERT2$^{0/0}$ Male f/f × *Ndrg1*-CreERT2$^{+/0}$
F2	f/f × *Ndrg1*-CreERT2$^{0/0}$	f/f × *Ndrg1*-CreERT2$^{+/0}$	f/f × *Ndrg1*-CreERT2$^{0/0}$ f/f × *Ndrg1*-CreERT2$^{+/0}$ Both males and females—Experiment

for five consecutive days. Genotypes were determined prior to weaning and verified after termination by PCR of Cre transgene.

All mice were maintained in a barrier facility on a light:dark cycle of 14:10 h and fed a normal mouse laboratory diet after weaning. All study mice for atherosclerosis were in an LDL receptor −/− background. For mice containing *Ndrg1*-CreERT2 transgene, to induce Cre activity, mice at 4–6 weeks of age were injected intraperitoneally with tamoxifen 150 mg/kg/day for 5 days. Two weeks after the last injection of tamoxifen, mice were fed a diet containing saturated fat (milk fat 21% wt/wt) and cholesterol (0.2% wt/wt; Diet # TD.88137, Envigo, termed "Western diet"). Since we hypothesized that PTC-specific deletion of AT1aR or ACE would reduce atherosclerosis, we fed these mice Western diet for 12 weeks. This feeding duration leads to profound atherosclerosis in the ascending and arch aortic region as reported previously (11, 21–23).

To activate human AGT and/or renin transgenes in PTCs, testosterone pellets (20 mg/pellet for 90-day release or 15 mg/pellet for 60-day release) were implanted subcutaneously. Two weeks later, all mice were fed Western diet for either 8 or 6 weeks. LDL receptor −/− mice fed Western diet for 6–8 weeks have early to intermediate stages of atherosclerosis. We hypothesized that increased human AGT and renin in PTCs leads to augmentation of atherosclerosis. Therefore, a shorter duration of Western diet feeding (either 6 or 8 weeks) was used.

To induce synthesis of human AGT in hepatocytes, an adeno-associated viral vector (AAV; 3×10^{10} genome copies/mouse) serotype 2/8 containing human AGT with a liver-specific promoter thyroxine-binding globulin (TBG) was injected intraperitoneally. Three groups of male littermates were administered testosterone to activate human renin expression in PTCs: (1) wild type mice administered null.AAVs, (2) *Kap*-hREN transgenic mice administered null.AAVs, and (3) *Kap*-hREN transgenic mice administered AAVs containing human AGT.

Both male and female mice were used for the experiments reported in this manuscript following the recent ATVB Council Statement (23) except for the data reported in **Figures 5**, **6**. Testosterone administration is required to activate human AGT or renin transgene. Shortly after testosterone pellet implantation, many female mice suffered from uterine prolapse that required euthanasia prior to the endpoint. Therefore, we excluded female mice for studies presented in **Figures 5**, **6**. Euthanasia before the endpoint was performed using CO_2 (fill rate >50% of the chamber volume/minute) followed by cervical dislocation.

At termination, mice were euthanized by a ketamine (90 mg/kg) and xylazine (10 mg/kg) cocktail. All animal studies performed were approved by the University of Kentucky Institutional Animal Care and Use Committee (Protocol number 2018–2968).

Administration of losartan

Mini osmotic minipumps (Alzet Model 1004, Durect Corporation) filled with either water (vehicle) or losartan (12.5 mg/kg/day, Cat # 61188, MilliporeSigma) were implanted subcutaneously into LDL receptor −/− mice, as described in our previous studies (24). After anesthetized using inhaled isoflurane (2%–3% vol/vol), mice at ∼9–10 weeks of age were implanted with mini osmotic pumps. Pumps were replaced after 4 and 8 weeks of the first pump implantation. All mice were fed Western diet for 12 weeks starting one day after the first pump implantation.

Plasma profiles

Blood samples were collected with EDTA (final concentration: ∼1.8 mg/ml) by submandibular bleeding during experiments and right ventricular punctures at termination. Then, plasma was collected by centrifugation at 3,000 rcf for 10 min, 4°C, and stored at −80°C. Plasma renin concentrations were evaluated by quantifying AngI generation after incubation with exogenous recombinant mouse AGT in the presence of EDTA (Cat # 51201, Lonza, final concentration: ∼14 mM) and PMSF for 60 min at 37°C. The reaction was terminated by placing samples at 100°C for 5 min and generated AngI was measured using a plasma renin activity ELISA kit (Cat # IB59131, IBL America). Plasma total cholesterol concentrations were measured using a commercial enzymatic kit (Cat # 999–02601, Wako Chemicals USA or Cat # C7510–120, Pointe Scientific).

Blood pressure measurement

Systolic blood pressure was measured on conscious mice by a non-invasive tail-cuff system (BP-2000, Visitech) following our standard protocol (25). Data were collected at the same time each day for three consecutive days. Criteria for accepted data were systolic blood pressure between 70 and 200 mmHg and standard deviation <30 mmHg for at least 5 successful recorded data/mouse/day. The mean systolic blood pressure of each mouse from the 3-day measurements was used for data analysis.

Quantification of atherosclerosis

Atherosclerotic lesions were evaluated on the intimal surface area of the aorta with an *en face* method following the AHA Statement (23) and our standard protocol (22). Briefly, the aorta was dissected and fixed with neutrally buffered formalin (10% wt/vol) overnight at room temperature. Periaortic tissues were removed gently. Then the intimal surface was exposed by a longitudinal cut, and pinned on a black wax surface. Images of *en face* aortas were taken using a Nikon digital camera (Nikon digital sight DS-Ri1) with a mm ruler for calibration. Lesions were traced manually from the beginning of the ascending region to the descending aortic region that is 1 mm distal from the left subclavian artery using Nikon NIS-Elements software (NIS-Elements

AR 5.11.00.) under a dissecting microscope. Lesion size was calculated as percent lesion area using the following formula.

$$\text{Percent lesion area} = \frac{\text{Atherosclerotic lesion area (mm}^2\text{)}}{\text{Intimal area of the aorta (mm}^2\text{)}} \times 100$$

Cryosectioning and imaging of mouse kidneys

Isolated whole kidneys from ROSA26R$^{mT/mG}$ × *Ndrg1*-CreERT2 mice were placed immediately in paraformaldehyde (PFA, 4% wt/vol) solution and fixed overnight. Following fixation, kidneys were incubated with 30% sucrose at 4°C overnight and embedded in O.C.T. for cryosectioning. Tissues were cut (10 μm/section) on a Leica CM1860 cryostat (Leica Biosystems). After washing with PBS, sections were mounted with mounting media containing DAPI, and images were captured using Axioscan 1 or 7 (Zeiss) or a confocal microscope (A1 HD25/A1R HD25, Nikon).

RNA isolation and quantitative PCR

Total RNA of the renal cortex was extracted using a commercial kit (Cat # AS1340, Promega) configured with a Maxwell RSC Instrument (Promega). To quantify mRNA abundance, total RNA was reversely transcribed with an iScript™ cDNA Synthesis kit (Cat # 170–8891, Bio-Rad), and quantitative PCR (qPCR) was performed using a SsoFast™ EvaGreen® Supermix kit (Cat # 172–5204, Bio-Rad) on a Bio-Rad CFX96 real-time system. Data were analyzed using $\Delta\Delta$Ct method and normalized by the geometric mean of 3 reference genes [*Actb*, *Gapdh*, and *Rplp2* (or *Ppia*)].

In situ hybridization

The distribution of mouse *Agtr1a* and human renin (*hREN*) mRNA in kidney tissue sections was examined by RNAscope® following the manufacturer's instructions (Advanced Cell Diagnostics). After fixation using 4% PFA, kidney tissues were processed and embedded into paraffin, and cut at a thickness of 4 μm. Subsequently, sections were deparaffinized using xylene followed by 2 washes with absolute ethanol. Target retrieval (Cat # 26043–05) was performed for 30 min at 100°C, and followed by a protease (Cat # 322331) incubation step for 15 min at 40°C. Target mRNA was hybridized with mouse *Agtr1a* (Cat # 481161) or human REN probe (Cat # 401921) for 2 h at 40°C, and amplified signals were detected using diaminobenzidine (Cat # 322310). Hematoxylin was used to stain nuclei. Images were captured using a Nikon Eclipse Ni microscope or Zeiss Axioscan 1 or 7.

Immunostaining

Immunostaining was performed on paraffin-embedded sections (4 μm) to determine the distribution of mouse ACE and human AGT in the kidney. Deparaffinized sections were incubated with an antigen retrieval reagent (Cat # HK547-XAK; BioGenex) for 20 min at 90°C. Non-specific binding sites were blocked using goat serum for 20 min at room temperature. Sections were then incubated with rabbit anti-mouse ACE antibody (Cat # ab254222; abcam) or anti-human AGT antibody (Cat # ab276132; abcam) diluted in primary antibody diluent (Cat #: GTX28208; GeneTex) for 12 h at 4°C. Goat anti-rabbit IgG conjugated with horseradish peroxidase (Cat # MP-7451; Vector laboratories) was used as the secondary antibody. ImmPACT® AEC (Cat # SK4205; Vector) was used as the chromogen, and hematoxylin (Cat # 26043–05; Electron Microscopy Sciences) was used for counterstaining. Histological images were captured using either an Eclipse Ni microscope or Zeiss Axioscan 1 or 7.

Statistical analysis

All statistical analyses were performed using SigmaPlot 14.5 or 15 or R Statistical Software (v4.1.1; R Core Team 2021). The assumption of normality was examined using QQ-plot and Shapiro–Wilk test. The homogeneous group variance assumption was assessed by Bartlett test. In studies including both sexes, two-way ANOVA was used to evaluate the interaction between sex and treatment or genotypes, and compare mean difference between groups in each sex, and *P*-value was adjusted using the Bonferroni method in the *post hoc* test. Non-normal distributed data were log-transformed to meet the normal distribution assumption. When heteroscedasticity was present, White-corrected covariance matrix was incorporated into the two-way ANOVA. In studies using only male mice with N ≤5/group, Mann–Whitney *U* test and Kruskal–Wallis one-way ANOVA on Ranks test were used in comparisons between two groups and among three- or four-groups, respectively. For N >5/group, mean comparisons were performed by one-way ANOVA test or Kruskal–Wallis one-way ANOVA on Ranks test depending on data distribution. $P < 0.05$ was considered statistically significant.

Results

Losartan reduced atherosclerosis in male and female hypercholesterolemic mice

Losartan inhibits both AT1aR and AT1bR, although our previous study demonstrated that AT1aR, but not AT1bR, contributes to atherosclerosis in mice (26). Losartan reduced atherosclerotic lesions in a dose-dependent manner (21). Losartan (12.5 mg/kg/day) led to a modest reduction of systolic blood pressure and atherosclerosis in male hypercholesterolemic mice, as demonstrated previously (21). To examine whether losartan had equivalent responses between sexes, male and female LDL receptor −/− mice were fed Western diet and

infused with either water (Vehicle) or losartan (12.5 mg/kg/day) for 12 weeks.

Losartan significantly increased plasma renin concentrations and decreased systolic blood pressure in both sexes (**Figures 1A,B**). Of note, losartan led to more profound increases of plasma renin concentrations and greater reduction of systolic blood pressure in female than in male mice (**Figures 1A,B**). Losartan did not change plasma total cholesterol concentrations in either male or female mice (**Figure 1C**), but attenuated atherosclerotic lesion size equivalently in male and female mice (**Figure 1D**). This study provides direct evidence that AT1R blockade has comparable effects on atherosclerosis in both sexes.

Validation of PTC-specific deletion induced by *Ndrg1*-CreERT2 activation

Genotyping of Cre was determined for all study mice (**Figure 2A**). To determine the specificity of *Ndrg1*-driven Cre, *Ndrg1*-CreERT2$^{+/0}$ mice were bred with either ROSA26R^{LacZ} or ROSA26R$^{mT/mG}$ reporter mice. These mice at 4–6 weeks of age were injected with 150 mg/kg/day of tamoxifen for 5 consecutive days. Kidneys were harvested at 2 weeks after completion of tamoxifen injection. X-gal staining revealed the presence of β-galactosidase activity predominantly in renal cortex of ROSA26R^{LacZ} × *Ndrg1*-CreERT2$^{+/0}$ mice (**Figure 2B**). In kidneys from ROSA26R$^{mT/mG}$ × *Ndrg1*-CreERT2$^{+/0}$ mice, fluorescent images were captured using a confocal microscope. tdTomato was exclusively expressed in all renal cells in ROSA26R$^{mT/mG}$ × *Ndrg1*-CreERT2$^{0/0}$ mice, while Cre activation in ROSA26R$^{mT/mG}$ × *Ndrg1*-CreERT2$^{+/0}$ mice induced EGFP expression on proximal tubules, including proximal convoluted tubules and some proximal straight tubules. These results confirm that *Ndrg1*-driven Cre is predominantly expressed in proximal convoluted tubules (S1 and S2) of *Ndrg1*-CreERT2$^{+/0}$ mice (**Figure 2C**), consistent with what was reported by Endo and colleagues (19).

AT1aR deletion in renal PTCs had no effect on atherosclerosis in both male and female mice

To examine whether AT1aR in PTCs contributes to atherosclerosis, PTC-AT1aR$^{-/-}$ mice and their wild type

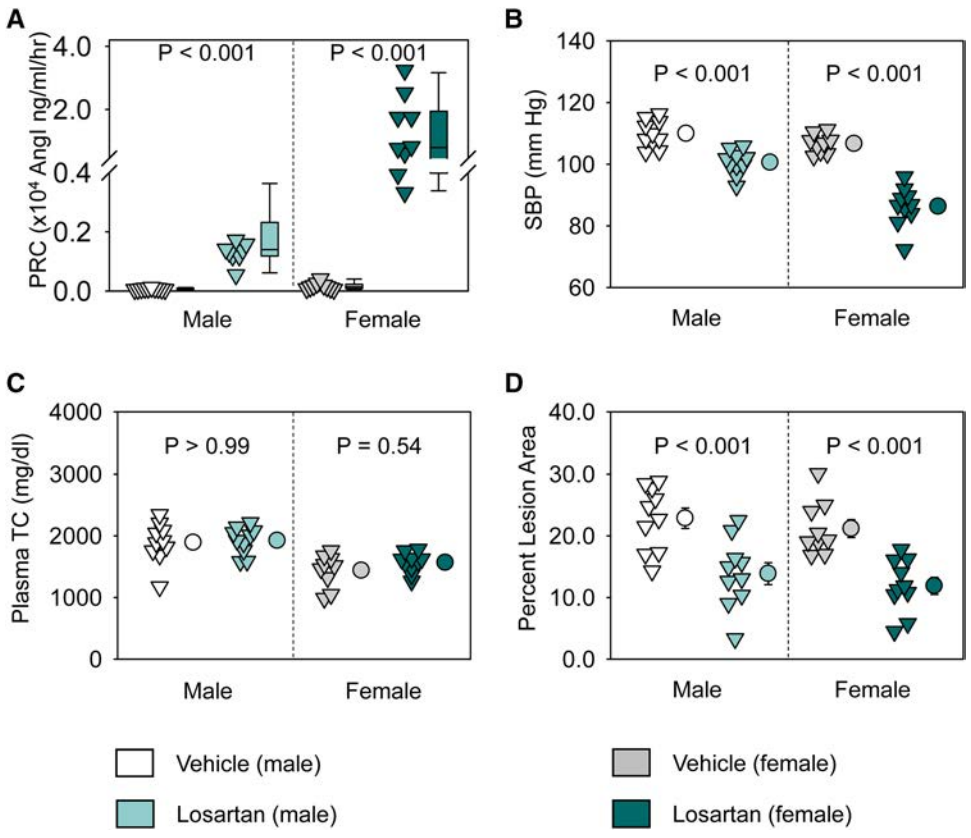

FIGURE 1
Losartan reduced systolic blood pressure and attenuated atherosclerosis in both male and female LDL receptor −/− mice. Both male and female LDL receptor −/− mice were fed Western diet and infused with either vehicle or losartan (12.5 mg/kg/day) for 12 weeks. *N* = 9–10/group. (**A**) Plasma renin concentrations (PRC), (**B**) systolic blood pressure (SBP), (**C**) plasma total cholesterol concentrations (TC), and (**D**) percent atherosclerotic lesion area. Data of PRC was log-transformed to meet normal distribution assumptions for statistical analysis. Two-way ANOVA was used to evaluate the interaction between sex and treatment. *P*-value was adjusted using the Bonferroni method in the *post hoc* test that examined the effect of losartan on each parameter in both sexes. *P* (sex × treatment) = 0.008 for (**A**) and 0.001 for (**B**), respectively.

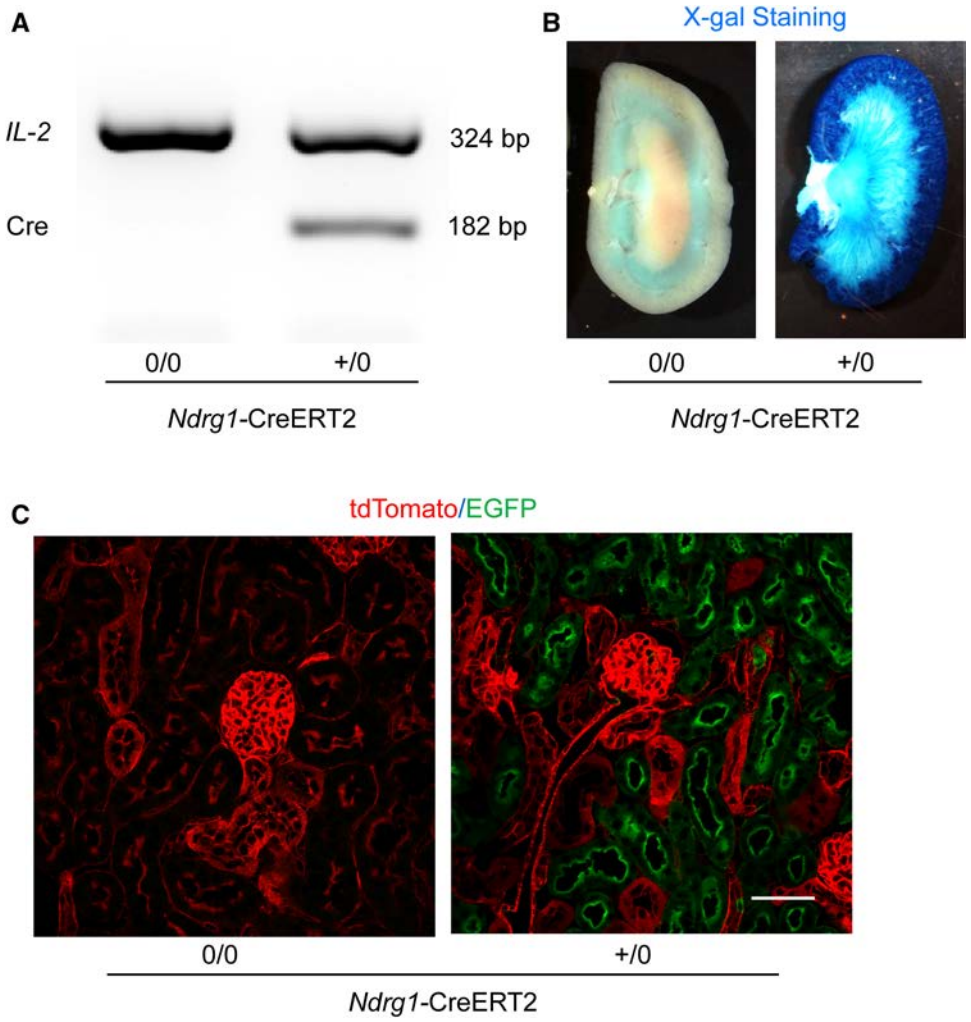

FIGURE 2
Validation of *Ndrg1*-Cre activation and distribution. *Ndrg1*-CreERT2$^{0/0}$ and *Ndrg1*-CreERT2$^{+/0}$ mice were injected intraperitoneally with tamoxifen 150 mg/kg/day for 5 consecutive days. Kidneys were harvested two weeks after the completion of tamoxifen injection. (**A**) PCR for detecting Cre recombinase in tail DNA, (**B**) X-gal staining of mouse kidneys, and (**C**) membrane-localized tdTomato and EGFP proteins detected by confocal microscopy in kidney sections.

littermates in an LDL receptor −/− background were fed Western diet for 12 weeks beginning 2 weeks after completion of tamoxifen injection (**Figure 3A**). Renal mRNA abundance of *Agtr1a* in PTC-AT1aR$^{-/-}$ mice was approximately 45% of that in their PCT-AT1aR$^{+/+}$ littermates (**Figure 3B**). Unfortunately, no antibodies have been demonstrated to authentic staining of AT1aR protein in mice (27–30). As an alternative mode of verifying PTC-specific AT1aR deletion in PTC-AT1aR$^{-/-}$ mice after Cre activation, we performed RNAscope using paraffin-embedded renal sections. AT1aR mRNAs were detected in PTCs, glomeruli, and interstitial cells of PTC-AT1aR$^{+/+}$ mice (**Figure 3C**), consistent with previous reports (31). While mRNA of *Agtr1a* in glomeruli and interstitial cells was observed, its mRNA in PTCs was not detected in PTC-AT1aR$^{-/-}$ mice (**Figure 3C**). These results confirm that *Ndrg1*-Cre activation led to effective AT1aR deletion in PTCs of PTC-AT1aR$^{-/-}$ mice.

Plasma renin concentrations (**Figure 3D**) and systolic blood pressure (**Figure 3E**) were not different between PCT-AT1aR$^{+/+}$ and PCT-AT1aR$^{-/-}$ littermates within each sex. Western diet induced hypercholesterolemia in both sexes, but plasma total cholesterol concentrations were not different (**Figure 3F**) and percent atherosclerotic lesion area was equivalent between the two genotypes within each sex (**Figure 3G**).

Renal PTC-specific deletion of ACE did not affect atherosclerosis in both male and female mice

To determine whether ACE in PTCs contributed to atherosclerosis, PTC-ACE$^{-/-}$ mice and their PTC-ACE$^{+/+}$ littermates in an LDL receptor −/− background were fed Western diet for 12 weeks beginning at 2 weeks after completion

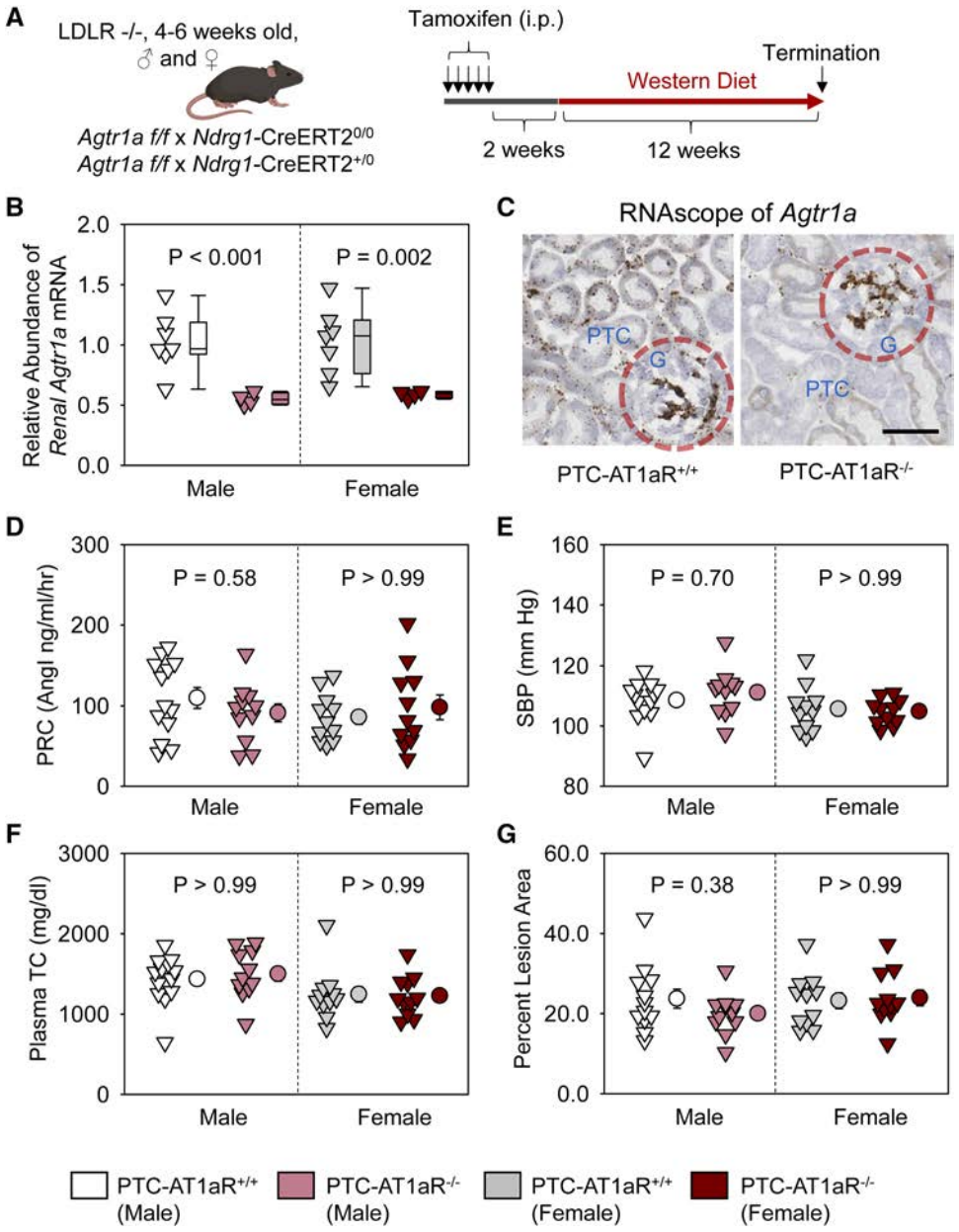

FIGURE 3
AT1aR deletion in PTCs had no effect on atherosclerosis in hypercholesterolemic mice. (**A**) Experimental protocol, (**B**) qPCR of renal *Agtr1a*, (**C**) RNAscope of renal *Agtr1a*, (**D**) plasma renin concentrations (PRC), (**E**) systolic blood pressure (SBP), (**F**) plasma total cholesterol concentrations (TC), and (**G**) percent atherosclerotic lesion area. *N* = 11–13/group. Two-way ANOVA was used to evaluate the interaction between sex and treatment (**B**,**D**–**G**). *P*-value was adjusted using the Bonferroni method in the *post hoc* test that examined the effect of AT1aR deletion in PTCs. G, glomerulus; PTC, proximal tubule cells.

of tamoxifen injection (Figure 4A). Renal mRNA abundance of ACE was 60% lower in male and 40% lower in female PTC-ACE$^{-/-}$ mice, compared to their sex- and age-matched PTC-ACE$^{+/+}$ littermates, respectively (Figure 4B). Deletion of ACE protein in PTCs was also confirmed by immunostaining of ACE in kidney (Figure 4C). PTC-specific ACE deletion did not change systolic blood pressure in either male or female mice (Figure 4D). Western diet induced hypercholesterolemia in both male and female mice. Plasma total cholesterol concentrations were comparable between the two genotypes in either sex (Figure 4E). Despite the profound deletion of ACE in PTCs, atherosclerotic lesion size was not reduced in either sex (Figure 4F).

Presence of human AGT and human renin in renal PTCs had no effect on atherosclerosis in male mice

To activate human AGT and/or renin transgene in PTCs, testosterone pellets were implanted subcutaneously (Figure 5A).

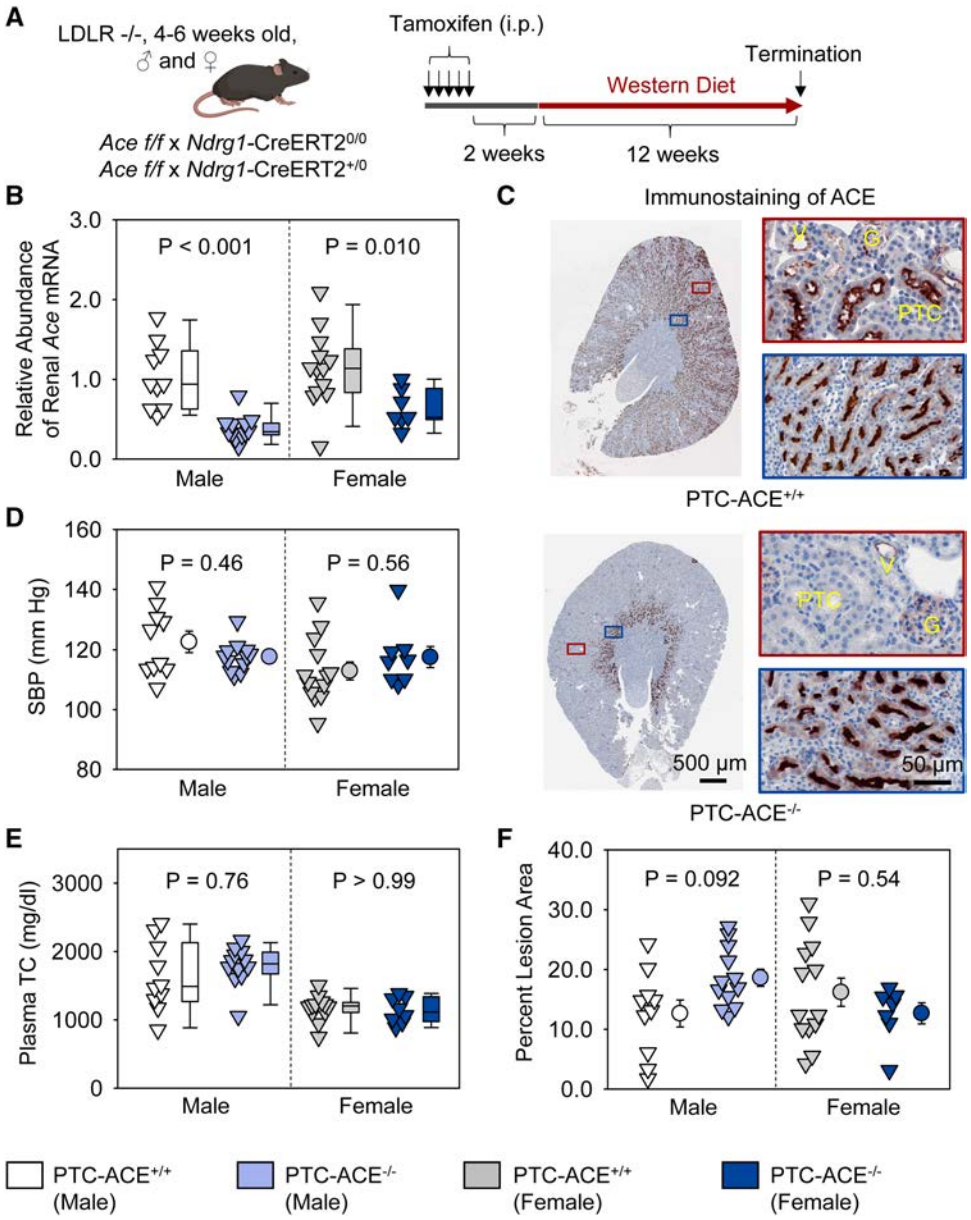

FIGURE 4
ACE deletion in PTCs had no effect on atherosclerosis in hypercholesterolemic mice. (**A**) Experimental protocol, (**B**) qPCR of renal *Ace*, (**C**) immunostaining of ACE in kidney, (**D**) systolic blood pressure (SBP), (**E**) plasma total cholesterol concentrations (TC), and (**F**) percent atherosclerotic lesion area. *N* = 7–13/group. Two-way ANOVA was used to evaluate the interaction between sex and genotypes (**B**,**D**–**F**). White-corrected covariance matrix was incorporated into the two-way ANOVA for analyzing data with heteroscedasticity (**B**,**E**). G, glomerulus; PTC, proximal tubule cells; V, vessel.

To examine whether co-presence of human AGT and renin in PTCs contributed to atherosclerosis, *Kap*-hAGT, *Kap*-hREN, *Kap*-hAGT × *Kap*-hREN, and their wild type littermates in an LDL receptor −/− background were fed Western diet for 8 weeks beginning two weeks after testosterone pellet implantation. As confirmed by qPCR of human AGT in mouse kidney (**Figure 5B**), mRNA abundance of human AGT was high in mice with *Kap*-hAGT or *Kap*-hAGT × *Kap*-hREN, but not detectable in mice with *Kap*-hREN or their wild type littermates. mRNA abundance of human renin (**Figure 5C**) was high in mice with *Kap*-hREN or *Kap*-hAGT × *Kap*-hREN, but not detectable in mice with *Kap*-hAGT or their wild type littermates. Presence of human AGT protein was also confirmed by immunostaining of human AGT that does not have cross-reaction with mouse AGT (**Figure 5D**). Unfortunately, we were not able to demonstrate the presence of human renin since human renin antibodies have cross-reactivity with mouse renin. Plasma renin concentrations (**Figure 5E**) and systolic blood pressure (**Figure 5F**) were not different among groups. Western diet induced hypercholesterolemia in all mice. Plasma total cholesterol concentrations (**Figure 5G**) were not different among groups. Presence of human AGT, human renin, or both human

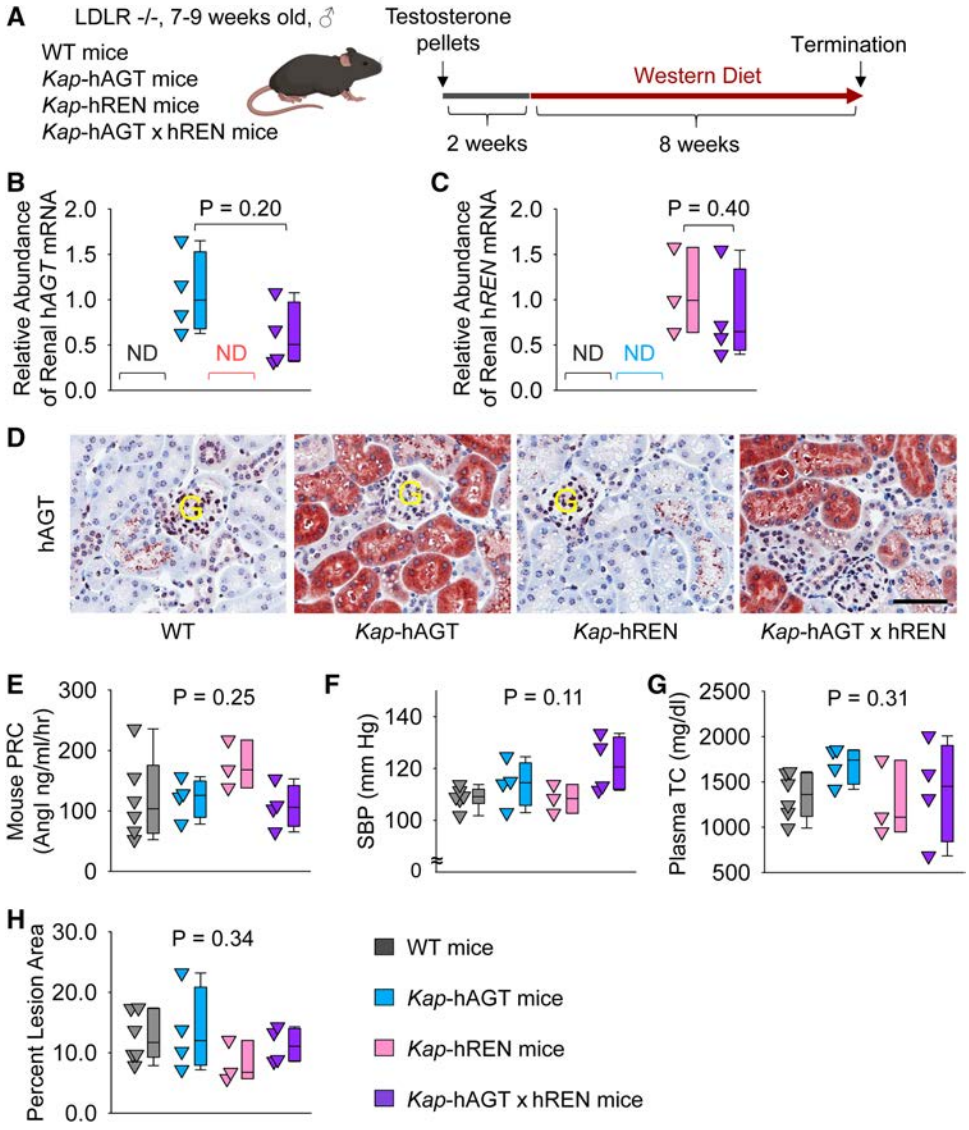

FIGURE 5
Human AGT and renin in PTCs had no effect on atherosclerosis in hypercholesterolemic mice. (A) Experimental protocol, (B) qPCR of renal human AGT (h*AGT*), (C) qPCR of renal human renin (h*REN*), (D) immunostaining of human AGT (hAGT) in kidney, (E) plasma renin concentrations (PRC), (F) systolic blood pressure (SBP), (G) plasma total cholesterol concentrations (TC), and (H) percent atherosclerotic lesion area. *N* = 3–6/group. Mann–Whitney *U* test was performed to determine the difference in the abundance of renal h*AGT* (B) or h*REN* (C) mRNA between two groups. Kruskal–Wallis one-way ANOVA on Ranks test was performed to determine the difference in each parameter among four groups (E–H). ND, not detectable; G, glomerulus.

AGT and renin in PTCs did not augment atherosclerotic lesions (Figure 5H).

Population of human AGT in liver and human renin in renal PTCs had no effect on atherosclerosis in male mice

Liver AGT is the major contributor to atherosclerosis and liver supplies AGT to renal proximal tubules (13, 32–34). Therefore, we populated human AGT in hepatocytes by intraperitoneally injecting an AAV encoding human AGT (Figure 6A). Since human AGT cannot be cleaved by mouse renin to produce AngI (35), we used *Kap*-hREN transgenic mice to express human renin specifically in PTCs. To activate human renin transgene in PTCs, testosterone pellets were implanted subcutaneously. Two weeks after administration of testosterone and AAVs, mice were fed Western diet for 6 weeks. mRNA of hAGT in liver (Figure 6B) and human AGT protein in plasma (Figure 6C) were only detected in mice infected with hAGT.AAVs. The presence of human AGT in mice infected with hAGT.AAVs was confirmed by immunostaining of human AGT in kidney sections of mice, supporting that human AGT protein was retained in mouse PTCs (Figure 6D). mRNA abundance of human renin was high in *Kap*-hREN mice, but it was not detected in mice without human renin transgene (Figure 6E). The presence of

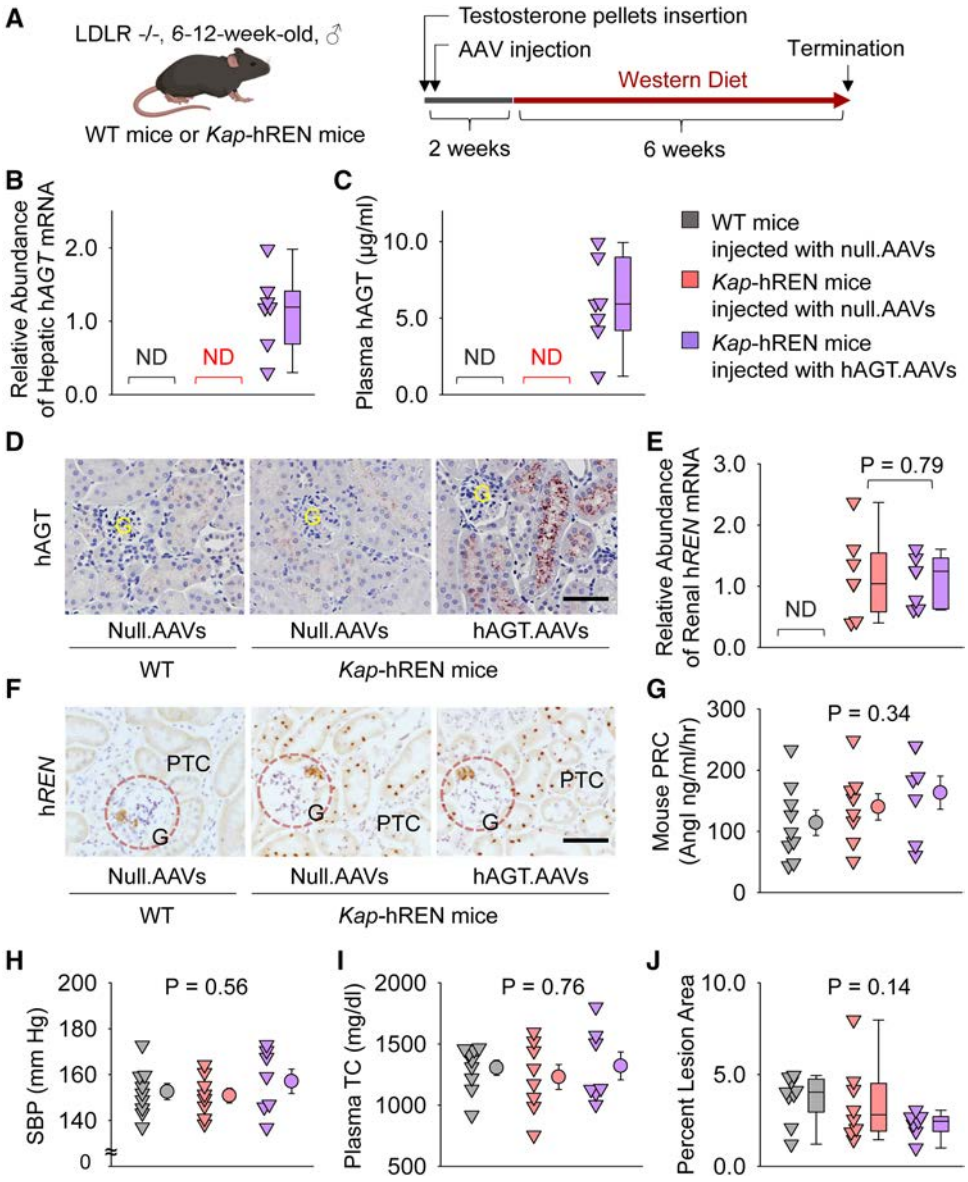

FIGURE 6
Human AGT in liver and human renin in PTCs had no effect on atherosclerosis in hypercholesterolemic mice. (**A**) Experimental protocol, (**B**) qPCR of renal human AGT (h*AGT*), (**C**) ELISA of plasma human AGT (hAGT), (**D**) immunostaining of human AGT (hAGT) in kidney, (**E**) qPCR of renal human renin (h*REN*), (**F**) RNAscope of human renin (h*REN*) in kidney, (**G**) plasma renin concentrations (PRC), (**H**) systolic blood pressure (SBP), (**I**) plasma total cholesterol concentrations (TC), and (**J**) percent atherosclerotic lesion area. $N = 7–9$/group. Mann–Whitney *U* test was performed to compare renal abundance of h*REN* mRNA between two *Kap*-hREN transgenic mouse groups (**E**) Kruskal–Wallis one-way ANOVA on Ranks test (**G–I**) or one-way ANOVA test (**J**) was performed to compare each parameter among the three groups. ND, not detectable; G, glomerulus; PTC, proximal tubule cells.

hREN mRNA in PTCs was also evaluated by RNAscope. Since the probe has a cross-reactivity for mouse renin, juxtaglomerular apparatus of both *Kap*-hREN transgenic mice and their wild-type littermate mice showed positive staining; however, positive staining of hREN in PTCs exhibited only in *Kap*-hREN transgenic mice (**Figure 6F**). Induction of human AGT in liver and human renin in PTCs did not change mouse plasma renin concentrations (**Figure 6G**) or systolic blood pressure (**Figure 6H**). All mice were equivalently hypercholesterolemic (**Figure 6I**) with indistinguishable atherosclerotic lesion size among the 3 groups (**Figure 6J**).

Discussion

The present study has three major findings. First, pharmacological inhibition of AT1R by losartan attenuates atherosclerosis in both male and female mice equivalently, although losartan suppresses blood pressure and increases plasma renin concentrations more profoundly in female mice. Second, inducible PTC-specific AT1aR or ACE deletion does not affect systolic blood pressure and atherosclerosis in hypercholesterolemic mice. Third, presence of human AGT and renin in PTCs does not augment atherosclerosis in mice.

AT1 receptor blockers (ARBs) have been used widely to treat high blood pressure and atherosclerosis in both men and women (36, 37). Human and rodent studies implicate that females might be more sensitive to the blood pressure-lowering effects of ARBs. We found that 12.5 mg/kg/d of losartan led to enhanced reductions of blood pressure in female mice, although systolic blood pressure in vehicle group between the two sexes was comparable. It is also interesting that losartan led to higher plasma renin concentrations in female mice than in male mice, implicating stronger negative feedback on AngII and AT1aR interaction in female mice.

Consistent with the effects of ARBs on blood pressure, genetic whole body AT1aR deletion in mice reduced blood pressure. Three studies reported effects of AT1aR deletion in PTCs on blood pressure in mice (38–40). Constitutive deletion of AT1aR on PTCs using *Pepck*-Cre (38) or *Sglt2*-Cre (39) resulted in lower systolic blood pressure, compared to their relative wild type mice; however, blood pressure was higher in mice with PTC-specific deletion of AT1aR than in mice with global AT1aR deletion, indicating that AT1aR in PTCs is not the only contributor to AngII-mediated blood pressure regulation (39). In contrast to blood pressure changes in mice with constitutive PTC-specific AT1aR deletion, testosterone inducible PTC-specific AT1aR deletion in adult mice by *Kap*-Cre did not affect blood pressure (40). This result is consistent with data from using tamoxifen-inducible *Ndrg1*-CreERT2$^{+/0}$ to delete AT1aR on PTCs in adult mice. One possibility is that constitutive vs. inducible deletion of AT1aR may have differential effects on blood pressure regulation. PTCs are composed of two different segments, proximal convoluted tubules (PCTs) and proximal straight tubules (PSTs). X-gal staining illustrated that Cre activity is present in ∼70% of PCTs and all PSTs in ROSA26R^{LacZ} × *Pepck*-Cre$^{+/0}$ mice (41). *Sglt2*-Cre activity was detected in 96% of all PTCs as defined by an anti-megalin antibody (42). *Kap*-Cre is mainly expressed in PTCs of the outer medulla, namely, PSTs (40, 43). We and Endo et al. found that *Ndrg1*-Cre predominantly leads to genetic deletions in PCTs (19). These results indicate that *Pepck*-Cre and *Sglt2*-Cre are more widely expressed in PTCs, compared to *Ndrg1*-Cre and *Kap*-Cre. Therefore, discrepancies of the blood pressure data may also relate to the magnitude of AT1aR deletion in renal proximal tubules.

Hypercholesterolemia leads to the RAS activation and promotes atherosclerosis (3, 44). There is a highly consistent literature that inhibition of ACE (21, 45, 46) or blockade of AT1R (21, 47, 48) have protective effects on hypercholesterolemia-induced atherosclerosis, although most studies only reported male mice. In one study, olmesartan (0.5 or 3 mg/kg/day) was administered to both male and female ApoE (apolipoprotein E) −/− mice fed a high cholesterol diet (49). The dose 0.5 mg/kg/day of olmesartan modestly reduced atherosclerosis in female mice, while 3 mg/kg/day reduced atherosclerosis equivalently in both sexes. In contrast to this study, Zhou et al. reported that female ApoE −/− mice had larger atherosclerotic lesions than male mice, and losartan (5 or 25 mg/kg/day) attenuated atherosclerosis only in female, but not in male, mice (50). We used LDL receptor −/− mice fed Western diet for 12 weeks. Despite the more profound blood pressure reduction in female mice, atherosclerotic lesion area was not different between male and female mice administered losartan. Our findings, in a study that has been performed simultaneously in both male and female mice, are consistent with losartan reducing atherosclerosis independent of blood pressure and sex. However, the mechanisms related to the different regulation of blood pressure and atherosclerosis remain to be defined.

Inhibition of the RAS components attenuates atherosclerosis with reductions in concentrations of renal AngII (12, 14, 21). Despite the associations between renal AngII and atherosclerosis, there has not been a determination whether manipulations in the renal RAS directly impact atherosclerosis. The present study provided direct evidence that AT1aR or ACE deletion on PTCs in adult mice does not affect hypercholesterolemia-induced atherosclerosis. Data generated by RNAscope demonstrated that *Agtr1a* mRNA is present in PTCs, glomeruli, and interstitial cells. AT1aR on podocytes and mesangial cells in glomeruli is important for the homeostasis of the glomerular wall, and interstitial cells communicate with PTCs through a paracrine system (51, 52). As shown by immunostaining, ACE is present predominantly in S3 of PTCs, whereas *Ndrg1*-Cre activation predominantly targets PCTs, but has a modest effect on PSTs. In addition to PTCs, ACE is abundant in endothelial cells of glomeruli and renal vessels. Our previous study has demonstrated that deletion of AT1aR or ACE on endothelial cells does not contribute to atherosclerosis (10, 17). Therefore, we do not predict that the presence of AT1aR or ACE on endothelial cells would affect atherosclerosis in PTC-specific AT1aR or ACE deficient mice. However, the present study cannot rule out that deletion of AT1aR or ACE in the entire kidney contributes to atherosclerosis. Unfortunately, there are no optimal mouse models available to study whether AT1aR or ACE in the whole kidney contributes to hypercholesterolemia-induced atherosclerosis.

Consistent with our findings of genetic deletion, increases of human AGT and renin in PTCs, with either direct increases of human AGT in PTCs (transgenic approach) or via population of human AGT in liver (AAV approach), has no effects on atherosclerosis in hypercholesterolemic mice. Although we have confirmed the high abundance of human AGT protein, we were not able to confirm whether human renin protein was highly abundant in PTCs due to lack of renin antibody specifically targeting human renin. We have also not been able to determine whether human AGT and renin could increase AngII in PTCs. Further studies on whether renal renin-angiotensin components affect atherosclerosis by deletion or increase of either renal AT1aR or AngII production in whole kidney will be considered when appropriate transgenic mice are available.

In summary, losartan leads to different magnitude of responsiveness on plasma renin concentrations and blood pressure between male and female mice, but comparable reductions in atherosclerosis in both sexes. Inducible PTC-specific deletion of AT1aR or ACE or increases of human AGT

and renin in adult mice does not affect blood pressure and atherosclerosis in hypercholesterolemic mice.

Data availability statement

The original contributions presented in the study are included in the article/**Supplementary Material**, further inquiries can be directed to the corresponding authors.

Ethics statement

The animal study was approved by the University of Kentucky Institutional Animal Care and Use Committee (Protocol number 2018–2968). The study was conducted in accordance with the local legislation and institutional requirements.

Author contributions

AD and HL designed the study and coordinated all experimental work. MK, NA, DY, HC, JM, CL, DH, and HS carried out the experimental work. MY provided protocol and advice for activation of *Ndrg1*-CreERT2 in mice. MK, NA, YK, and HL analyzed and interpreted the data. MK, NA, AD, and HL wrote the manuscript with valuable input from all other authors. All authors contributed to the article and approved the submitted version.

Funding

This research work was supported by the National Heart, Lung, and Blood Institute of the National Institutes of Health under award numbers R01HL139748. The content in this manuscript is solely the responsibility of the authors and does not necessarily represent the official views of the National Institutes of Health.

Acknowledgments

Histological and immunohistological images were taken using Zeiss Axioscan 1 or 7 or Nikon A1R confocal microscope in the Light Microscopy Core at the University of Kentucky.

Conflict of interest

The authors declare that the research was conducted in the absence of any commercial or financial relationships that could be construed as a potential conflict of interest.

Publisher's note

Supplementary material

The Supplementary Material for this article can be found online at: https://www.frontiersin.org/articles/10.3389/fcvm.2023.1250234/full#supplementary-material

References

1. Robinet P, Milewicz DM, Cassis LA, Leeper NJ, Lu HS, Smith JD. Consideration of sex differences in design and reporting of experimental arterial pathology studies-statement from ATVB council. *Arterioscler Thromb Vasc Biol.* (2018) 38:292–303. doi: 10.1161/ATVBAHA.117.309524

2. Wu CH, Mohammadmoradi S, Chen JZ, Sawada H, Daugherty A, Lu HS. Renin-angiotensin system and cardiovascular functions. *Arterioscler Thromb Vasc Biol.* (2018) 38:e108–16. doi: 10.1161/ATVBAHA.118.311282

3. Rader DJ, Daugherty A. Translating molecular discoveries into new therapies for atherosclerosis. *Nature.* (2008) 451:904–13. doi: 10.1038/nature06796

4. Wu C, Lu H, Cassis LA, Daugherty A. Molecular and pathophysiological features of angiotensinogen: a mini review. *N Am J Med Sci (Boston).* (2011) 4:183–90. doi: 10.7156/v4i4p183

5. Daugherty A, Rateri DL, Lu H, Inagami T, Cassis LA. Hypercholesterolemia stimulates angiotensin peptide synthesis and contributes to atherosclerosis through the AT1A receptor. *Circulation.* (2004) 110:3849–57. doi: 10.1161/01.CIR.0000150540.54220.C4

6. Dzau VJ, Bernstein K, Celermajer D, Cohen J, Dahlof B, Deanfield J, et al. The relevance of tissue angiotensin-converting enzyme: manifestations in mechanistic and endpoint data. *Am J Cardiol.* (2001) 88:1l–20l. doi: 10.1016/S0002-9149(01)01878-1

7. Potter DD, Sobey CG, Tompkins PK, Rossen JD, Heistad DD. Evidence that macrophages in atherosclerotic lesions contain angiotensin II. *Circulation.* (1998) 98:800–7. doi: 10.1161/01.CIR.98.8.800

8. Dzau VJ. Tissue angiotensin and pathobiology of vascular disease—a unifying hypothesis. *Hypertension.* (2001) 37:1047–52. doi: 10.1161/01.HYP.37.4.1047

9. Cassis LA, Rateri DL, Lu H, Daugherty A. Bone marrow transplantation reveals that recipient AT1a receptors are required to initiate angiotensin II-induced atherosclerosis and aneurysms. *Arterioscler Thromb Vasc Biol.* (2007) 27:380–6. doi: 10.1161/01.ATV.0000254680.71485.92

10. Rateri DL, Moorleghen JJ, Knight V, Balakrishnan A, Howatt DA, Cassis LA, et al. Depletion of endothelial or smooth muscle cell-specific angiotensin II type 1a receptors does not influence aortic aneurysms or atherosclerosis in LDL receptor deficient mice. *PLoS One.* (2012) 7:e51483. doi: 10.1371/journal.pone.0051483

11. Lu H, Rateri DL, Feldman DL, Charnigo RJ Jr, Fukamizu A, Ishida J, et al. Renin inhibition reduces hypercholesterolemia-induced atherosclerosis in mice. *J Clin Invest.* (2008) 118:984–93. doi: 10.1172/JCI32970

12. Ye F, Wang Y, Wu C, Howatt DA, Wu CH, Balakrishnan A, et al. Angiotensinogen and megalin interactions contribute to atherosclerosis. *Arterioscler Thromb Vasc Biol.* (2019) 39:150–5. doi: 10.1161/ATVBAHA.118.311817

13. Wu CH, Wu C, Howatt DA, Moorleghen JJ, Cassis LA, Daugherty A, et al. Two amino acids proximate to the renin cleavage site of human angiotensinogen do not affect blood pressure and atherosclerosis in mice. *Arterioscler Thromb Vasc Biol.* (2020) 40:2108–13. doi: 10.1161/ATVBAHA.120.314048

14. Kukida M, Sawada H, Ohno-Urabe S, Howatt DA, Moorleghen JJ, Poglitsch M, et al. Effects of endogenous angiotensin II on abdominal aortic aneurysms and

atherosclerosis in angiotensin II-infused mice. *J Am Heart Assoc*. (2021) 10:e020467. doi: 10.1161/JAHA.121.020467

15. Lavoie JL, Lake-Bruse KD, Sigmund CD. Increased blood pressure in transgenic mice expressing both human renin and angiotensinogen in the renal proximal tubule. *Am J Physiol Renal Physiol*. (2004) 286:F965–971. doi: 10.1152/ajprenal.00402.2003

16. Rateri DL, Moorleghen JJ, Balakrishnan A, Owens AP, Howatt DA, Subramanian V, et al. Endothelial cell-specific deficiency of Ang II type 1a receptors attenuates Ang II-induced ascending aortic aneurysms in LDL receptor −/− mice. *Circ Res*. (2011) 108:574–81. doi: 10.1161/CIRCRESAHA.110.222844

17. Chen X, Howatt DA, Balakrishnan A, Moorleghen JJ, Wu C, Cassis LA, et al. Angiotensin-converting enzyme in smooth muscle cells promotes atherosclerosis. *Arterioscler Thromb Vasc Biol*. (2016) 36:1085–9. doi: 10.1161/ATVBAHA.115.307038

18. Sawada H, Kukida M, Chen X, Howatt DA, Moorleghen JJ, Balakrishnan A, et al. Angiotensin I infusion reveals differential effects of angiotensin-converting enzyme in aortic resident cells on aneurysm formation. *Circ J*. (2020) 84:825–9. doi: 10.1253/circj.CJ-19-0955

19. Endo T, Nakamura J, Sato Y, Asada M, Yamada R, Takase M, et al. Exploring the origin and limitations of kidney regeneration. *J Pathol*. (2015) 236:251–63. doi: 10.1002/path.4514

20. Lavoie JL, Bianco RA, Sakai K, Keen HL, Ryan MJ, Sigmund CD. Transgenic mice for studies of the renin-angiotensin system in hypertension. *Acta Physiol Scand*. (2004) 181:571–7. doi: 10.1111/j.1365-201X.2004.01332.x

21. Lu H, Balakrishnan A, Howatt DA, Wu C, Charnigo R, Liau G, et al. Comparative effects of different modes of renin angiotensin system inhibition on hypercholesterolaemia-induced atherosclerosis. *Br J Pharmacol*. (2012) 165:2000–8. doi: 10.1111/j.1476-5381.2011.01712.x

22. Chen H, Howatt DA, Franklin MK, Amioka N, Sawada H, Daugherty A, et al. A mini-review on quantification of atherosclerosis in hypercholesterolemic mice. *Glob Transl Med*. (2022) 1:72. doi: 10.36922/gtm.v1i1.76

23. Daugherty A, Tall AR, Daemen M, Falk E, Fisher EA, Garcia-Cardena G, et al. Recommendation on design, execution, and reporting of animal atherosclerosis studies: a scientific statement from the American heart association. *Arterioscler Thromb Vasc Biol*. (2017) 37:e131–57. doi: 10.1161/ATV.0000000000000062

24. Lu H, Howatt DA, Balakrishnan A, Moorleghen JJ, Rateri DL, Cassis LA, et al. Subcutaneous angiotensin II infusion using osmotic pumps induces aortic aneurysms in mice. *J Vis Exp*. (2015) 103:53191. doi: 10.3791/53191

25. Daugherty A, Rateri D, Lu H, Balakrishnan A. Measuring blood pressure in mice using volume pressure recording, a tail-cuff method. *J Vis Exp*. (2009) 27:1291. doi: 10.3791/1291

26. Poduri A, Owens AP 3rd, Howatt DA, Moorleghen JJ, Balakrishnan A, Cassis LA, et al. Regional variation in aortic AT1b receptor mRNA abundance is associated with contractility but unrelated to atherosclerosis and aortic aneurysms. *PLoS One*. (2012) 7:e48462. doi: 10.1371/journal.pone.0048462

27. Elliott KJ, Kimura K, Eguchi S. Lack of specificity of commercial antibodies leads to misidentification of angiotensin type-1 receptor protein. *Hypertension*. (2013) 61:e31. doi: 10.1161/HYPERTENSIONAHA.111.00943

28. Benicky J, Hafko R, Sanchez-Lemus E, Aguilera G, Saavedra JM. Six commercially available angiotensin II AT(1) receptor antibodies are non-specific. *Cell Mol Neurobiol*. (2012) 32:1353–65. doi: 10.1007/s10571-012-9862-y

29. Herrera M, Sparks MA, Alfonso-Pecchio AR, Harrison-Bernard LM, Coffman TM. Lack of specificity of commercial antibodies leads to misidentification of angiotensin type 1 receptor protein. *Hypertension*. (2013) 61:253–8. doi: 10.1161/HYPERTENSIONAHA.112.203679

30. Herrera M, Sparks MA, Alfonso-Pecchio AR, Harrison-Bernard LM, Coffman TM. Response to lack of specificity of commercial antibodies leads to misidentification of angiotensin type-1 receptor protein. *Hypertension*. (2013) 61:e32. doi: 10.1161/hypertensionaha.111.00982

31. Schrankl J, Fuchs M, Broeker K, Daniel C, Kurtz A, Wagner C. Localization of angiotensin II type 1 receptor gene expression in rodent and human kidneys. *Am J Physiol Renal Physiol*. (2021) 320:F644–f653. doi: 10.1152/ajprenal.00550.2020

32. Lu H, Wu C, Howatt DA, Balakrishnan A, Moorleghen JJ, Chen X, et al. Angiotensinogen exerts effects independent of angiotensin II. *Arterioscler Thromb Vasc Biol*. (2016) 36:256–65. doi: 10.1161/ATVBAHA.115.306740

33. Wu C, Xu Y, Lu H, Howatt DA, Balakrishnan A, Moorleghen JJ, et al. Cys18-Cys137 disulfide bond in mouse angiotensinogen does not affect Ang II-dependent functions in vivo. *Hypertension*. (2015) 65:800–5. doi: 10.1161/HYPERTENSIONAHA.115.05166

34. Amioka N, Wu CH, Sawada H, Ito S, Pettey AC, Wu C, et al. Functional exploration of conserved sequences in the distal face of angiotensinogen. *Arterioscler Thromb Vasc Biol*. (2023) 43:1524–32. doi: 10.1161/ATVBAHA.122.318930

35. Fukamizu A, Sugimura K, Takimoto E, Sugiyama F, Seo MS, Takahashi S, et al. Chimeric renin-angiotensin system demonstrates sustained increase in blood pressure of transgenic mice carrying both human renin and human angiotensinogen genes. *J Biol Chem*. (1993) 268:11617–21. doi: 10.1016/S0021-9258(19)50246-0

36. Law MR, Morris JK, Wald NJ. Use of blood pressure lowering drugs in the prevention of cardiovascular disease: meta-analysis of 147 randomised trials in the context of expectations from prospective epidemiological studies. *Br Med J*. (2009) 338:b1665. doi: 10.1136/bmj.b1665

37. McAlister FA. Angiotensin-converting enzyme inhibitors or angiotensin receptor blockers are beneficial in normotensive atherosclerotic patients: a collaborative meta-analysis of randomized trials. *Eur Heart J*. (2012) 33:505–14. doi: 10.1093/eurheartj/ehr400

38. Gurley SB, Riquier-Brison AD, Schnermann J, Sparks MA, Allen AM, Haase VH, et al. AT1A Angiotensin receptors in the renal proximal tubule regulate blood pressure. *Cell Metab*. (2011) 13:469–75. doi: 10.1016/j.cmet.2011.03.001

39. Li XC, Leite APO, Zheng X, Zhao C, Chen X, Zhang L, et al. Proximal tubule-specific deletion of angiotensin II type 1a receptors in the kidney attenuates circulating and intratubular angiotensin II-induced hypertension in PT-Agtr1a(−/−) mice. *Hypertension*. (2021) 77:1285–98. doi: 10.1161/HYPERTENSIONAHA.120.16336

40. Li H, Weatherford ET, Davis DR, Keen HL, Grobe JL, Daugherty A, et al. Renal proximal tubule angiotensin AT1A receptors regulate blood pressure. *Am J Physiol Regul Integr Comp Physiol*. (2011) 301:R1067–1077. doi: 10.1152/ajpregu.00124.2011

41. Rankin EB, Tomaszewski JE, Haase VH. Renal cyst development in mice with conditional inactivation of the von hippel-lindau tumor suppressor. *Cancer Res*. (2006) 66:2576–83. doi: 10.1158/0008-5472.CAN-05-3241

42. Rubera I, Poujeol C, Bertin G, Hasseine L, Counillon L, Poujeol P, et al. Specific Cre/Lox recombination in the mouse proximal tubule. *J Am Soc Nephrol*. (2004) 15:2050–6. doi: 10.1097/01.ASN.0000133023.89251.01

43. Ding Y, Davisson RL, Hardy DO, Zhu LJ, Merrill DC, Catterall JF, et al. The kidney androgen-regulated protein promoter confers renal proximal tubule cell-specific and highly androgen-responsive expression on the human angiotensinogen gene in transgenic mice. *J Biol Chem*. (1997) 272:28142–8. doi: 10.1074/jbc.272.44.28142

44. Daugherty A, Lu H, Rateri DL, Cassis LA. Augmentation of the renin-angiotensin system by hypercholesterolemia promotes vascular diseases. *Future Lipidol*. (2008) 3:625–36. doi: 10.2217/17460875.3.6.625

45. Hayek T, Attias J, Smith J, Breslow JL, Keidar S. Antiatherosclerotic and antioxidative effects of captopril in apolipoprotein E-deficient mice. *J Cardiovasc Pharmacol*. (1998) 31:540–4. doi: 10.1097/00005344-199804000-00011

46. Keidar S, Attias J, Coleman R, Wirth J, Scholkens B, Hayek T. Attenuation of atherosclerosis in apolipoprotein E-deficient mice by ramipril is dissociated from its antihypertensive effect and from potentiation of bradykinin. *J Cardiovasc Pharmacol*. (2000) 35:64–72. doi: 10.1097/00005344-200001000-00008

47. Keidar S, Attias J, Smith J, Breslow JL, Hayek T. The angiotensin-II receptor antagonist, losartan, inhibits LDL lipid peroxidation and atherosclerosis in apolipoprotein E-deficient mice. *Biochem Biophys Res Comm*. (1997) 236:622–5. doi: 10.1006/bbrc.1997.6844

48. Matsumura T, Kinoshita H, Ishii N, Fukuda K, Motoshima H, Senokuchi T, et al. Telmisartan exerts antiatherosclerotic effects by activating peroxisome proliferator-activated receptor-gamma in macrophages. *Arterioscler Thromb Vasc Biol*. (2011) 31:1268–75. doi: 10.1161/ATVBAHA.110.222067

49. Tsuda M, Iwai M, Li JM, Li HS, Min LJ, Ide A, et al. Inhibitory effects of AT1 receptor blocker, olmesartan, and estrogen on atherosclerosis via anti-oxidative stress. *Hypertension*. (2005) 45:545–51. doi: 10.1161/01.HYP.0000157409.88971.fc

50. Zhou Y, Chen R, Catanzaro SE, Hu L, Dansky HM, Catanzaro DF. Differential effects of angiotensin II on atherogenesis at the aortic sinus and descending aorta of apolipoprotein-E-deficient mice. *Am J Hypertens*. (2005) 18:486–92. doi: 10.1016/j.amjhyper.2004.11.005

51. Suzuki K, Han GD, Miyauchi N, Hashimoto T, Nakatsue T, Fujioka Y, et al. Angiotensin II type 1 and type 2 receptors play opposite roles in regulating the barrier function of kidney glomerular capillary wall. *Am J Pathol*. (2007) 170:1841–53. doi: 10.2353/ajpath.2007.060484

52. Nishiyama A, Nakagawa T, Kobori H, Nagai Y, Okada N, Konishi Y, et al. Strict angiotensin blockade prevents the augmentation of intrarenal angiotensin II and podocyte abnormalities in type 2 diabetic rats with microalbuminuria. *J Hypertens*. (2008) 26:1849–59. doi: 10.1097/HJH.0b013e3283060efa

frontiers | Frontiers in Cardiovascular Medicine

TYPE Original Research
PUBLISHED 28 August 2023
DOI 10.3389/fcvm.2023.1198486

OPEN ACCESS

EDITED BY
Natarajaseenivasan Kalimuthusamy,
Bharathidasan University, India

REVIEWED BY
Yubi Lin,
Sun Yat-sen University, China
Georgia Ragia,
Democritus University of Thrace, Greece

*CORRESPONDENCE
Sheng-Hua Zhou
✉ zhoushenghua@csu.edu.cn
Yi-Chao Xiao
✉ yichaoxiao@csu.edu.cn

RECEIVED 01 April 2023
ACCEPTED 27 June 2023
PUBLISHED 28 August 2023

CITATION
Wu C-K, Teng S, Bai F, Liao X-B, Zhou X-M, Liu Q-M, Xiao Y-C and Zhou S-H (2023) Changes of ubiquitylated proteins in atrial fibrillation associated with heart valve disease: proteomics in human left atrial appendage tissue.
Front. Cardiovasc. Med. 10:1198486.
doi: 10.3389/fcvm.2023.1198486

Changes of ubiquitylated proteins in atrial fibrillation associated with heart valve disease: proteomics in human left atrial appendage tissue

Chen-Kai Wu[1], Shuai Teng[1], Fan Bai[1], Xiao-Bo Liao[2], Xin-Min Zhou[2], Qi-Ming Liu[1], Yi-Chao Xiao[1]* and Sheng-Hua Zhou[1]*

[1]Department of Cardiology, The Second Xiangya Hospital, Central South University, Changsha, China, [2]Department of Cardiovascular Surgery, The Second Xiangya Hospital, Central South University, Changsha, China

Background: Correlations between posttranslational modifications and atrial fibrillation (AF) have been demonstrated in recent studies. However, it is still unclear whether and how ubiquitylated proteins relate to AF in the left atrial appendage of patients with AF and valvular heart disease.
Methods: Through LC–MS/MS analyses, we performed a study on tissues from eighteen subjects (9 with sinus rhythm and 9 with AF) who underwent cardiac valvular surgery. Specifically, we explored the ubiquitination profiles of left atrial appendage samples.
Results: In summary, after the quantification ratios for the upregulated and downregulated ubiquitination cutoff values were set at >1.5 and <1:1.5, respectively, a total of 271 sites in 162 proteins exhibiting upregulated ubiquitination and 467 sites in 156 proteins exhibiting downregulated ubiquitination were identified. The ubiquitylated proteins in the AF samples were enriched in proteins associated with ribosomes, hypertrophic cardiomyopathy (HCM), glycolysis, and endocytosis.
Conclusions: Our findings can be used to clarify differences in the ubiquitination levels of ribosome-related and HCM-related proteins, especially titin (TTN) and myosin heavy chain 6 (MYH6), in patients with AF, and therefore, regulating ubiquitination may be a feasible strategy for AF.

KEYWORDS

atrial fibrillation, ubiquitination, proteomics, protein-protein interaction networks, TTN, MYH6

1. Introduction

One of the major causes of systemic embolism and cardioembolic stroke is atrial fibrillation (AF), which is caused by hemodynamic instability and blood hypercoagulability in clinical practice. Overall, the prevalence of AF will continue to grow with population aging. In the Chinese population over 40 years of age, the prevalence of AF was 1.57% in 2013 (1). AF is still an important public health concern. Drugs and radiofrequency ablation exhibit finite efficiency and safety, and the molecular mechanism underlying the progression of AF remains unclear.

Posttranslational modifications (PTMs) of proteins are covalent modifications. PTMs include ubiquitination, which involves the addition of ubiquitin to a protein, methylation, glycosylation, phosphorylation, acylations, acetylation, and lipidation (2). Ubiquitination is a dynamic multifaceted posttranslational modification where a small protein called

ubiquitin is added to a target protein, and ubiquitin, a protein consisting of 76 AAs, is the fundamental unit of ubiquitination. The ubiquitin–proteasome system (UPS) is vital for targeting specific proteins for degradation and controls cellular processes such as protein sorting, signal transduction and DNA repair. Ubiquitination also regulates protein localization and function independent of its effect on protein degradation (3, 4). Ubiquitination plays a central role in cardiovascular diseases (5), such as cardiac hypertrophy (6), congenital heart defects (7), diabetic heart diseases (8–11), and cardiac arrhythmias (12–16), functions with myocardial β 1-adrenergic receptor under physiological conditions (17), and is involved in redox homeostasis, such that it can create an imbalance that leads to cardiovascular complications (18). Furthermore, ubiquitination also plays a role in the occurrence and development of atrial fibrillation. For example, in atrial cardiomyocytes of rabbits with atrial fibrillation, Rfp2 has been found to be upregulated, which leads to the ubiquitination of Cav1.2 to autophagosomes, and these changes induce atrial electrical remodeling (19). Another recent study clarified the relationship between the E3 ubiquitin protein ligase tripartite motif-containing protein 21 and atrial remodeling and AF after myocardial infarction atrial remodeling (20). The degradation of Smad7 by Arkadia-mediated polyubiquitination plays an important role in AF-induced atrial fibrosis (21). Although several studies report evaluations of ubiquitination in the context of AF, proteome-wide analyses have not yet been conducted. The purpose of this study is to clarify whether there are changes in ubiquitination during atrial fibrillation, what specific alterations occur, and how they relate to functional changes.

In this study, we performed LC–MS/MS analysis to identify proteins with ubiquitination that were altered in AF tissues. A total of 271 sites in 162 proteins exhibiting upregulated ubiquitination and 467 sites in 156 proteins exhibiting downregulated ubiquitination were identified. Most upregulated and downregulated ubiquitylated proteins were located in the cytoplasm. A protein–protein interaction (PPI) network analysis revealed that glycolysis-related, ribosome-related, endocytosis-related, and hypertrophic cardiomyopathy-related proteins were highly associated with ubiquitination in AF tissues.

2. Subjects and methods

2.1. Study design

A single-center study was conducted with patients undergoing cardiac valvular replacement surgery at the Second Xiangya Hospital of Central South University. Based on their symptoms and results of 12-channel electrocardiography or 24-h Holter electrocardiography, the subjects were assigned to a chronic AF group (onset time ≥1 year) or a sinus rhythm (SR) group. All patients underwent transthoracic echocardiography (TTE) before surgery, and other general patient data were collected. Based on coronary angiography (CAG), patients with coronary artery disease (CAD) were excluded from the study. A piece of tissue was sliced from the left atrial appendages (LAA) of the enrolled patients during surgery.

We obtained ethical approval for the study from the Ethics Committee of the Second Xiangya Hospital of Central South University. Written informed consent was obtained by all the subjects or their legal representatives. The study was conducted based on the Declaration of Helsinki. The flow chart of the study is illustrated in **Figure 1A**.

2.2. Protein extraction and trypsin digestion

The specimens were obtained from the LAA during mitral valve surgery and were immediately flash-frozen in liquid nitrogen and stored in liquid nitrogen. To analyze the ubiquitination characteristics of the samples, a mixture of 3 tissue samples from the same group was considered to be one sample. We obtained 3 of these mixed samples for each group. The ground tissue was lysed by sonication in lysis buffer. Debris was removed through centrifugation. Finally, a BCA kit was used to measure the protein concentration of the prepared samples.

Equal amounts of protein were taken based on concentration measurement, and the volume was adjusted with lysis buffer. The samples were then treated with 20% TCA and incubated at 4°C for 2 h. After centrifugation at 4,500 × *g* for 5 min at 4°C, the supernatant was discarded, and the protein pellet was washed three times with cold acetone. The protein pellet was air-dried and then resuspended in 200 mM TEAB followed by sonication to disperse the precipitate. Trypsin was added at a ratio of 1:50 and incubated overnight at 37°C. Dithiothreitol (DTT) was subsequently added to a final concentration of 5 mM and incubated at 56°C for 30 min, followed by alkylation with IAA at a final concentration of 11 mM at room temperature in the dark for 15 min. After that, trypsin was added again at a ratio of 1:100, and the samples were further digested for 4 h.

2.3. Affinity enrichment

The peptides obtained were dissolved in IP buffer solution, and the supernatant was poured into a flask containing prewashed antibody-loaded beads, placed on a rotating shaker at 4°C, and gently shaken overnight. After incubation, the beads were washed 4 times with IP buffer and twice with deionized water. Finally, 0.1% trifluoroacetic acid eluent was used 3 times to elute the bead-bound peptides. Finally, the eluted fractions were combined and vacuum-dried. After drying, the resulting peptides were desalted and used for LC–MS/MS analysis.

2.4. LC−MS/MS analysis

The peptides were dissolved and then separated using NanoElute Ultra Performance Liquid Chromatography (UPLC). Solvent A was an aqueous solution containing 0.1% formic acid and 2% acetonitrile; solvent B was an acetonitrile solution

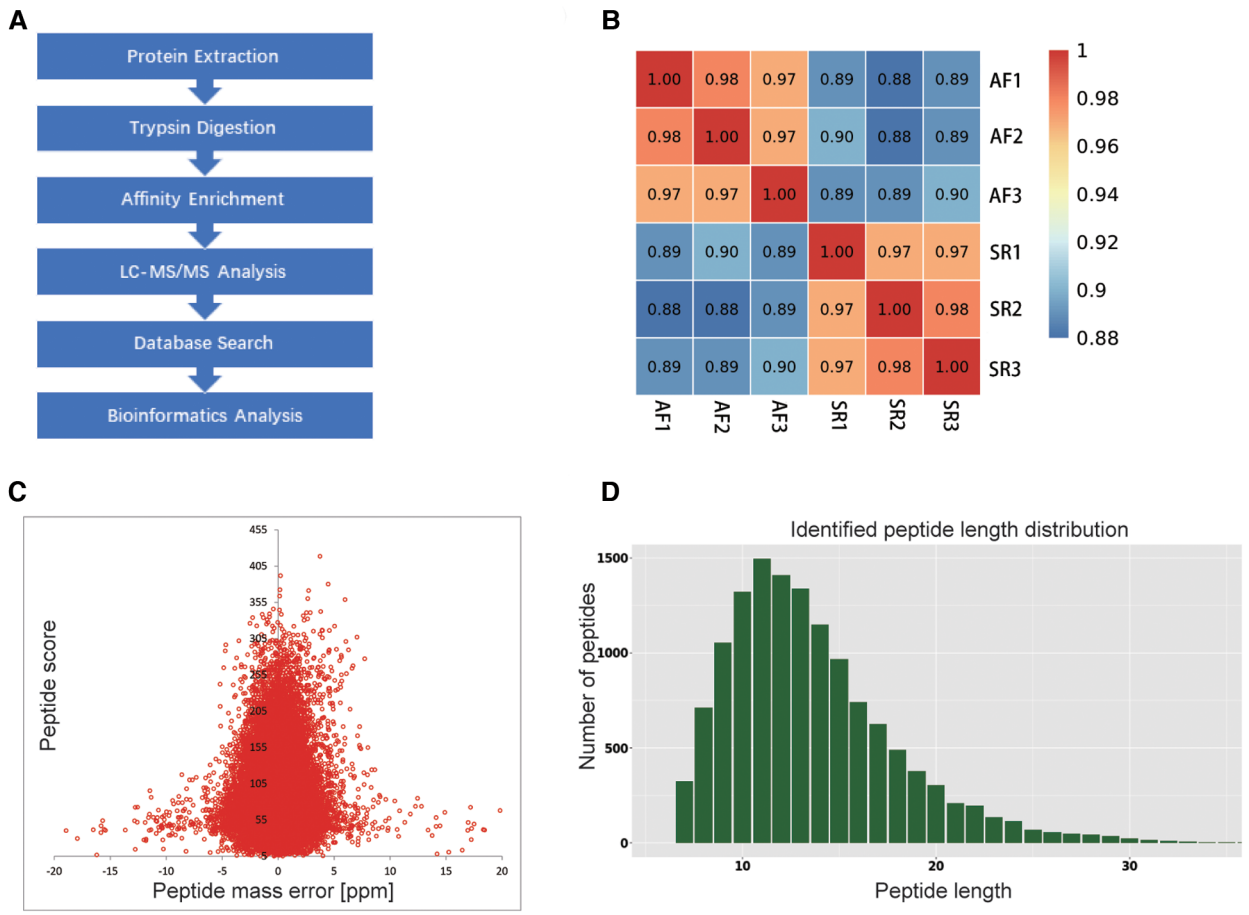

FIGURE 1
Flow chart of the study and QC validation. (A) Flow chart showing the proteomic ubiquitination analysis of SR and AF samples. (B) Consistency among 3 mixed tissue sample replicates was indicated by Pearson's correlation coefficient. (C) QC validation of the MS data: the accuracy of the mass data was in line with that needed, and most mass errors were <5 ppm. (D) The length of most peptides ranged from 7 to 20 AAs.

containing 0.1% formic acid. The gradient consisted of solvent B increasing from 6% to 22% for 43 min, from 22% to 30% for 13 min, and from 30% to 80% for 3 min, all at a constant flow rate of 450 nl/min.

The peptides were separated by UPLC, injected into the NSI source for ionization and then analyzed by a tims-TOF Pro mass spectrometer. The electrospray voltage was set at 1.6 kV, and the peptide precursor ions and their secondary fragments were detected and analyzed by TOF. The m/z scan range of the secondary mass spectrum was set to 100–1,700 m/z, and intact peptides were detected in the Orbitrap at a resolution of 70,000. The data acquisition mode applied was parallel accumulation and serial fragmentation (PASEF). After the first-level mass spectra were collected, the second-level spectra with precursor ion charges in the range of 0–5 were collected in PASEF mode 10 times, and the dynamic rejection time applied to the tandem mass spectrum scan was 24 s to avoid repeated scans of the precursor ions. The concentration of the injection was 2 mg, the analysis temperature was set as 50°C, and the runtime of analysis was set as 60 min. We used a homemade reversed-phase analytical column (100 µm i.d. × 25 cm) packed with 1.9 µm/120 Å ReproSil PurC18 resins (Dr. Maisch GmbH, Ammerbuch, Germany).

2.5. Database search

Secondary mass spectrum data were searched using MaxQuant (v1.6.6.0). The following search parameter settings were used: The database was Homo_sapiens_9606_SP_20191115 (20380 sequences), a reverse database was applied to calculate the false-positive rate (FDR) caused by random matching, and a common contamination library was applied to eliminate the impact of contaminating proteins on the identification results; the cleavage enzyme was set to Trypsin/P. The FDR for protein identification and peptide-spectrum match (PSM) identification was adjusted to <1%.

2.6. Bioinformatics methods

The UniProt-GOA database (http://www.ebi.ac.uk/GOA/) was used for Gene Ontology (GO) annotation of the proteome. GO covers three domains: cellular component, molecular function, and biological process. Kyoto Encyclopedia of Genes and Genomes (KEGG) pathway annotation was derived from the KEGG database (http://www.genome.jp/kegg/).

The subcellular localization prediction software WoLF PSORT (https://wolfpsort.hgc.jp/) was used. The motif characteristics of the ubiquitylated AAs were analyzed using MoMo software (the motif-x algorithm). A protein–protein interaction enrichment analysis was performed with the STRING database version 11.0. A corrected *P value* <0.05 was considered statistically significant in the bioinformatics analysis. The methodology used for the validation analysis was a two-sample *t* test.

2.7. Data availability

The primary proteomics data produced in this study are uploaded to PRIDE: Project PXD030397 https://www.ebi.ac.uk/pride/archive/projects/PXD030397.

3. Results

3.1. Subject characteristics

Table 1 summarizes the demographic and baseline characteristics of the patients. The parameters in the SR and AF groups were matched with respect to gender ratio, BMI (25.25 ± 5.09 vs. 22.33 ± 3.33 kg/m^2, $P = 0.169$), age (59.22 ± 6.72 vs. 56.44 ± 9.26 years, $P = 0.477$), fasting blood glucose (4.81 ± 072 vs. 5.03 ± 0.69 mmol/L, $P = 0.493$), triglycerides levels (1.34 ± 0.56 vs. 1.06 ± 0.54 mmol/L, $P = 0.308$), total cholesterol levels (4.08 ± 0.70 vs. 3.81 ± 0.27 mmol/L, $P = 0.303$), EF (64.22 ± 9.51% vs. 59.44 ± 7.76%, $P = 0.260$), comorbidities and pharmacological treatment. The difference observed in LA size was significant (35.00 ± 5.92 vs. 59.44 ± 7.76 mm, $P = 0.000$).

TABLE 1 Demographic and baseline data of the subjects.

	SR ($n = 9$)	AF ($n = 9$)	*P* value
Male/female (*n*, %)	3 (33.3%)/6 (66.6%)	5 (55.5%)/4 (44.4%)	0.343
BMI (kg/m^2)	25.25 ± 5.09	22.33 ± 3.33	0.169
Age (year)	59.22 ± 6.72	56.44 ± 9.26	0.477
Fasting blood glucose (mmol/L)	4.81 ± 072	5.03 ± 0.69	0.493
Triglycerides (mmol/L)	1.34 ± 0.56	1.06 ± 0.54	0.308
Total cholesterol (mmol/L)	4.08 ± 0.70	3.81 ± 0.27	0.303
LA size (mm)	35.00 ± 5.92	58.89 ± 8.37	0.000
EF (%)	64.22 ± 9.51	59.44 ± 7.76	0.260
Mitral valve area (mm^2)	137.00 ± 26.42	141.00 ± 51.25	0.282
Mitral regurgitation			0.653
Grade II (*n*)	6	5	
Grade III (*n*)	3	4	
NYHA class (II/III) (*n*)	2/7	1/8	0.555
Comorbidities			
Hypertension (*n*, %)	2 (22.2%)	2 (22.2%)	1.000
Congestive heart failure (*n*, %)	9 (100%)	9 (100%)	1.000
Diabetes (*n*, %)	2 (22.2%)	3 (33.3%)	0.599
Stroke or TIA (*n*, %)	0 (0.00%)	0 (0.00%)	1.000
Pharmacological treatment			
Beta blockers (*n*, %)	8 (88.88%)	8 (88.88%)	1.000
ACE inhibitors (*n*, %)	6 (66.66%)	8 (88.88%)	0.257
Amiodarone (*n*, %)	0 (0.00%)	2 (0.00%)	0.134

3.2. Quantitative analysis of lysine ubiquitination in LAA

To explore whether the ubiquitination rate was influenced by AF status. A quantitative ubiquitination analysis was performed based on UPLC–MS/MS data. A mixture of every 3 tissues from the same group was recognized as one sample. Consistency in the analysis of 3 mixed-tissue samples (triplicate samples) was indicated through Pearson's correlation analysis (**Figure 1B**). The overall accuracy of the mass data acquired by MS was in line with that required for the analysis, with most mass errors <5 ppm (**Figure 1C**). As illustrated in **Figure 1D**, most peptide lengths ranged from 7 to 20 AAs. In general, as illustrated in **Figure 2A**, changes in ubiquitination were observed in 4,788 quantifiable sites and 1,631 quantifiable proteins. There were <5 modified sites in most proteins (**Figure 2B**). The quantification ratios for the downregulated and upregulated ubiquitination cutoff values were set at <1:1.5 and >1.5, respectively; 156 downregulated ubiquitinated proteins and 162 upregulated ubiquitinated proteins were identified. As illustrated in **Figures 2C,D**, ubiquitination was downregulated at 467 sites, and ubiquitination was upregulated at 271 sites.

Among these differentially ubiquitylated proteins, titin (TTN), contributing to sarcomere assembly and conferring stability during the cardiac cycle, harbored the most sites (174). Myosin heavy chain 6 (MYH6) harbored 38 sites, and myosin heavy chain 7 (MYH7) harbored 11 sites. Mutations in MYH6 and MYH7 are associated with hypertrophic cardiomyopathy. MYH6 and MYH7 are the alpha heavy chain subunit and beta (or slow) heavy chain subunit of cardiac myosin, respectively. Myomesin 1 (MYOM1), myomesin 3 (MYOM3) and myomesin 2 (MYOM2) harbored 14 ubiquitination sites, 12 ubiquitination sites and 7 ubiquitination sites, respectively. MYOM1, MYOM2 and MYOM3 are highly expressed in the heart. MYOM1 and MYOM2, parts of an M-band, bind tightly to TTN in the M-line; in addition, MYOM3 is a recently discovered part of the M-band (22). The number of ubiquitination sites in the remaining proteins was as follows: 9 in HSPA1B, 8 in GJA1, 8 in DSP, 7 in HSPA8, 6 in TPM1 and 6 in TUBA1B (**Table 2**).

3.3. Subcellular location analysis of differentially expressed ubiquitylated proteins

The subcellular localization of the differentially expressed proteins (DEGs) is presented in **Supplementary Figure S1**. The proteins exhibiting upregulated ubiquitination were mainly in the

A

Summary of identified and quantified sites and proteins

Name	Identified	Quantifiable
Proteins	2243	1631
Sites	7275	4788

Summary of differentially quantified sites and proteins

Name	Type	Up-regulated (>1.5)	Down-regulated (<1/1.5)
AF/SR	Proteins	162	156
	Sites	271	463

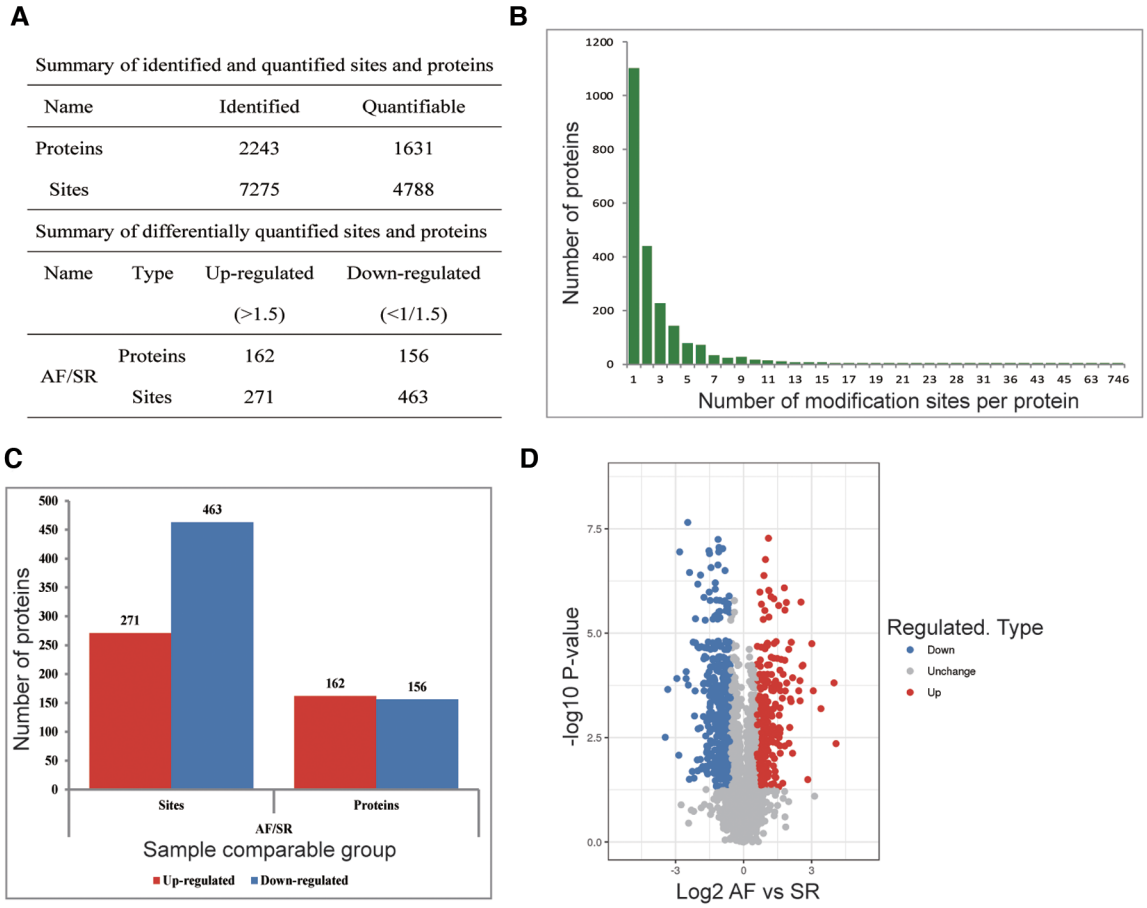

FIGURE 2
Ubiquitination analysis of SR and AF tissue samples. (A) Changes were observed at 4,788 quantifiable sites and in 1,631 quantifiable proteins. (B) Identified protein site number distribution: most proteins harbored <5 modification sites. (C) Differential ubiquitination sites and protein numbers: A total of 271 sites in 162 proteins exhibiting upregulated ubiquitination and 467 sites in 156 proteins exhibiting downregulated ubiquitination were identified. (D) Volcano plot showing differentially ubiquitylated proteins and sites.

cytoplasm ($n = 69$, 42.86%), nucleus ($n = 36$, 22.36%) and plasma membrane ($n = 23$, 14.29%). The others were in mitochondria, the extracellular space and other locations. The proteins exhibiting downregulated ubiquitination were mainly in the cytoplasm ($n = 69$, 44.52%), nucleus ($n = 42$, 27.1%), extracellular space ($n = 12$, 7.74%) and mitochondria ($n = 11$, 7.1%).

3.4. GO enrichment-based functional classification of differentially expressed ubiquitylated proteins

We classified sites with different modification abundances into 4 quantiles according to their AF/SR modification multiples; these

TABLE 2 Summary of the 11 proteins with the greatest difference in ubiquitination.

Protein accession	Gene name	Number of sites	Upregulated sites	Downregulated sites
Q8 WZ42	TTN	174	5	169
P13533	MYH6	38	34	4
P52179	MYOM1	14	0	14
Q5VTT5	MYOM3	12	0	12
P12883	MYH7	11	2	9
P0DMV9	HSPA1B	9	9	0
P17302	GJA1	8	8	0
P15924	DSP	8	1	7
P11142	HSPA8	7	7	0
P54296	MYOM2	7	1	6
P09493	TPM1	6	1	5
P68363	TUBA1B	6	6	0

quantiles were called Q1–Q4 (Q1 < 0.500, Q2: 0.500–0.667, Q3: 1.5–2.0, and Q4 > 2.0) (Figure 3A). As illustrated in Figures 3B–D, GO enrichment-based functional classification indicated a relationship among the sites in the same quantile. Figure 3B shows the ubiquitination of sites associated with AF. The results revealed that the downregulated proteins with downregulated ubiquitination in Q1 were mainly involved in processes related to heart development, protein localization to organelles, viral gene expression, protein localization to the endoplasmic reticulum, the response to interleukin-6, animal organ morphogenesis, actomyosin structure organization, and actin filament organization. It also revealed that the ubiquitylated proteins in Q3 were mainly involved in processes related to heart contraction, blood circulation, ribose phosphate metabolism, nucleoside metabolism, metal ion transport, cation transport, and receptor recycling. The proteins with upregulated ubiquitination in Q4 were enriched mainly in macroautophagy, the regulation of organelle organization, and the establishment of monopolar cell polarity.

In the cellular component category, the distributions of proteins with downregulated ubiquitination in Q1 were ribosomes, cytosolic ribosomes and ribosomal subunits. In contrast, proteins in Q3 exhibiting upregulated ubiquitination were highly enriched in sarcolemma and synapses. Q4 proteins were involved in organelle outer membranes and the mitochondrial outer membrane (Figure 3C).

Ubiquitination rates were also analyzed based on molecular functions (Figure 3D). In Q1, the proteins with downregulated ubiquitination exhibited fructose-bisphosphate aldolase activity. The proteins in Q3 exhibiting upregulated ubiquitination were mainly involved in ion transmembrane transporter activity, cation-transporting ATPase activity and transmembrane transporter activity. The Q4 proteins were closely associated with structural constituents of the cytoskeleton, GTPase activity GTP binding, guanyl binding, wide pore channel activity, and porin activity.

3.5. Protein domain and KEGG pathway analysis of differentially expressed ubiquitylated proteins

Ubiquitination rates were also analyzed based on protein domain analysis. In Q1, the proteins were distributed in the ribosomal protein L23/L15e core domain. In Q3, the proteins were enriched in ATPase, GAT, VHS, cyclic nucleotide-binding-like and EF-hand domains. The proteins with upregulated ubiquitination in Q4 were involved in the tubulin, connexin, ezrin/radixin/moesin, moesin tail, and porin domains, gap junction proteins, and P-loop-containing nucleoside triphosphate hydrolase (Figure 4C).

Figure 4A reveals the results of the KEGG pathway analysis of ubiquitylated proteins associated with AF. In the Q1 quantile, the proteins with downregulated ubiquitination were distributed mainly in pathways related to ribosome and arachidonic acid metabolism. In Q3, the proteins with upregulated ubiquitination were distributed mainly in pathways related to arrhythmogenic right ventricular cardiomyopathy. The Q4-enriched proteins were involved in parathyroid hormone synthesis, secretion and action, legionellosis, pathogenic *Escherichia coli* infection, the NOD-like receptor signaling pathway, longevity regulating pathway, gap junctions, tight junctions, and cholesterol metabolism. Figure 4B reveals that in all KEGG pathways, the proteins were highly enriched in hsa05410 hypertrophic cardiomyopathy (HCM). Among the 17 proteins associated with the hsa05410 hypertrophic cardiomyopathy (HCM) KEGG pathway, TTN harbored the highest number of modification sites (174), followed by MYH6 (with 38) (Figure 4D).

3.6. Motif analysis of differentially altered ubiquitylated proteins

Based on MoMo software (the motif-x algorithm), a motif analysis of differentially ubiquitylated proteins was conducted to evaluate the 10 bilateral AAs down- and upstream of a ubiquitylated lysine (Figures 5A,B). Sequences enriched with valine (V), glutamic acid (E), aspartic acid (D) and alanine (A) residues were found downstream of a ubiquitylated lysine, whereas sequences enriched with valine (V) and alanine (A) residues were found upstream. Among these motifs, A was at the +4/+3/+2 positions, and L was at the +2 position (Figure 5A).

The results revealed nine significantly enriched ubiquitination site motifs among the quantifiable ubiquitylated sites: YxxRxxAxNKacxG, ExxxxxxKac, KacxxxxxxxK, KacxxxxxK, KxxxxxxxKac, KacE, RxxxxxxxKac, KacD, and AKac (Figure 5B), where x stands for a random AA and Kac stands for a ubiquitylated lysine.

3.7. PPI network analysis of differentially ubiquitylated proteins

Based on PPI networks and the STRING database, we analyzed the key genes associated with AF. The results revealed that ubiquitylated proteins in AF were mainly glycolysis-, ribosome-, endocytosis-, and hypertrophic cardiomyopathy-related proteins (Figures 6A–D). The ubiquitylated proteins associated with glycolysis harbored five upregulated ubiquitination sites and five downregulated ubiquitination sites (Figure 6A). The HCM-related sites included two sites with upregulated modification and eleven sites exhibiting downregulated modifications (Figure 6B). Sixteen sites in the ribosome-related ubiquitination PPI network showed downregulated ubiquitination, and two sites showed upregulated ubiquitination (Figure 6C). The PPI network associated with endocytosis-related proteins included 9 upregulated ubiquitination sites and two downregulated ubiquitination sites (Figure 6D). MYH6 and TTN were identified as candidate key genes highly related to AF. The cluster identification assay shown in Figure 6C suggested that RPS27A played the most important role in AF.

10.3389/fcvm.2023.1198486

FIGURE 3
GO enrichment-based functional classification of differentially ubiquitylated proteins. (**A**) We classified the sites with different modification abundances into 4 quartiles, called Q1–Q4, according to their different modification multiples. (**B**) Biological process analysis based on Q1–Q4 quantiles. (**C**) Cellular component analysis based on Q1–Q4 quantiles. (**D**) Molecular function analysis based on Q1–Q4 quantiles.

10.3389/fcvm.2023.1198486

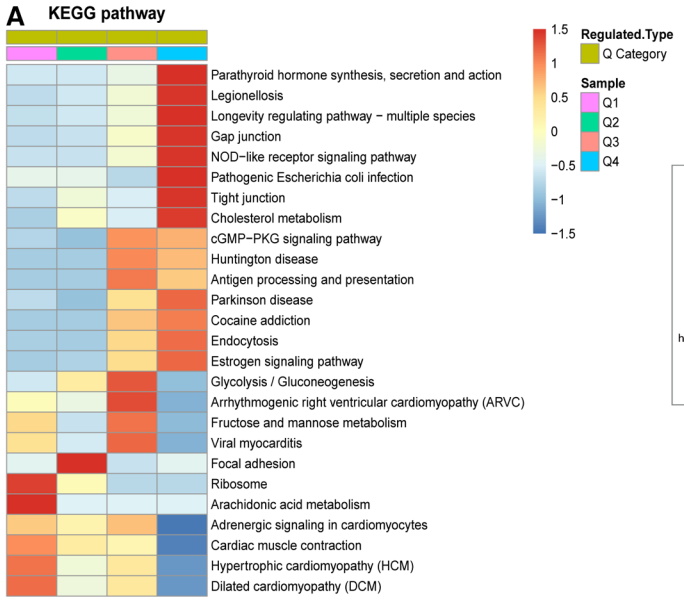

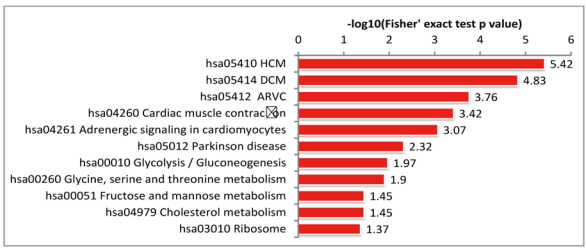

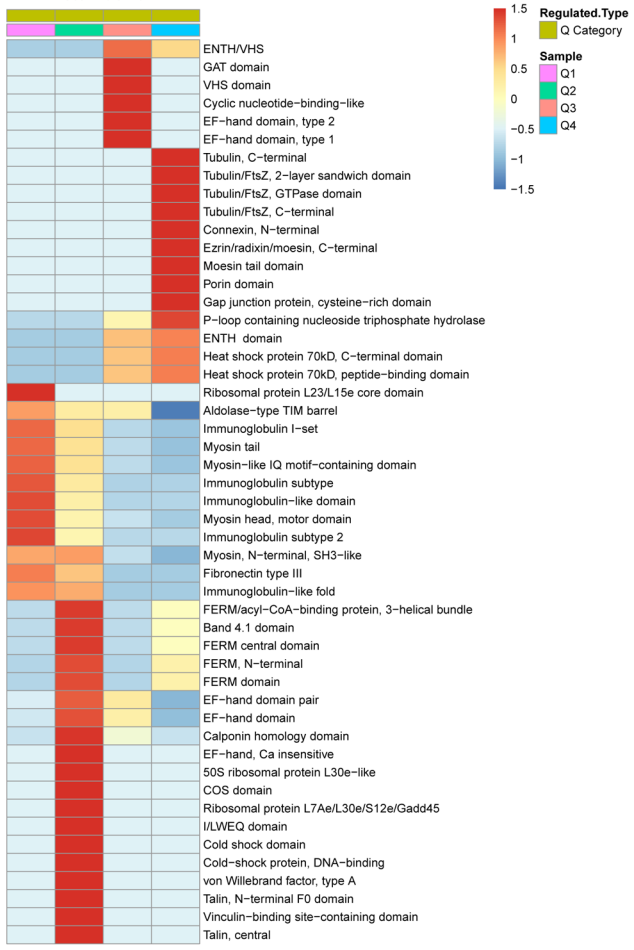

D

Summary of the 17 proteins in the hsa05410 HCM KEGG pathway

NO.	Protein accession	Gene name	Number of positions	Number of KEGG pathways
1	P67936	TPM4	2	4
2	P17661	DES	3	3
3	P06753	TPM3	2	6
4	P16615	ATP2A2	1	11
5	P18084	ITGB5	1	10
6	Q92736	RYR2	2	12
7	P12883	MYH7	11	7
8	P11532	DMD	1	4
9	Q13683	ITGA7	1	8
10	P09493	TPM1	6	5
11	Q8WZ42	TTN	174	2
12	Q9UGJ0	PRKAG2	2	15
13	P63316	TNNC1	2	5
14	P08590	MYL3	2	5
15	P45379	TNNT2	3	4
16	Q14896	MYBPC3	3	2
17	P13533	MYH6	38	7

FIGURE 4
Protein domain and KEGG pathway analysis of differentially expressed ubiquitylated proteins. (**A**) KEGG pathway analysis based on Q1-Q4 quantiles. (**B**) Top 11 pathways of all KEGG pathways. The proteins involved in all KEGG pathways were most highly enriched in hsa05410 hypertrophic cardiomyopathy (HCM). (**C**) Protein complex analysis. (**D**) Summary of the 17 proteins associated with hsa05410 HCM: TTN had the most (348) modifications in all enriched KEGG pathways, followed by MYH6 (266).

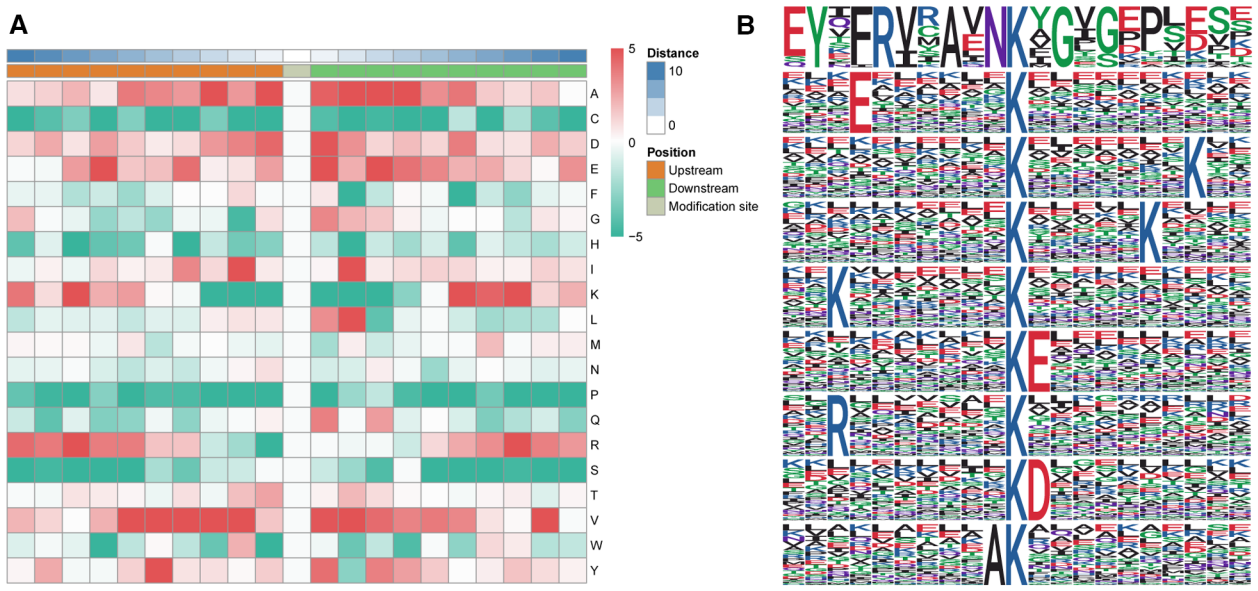

FIGURE 5
Motif analysis of differentially altered ubiquitylated proteins. (A) Heatmap of the 10 bilateral AAs down- and upstream of the ubiquitylated lysine. Enrichments of valine (V), glutamic acid (E), aspartic acid (D) and alanine (A) residues were found downstream of the ubiquitylated lysine, whereas enrichments of valine (V) and alanine (A) were found upstream of the ubiquitylated lysine. (B) Sequence logo of acetylation motifs. The results revealed nine significantly enriched ubiquitination site motifs from the quantifiable ubiquitylated sites, where x stands for a random AA and Kac stands for a ubiquitylated lysine.

3.8. Validation results

The identity of myomesin 1 (MYOM1) and myomesin 3 (MYOM3) was validated by immunoprecipitation (IP) combined with Western blotting (WB). MYOM1 and MYOM3 in the LAA tissues from the SR group were preferentially coimmunoprecipitated with ubiquitin compared with those from the AF group (both $P < 0.05$), confirming the differential interactions identified in the mass spectrometry analysis (**Figure 7**), which demonstrated the reliability of the results in this study (**Table 2**).

4. Discussion

To date, this report is the only description of protein ubiquitination in AF patients based on quantitative proteomics. Our results revealed that the degree of protein ubiquitination was different in AF tissues than in non-AF tissues, leading to upregulated or downregulated ubiquitination. We also identified ubiquitination sites. A total of 271 sites in 162 proteins exhibiting upregulated ubiquitination and 467 sites in 156 proteins exhibiting downregulated ubiquitination were identified. Interestingly, both upregulated lysine ubiquitination and downregulated lysine ubiquitination were identified in some proteins. Furthermore, the DEGs involved in ubiquitination events encoded proteins associated with glycolysis, ribosomes, endocytosis, and hypertrophic cardiomyopathy. These results revealed that ubiquitination is essential to the development of AF.

PTMs are indispensable in numerous cellular processes. Among twenty AAs, modifications are deposited mainly on a lysine residue, the only AA with a side chain amine, which can be covalently modified by glycosyl, propionyl, butyryl, acetyl, hydroxy, crotonyl, ubiquitin and ubiquitin-like groups. Ubiquitination is vital for myocardial ischemia/reperfusion (I/R) injury, cardiomyopathy, and heart failure (23). It has been reported that parkin, cooperating with the ubiquitin-conjugating enzyme UbcH7, functions as a ubiquitin ligase to promote protein degradation (24). Shimura H and his colleague identified a new mechanism that can alleviate myocardial injury. Mitochondrial permeability transition pore (mPTP) opening was suppressed by parkin through the catalyzed ubiquitination of CypD, which is involved in necrotic cascades. Thus, parkin benefits cardiac function (25). The results obtained by Tsushima et al. described a novel mechanism underlying lipotoxic cardiomyopathy. An increasing rate of A-kinase anchor protein 121 (AKAP121) ubiquitination changed the phosphorylation rate of Ser637 in dynamin-related protein 1 (DRP1), which was caused by altered mitochondrial redox status (26). Furthermore, ubiquitination has been associated with ubiquitination in myocardial infarction (MI). Phosphorylation of GSK3 was necessary for the ubiquitination-dependent degradation of OMA1, which promoted leptin-regulated mitochondrial integrity. Leptin enhances the survival and mitochondrial integrity of hMSCs. Therefore, enforcing ubiquitination may be a feasible strategy against cardiovascular diseases such as MI (27).

Our own bioinformatics analysis showed that TTN harbored the most ubiquitination sites (with 174 sites), followed by MYH6, which harbored 38 sites. In addition, TTN harbored the most

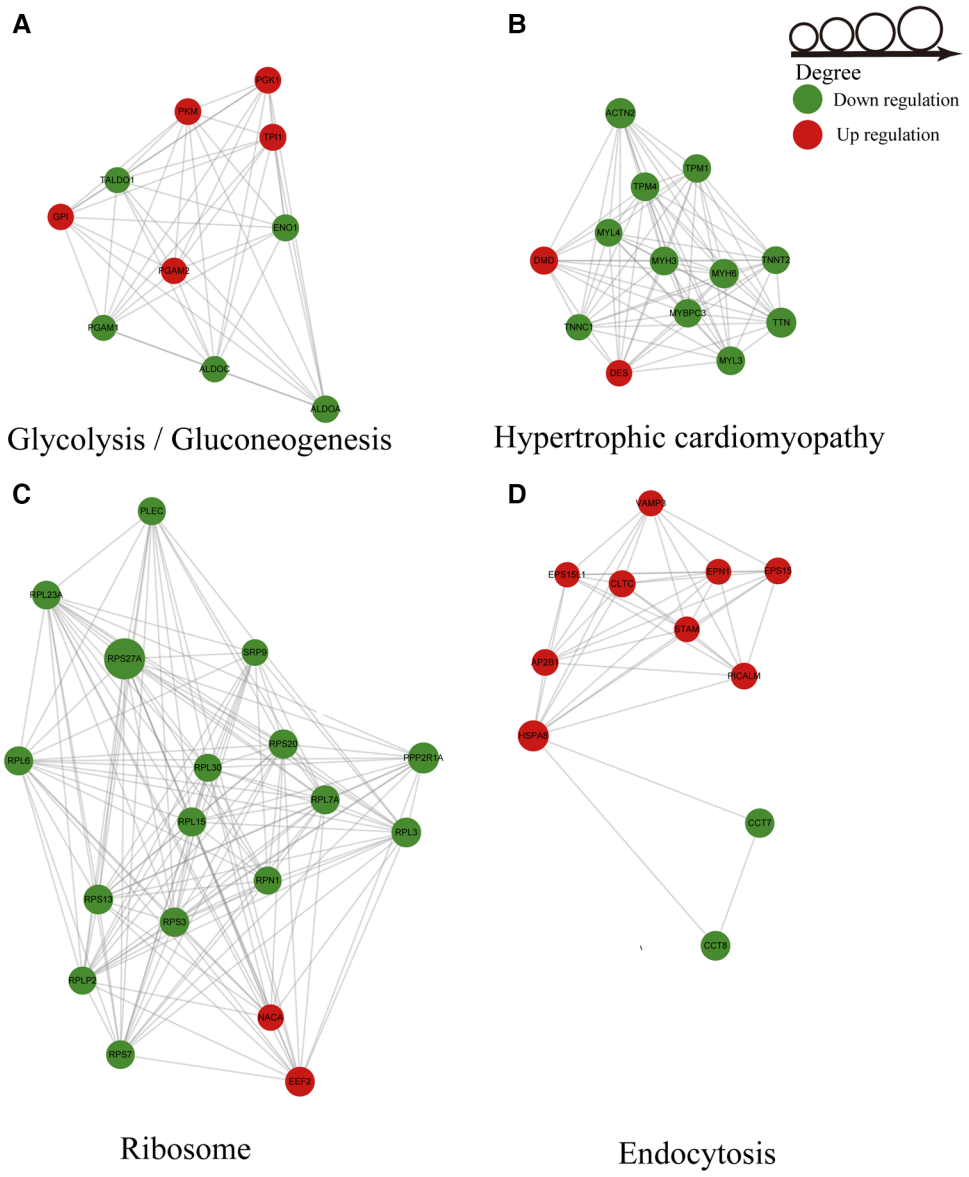

FIGURE 6
Ubiquitylated PPI network analysis. (A) PPI of glycolysis-related proteins. (B) PPI of hypertrophic cardiomyopathy-related proteins. (C) PPI of ribosome-related proteins. (D) PPI of endocytosis-related proteins.

modified sites (348) in all the enriched KEGG pathways, followed by MYH6 (266). Therefore, the TTN and MYH6 genes were significantly and highly expressed in AF compared with SR tissues. We speculated that these two highly expressed genes may play a role in the incidence of AF in valvular heart disease patients. There have been several studies on the correlation between AF and these two highly expressed genes, TTN and MYH6.

TTN, the largest known protein [$M(r)$ 3,000 kDa], plays an important role in sarcomere assembly and confers stability during the cardiac cycle (28). A study by Choi et al. indicated a close correlation between early-onset AF and a loss-of-function (LOF) TTN variant (29). In another study, Ahlberg et al. revealed that early-onset AF was closely associated with titin truncation variants (TTNtvs) (30, 31). Furthermore, Chalazan et al. indicated that in ethnic minority groups, there was a close correlation between early-onset AF and TTN variants (32). In addition, TTN has been correlated with other diseases, such as dilated cardiomyopathy, hypertrophic cardiomyopathy, and neuromuscular disorders (33–35). The underlying mechanisms by which TTN leads to AF remain unclear. One possible mechanistic explanation for the highly expressed TTN association with AF is that DCM or HCM caused by TTN increases patient susceptibility to AF. However, none of the patients recruited in this study suffered from DCM or HCM. Further research is required to elucidate the mechanisms underlying TTN function.

As the α-heavy chain subunit of cardiac myosin, MYH6 is the fastest molecular motor comprising thick filaments (36). There are close correlations between MYH6 variants and congenital heart

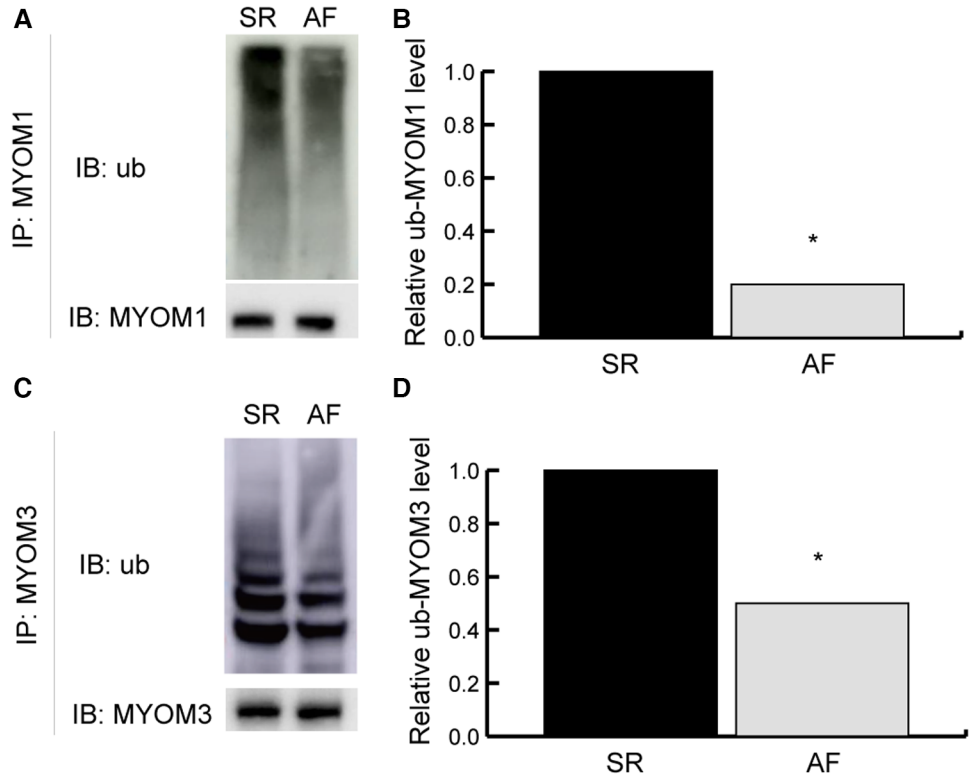

FIGURE 7
Validation results. Validation of ubiquitylated MYOM1 and ubiquitylated MYOM3 as determined by coimmunoprecipitation (co-IP) combined with Western blotting (WB). (**A**,**B**) Ubiquitinated MYOM1. (**C**,**D**) Ubiquitinated MYOM3. IP, immunoprecipitation; IB, immunoblotting; MYOM1, myomesin 1; MYOM3, myomesin 3; ub, ubiquitylated. *$P < 0.05$.

defects (CHDs) (37), nonsyndromic coarctation of the aorta (38), familial dilated cardiomyopathy (39), ischemic cardiomyopathy (40), and hypertrophic cardiomyopathy (41). Holm and colleagues found a close correlation between sick sinus syndrome (SSS) and MYH6 missense mutations (42). Thorolfsdottir et al. indicated that atrial fibrillation was associated with rare MYH6 variants, which exerted important effects on the passive elasticity of the heart (43). None of the patients recruited for this study suffered from CHD, coarctation of the aorta, DCM or SSS. The underlying mechanisms by which MYH6 leads to AF remain unclear, and further research is needed.

Ribosomal proteins (RPs) are abundant RNA-binding proteins with multiple functions. One RP, ribosomal protein S27a (RPS27A), actively promotes proliferation in breast cancer (44), renal cancer (45), colon cancer (46), and chronic myeloid leukemia (47). Several studies have revealed the ubiquitination functions of RPS27A. Montellese et al. indicated that USP16-mediated deubiquitination and RPS27a ubiquitination were essential for the entry of maturing pre-40S particles into a pool of translating ribosomes (48). Holm et al. found that P-3F enhances P53 stability by changing the translocation of RPS27a. The release of RPS27a from the nucleolus, from which it enters the nucleoplasm, decreased the phosphorylation of Mdm2 and downregulated the ubiquitination of P53 (49). These reports demonstrated the potential function of RPS27a in translation. A similar mechanism may be involved in AF and needs to be identified.

Accumulated evidence suggests that AF risk is associated with multiomics profiles, including genomics, epigenomics, transcriptomics, proteomics, and metabolomics. Our study found 156 downregulated ubiquitinated proteins and 162 upregulated ubiquitinated proteins in AF patients. In another study based on clinical samples, Amrish Deshmukh et al. revealed 1,011 differentially expressed mRNAs in the LAA tissues between AF and SR patients (50). As Venn diagrams in **Supplementary Figures S2A,C** show, 8 genes related to downregulated ubiquitinated proteins and increased expression probes simultaneously were obtained in **Supplementary Figure S2B**, while 8 genes related to upregulated ubiquitinated proteins and decreased expression probes simultaneously were obtained simultaneously in **Supplementary Figure S2D**. Apart from the proteins mentioned earlier, such as MYH7, MYOM2, MYOM1, and DSP, significant changes in protein ubiquitination levels were observed in FLNC, HSPA1B, and GFPT1 among these intersecting proteins. Filamin C (FLNC) is a protein that plays a vital role in the cytoskeleton structure of cells, and it is highly expressed in cardiac muscle. Numerous studies have suggested a strong correlation between FLNC and the development of cardiomyopathy (51–53). HSPA1B, which encodes heat-shock protein 70 kDa (Hsp70), protects against stroke in AF patients. In our study, HSPA1B was associated with upregulated ubiquitination, and its protection against stroke might be weakened. However, there were no strokes in the enrolled

patients (54). Although an increase in ubiquitination level does not necessarily imply protein degradation, combining the results of ubiquitination with results of different -omics layers may help to identify genes that are more relevant to the occurrence and progression of atrial fibrillation.

Multiomics approaches have emerged as a powerful tool with several advantages in studying cardiovascular diseases. One study investigated the association between single-nucleotide polymorphisms (SNPs) and AF by tissue-specific multiomics analysis in a case–control cohort of AF (55). In their study, genomics, transcriptomics, and proteomics were applied, and correlations between the transcription factor NKX2-5 and AF were elucidated. Multiomics approaches can identify key drivers of disease. As illustrated in the above study, abundant disease-associated SNPs were discovered by genome-wide association studies (GWAS); however, their underlying molecular mechanisms remain largely elusive. With the help of multiomics approaches, the role of NKX2-5 as a link between AF and the GWAS SNP rs9481842 was clarified. The most important advantage of multiomics approaches is that by integrating data from various levels, multiomics approaches can provide a more comprehensive understanding of the molecular mechanisms underlying these complex diseases and the interactions between different biological pathways and networks involved in cardiovascular diseases. Moreover, multiomics approaches can identify new biomarkers and therapeutic targets. Finally, by using multiomics approaches, researchers can develop more precise and personalized approaches to disease diagnosis and treatment. Our study, focused on proteomic changes in the form of ubiquitination, forms an essential piece of this multiomics puzzle. Future studies could use our findings as a stepping stone, integrating them with genomic, transcriptomic, and metabolomic data to fully comprehend the pathogenesis of atrial fibrillation.

Despite being the first study to focus on ubiquitination changes in atrial fibrillation by quantitative proteomics and identifying some valuable proteins with ubiquitination changes, this study still has several limitations. First, because obtaining left atrial appendage tissue during cardiac surgery poses a high risk of perforation and difficulty in obtaining specimens, the sample size was small. Second, current ubiquitin proteomics technology and limited specimen weight per patient may have led to the underrepresentation of ubiquitinated proteins, possibly overlooking some crucial proteins with key functional roles. Third, our center lacks conditions for establishing pig or dog models of atrial fibrillation, precluding functional validation in atrial fibrillation animal models. Finally, differences in amino acid sequences between humans and common animal models used in studying atrial fibrillation (pigs, dogs) may make it difficult to conduct functional studies of some identified proteins using animal models.

In conclusion, significant alterations in ubiquitination were observed between the SR and AF groups. Most DEGs were distributed in ribosome-related proteins with downregulated ubiquitination. The results indicated that alterations in ribosome-associated protein ubiquitination influence the development of AF. Our findings may provide a more feasible strategy against AF.

Data availability statement

The datasets presented in this study can be found in online repositories. The names of the repository/repositories and accession number(s) can be found in the article/**Supplementary Material**.

Ethics statement

The studies involving human participants were reviewed and approved by the Ethics Committee of the Second Xiangya Hospital of Central South University. The patients/participants provided their written informed consent to participate in this study.

Author contributions

C-KW, ST, FB, X-BL, X-MZ, Q-ML, Y-CX, and S-HZ contributed to the conception, design and sample collection for the study. C-KW performed the laboratory analysis. C-KW and Y-CX performed the statistical analysis and wrote the first draft of the manuscript. C-KW, Y-CX, and S-HZ acquired funding and supervised the project. All authors contributed to the article and approved the submitted version.

Funding

This research was supported by the Fundamental Research Funds for the Central Universities of Central South University (2019zzts353), the National Natural Science Foundation of China (81870258, 81670269) and the Natural Science Foundation of Hunan Province, China (No. 2023JJ30791). There are no conflicts with industry.

Acknowledgments

We thank the Fundamental Research Funds for the Central Universities of Central South University and the National Natural Science Foundation of China for supporting us in conducting our research.

Conflict of interest

The authors declare that the research was conducted in the absence of any commercial or financial relationships that could be construed as a potential conflict of interest.

Publisher's note

that may be evaluated in this article, or claim that may be made by its manufacturer, is not guaranteed or endorsed by the publisher.

Supplementary material

The Supplementary Material for this article can be found online at: https://www.frontiersin.org/articles/10.3389/fcvm.2023.1198486/full#supplementary-material

SUPPLEMENTARY FIGURE S1
Subcellular location of upregulated ubiquitylated proteins (A) and downregulated ubiquitylated proteins (B).

SUPPLEMENTARY FIGURE S2
The Venn diagram illustrates the relationship between proteins exhibiting elevated levels of ubiquitination and genes displaying decreased expression (A), and the overlapping genes are provided in list form (B). Similarly, the Venn diagram depicts the association between proteins exhibiting reduced levels of ubiquitination and genes displaying increased expression (C), with the corresponding overlapping genes listed (D).

References

1. Li Q, Wu H, Yue W, Dai Q, Liang H, Bian H, et al. Prevalence of stroke and vascular risk factors in China: a nationwide community-based study. *Sci Rep*. (2017) 7(1):6402. doi: 10.1038/s41598-017-06691-1

2. Leutert M, Entwisle SW, Villén J. Decoding post-translational modification crosstalk with proteomics. *Mol Cell Proteomics*. (2021) 20:100129. doi: 10.1016/j.mcpro.2021.100129

3. Clague MJ, Heride C, Urbé S. The demographics of the ubiquitin system. *Trends Cell Biol*. (2015) 25(7):417–26. doi: 10.1016/j.tcb.2015.03.002

4. Swatek KN, Komander D. Ubiquitin modifications. *Cell Res*. (2016) 26 (4):399–422. doi: 10.1038/cr.2016.39

5. Su H, Li J, Zhang H, Ma W, Wei N, Liu J, et al. COP9 signalosome controls the degradation of cytosolic misfolded proteins and protects against cardiac proteotoxicity. *Circ Res*. (2015) 117(11):956–66. doi: 10.1161/circresaha.115.306783

6. Yan K, Ponnusamy M, Xin Y, Wang Q, Li P, Wang K. The role of K63-linked polyubiquitination in cardiac hypertrophy. *J Cell Mol Med*. (2018) 22(10):4558–67. doi: 10.1111/jcmm.13669

7. Mukherjee R, Chakrabarti O. Ubiquitin-mediated regulation of the E3 ligase GP78 by MGRN1 in trans affects mitochondrial homeostasis. *J Cell Sci*. (2016) 129 (4):757–73. doi: 10.1242/jcs.176537

8. Wu J, Tian Z, Sun Y, Lu C, Liu N, Gao Z, et al. Exogenous H(2)S facilitating ubiquitin aggregates clearance via autophagy attenuates type 2 diabetes-induced cardiomyopathy. *Cell Death Dis*. (2017) 8(8):e2992. doi: 10.1038/cddis.2017.380

9. Sun Y, Lu F, Yu X, Wang B, Chen J, Lu F, et al. Exogenous H(2)S promoted USP8 sulfhydration to regulate mitophagy in the hearts of db/db mice. *Aging Dis*. (2020) 11 (2):269–85. doi: 10.14336/ad.2019.0524

10. Tseng JF, Chen SR, Au HK, Chipojola R, Lee GT, Lee PH, et al. Effectiveness of an integrated breastfeeding education program to improve self-efficacy and exclusive breastfeeding rate: a single-blind, randomised controlled study. *Int J Nurs Stud*. (2020) 111:103770. doi: 10.1016/j.ijnurstu.2020.103770

11. Yu M, Du H, Wang B, Chen J, Lu F, Peng S, et al. Exogenous H(2)S induces Hrd1 S-sulfhydration and prevents CD36 translocation via VAMP3 ubiquitylation in diabetic hearts. *Aging Dis*. (2020) 11(2):286–300. doi: 10.14336/ad.2019.0530

12. Basheer WA, Harris BS, Mentrup HL, Abreha M, Thames EL, Lea JB, et al. Cardiomyocyte-specific overexpression of the ubiquitin ligase Wwp1 contributes to reduction in connexin 43 and arrhythmogenesis. *J Mol Cell Cardiol*. (2015) 88:1–13. doi: 10.1016/j.yjmcc.2015.09.004

13. Marionneau C, Abriel H. Regulation of the cardiac Na+ channel NaV1.5 by post-translational modifications. *J Mol Cell Cardiol*. (2015) 82:36–47. doi: 10.1016/j.yjmcc.2015.02.013

14. Zhao C, Wang L, Ma X, Zhu W, Yao L, Cui Y, et al. Cardiac Nav 1.5 is modulated by ubiquitin protein ligase E3 component n-recognin UBR3 and 6. *J Cell Mol Med*. (2015) 19(9):2143–52. doi: 10.1111/jcmm.12588

15. Huang Y, Wang Z, Liu Y, Xiong H, Zhao Y, Wu L, et al. αB-Crystallin interacts with Nav1.5 and regulates ubiquitination and internalization of cell surface Nav1.5. *J Biol Chem*. (2016) 291(21):11030–41. doi: 10.1074/jbc.M115.695080

16. Roder K, Kabakov A, Moshal KS, Murphy KR, Xie A, Dudley S, et al. Trafficking of the human ether-a-go-go-related gene (hERG) potassium channel is regulated by the ubiquitin ligase rififylin (RFFL). *J Biol Chem*. (2019) 294(1):351–60. doi: 10.1074/jbc.RA118.003852

17. Yu SM, Jean-Charles PY, Abraham DM, Kaur S, Gareri C, Mao L, et al. The deubiquitinase ubiquitin-specific protease 20 is a positive modulator of myocardial β(1)-adrenergic receptor expression and signaling. *J Biol Chem*. (2019) 294 (7):2500–18. doi: 10.1074/jbc.RA118.004926

18. Pan JA, Sun Y, Jiang YP, Bott AJ, Jaber N, Dou Z, et al. TRIM21 Ubiquitylates SQSTM1/p62 and suppresses protein sequestration to regulate redox homeostasis. *Mol Cell*. (2016) 61(5):720–33. doi: 10.1016/j.molcel.2016.02.007

19. Yuan Y, Zhao J, Gong Y, Wang D, Wang X, Yun F, et al. Autophagy exacerbates electrical remodeling in atrial fibrillation by ubiquitin-dependent degradation of L-type calcium channel. *Cell Death Dis*. (2018) 9(9):873. doi: 10.1038/s41419-018-0860-y

20. Liu X, Zhang W, Luo J, Shi W, Zhang X, Li Z, et al. TRIM21 deficiency protects against atrial inflammation and remodeling post myocardial infarction by attenuating oxidative stress. *Redox Biol*. (2023) 62:102679. doi: 10.1016/j.redox.2023.102679

21. He X, Gao X, Peng L, Wang S, Zhu Y, Ma H, et al. Atrial fibrillation induces myocardial fibrosis through angiotensin II type 1 receptor-specific arkadia-mediated downregulation of Smad7. *Circ Res*. (2011) 108(2):164–75. doi: 10.1161/circresaha.110.234369

22. Schoenauer R, Lange S, Hirschy A, Ehler E, Perriard J-C, Agarkova I. Myomesin 3, a novel structural component of the M-band in striated muscle. *J Mol Biol*. (2008) 376(2):338–51. doi: 10.1016/j.jmb.2007.11.048

23. Liu J, Zhong L, Guo R. The role of posttranslational modification and mitochondrial quality control in cardiovascular diseases. *Oxid Med Cell Longev*. (2021) 2021:6635836. doi: 10.1155/2021/6635836

24. Shimura H, Hattori N, Kubo S, Mizuno Y, Asakawa S, Minoshima S, et al. Familial Parkinson disease gene product, parkin, is a ubiquitin-protein ligase. *Nat Genet*. (2000) 25(3):302–5. doi: 10.1038/77060

25. Sun T, Ding W, Xu T, Ao X, Yu T, Li M, et al. Parkin regulates programmed necrosis and myocardial ischemia/reperfusion injury by targeting cyclophilin-D. *Antioxid Redox Signal*. (2019) 31(16):1177–93. doi: 10.1089/ars.2019.7734

26. Tsushima K, Bugger H, Wende AR, Soto J, Jenson GA, Tor AR, et al. Mitochondrial reactive oxygen species in lipotoxic hearts induce post-translational modifications of AKAP121, DRP1, and OPA1 that promote mitochondrial fission. *Circ Res*. (2018) 122(1):58–73. doi: 10.1161/circresaha.117.311307

27. Yang F, Wu R, Jiang Z, Chen J, Nan J, Su S, et al. Leptin increases mitochondrial OPA1 via GSK3-mediated OMA1 ubiquitination to enhance therapeutic effects of mesenchymal stem cell transplantation. *Cell Death Dis*. (2018) 9(5):556. doi: 10.1038/s41419-018-0579-9

28. Labeit S, Gautel M, Lakey A, Trinick J. Towards a molecular understanding of titin. *EMBO J*. (1992) 11(5):1711–6. doi: 10.1002/j.1460-2075.1992.tb05222.x

29. Choi SH, Weng LC, Roselli C, Lin H, Haggerty CM, Shoemaker MB, et al. Association between titin loss-of-function variants and early-onset atrial fibrillation. *J Am Med Assoc*. (2018) 320(22):2354–64. doi: 10.1001/jama.2018.18179

30. Ahlberg G, Refsgaard L, Lundegaard PR, Andreasen L, Ranthe MF, Linscheid N, et al. Rare truncating variants in the sarcomeric protein titin associate with familial and early-onset atrial fibrillation. *Nat Commun*. (2018) 9(1):4316. doi: 10.1038/s41467-018-06618-y

31. Choi SH, Jurgens SJ, Weng LC, Pirruccello JP, Roselli C, Chaffin M, et al. Monogenic and polygenic contributions to atrial fibrillation risk: results from a national biobank. *Circ Res*. (2020) 126(2):200–9. doi: 10.1161/circresaha.119.315686

32. Chalazan B, Mol D, Darbar FA, Ornelas-Loredo A, Al-Azzam B, Chen Y, et al. Association of rare genetic variants and early-onset atrial fibrillation in ethnic minority individuals. *JAMA Cardiol*. (2021) 6(7):811–9. doi: 10.1001/jamacardio.2021.0994

33. Gerull B, Gramlich M, Atherton J, McNabb M, Trombitás K, Sasse-Klaassen S, et al. Mutations of TTN, encoding the giant muscle filament titin, cause familial dilated cardiomyopathy. *Nat Genet*. (2002) 30(2):201–4. doi: 10.1038/ng815

34. Hackman P, Vihola A, Haravuori H, Marchand S, Sarparanta J, De Seze J, et al. Tibial muscular dystrophy is a titinopathy caused by mutations in TTN, the gene encoding the giant skeletal-muscle protein titin. *Am J Hum Genet*. (2002) 71 (3):492–500. doi: 10.1086/342380

35. Gerull B. Between disease-causing and an innocent bystander: the role of titin as a modifier in hypertrophic cardiomyopathy. *Can J Cardiol*. (2017) 33(10):1217–20. doi: 10.1016/j.cjca.2017.07.010

36. Nielsen JB, Thorolfsdottir RB, Fritsche LG, Zhou W, Skov MW, Graham SE, et al. Biobank-driven genomic discovery yields new insight into atrial fibrillation biology. *Nat Genet*. (2018) 50(9):1234–9. doi: 10.1038/s41588-018-0171-3

37. Granados-Riveron JT, Ghosh TK, Pope M, Bu'Lock F, Thornborough C, Eason J, et al. Alpha-cardiac myosin heavy chain (MYH6) mutations affecting myofibril formation are associated with congenital heart defects. *Hum Mol Genet*. (2010) 19 (20):4007–16. doi: 10.1093/hmg/ddq315

38. Bjornsson T, Thorolfsdottir RB, Sveinbjornsson G, Sulem P, Norddahl GL, Helgadottir A, et al. A rare missense mutation in MYH6 associates with non-syndromic coarctation of the aorta. *Eur Heart J*. (2018) 39(34):3243–9. doi: 10.1093/eurheartj/ehy142

39. Klos M, Mundada L, Banerjee I, Morgenstern S, Myers S, Leone M, et al. Altered myocyte contractility and calcium homeostasis in alpha-myosin heavy chain point mutations linked to familial dilated cardiomyopathy. *Arch Biochem Biophys*. (2017) 615:53–60. doi: 10.1016/j.abb.2016.12.007

40. Chen JH, Wang LL, Tao L, Qi B, Wang Y, Guo YJ, et al. Identification of MYH6 as the potential gene for human ischaemic cardiomyopathy. *J Cell Mol Med*. (2021) 25(22):10736–46. doi: 10.1111/jcmm.17015

41. Carniel E, Taylor MR, Sinagra G, Di Lenarda A, Ku L, Fain PR, et al. Alpha-myosin heavy chain: a sarcomeric gene associated with dilated and hypertrophic phenotypes of cardiomyopathy. *Circulation*. (2005) 112(1):54–9. doi: 10.1161/circulationaha.104.507699

42. Holm H, Gudbjartsson DF, Sulem P, Masson G, Helgadottir HT, Zanon C, et al. A rare variant in MYH6 is associated with high risk of sick sinus syndrome. *Nat Genet*. (2011) 43(4):316–20. doi: 10.1038/ng.781

43. Thorolfsdottir RB, Sveinbjornsson G, Sulem P, Helgadottir A, Gretarsdottir S, Benonisdottir S, et al. A missense variant in PLEC increases risk of atrial fibrillation. *J Am Coll Cardiol*. (2017) 70(17):2157–68. doi: 10.1016/j.jacc.2017.09.005

44. Adams SM, Sharp MG, Walker RA, Brammar WJ, Varley JM. Differential expression of translation-associated genes in benign and malignant human breast tumours. *Br J Cancer*. (1992) 65(1):65–71. doi: 10.1038/bjc.1992.12

45. Kanayama H, Tanaka K, Aki M, Kagawa S, Miyaji H, Satoh M, et al. Changes in expressions of proteasome and ubiquitin genes in human renal cancer cells. *Cancer Res*. (1991) 51(24):6677–85.

46. Wong JM, Mafune K, Yow H, Rivers EN, Ravikumar TS, Steele GD Jr, et al. Ubiquitin-ribosomal protein S27a gene overexpressed in human colorectal carcinoma is an early growth response gene. *Cancer Res*. (1993) 53(8):1916–20.

47. Wang H, Yu J, Zhang L, Xiong Y, Chen S, Xing H, et al. RPS27a promotes proliferation, regulates cell cycle progression and inhibits apoptosis of leukemia cells. *Biochem Biophys Res Commun*. (2014) 446(4):1204–10. doi: 10.1016/j.bbrc.2014.03.086

48. Montellese C, van den Heuvel J, Ashiono C, Dörner K, Melnik A, Jonas S, et al. USP16 counteracts mono-ubiquitination of RPS27a and promotes maturation of the 40S ribosomal subunit. *Elife*. (2020) 9:e54435. doi: 10.7554/eLife.54435

49. Wang H, Feng J, Zhou T, Wei L, Zhou J. P-3F, a microtubule polymerization inhibitor enhances P53 stability through the change in localization of RPS27a. *Int J Biochem Cell Biol*. (2017) 92:53–62. doi: 10.1016/j.biocel.2017.09.010

50. Deshmukh A, Barnard J, Sun H, Newton D, Castel L, Pettersson G, et al. Left atrial transcriptional changes associated with atrial fibrillation susceptibility and persistence. *Circ Arrhythm Electrophysiol*. (2015) 8(1):32–41. doi: 10.1161/circep.114.001632

51. Ortiz-Genga MF, Cuenca S, Dal Ferro M, Zorio E, Salgado-Aranda R, Climent V, et al. Truncating FLNC mutations are associated with high-risk dilated and arrhythmogenic cardiomyopathies. *J Am Coll Cardiol*. (2016) 68(22):2440–51. doi: 10.1016/j.jacc.2016.09.927

52. Paldino A, Dal Ferro M, Stolfo D, Gandin I, Medo K, Graw S, et al. Prognostic prediction of genotype vs phenotype in genetic cardiomyopathies. *J Am Coll Cardiol*. (2022) 80(21):1981–94. doi: 10.1016/j.jacc.2022.08.804

53. Patel AP, Dron JS, Wang M, Pirruccello JP, Ng K, Natarajan P, et al. Association of pathogenic DNA variants predisposing to cardiomyopathy with cardiovascular disease outcomes and all-cause mortality. *JAMA Cardiol*. (2022) 7(7):723–32. doi: 10.1001/jamacardio.2022.0901

54. Allende M, Molina E, Guruceaga E, Tamayo I, González-Porras JR, Gonzalez-López TJ, et al. Hsp70 protects from stroke in atrial fibrillation patients by preventing thrombosis without increased bleeding risk. *Cardiovasc Res*. (2016) 110 (3):309–18. doi: 10.1093/cvr/cvw049

55. Assum I, Krause J, Scheinhardt MO, Müller C, Hammer E, Börschel CS, et al. Tissue-specific multi-omics analysis of atrial fibrillation. *Nat Commun*. (2022) 13 (1):441. doi: 10.1038/s41467-022-27953-1

frontiers | Frontiers in Cardiovascular Medicine

TYPE Original Research
PUBLISHED 30 August 2023
DOI 10.3389/fcvm.2023.1187490

OPEN ACCESS

EDITED BY
Gianfranco Pintus,
University of Sharjah, United Arab Emirates

REVIEWED BY
Francisco I. Ramirez-Perez,
University of Missouri, United States
Jeannette Vasquez-Vivar,
Medical College of Wisconsin, United States

*CORRESPONDENCE
Jun-ichi Abe
jabe@mdanderson.org
Nhat-Tu Le
nhle@houstonmethodist.org

†These authors have contributed equally to this work

‡These authors share senior authorship, contributing equally to the supervision and guidance of the project

RECEIVED 21 March 2023
ACCEPTED 24 July 2023
PUBLISHED 30 August 2023

CITATION
Nguyen MTH, Imanishi M, Li S, Chau K, Banerjee P, Velatooru Lr, Ko KA, Samanthapudi VSK, Gi YJ, Lee L-L, Abe RJ, McBeath E, Deswal A, Lin SH, Palaskas NL, Dantzer R, Fujiwara K, Borchrdt MK, Turcios EB, Olmsted-Davis EA, Kotla S, Cooke JP, Wang G, Abe J-i and Le Nhat-Tu (2023) Endothelial activation and fibrotic changes are impeded by laminar flow-induced CHK1-SENP2 activity through mechanisms distinct from endothelial-to-mesenchymal cell transition.
Front. Cardiovasc. Med. 10:1187490.
doi: 10.3389/fcvm.2023.1187490

Endothelial activation and fibrotic changes are impeded by laminar flow-induced CHK1-SENP2 activity through mechanisms distinct from endothelial-to-mesenchymal cell transition

Minh T. H. Nguyen[1,2†], Masaki Imanishi[3†], Shengyu Li[1†], Khanh Chau[1†], Priyanka Banerjee[1], Loka reddy Velatooru[1], Kyung Ae Ko[3], Venkata S. K. Samanthapudi[3], Young J. Gi[3], Ling-Ling Lee[3], Rei J. Abe[1], Elena McBeath[3], Anita Deswal[3], Steven H. Lin[3], Nicolas L. Palaskas[3], Robert Dantzer[4], Keigi Fujiwara[3], Mae K. Borchrdt[1], Estefani Berrios Turcios[1], Elizabeth A. Olmsted-Davis[1], Sivareddy Kotla[3], John P. Cooke[1], Guangyu Wang[1‡], Jun-ichi Abe[3*‡] and Nhat-Tu Le[1*‡]

[1]Center for Cardiovascular Regeneration, Department of Cardiovascular Sciences, Houston Methodist Research Institute, Houston, TX, United States, [2]Department of Life Science, Vietnam Academy of Science and Technology, University of Science and Technology of Hanoi, Hanoi, Vietnam, [3]Department of Cardiology, The University of Texas MD Anderson Cancer Center, Houston, TX, United States, [4]Department of Symptom Research, The University of Texas MD Anderson Cancer Center, Houston, TX, United States

Background: The deSUMOylase sentrin-specific isopeptidase 2 (SENP2) plays a crucial role in atheroprotection. However, the phosphorylation of SENP2 at T368 under disturbed flow (D-flow) conditions hinders its nuclear function and promotes endothelial cell (EC) activation. SUMOylation has been implicated in D-flow-induced endothelial-to-mesenchymal transition (endoMT), but the precise role of SENP2 in counteracting this process remains unclear.

Method: We developed a phospho-specific SENP2 S344 antibody and generated knock-in (KI) mice with a phospho-site mutation of SENP2 S344A using CRISPR/Cas9 technology. We then investigated the effects of SENP2 S344 phosphorylation under two distinct flow patterns and during hypercholesteremia (HC)-mediated EC activation.

Abbreviations

AAV, adeno-associated virus; ATR, the ataxia telangiectasia mutated- and rad3-related kinase; ATM, ataxia-telangiectasia mutated kinase; BMT, bone marrow transplantation; CHK1, Checkpoint kinase 1; CRISPR/Cas9, RNA-guided endonuclease Cas9 from microbial type II CRISPR; DAPI, 4′,6-diamidino-2-phenylindole; DEG, differentially expressed gene; DDR, DNA damage response; DDIAS, DNA damage induced apoptosis suppressor; D-flow, disturbed flow; EC, endothelial cell; endoMT, endothelial-to-mesenchymal transition; Gy, Gray; GO, Gene Ontology; GSEA, gene set enrichment analysis; γH2AX, phosphorylated S139 histone H2A; H&E, hematoxylin and eosin; HDL, high-density lipoprotein; HFD, high fat diet; HUVEC, human umbilical vein EC; IPA, ingenuity pathway analysis; ICAM1, intercellular adhesion molecule 1; IR, ionizing radiation; KI, knock-in; L-flow, laminar flow; LDL, low-density lipoprotein; MS, mass spectrometry; PBS, phosphate buffered saline; qRT-PCR, quantitative reverse-transcriptase polymerase chain reaction; RNA-seq, RNA sequencing; SMA, α-smooth muscle actin; SENP2, sentrin-specific isopeptidase 2; TWIST1, twist-related protein 1; siRNA, small interfering RNA; SUMO, small ubiquitin-related modifier; TGF-β, transforming growth factor-β; VCAM1, vascular cell adhesion molecule 1; VE-cad, vascular-endothelial cadherin; WT, wild type.

Result: Our findings demonstrate that laminar flow (L-flow) induces phosphorylation of SENP2 at S344 through the activation of checkpoint kinase 1 (CHK1), leading to the inhibition of ERK5 and p53 SUMOylation and subsequent suppression of EC activation. We observed a significant increase in lipid-laden lesions in both the aortic arch (under D-flow) and descending aorta (under L-flow) of female hypercholesterolemic SENP2 S344A KI mice. In male hypercholesterolemic SENP2 S344A KI mice, larger lipid-laden lesions were only observed in the aortic arch area, suggesting a weaker HC-mediated atherogenesis in male mice compared to females. Ionizing radiation (IR) reduced CHK1 expression and SENP2 S344 phosphorylation, attenuating the pro-atherosclerotic effects observed in female SENP2 S344A KI mice after bone marrow transplantation (BMT), particularly in L-flow areas. The phospho-site mutation SENP2 S344A upregulates processes associated with EC activation, including inflammation, migration, and proliferation. Additionally, fibrotic changes and up-regulated expression of EC marker genes were observed. Apoptosis was augmented in ECs derived from the lungs of SENP2 S344A KI mice, primarily through the inhibition of ERK5-mediated expression of DNA damage-induced apoptosis suppressor (DDIAS).
Summary: In this study, we have revealed a novel mechanism underlying the suppressive effects of L-flow on EC inflammation, migration, proliferation, apoptosis, and fibrotic changes through promoting CHK1-induced SENP2 S344 phosphorylation. The phospho-site mutation SENP2 S344A responds to L-flow through a distinct mechanism, which involves the upregulation of both mesenchymal and EC marker genes.

KEYWORDS

atherosclerosis, endothelial activation, laminar flow, CHK1, SENP2, SUMOylation, fibrotic changes

Introduction

Blood flow patterns have a significant impact on disease progression *in vivo*, but the underlying biological mechanisms are not fully understood. It has been observed that exposure to D-flow, but not L-flow (1, 2), in vascular regions of ECs contributes to the development of atherosclerosis (2). The deSUMOylation enzyme SENP2, containing nuclear localization and export signals with nucleocytoplasmic shuttling activity, plays a crucial role in regulating the SUMOylation of various proteins involved in important cellular processes. These proteins include extracellular signal-regulated kinase 5 (ERK5), tumor suppressor protein p53, focal adhesion kinase (FAK), and membrane associated guanylate kinase WW and PDZ domain containing 1 (MAGI1) (3–9). Our previously studies have demonstrated that D-flow activates a redox sensitive ribosomal S6 kinase p90RSK, leading to phosphorylation of SENP2 at T368. This phosphorylation event subsequently triggers the SUMOylation of ERK5 and p53, promoting EC inflammation and apoptosis. Consequently, EC dysfunction ensues, contributing to the development of atherosclerosis (3–5, 9–12). In contrast, we have also observed that L-flow inhibits the SUMOylation of ERK5 and p53 without affecting SENP2 T368 phosphorylation (2–4, 14). This suggests that the atheroprotective effects of L-flow are independent of SENP2 T368 phosphorylation.

Atherogenesis is closely associated with DNA damage in cells of the vessel walls, leading to the activation of DNA damage response (DDR) pathways (14–16). DDR plays a crucial role in maintaining the genetic stability and integrity of cells exposed to DNA-damaging agents such as radiotherapy and chemotherapy, commonly used in cancer treatment (17). DDR achieves this by initiating cell cycle arrest for DNA repair and promoting cell apoptosis and senescence to prevent the propagation of damaged DNA. The main DDR pathways are governed by the ataxia-telangiectasia-mutated (ATM) and ataxia-telangiectasia and Rad3-related (ATR) kinases, which phosphorylate proteins at sites of DNA damage. For instance, phosphorylation of the Serine 139 residue of the histone variant H2AX leads to the formation of γH2AX and activates check point kinase (CHK) (18). CHK1 is activated by ATR and plays a critical role in regulating DDR to prevent the propagation of DNA damage. It induces cell cycle arrest, senescence, and apoptosis, thereby halting the progression of cell with damaged DNA (18, 19). CHK1 activation is particularly important in preventing cells with defective G1 checkpoint, often observed due to p53 mutations, from entering mitosis. Moreover, CHK1 also suppresses replicative stress by inhibiting excess origin firing, especially in cells with activated oncogenes.

EC activation is a significant contributor to atherosclerosis. Various mechanisms contribute to EC activation, including the generation of adhesion molecules and chemokines (inflammation), migration, proliferation, and apoptosis. L-flow inhibits these processes, while D-flow promotes them (20). ECs can undergo transdifferentiation to a mesenchymal phenotype through a process called endothelial-to-mesenchymal transition (endoMT) (21, 22). During endoMT, the expression of EC-specific genes such as cluster of differentiation 31 [CD31 or platelet endothelial cells adhesion molecule 1 (PECAM1)], vascular endothelial cadherin (VE-Cadherin or CDH5), von Willebrand factor (vWF), tyrosine kinase with immunoglobulin-like and EGF-like domains 1 (TIE1), and TEK receptor tyrosine kinase (TIE2) is downregulated (21, 23, 24) while the expression of mesenchymal cell-specific genes such as α-smooth muscle

actin (αSMA), extra domain A (EDA) of fibronectin, N-cadherin, vimentin, fibroblast specific protein 1 (FSP1), fibroblast activating protein (FAP), and Twist-related protein 1 (TWIST1) is upregulated (23, 24). Although endoMT was initially discovered during embryonic cardiac development, recent studies have suggested its involvement in atherosclerosis (25–30). Importantly, blood flow plays a critical role in regulating endoMT. Moonen and colleagues have shown that L-flow-induced activation of ERK5 can suppress endoMT (31). It has become evident that the two different flow patterns, L-flow and D-flow, regulate EC activation and endoMT differently but in concert. While several studies have focused on how flow regulates individual biological responses, to the best of our knowledge, it remains unclear how flow regulates all the processes associated with EC activation and endoMT and their contribution to atherosclerosis.

Radiation therapy-induced cardiovascular disease is a significant cause of morbidity and mortality among cancer survivors, particularly in breast cancer (32), lymphoma (33, 34), and lung cancer (35, 36). A study by Darby and colleagues revealed that there is an increase of 7.4% in major coronary events per gray (Gy) of mean heart dose, and within the first 4 years of radiation therapy, there is an increase of 16.3% per Gy of mean heart dose. Even small increments in mean heart dose are associated with an elevated risk of major coronary events (2 Gy: 10%; 2–4 Gy: 30%; 5–9 Gy: 40%; ≥10 Gy: 116%) compared to patients receiving no heart dose (37). Radiation therapy leads to acute macro- and micro-vascular injury by causing EC injury and activating cardiac monocyte and macrophage. However, the regulatory mechanisms underlying these effects remain unclear, and there are currently no effective treatment available to prevent radiation-induced cardiovascular disease.

In our research, we explored publicly available datasets to investigate other phosphorylation sites of SENP2, as the atheroprotective effect of L-flow seemed independent of SENP2 T368 phosphorylation. Our analysis revealed that SENP2 can undergo phosphorylation at S344 (38, 39) by CHK1, a kinase identified through chemical and genetic approaches combined with high-resolution mass-spectrometry (19, 38, 39). Additionally, we found that exposure to L-flow enhances the phosphorylation of CHK1 at S280 and SENP2 at S344 in ECs. Intriguingly, we observed that radiation disrupts this pathway by reducing CHK1 expression. However, the functional role, regulatory mechanism, and contribution of CHK1-mediated SENP2 S344 phosphorylation to EC activation, endoMT, and atherogenesis are still poorly understood. Therefore, our study aims to investigate the functional role and regulatory mechanism of CHK1-mediated SENP2 S344 phosphorylation induced by L-flow and its subsequent impact on atherogenesis.

Methods

The data supporting the findings of this study are available from the corresponding authors upon reasonable request.

Plasmids, adeno-associated virus (AAV), and adenoviruses

The plasmid containing human SENP2 WT was obtained from Addgene (#18047) (40). To generate the phospho-site mutation SENP2 S344A, a Quik Change site-directed mutagenesis kit (Agilent Technologies) was used following the manufacturer's instructions. Adenoviruses expressing human SENP2 WT and S344A (Ad SENP2 WT, Ad SENP2 S344A) were generated by cloning each corresponding insert from the pCMV vector into the pENTR1A vector (Life Technologies, #A10462) at sites recognized by the restriction enzymes EcoRI and SalI. A recombinase reaction was performed to obtain a pDEST-based vector using the Invitrogen Gateway LR Clonase II Enzyme mix (#11791100) according to the manufacturer's instructions. For control purposes, adenovirus containing b-galactosidase (Ad-LacZ) was used (9). Plasmids containing human DDIAS (C11orf82, #RC206347) and pCMV6-Entry with C-terminal Myc-DDK Tag (#PS100001) were purchased from OriGene Technologies, Inc. Additionally, a plasmid encoding mPCSK9 was obtained from Addgene (#58376) (41). A recombinant adeno-associated virus serotype 8 (rAAV8) expressing mPCSK9 under the control of the liver-specific promoter controlling region-apolipoprotein enhancer/alpha1-antitrypsin (rAAV8-HCRApoE/hAAT) was produced by the University of North Carolina Vector Core (Chapel Hill, NC).

Antibodies and reagents

Phospho-specific SENP2 S344 antibody was custom produced by Pierce Biotechnology Inc. Rabbits were immunized with a synthesized peptide corresponding to amino acids 334–354 of the human SENP2 sequence (Ac-GSNGLLRRKVS*IIETKEKNCS). Adverse reactions, including lesion formation, loss of appetite, and non-responsiveness, were monitored during the immunization process. Once the rabbits passed the initial evaluation, the remaining immunization protocol was carried out according to the manufacturer's protocol. After the completion of the immunization process, the rabbits were euthanized, and the obtained sera were affinity purified. The following antibodies were purchased from Cell Signaling Technology (Beverly, MA, USA): ERK5 (#3372), cleaved caspase 3 (#9661), ICAM1 (#4915, #67836), p53 (#9282), VCAM1 (#13662), phospho-CHK1 S280 (#2347S), phospho-CHK1 S345 (#2348S), and phospho-CHK1 S317 (#12302S). The following antibodies were purchased from Abcam (Waltham, MA, USA) SENP2 (#58418), VCAM1 (#13407), α-SMA (#ab5694). CHK1 (sc-8408) was purchased from Santa Cruz biotechnology (Dallas, TX). SENP2 antibody (NBP1-31217) and β-actin antibody (NB600-532) were purchased from Novus Biologicals (Briarwood Ave, CO, USA). The following antibodies and reagents were purchased from Sigma-Aldrich (St. Louis, MO, USA): DDIAS (HPA038541), TWIST1 (ABD29), protease inhibitor cocktail (P8340), PMSF (#36978), NEM (E3876), and diphenyleneiodonium chloride (D2926). SUMO2/3 antibody (AP1224a) was purchased from Abcepta, Inc

(San Diego, CA). The Quick ChangeII Site-Directed Mutagenesis Kit (#200523) was purchased from Agilent Technology (Santa Clara, CA, USA). Lipofectamine 2,000 transfection reagent (#11668027) was purchased from Thermo Fisher Scientific, Waltham, MA). CHK1 inhibitor (GDC 0575) and ERK5 inhibitor (XMD8-92, #S7525) were purchased from Selleck Chemicals LLC (Houston, TX, USA), dissolved in DMSO, and pretreated to ECs prior to flow exposure at the doses indicated in the figures.

Animal studies

Procedures involving mice conducted in accordance with the guidelines and regulations set forth by the Institutional Care and Use Committees (IACUC) of the Texas A&M Institute of Biosciences and Technology (2014-0231, 2017-0154) and the University of Texas MD Anderson Cancer Center (UTMDACC; 00001652, 00001109), adhering to the NIH standards outlined in the Guide for the Care and Use of Laboratory Animals (DHHS pub. NIH 85-23 Rev.1985). The mice were provided with an appropriate irradiated diet and ultra-filtered water. They were housed in a facility at UTMDACC, which is AAALAC certified and maintained with an ambient temperature of 22°C with a 12 h light/12 h dark cycle (42). The mice were housed in a cage-level barrier system with heat-treated wood chip bedding and enrichment material (nestlets). Cages and water were changed on a weekly basis. To study the mouse counterpart of human SENP2 S344 (S343, referred to as "mouse SENP2 S344" for consistency), we generated SENP2 S344A knock-in (KI) mice using CRISPR/Cas9 technology. The gRNAs for targeting SENP2 S344 were selected based on minimal off-target cuts using an off-target program (http://crispr.mit.edu/), and their *in vivo* cutting efficiency was assessed using an efficiency-of-cutting program (http://crispr.dfci.harvard.edu/SSC/). Three gRNAs that cut closest to the S344 codon while meeting the off-target and efficiency criteria were chosen for further testing. The gRNAs, along with an unrelated gRNA, were incubated with an SENP2 plasmid and Cas9 following the instructions provided with the Clontech Cas9 guide-it Screening Kit. Gel electrophoresis confirmed 100% accuracy of the three SENP2 S344 gRNAs in cutting target sequence, while the control gRNA did not show any cutting activity (data not shown). The 110 bp donor DNAs containing the S344A mutation, along with a silent mutation in the PAM sequence (resulting in the same amino acid but with a different codon), were synthesized by Sigma-Aldrich. Excess single-strand donor DNAs were used for asymmetric PCR and PCR clean-up. The final product was then sent to the Genetically Engineered Mouse Facility at UTMDACC. Each donor DNA, along with its corresponding gRNA and Cas9, was microinjected into the pronucleus of fertilized C57/BL6 mouse eggs and implanted into recipient mice.

To measure the levels of HDL and LDL cholesterol, a cholesterol assay kit for mice (#EHDL-100, Bioassay System, Hayward, CA) was used (43).

Tissue preparation, histologic evaluation, and quantification of lesion size

We administered a single dose of rAAV8-mPCSK9 (1×10^{11}/mouse) via tail veins of eight-week-old mice, which were then fed a high-fat diet (HFD) consisting of 21% fat, 0.15% cholesterol, 19.5% casein (#TD.88137; Envigo, NJ) (44) for 16 weeks. Mouse body weight was recorded before and after HFD. At the end of the experiment, mice were euthanized using CO_2 inhalation, and blood samples were collected for LDL cholesterol assay (45). The arterial tree was perfused through the left ventricle with saline containing heparin (40 USP U/ml), followed by 10% neutral-buffered formalin in PBS (10 min). The aorta was dissected from the heart to the iliac bifurcation and opened along the ventral midline. En face prepared aortas were washed in PBS, dipped in 60% isopropyl alcohol, and stained with 0.3% Oil Red O (ORO) in 60% isopropyl alcohol for 30 min. Images were captured using a digital camera mounted on a Nikon SMZ1000 stereomicroscope, and image analysis was performed using the ImageJ software (5, 46) in a double-blinded manner.

Bone marrow transplantation (BMT)

To perform BMT, lethally irradiated bone marrow cells obtained from eight-to-nine-week-old SENP2 S344A KI or WT mice were replaced with bone marrow cells obtained from WT mice (47). Following a recovery period of 6 weeks, the recipient mice were administered a single dose of rAAV8-mPCSK9 and were fed a HFD for 22 weeks (45). To confirm the successful completion of the BMT, PCR was conducted on genomic DNA extracted from peripheral blood of the recipient mice, using specific primers for WT (forward: CAC GTA TTC ACT ACC CAA TGT GGA GTT C; reverse: AAG TTC TTT TCC TTT ATC TCA AGC ACT GA) and SENP2 S344A KI (forward: CAC GTA TTC ACT ACC CAA TGT GGA GTT C, reverse: GTT CTT TTC CTT AAT CTC AAG CAC TGC). Lipid-laden lesions in the mouse aortas were identified through Oil Red O staining of *en-face* preparations. The aortic valve leaflets, sectioned at the center area between the free edge and attachment site at the annulus, were stained using Trichrome Stain Kit (ab150686; abcam). Histological evaluation was performed to assess the changes in the aortic valves of the BMT recipients.

Isolation and culture of human umbilical vein ECs (HUVECs)

HUVECs were isolated by performing a collagenase digestion of the endothelium obtained from human umbilical cord veins. Subsequently, we cultured the cells on dishes or flasks that were coated with 0.2% gelatin type A (#901771; MP Biomedicals, Santa Ana, CA, USA) in EC medium [ECM, #1001, Science Cell, San Diego, CA, USA]. The study received approval from the Institutional Review Board (IRB Pro00020559) at the Houston Methodist

Research Institute (HMRI) and UTMDACC (IRB RM00000535-RN01). Informed consent was not required for this particular study.

Isolation and culture of mouse lung ECs

The isolation of ECs from mouse lungs was approved by the IACUC at the HMRI (IS00006725), and the procedure followed previously described method (16, 21, 22). Lungs from mice aged six to eight weeks were carefully washed with cold PBS, finely minced using scissors, and then digested using collagenase. To capture the ECs from the mouse lungs, we utilized sheep anti-rat PECAM-1-conjugated Dynabeads (#11035, Invitrogen, Carlsbad, CA, USA). Subsequently, the captured cells were cultured in DMEM (#SH30243.0, Hyclone, Logan, UT, USA) supplemented with 10% FBS (#F2442, Sigma-Aldrich, Saint Louis, MO), 1% ECGS (Promo Cell, Heidelberg, Germany), 25 mM HEPES (#25-060-CI, Corning, Manassas, VA, USA), 1% non-essential amino acid solution (#25-025-CI, Corning, Manassas, VA, USA), 100 mg/ml heparin (#67457037399, Mylan Institutional, Rockford, IL, USA) and 1% penicillin/streptomycin (#30-002-CI, Corning, Manassas, VA, USA).

siRNA and plasmid transfection

To degrade human CHK1, we utilized siRNA targeting nucleotides in the coding sequence 281–301 (AAGCGUGCCGUAGACUGUCCA), along with non-target control sequences, which were purchased from Sigma-Aldrich (Burlington, MA, USA). The siRNA and plasmid transfection procedure was conducted following our previously described methods (5, 44). GIBCO Opti-MEM reduced serum medium (#31985070; Thermo Fisher Scientific) supplemented with Plus (#11514015) and Lipofectamine (#18324020) obtained from Life Technologies were used during transfection. Following transfection, the cells were allowed to recover for 24–48 h before further processing.

RNA-sequencing-based genome wide gene expression study

Total RNA was extracted from ECs isolated from the lungs of SENP2 S344A KI and WT mice following 24 h of L-flow exposure. The RNeasy Plus Micro Kit (#74034, QIAGEN, Germ: antown, MD) was used for RNA extraction. Subsequently, we shipped the RNA samples to Beijing Genomic Institution (BGI, Shenzhen, China) for mRNA preparation, library construction, and sequencing using the BGISEQ-500 platform. The clean tags obtained from sequencing were mapped to the reference genome and genes available at the Mice Genome Annotation Project 2, allowing for up to one mismatch. The original sequencing data have been deposited in the Gene Expression Omnibus (GEO) databse with the accession number GSE222511 and token snyjiikwrdwntcz. Aligment of the paired-end RNA-seq reads to the mouse genome (gencode.vM27) was performed using Kallisto (v0.46.0) with default parameters. DESeq2 (v2.0.12) was used to calculate gene expression levels and identify differently expressed genes (DEGs). Gene expression was measured in transcripts per million (TPM), and DEGs were defined based on Q value $\leq$0.05 as a threshold. Pathway enrichment analysis was conducted using DAVID (https://david-d.ncifcrf.gov) by calculating p-values for each Gene Ontology (GO) term with a modified Fisher's exact test. Significantly enriched GO terms were selected using a Q value <0.05 as the threshold, and a Venn diagram was constructed to identify co-expressed DEGs among the samples using R (v3.5.1). The transcriptional profiles of the KI and WT groups were analyzed, and heatmaps were generated using MORPHEUS https://software.broadinstitute.org/morpheus/.

Immunoblotting and SUMOylation

Protein extraction was performed using radioimmunoprecipitation assay (RIPA) buffer (Tris-HCl pH 7.4 50 mM, NaCl 150 mM, ethylenediaminetetraacetic acid 1 mM, Nonidet P-40 1%, sodium dodecyl sulfate 0.1%, sodium deoxycholate 0.25%) or obtained from EMD Millipore (#20-118, Billerica MA, USA) suplemented with mammalian protease inhibitor cocktail (#p8340; Sigma-Roche, Mannheim, Germany), phenylmethylsulfonyl fluoride 1 mM (#36978; Thermo Fisher Scientific), and N-ethylmaleimide 10 mM (#E3876; Sigma-Roche, Mannheim, Germany) (5). Lysates were centrifuged (15,000 rpm/20 min/4°C) to remove debris, and protein concentration was determined using DC^{TM} Protein Assay Kit I (#5000111; Bio-Rad, Hercules CA, USA). Equal amounts of protein were loaded onto sodium dodecyl sulfate (SDS)-polyacrylamide gel electrophoresis (SDS-PAGE) gels and then transferred onto Immobilon-P transfer membranes (#IPVH00010; Merc Millipore, Tullagreen, IRL). The membranes were incubated in 3% BSA/TBST solution (10 mM Tris-HCl, 0.15 M NaCl, 0.1% Tween 20, pH 8.0) at room temperature (1 h), washed in TBST, and then incubated with specific antibodies (500–1,000 dilution) with mild agitation overnight at 4°C. After washing three times (10 min each), the membranes were incubated with HRP-conjugated secondary antibodies (4,500–5,500 dilution), washed again, and chemiluminescence was detected using an ECL substrate (NEL105001EA; Perkin Elmer. Inc, Waltham, MA, USA). Signal intensities from the immunoblotted membranes were quantified using ImageJ. For SUMOylation, lysates were immunoprecipitated with an antibody that specifically recognizes SUMO2/3 (Signal-Seeker^{TM} SUMOylation 2/3 Detection Kit #BK162; Cytoskeleton, Inc.) and then immunoblotted with ERK5 or p53 antibody to detect SUMOylated ERK5 or p53. The same pulldown samples were also immunoblotted with a SUMO2/3 antibody to confirm equal amounts of SUMO2/3 were pulled down. A control bead was used as a reference.

Automated capillary electrophoresis Western analysis (Wes; proteinSimple, San Jose, Ca, USA)

Lysates were mixed with a 5X fluorescent master mix containing 200 mM DTT, heated at 95°C for 5 min, and 5 µl

of 0.4–1 mg/ml protein was loaded onto a Wes plate (#004-600) using a 12–230 kDa Separation Module (#SM-W003) with either a rabbit (#DM-001) or mouse (#DM-002) detection module. Lysates, blocking buffer, primary antibodies, HRP-conjugated secondary antibodies, and luminol-peroxide were dispensed onto the Wes plate. β-actin antibody was used as a loading control and was multiplexed with the primary antibodies for all samples. Capillary electrophoresis was performed using the instrument's default settings: separation time of 25 min, separation voltage of 375 V, blocking for 5 min, and primary and secondary antibodies incubation for 30 min. Automatically detected standards and peaks were manually inspected, and the data were analyzed using the built-in Compass software (ProteinSimple) (48, 49).

Cone-and-plate devices for studying different flow patterns *in vitro*

In our study, we utilized cone-and-plate devices to investigate the impact of various flow patterns on HUVECs *in vitro* (50). The cone-and-plate method's principle has been described in detail elsewhere (51). To generate D-flow, we used cones with 1-mm deep radial grooves, which induced cobble stone-like cell shapes, mimicking the *in vivo* d-flow conditions (50). It is important to note that D-flow exhibits a turbulent flow pattern, making shear stress calculations unfeasible, unlike oscillatory flow. For L-flow experiments, we utilized flat cones (smooth cones) and observed that HUVECs assumed elongated shapes, resembling the condition observed under L-flow *in vivo* (50). Furthermore, we confirmed the successful generation of L-flow by detecting the phosphorylation of ERK5 at T-E-Y residues (50, 52). As L-flow inhibits EC inflammation while d-flow promotes it, interpreting an increase in EC inflammatory gene expression becomes challenging. It remains unclear whether such increase is due to the heightened proinflammatory effects of D-flow or the diminished anti-inflammatory effects of L-flow. To isolate the effect of each flow pattern, we included a control group with no flow (static conditions).

In vitro EC migration assay

Sub-confluent HUVECs were transduced with Ad-SENP2 WT or S344A. The following day, a vertical region at the center of the HUVEC layer was scratched using a sterile 200 µl pipette tip. The culture media was then aspirated, and the cells were washed three times in PBS to remove any detached cells. Fresh ECM was added to the wells. After 6 h of L-flow exposure, the cells were photographed under a microscope, and the images were analyzed using Image J software. The cell migration rate was calculated as follows: length of initial cell-free vertical scratch − length of remaining cell-free region after L-flow) / length of initial cell-free vertical scratch × 100%.

Statistical analysis

To assess the statistical significance of the differences between experimental groups, we initially conducted a Shapiro-Wilk test to evaluate the normality of each group. For normality distributed data, we performed an ordinary one-way ANOVA followed by Fisher's LSD test for multiple group comparisons or an unpaired Student *t*-test for two group comparisons. In the case of 2-by-2 experiments, we employed a two-way ANOVA analysis instead of a one-way ANOVA. If the data did not meet the assumptions of normality, we employed a Brown-Forsythe and Welch ANOVA or unpaired *t*-test with Welch's correction using Prism software (GraphPad Software). We considered *p*-values less than 0.05 as statistically significant.

Data availability

The RNA-sequencing data generated in this study have been deposited into the NCBI's Gene Expression Omnibus database under accession GSE95066. The sequence of SENP2 has been deposited in GenBank under accession KY651081. All other data, analytic methods, and study materials that support the findings of this study are included in the Data supplement or can be obtained from the corresponding authors upon reasonable request.

Results

CHK1 regulates L-flow-induced phosphorylation of SENP2 at S344 residue, subsequently suppressesing the SUMOylation of ERK5 and p53

Based on publicly available mass spectrometry-based phosphoproteomic datasets that revealed phosphorylation of SENP2 at the Serine344 (S344) residue (38, 39), we aimed to investigate if this phosphorylation occurs in ECs in response to L-flow. To address this, we generated a phospho-specific SENP2 S344 antibody and transduced HUVECs with adenovirus expressing either the phospho-site mutation SENP2 S344A or the wild-type form (Ad-SENP2 S344A or Ad-SENP2 WT). Subsequently, these HUVECs were exposed to L-flow. Following L-flow, we observed an increase in SENP2 S344 phosphorylation, which was effectively abolished by transduction with Ad-SENP2 S344A (**Figures 1A,C, D**). By contrast, there was no significant increase in SENP2 S344 phosphorylation in response to D-flow (**Figures 1B,D**).

Another publicly available mass spectrometry-based dataset revealed that CHK1 phosphorylates SENP2 at the S344 residue. However, the functional consequence of this phosphorylation has not been characterized yet (19). To investigate the involvement of CHK1 in L-flow-mediated SENP2 S344 phosphorylation, we pre-treated HUVECs with the CHK1 inhibitor, GDC 0575 (53), prior to L-flow exposure. Remarkably, the pretreatment with GDC 0575 resulted in a significant decrease in SENP2 S344

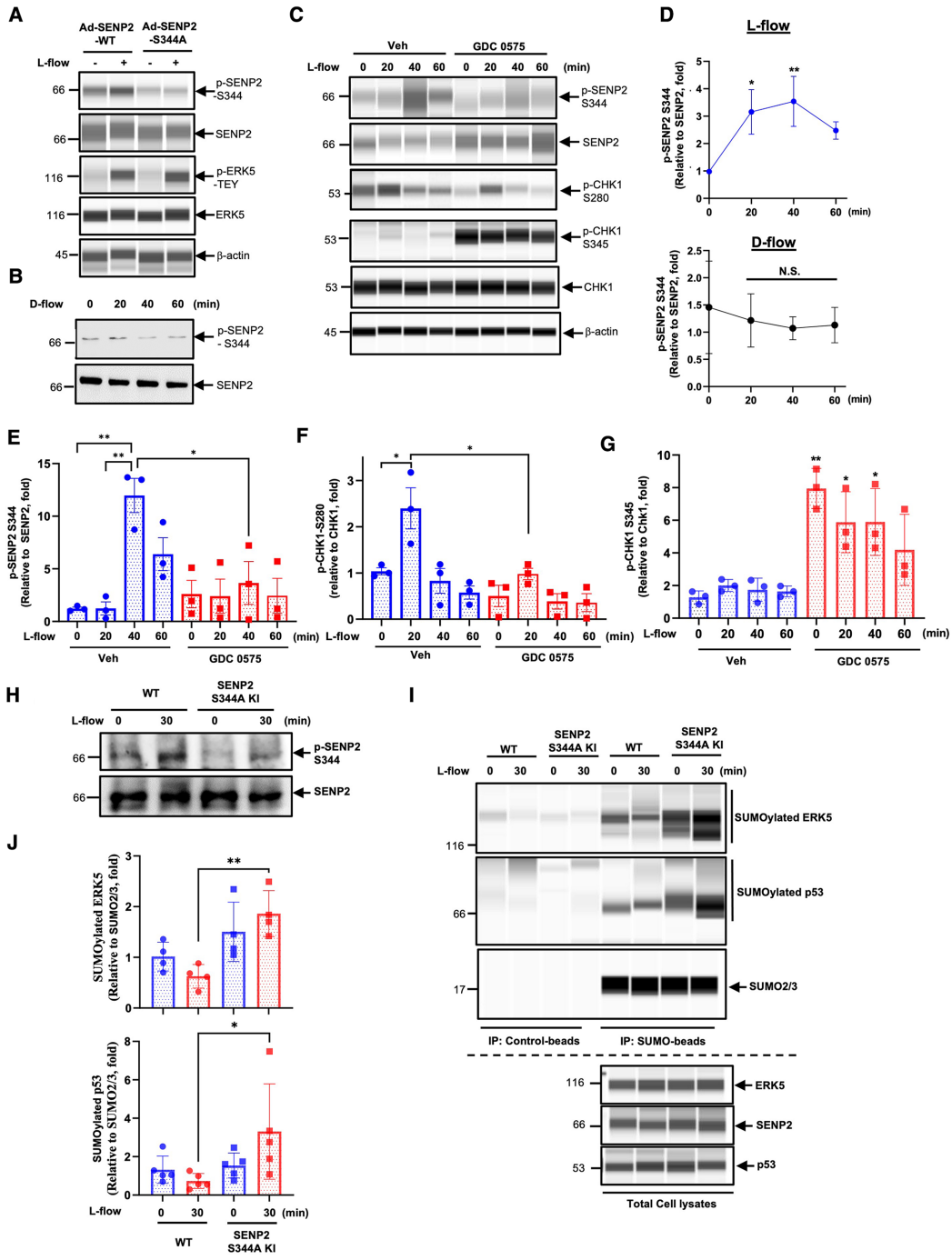

FIGURE 1
CHK1 regulates L-flow-induced SENP2 S344 phosphorylation, subsequently suppresses ERK5 and p53 SUMOylation: (**A**) HUVECs transduced with Ad-SENP2 WT or Ad-SENP2 S344A were exposed to L-flow for 0 and 30 min, and the levels of SENP2 (p-S344 and total), ERK5 (p-T-E-Y and total), and actin (loading control) were determined using Wes. An increase in p-ERK5-T-E-Y indicated successful generation of L-flow, in addition to elongated cell shape (50, 52). (**B**) HUVECs were exposed to D-flow for 0, 20, 40, and 60 min, and the levels of SENP2 (p-S344 and total) were determined using immunoblotting. (**C**) HUVECs pretreated with 250 nM GDC 0575 were exposed to L-flow for 0, 20, 40, and 60 min, and the levels of SENP2 (p-S344 and total), CHK1 (p-S280, p-S345, and total), and actin were determined using Wes. (**D**, upper panel) The graphs present quantified data from 3 independent experiments from (**C**) ($n = 3$) (*$p < 0.05$, **$p < 0.01$, two-way ANOVA). (**D**, lower panel) The graphs present quantified data from 3 independent experiments from (**B**) ($n = 3$). N.S. indicates no significance. (**E–G**) The graphs present quantified data from 3 independent experiments from (**C**) ($n = 3$) (*$p < 0.05$, **$p < 0.01$, two-way ANOVA). (**H**) WT mouse lung ECs (WT MLECs) and SENP2 S344A KI MLECs were exposed to L-flow for 0 and 30 min, and the levels of SENP2 (p-S344 and total) were determined by immunoblotting. (**I**) WT MLECs and SENP2 S344A KI MLECs were exposed to L-flow for 0 and 30 min. Lysates were immuno-precipitated with the SUMO2/3 antibody (Signal-Seeker™ SUMOylation 2/3 Detection Kit, #BK162; Cytoskeleton, Inc.), and ERK5 or p53 antibody was used to detect SUMOylated ERK5 or p53 using Wes, respectively. The SUMO2/3 antibody was also used to confirm equal immunoprecipitation across the samples. Control beads were used as the negative control. ERK5, SENP2, and p53antibodies were used to detect their expression in total cell lysates using Wes. (**J**) The graphs present quantified data from 4 (upper panel) and 5 (lower panel) independent experiments (*$p < 0.05$, two-way ANOVA).

phosphorylation (Figures 1C,E). These findings suggest that CHK1 plays a role in L-flow-mediated SENP2 S344 phosphorylation.

Moreover, since CHK1 activation is known to be regulated by the CHK1-mediated phosphatase 2A circuit (54), we assessed the effect of GDC 0575 on CHK1 activation. Interestingly, treatment with GDC 0575 led to an increase in CHK1 S345 phosphorylation, indicates effective suppression of CHK1 activation due to the inhibition of phosphatase 2A activity (Figures 1C,G). Notably, we observed an increase in CHK1 phosphorylation at S280, but not S345, in the vehicle-treated HUVECs after L-flow, which was abolished by GDC 0575 (Figures 1C,F,G). It is worth noting that phosphorylation of CHK1 at S280, but not S345, promotes CHK1 nuclear translocation (45, 55, 56). Therefore, it is possible that CHK1-mediated SENP2 S344 phosphorylation following L-flow is regulated by CHK1 S280 phosphorylation-driven CHK1 nuclear translocation rather than CHK1 S345 phosphorylation-dependent kinase activation.

To investigate the functions and regulatory mechanisms of SENP2 S344 phosphorylation, we utilized CRISPR/Cas9 technology to generate mice with a phospho-site mutation in SENP2 at S344 (SENP2 S344A KI mice) (47). We isolated ECs from the lungs of the SENP2 S344A KI mice (SENP2 S344A KI MLECs) and examined the effects of L-flow on SENP2 S344 phosphorylation. Notably, we observed that L-flow-induced SENP2 S344 phosphorylation was significantly inhibited in SENP2 S344A KI MLECs (Figure 1H). Furthermore, we investigated the impact of SENP2 S344 phosphorylation on the SUMOylation of ERK5 and p53. Interestingly, we observed an increase in the SUMOylation of ERK5 and p53 in SENP2 S344A KI MLECs specifically after L-flow stimulation, while no significant changes were observed under static conditions, compared to those in WT MLECs (Figures 1I,J). These findings strongly suggest that SENP2 S344 phosphorylation induced by L-flow plays a crucial role in inhibiting the SUMOylation of ERK5 and p53 through modulating SENP2 deSUMOylation activity.

SENP2 S344 phosphorylation suppresses EC inflammation and apoptosis *in vivo*

We have previously reported that SENP2 plays a crucial role in inhibiting EC inflammation and apoptosis by suppressing the SUMOylation of ERK5 and p53 (10, 57). While we did not observe an increase in SENP2 S344 phosphorylation in HUVECs exposed to D-flow *in vitro* (Figures 1B,D), our previous study has demonstrated that depletion of SENP2 leads to increased adhesion molecule expression and apoptosis in both L-flow and D-flow conditions in SENP2 knock-out mice (9). To further investigate the impact of SENP2 S344 phosphorylation on EC inflammation and apoptosis, we examined the effects in both L-flow and D-flow conditions using mice carrying the phospho-site mutation SENP2 S344A KI. Immunofluorescence staining revealed increased expression of VCAM1, a marker of EC inflammation, in the D-flow condition of the phospho-site mutation SENP2 S344A KI mice (Figure 2A). Additionally, TUNEL staining revealed an increased number of TUNEL-positive cells, indicating apoptosis, in the D-flow condition of the phospho-site mutation SENP2 S344A KI mice (Figure 2B). These findings provide further evidence supporting the role of SENP2 S344 phosphorylation in suppressing EC inflammation and apoptosis by preserving the deSUMOylation activity of SENP2 in an *in vivo* context.

The phospho-site mutation SENP2 S344a KI mice exhibit larger lipid-laden lesions

To assess the effect induced by SENP2 S344 phosphorylation in atherogenesis, we injected both WT control mice and phospho-site mutation SENP2 S344A KI mice with a single dose of rAAV8-mPCSK9 and fed them a high fat diet (HFD) for 16 weeks (42, 46). There were no differences in body weight and cholesterol levels between the WT and the phospho-site mutation SENP2 S344A KI mice (Supplementary Figures S1A,B). However, en face Oil Red O staining of mouse aortas showed significantly larger lipid-laden lesions in both the aortic arch (D–flow) and descending aorta (L-flow) of the female phospho-site mutation hypercholesteremic (HC) SENP2 S344A KI mice (Figures 3A,B, lower panel). In the male HC phospho-site mutation SENP2 S344A KI mice, significantly larger lipid-laden lesions were only observed in the aortic arch area (D-flow, Figure 3B, upper panel), suggesting that HC-mediated EC activation and atherogenesis are weaker in males compared to females. Because DNA damage-induced activation in cells of the vessel walls, i.e., ECs (14–16), is associated with atherogenesis, we determined whether the pro-atherosclerotic property of the phospho-site mutation SENP2 S344A KI is due to deficient SENP2 S344 phosphorylation in the cells of the vessel walls. Bone marrow cells in eight-to-nine-week-old SENP2 S344A KI or WT mice were ablated through lethal irradiation, then grafted with bone marrow cells extracted from WT donors of the same age (Figure 3C). Six weeks of recovery from bone marrow transplantation (BMT) (58), both WT → WT and WT → SENP2 S344A KI mice (Figure 3C) were injected with a single dose of rAAV8-mPCSK9 and fed a HFD (42) (Figure 3C). Twenty-two weeks after HFD, genomic DNA was extracted from peripheral blood and used for PCR to verify if BMT was successful (Figure 3D). There was no difference in body weight and cholesterol levels between WT→ WT and WT→SENP2 S344A KI (Supplementary Figures S1C,D) in both male and female mice. Although HC-mediated formation of lipid-laden lesions is weaker in systemic SENP2 S344A KI male mice compared to that of female mice, male WT→SENP2 S344A KI mice displayed larger lipid-laden lesions in D-flow areas (Figures 3E,F). Larger plaque lesions in the aortic valve cross-sectional areas were observed in WT → SENP2 S344A KI male mice compared to those in WT → WT male mice, suggesting that SENP2 S344 phosphorylation in the vessel wall plays a crucial role in inhibiting atherosclerotic formation, especially in D-flow areas (Figures 3G,H). Although the percentage of necrotic core formation per total lipid-laden areas was almost identical between male WT → SENP2 S344A KI and male WT → WT

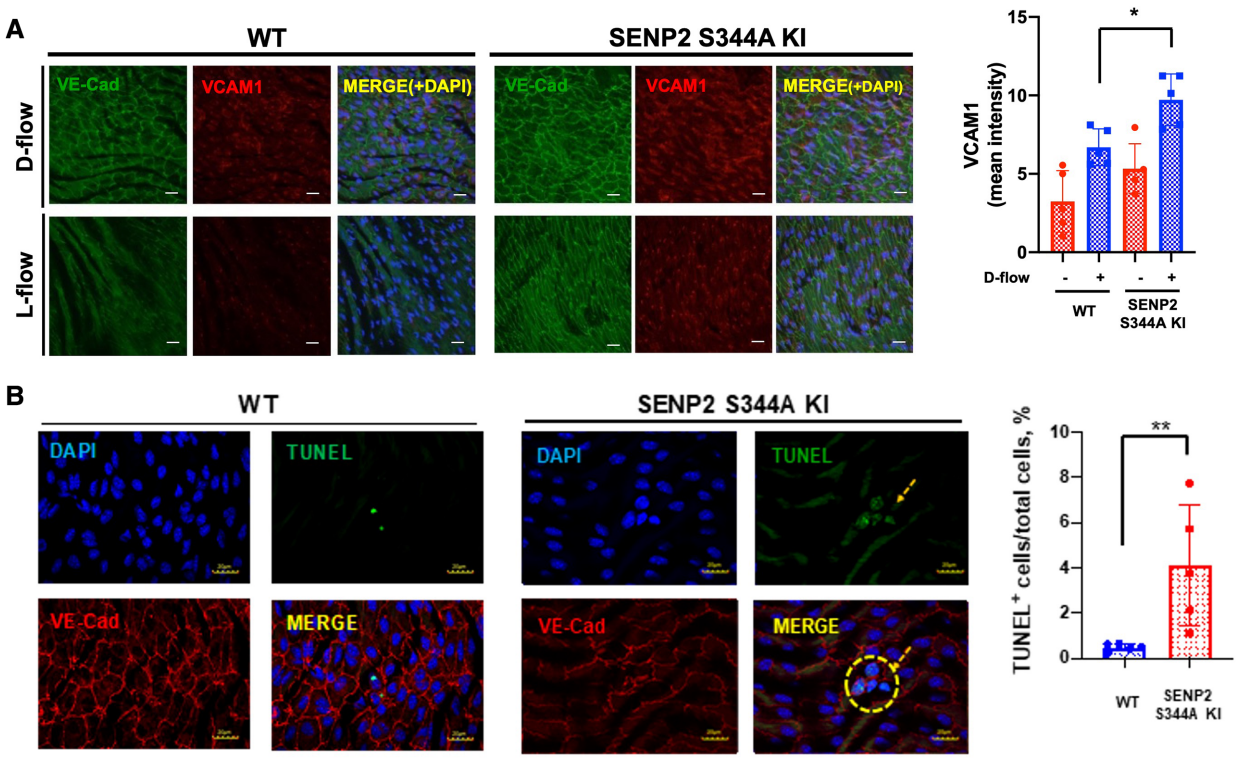

FIGURE 2
Increased EC inflammation and apoptosis in SENP2 S344A KI mice: (**A**) En face preparation of WT and SENP2 S344A KI aortas were immunofluorescence-stained with VCAM1 (red, EC inflammation) and VE-Cad (green, EC marker). (**B**) Aortic sections were stained with TUNEL (green, EC apoptosis (106)) and DAPI (blue, nucleus (9)). TUNEL-positive apoptotic nuclei were counted, indicating the colocalization between the TUNEL signal (representing fragmented DNA) and the DAPI signal (representing cell nuclei) (28). The graphs present quantified data from 5 independent samples ($n = 5$) (*$p < 0.05$, **$p < 0.01$, two-way ANOVA for (**A**); unpaired *t*-test for (**B**)).

mice (Figure 3I), the fibrotic caps covering necrotic cores were thinner in male WT → SENP2 S344A KI (Figure 3J), suggesting that SENP2 S344 phosphorylation in cells of the vessels prevents vulnerable plaque formation (Figures 3I,J).

Radiation accelerates EC activation through the downregulation of CHK1 expression

Although en face Oil Red O staining showed that lipid-laden lesions in female SENP2 S344A KI mice were larger than in female WT mice (Figures 3A,B), when these female mice underwent BMT for vascular-specific models, the lipid-laden lesions in female WT → SENP2 S344A KI mice were almost identical to those in female WT → WT mice (Figure 4A). During BMT, mice were irradiated; therefore, we hypothesized that radiation may alter CHK1 and/or SENP2 activity. To address this possibility, we irradiated HUVECs and observed a dose-dependent reduction in both SENP2 S344 phosphorylation and CHK1 expression, accompanied by elevated expression of VCAM1 and ICAM1. The changes in VCAM1 and ICAM1 expression showed an inverse correlation with changes in CHK1 expression and SENP2 S344 phosphorylation (Figures 4B,C). Furthermore, CHK1 depletion accelerated ERK5 SUMOylation (Figure 4D) and D-flow-induced ICAM1 expression (Figure 4E), while counteracting the anti-inflammatory effect of L-flow (Figures 4F,G). These data suggest that radiation induces EC activation by suppressing the CHK1-SENP2 S344 phosphorylation axis. Therefore, the effect of the phospho-site mutation SENP2 S344A KI mice on atherosclerotic plaque formation became unclear, especially in female mice after BMT (Figure 4A), compared to the phospho-site mutation SENP2 S344A KI mice that did not receive radiation (Figures 3A,B lower panel).

SENP2 S344 phosphorylation suppresses various processes contributing to EC activation

To elucidate the functional role of L-flow-induced SENP2 S344 phosphorylation, SENP2 S344A KI MLECs and WT MLECs were exposed to L-flow for 24 h, and RNA-seq was performed. We identified 427 differentially expressed genes (DEGs) in SENP2 S344A KI MLECs compared to WT MLECs (Figure 5A). Among these DEGs, 259 out of 427 DEGs were regulated by L-flow (Figure 5B). GO analysis revealed that these 427 DEGs are associated with migration, positive regulation of epithelial cell proliferation, multicellular organism development, positive regulation of angiogenesis, and cell adhesion, all of which are known to contribute to EC activation (Figures 5D,E). GO Circle analysis revealed positive *Z*-scores (indicating activation) of all these

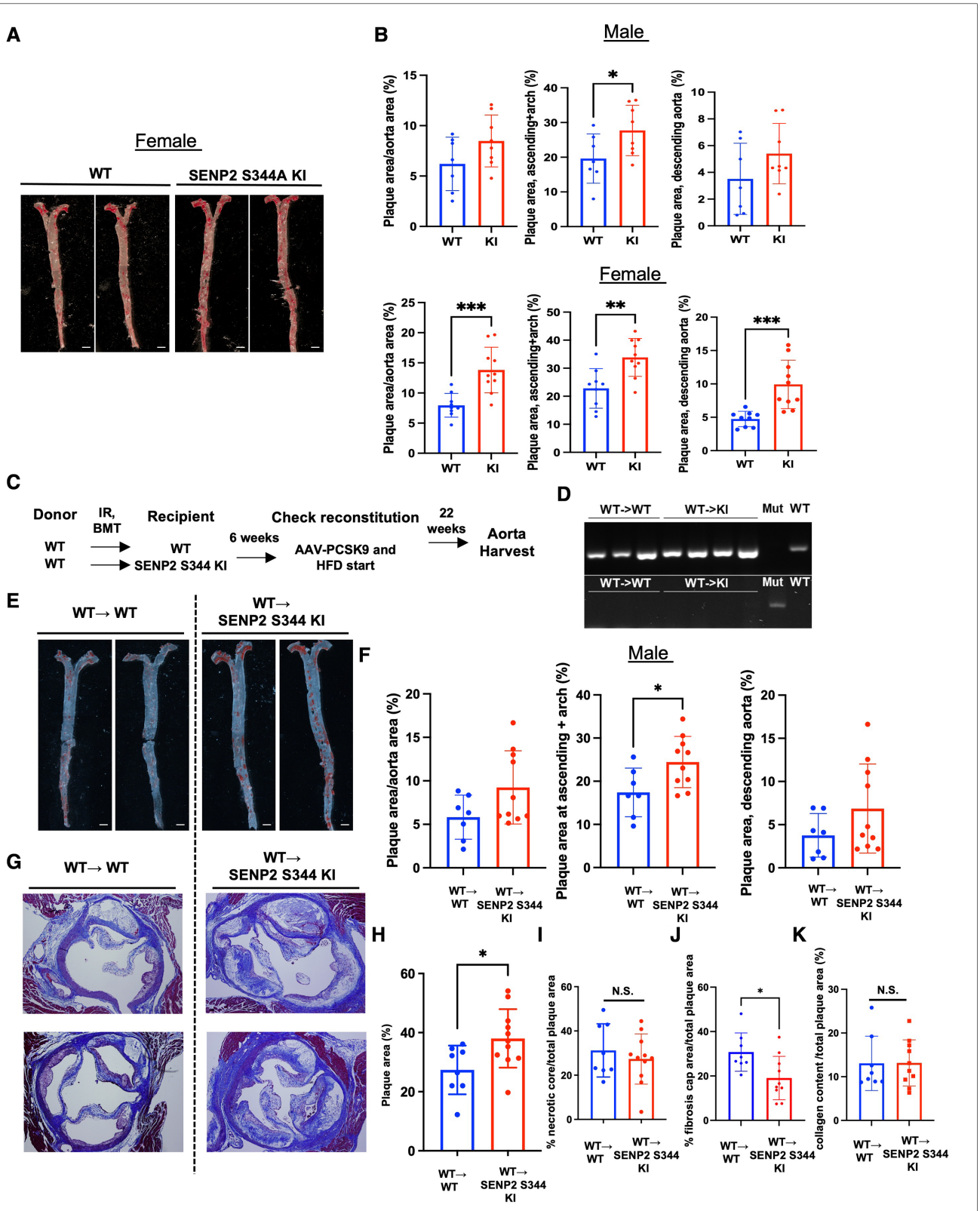

FIGURE 3
Increased lipid-laden lesions and fibrotic caps in SENP2 S344A KI mice: SENP2 S344A KI and WT mice were injected with a single dose of rAAV8-mPCSK9 and fed a high fat diet (HFD) for 16 weeks (42). (**A**) En face Oil Red O staining was performed to quantify lipid abundance and distribution. (**C**) The bone marrow transplantation (BMT) procedure was conducted (58). (**D**) Representative PCR data demonstrate the success of the BMT. (**E**) En face Oil Red O staining was performed on the BMT-generated models. (**G**) Aortic valve leaflet sections were stained with Masson's trichrome to evaluate changes in the aortic valves. (**B**, **F**, **H**–**K**) The graphs present quantified data from samples ($n = 7$–10) (*$p < 0.05$, **$p < 0.01$, unpaired t-test). N.S. indicates non-significant.

10.3389/fcvm.2023.1187490

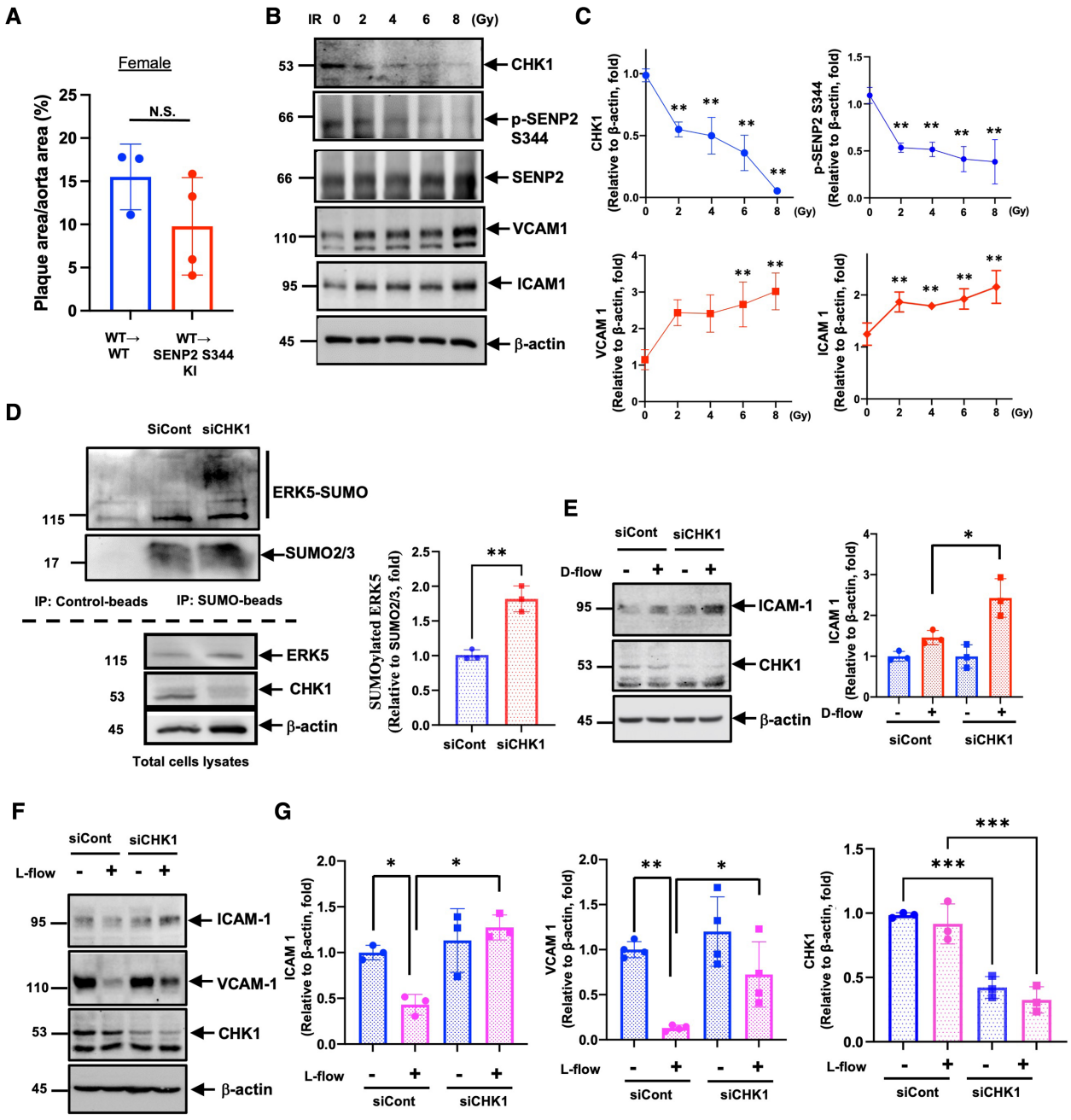

FIGURE 4
Radiation-induced EC activation through CHK1 downregulation: (A)there was no significant difference in lipid-laden lesions between female WT → WT and WT → SENP2 S344A KI mice ($n = 3–4$). (B) Expression levels of CHK1, SENP2 (p-S344 and total), VCAM1, ICAM1, and actin were evaluated in HUVECs exposed to 0, 2, 4, 6, 8 Gy of ionizing radiation (IR) for 24 h. (C) The graphs present quantified data from 3 independent experiments (**$p <$ 0.01, two-way ANOVA). (D, left panel) SUMOylated ERK5 was assessed in siRNA-treated HUVECs, and the lysates were immuno-precipitated as described in Figure 1I. (D, right panel) The graphs present quantified data from 3 independent experiments (**$p < 0.01$, t-test). (E, left panel) siRNA-treated HUVECs were exposed to D-flow for 24 h, and the expression of ICAM1, CHK1, and actin were determined using immunoblotting. (E, right panel) The graphs present quantified data from 3 independent experiments (*$p < 0.05$, two-way ANOVA). (F) Expression levels of ICAM1, VCAM1, CHK1, and actin were evaluated in siRNA-treated HUVECs exposed to L-flow for 24 h using immunoblotting. (G) The graphs present quantified data from 3 or 4 independent experiments (*$p < 0.05$, **$p < 0.01$, two-way ANOVA).

processes in SENP2 S344A KI MLECs (Figure 5E). Furthermore, an *in vitro* study showed that L-flow promotes the migration of HUVECs, and this effect was further enhanced by the transduction of Ad-SENP2 S344A phospho-site mutation (Figures 5F,G). Activation of ERK5 transcriptional activity can suppress EC migration (59), and our previous study has demonstrated that ERK5 SUMOylation can inhibit ERK5 transcriptional activity (49). Therefore, the increased migration of HUVECs driven by the transduction of Ad-SENP2 S344A can be attributed to an increase in ERK5 SUMOylation. Collectively, our findings suggest the involvement of SENP2 S344 phosphorylation in regulating various processes contributing to EC activation, including EC migration.

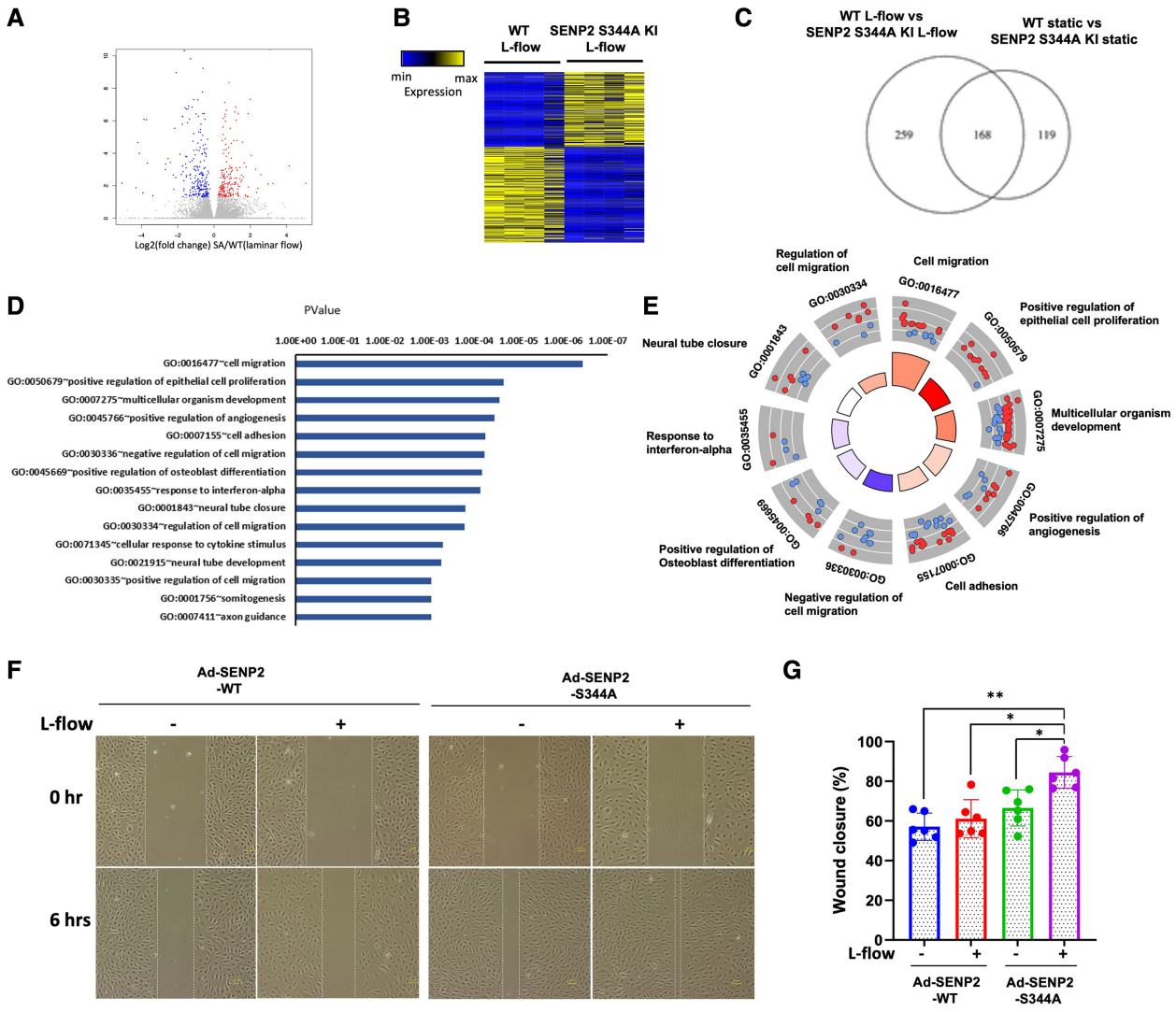

FIGURE 5
Increased EC pathophysiological stress response in SENP2 S344A KI MLECs: (**A**) the volcano plot illustrates the differentially expressed genes (DEGs) in WT MLECs compared to SENP2 S344A KI MLECs after L-flow; "red" dots represent upregulated DEGs, and "blue" dots represent downregulated DEGs. (**B**) A heatmap displaying hierarchical clustering of DEGs between WT MLECs vs. SENP2 S344A KI MLECs after L-flow for 24 h. (**C**) A Venn diagram indicating the total number of DEGs in WT MLECs and SENP2 S344A KI MLECs. (**D**) Annotation of EC activation-related gene ontology (GO) pathways identified in quadruplicate between WT MLECs vs. SENP2 S344A KI MLECs. (**E**) A molecular function Chord plot illustrating the enriched GO biological process terms associated with EC activation in SENP2 S344A KI MLEC transcripts, along with the corresponding genes arranged by their expression levels. (**F**) HUVECs transduced with Ad-SENP2 WT or Ad-SENP2 S344A were subjected to a scratch assay and exposed to L-flow for 6 h. Representative images of cell migration are shown. The dashed line represents the initial or final migration areas. (**G**) The graphs present quantified data from 6 independent experiments (*$p < 0.05$, **$p < 0.01$, two-way ANOVA).

SENP2 S344 phosphorylation suppresses fibrotic changes concurrent with upregulating EC-specific gene expression

Based on the knowledge-based database of Ingenuity Pathways Analysis (IPA), we identified the pulmonary fibrosis idiopathic signaling pathway as the top-ranked enriched IPA canonical pathway. Moreover, the *Z*-score (a measurement of activation) from IPA suggests that fibrotic changes-related processes in the pulmonary fibrosis idiopathic signaling pathway and hepatic fibrosis signaling pathway are positively upregulated in SENP2 S344A KI MLECs compared to WT MLECs after L-flow (**Figure 6A**; **Supplementary Table S1**). Even in static conditions, the *Z*-score of the pulmonary fibrosis idiopathic signaling pathway remains positive, further suggesting the pro-fibrotic effects of the phospho-site mutation SENP2 S344A KI MLECs (**Figure 6B**). Importantly, the *Z*-score of all processes contributing to EC activation, such as cell adhesion, angiogenesis, positive regulation of epithelial cell proliferation, and extracellular matrix organization, is also positive in SENP2 S344A KI MLECs under static conditions. These data strongly suggest the contribution of SENP2 S344 phosphorylation to EC activation (**Figures 6C,D**). Consistent with these findings, we observed an increase in DNA synthesis in SENP2 S344A KI MLECs

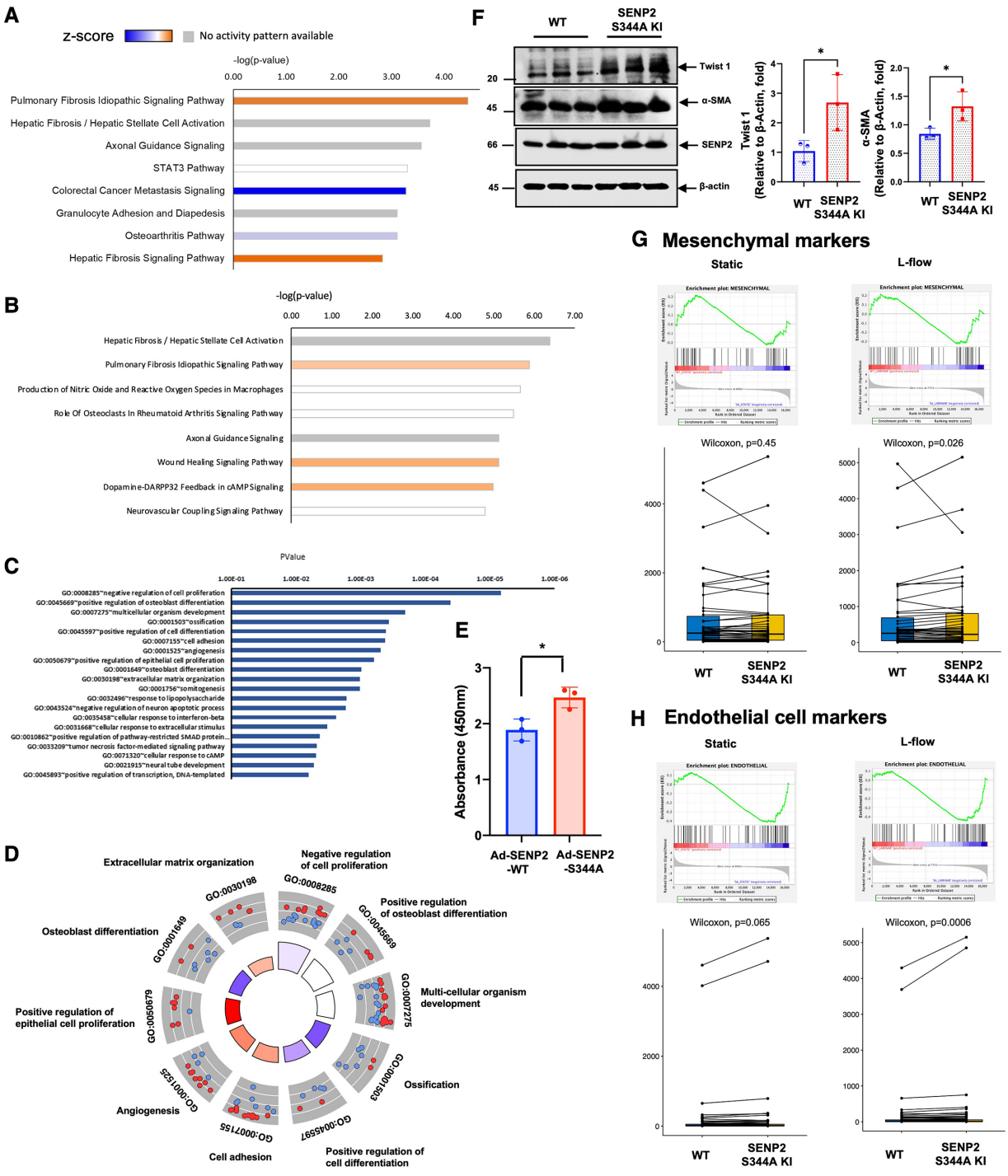

FIGURE 6
Increased EC activation-stimulated fibrosis in SENP2 S344A KI MLECs with upregulated expression of EC markers: (**A**) after L-flow, the *Z*-score of fibrosis-related processes is positively upregulated in SENP2 S344A KI MLECs, as determined by IPA analysis. (**B**) Under static condition, the *Z*-score of the pulmonary fibrosis idiopathic signaling pathway remains positive in SENP2 S344A KI MLECs. (**C**,**D**) Under static condition, the *Z*-score of EC activation-associated processes, including cell adhesion, angiogenesis, positive regulation of epithelial cell proliferation, and extracelular matrix organization, is positive in SENP2 S344A KI MLECs. (**E**) DNA synthesis is increased in HUVECs transduced with Ad-SENP2 S344A compared to HUVECs transduced with Ad-SENP2 WT, as demonstrated by data from 3 independent experiments. (**F**, left panel) The expression of mesenchymal markers (TWIST1, αSMA) is increased in SENP2 S344A KI MLECs. (**F**, right panel) The graphs present quantified data from 3 independent experiments (*$p < 0.05$, *t*-test). (**G**,**H**) The expression of both mesenchymal (**G**) and endothelial (**H**) markers is increased in SENP2 S344A KI MLECs.

compared to WT MLECs (Figure 6E). To evaluate the role of SENP2 S344 phosphorylation in fibrotic changes, we determined the expression levels of fibrotic and mesenchymal markers and found that both TWIST1 (fibrotic marker) and αSMA (mesenchymal marker) expression were increased in SENP2 S344A KI MLECs (Figure 6F). Since d-flow can activate

endoMT, we also assessed the expression of both mesenchymal and EC-specific genes. We found that the expression of both mesenchymal and EC-specific gene was upregulated in SENP2 S344A KI MLECs after L-flow (**Figures 6G,H**). These data suggest that the phospho-site mutation SENP2 S344A KI MLECs exhibit a distinct expression pattern, promoting fibrotic changes while maintaining EC phenotypes without inducing endoMT. This distinct expression pattern may account for the decrease in fibrotic cap area without changing collagen composition in phospho-site mutation SENP2 S344A KI mice (**Figure 3K**) because a decrease in fibrotic cap areas did not cause a parallel decrease in collagen composition.

Via SENP2 S344 phosphorylation and ERK5 activation, L-flow upregulates the expression of DDIAS, which inhibits EC apoptosis

Venn diagram analysis revealed 117 DEGs in the WT MLECs after L-flow. Among these DEGs, 14 out of 117 DEGs were regulated by SENP2 S344 phosphorylation (**Figure 7A**). Notably, *Ddias*, *Il6st*, *Kif18b*, *Pdgfrl*, *Podn*, *Ptpn18*, *Stc10a6*, *Slc7ab*, and *Tgfb3* were identified as 9 core genes regulated by L-flow-induced SENP2 S344 phosphorylation (**Figures 7A,B**). These 9 core genes likely play a critical role in various processes contributing to EC activation, as depicted in **Figures 6C,D**. Interestingly, we observed that the expression of transforming growth factor beta 3 (*Tgfb3*), a regulator of fibrotic changes (60), was inhibited by L-flow, and this inhibition was abolished in the SENP2 S344A KI MLECs (**Figure 7B**). These findings suggest that Tgfb3 is involved in the anti-fibrotic effects mediated by SENP2 S344 phosphorylation. Furthermore, a heatmap analysis of these 9 core genes revealed that *Ddias* was one of the most significantly upregulated genes (**Figure 7B**). As *Ddias* expression is regulated by ERK5 activation and has been shown to inhibit cell death (61, 62), we investigated whether L-flow-induced ERK5 activation regulates DDIAS expression. In HUVECs, we found that the upregulated expression of DDIAS induced by L-flow was abolished when treated with XMD8-92, an ERK5 specific inhibitor (**Figure 7C**). Previously, we reported that ERK5 transcriptional activity is involved in ionizing radiation (IR)-induced EC apoptosis (63). To assess the role of DDIAS expression in EC apoptosis, we exposed HUVECs expressing DDIAS to 2 Gy of IR and observed that the increase in cleaved caspase 3 expression induced by IR was attenuated (**Figure 7D**). These findings collectively highlight the crucial role of DDIAS in the anti-apoptotic effects mediated by L-flow.

Discussion

CHK1 phosphorylates SENP2 at S344 (19), which was discovered as a new residue through mass spectrometry-based phospho-proteomics but with uncharacterized functions (38, 39). In this study, we present evidence describing the functional role and regulatory mechanism governing SENP2 S344 phosphorylation in ECs after L-flow. L-flow enhances the phosphorylation of CHK1 S280 and SENP2 S344, leading to an increase in SENP2 deSUMOylation activity. This is supported by the suppression of ERK5 and p53 SUMOylation and the inhibition of EC inflammation and apoptosis. The phospho-site mutation SENP2 S344A KI mice exhibit an increase in adhesion molecule expression and apoptosis, as well as larger lipid-laden lesions in both female and male mice undergoing HC-mediated atherosclerosis compared to the WT mice, although HC-mediated atherogenesis is weaker in male mice. However, when these mice undergo BMT, lipid-laden lesions in the female WT → SENP2 S344A KI mice are almost identical to those of the female WT → WT mice. We found that radiation can alter the anti-atherosclerotic effect of SENP2 S344 phosphorylation by downregulating the expression of CHK1. Therefore, interpreting the anti-atherosclerotic effect of CHK1-SENP2 S344 phosphorylation in the model of atherosclerosis after BMT would be challenging. Importantly, we found that the CHK1-SENP2 S344 phosphorylation axis coordinately suppresses multiple processes associated with fibrotic changes concurrent with EC activation, such as inflammation, migration, proliferation, and apoptosis. The deficient SENP2 S344 phosphorylation instigates various processes associated with fibrotic changes, along with upregulated expression of EC-specific genes, suggesting that L-flow-induced CHK1-SENP2 S344 phosphorylation promotes fibrotic changes through a mechanism distinct from endoMT. Lastly, we found that by activating ERK5, L-flow upregulates the expression of DDIAS, which subsequently suppresses EC apoptosis by phosphorylating SENP2 S344. Taken together, our data suggest the key role of the CHK1-SENP2 S344 phosphorylation axis in regulating various processes contributing to both EC activation and fibrotic changes in concert. This process is initiated by DDR (CHK1) activation and inhibits both EC activation and fibrotic changes by inducing SENP2 deSUMOylation activity. Our findings suggest that the CHK1-SENP2 S344 phosphorylation axis may suppress excessive EC activation and fibrotic changes after various pathophysiological stresses for maintaining EC barrier function, especially under L-flow.

In this study, we found that L-flow induces the CHK1-SENP2 S344 phosphorylation axis, which inhibits EC inflammation (including adhesion molecule expression), migration, proliferation, apoptosis, and fibrotic changes. These components are critical in the EC response to pathophysiological stress. It is well known that L-flow inhibits these processes, while D-flow activates them (20). Our findings demonstrate that L-flow-induced CHK1-SENP2 S344 phosphorylation increases SENP2 deSUMOylation activity, leading to the inhibition of ERK5 and p53 SUMOylation. In contrast, our previous reports have shown that D-flow-induced p90RSK-SENP2 T368 phosphorylation inhibits SENP2 function in the nucleus, resulting in increased SUMOylation of ERK5 and p53 (9). Together, these findings highlight the crucial role of SENP2 deSUMOylation activity in regulating various processes associated with the EC response to pathophysiological stress, including inflammation, migration, proliferation, apoptosis, and fibrotic changes in concert. These

10.3389/fcvm.2023.1187490

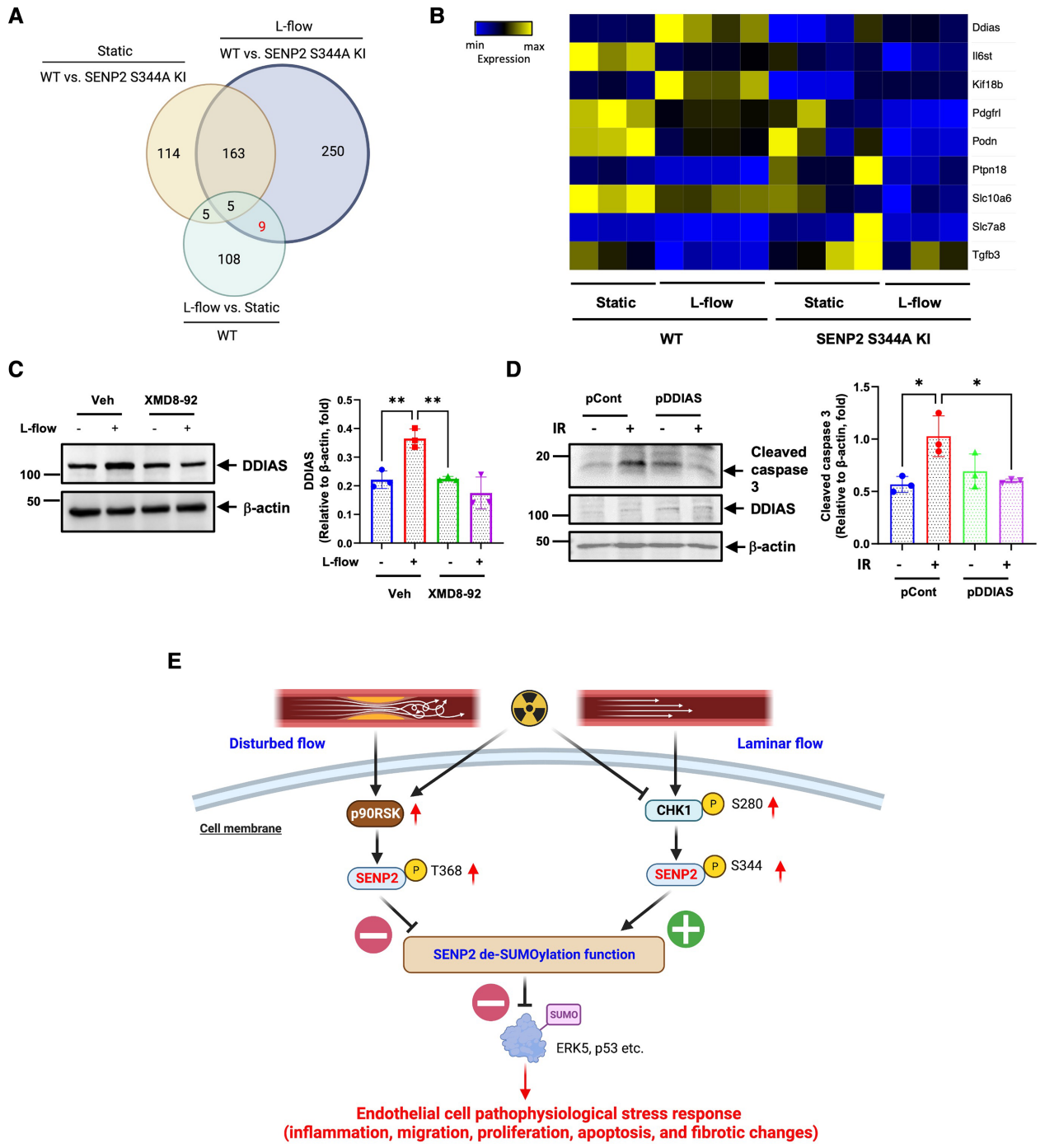

FIGURE 7
L-flow upregulates DDIAS expression via SENP2 S344 phosphorylation and ERK5 activation to suppress EC apoptosis: (**A**) the venn diagram illustrates the significant DEGs between the groups. (**B**) The heatmap displays the nine core genes, including DDIAS. (**C**, left panel) Pretreatment with XMD8-92 (5 μM), an ERK5-specific inhibitor, suppresses L-flow-mediated upregulation of DDIAS expression in HUVECs after 24 h. (**C**, right panel) The graphs present quantified data from 3 independent experiments (**$p < 0.01$, two-way ANOVA). (**D**, left panel) HUVECs were overexpressed with DDIAS using the DDIAS plasmid or control plasmid, then exposed to IR for 24 h. The increased expression of cleaved caspase-3 induced by IR is reversed by DDIAS overexpression. (**D**, right panel) The graphs present quantified data from 3 independent experiments (*$p < 0.05$, two-way ANOVA). "pCont" refers to the control plasmid, and "pDDIAS" refers to the DDIAS plasmid. (**E**) The scheme illustrates the mechanism of L-flow-induced SENP2 S344 phosphorylation in suppressing the EC pathophysiological stress response.

processes occur under two different flow patterns, utilizing two different SENP2 phosphorylation sites: T368 by p90RSK and S344 by CHK1. These phosphorylation sites play a vital role in determining SENP2 deSUMOylation function and subsequent pro- vs. anti-EC activation (Figure 7E). Furthermore, we have previously reported that IR increases p90RSK activation, which phosphorylates SENP2 T368 (63, 64). Therefore, through its dual effects of downregulating CHK1 expression and activating

p90RSK, IR can induce a severe EC response to pathophysiological stress, especially under flow conditions *in vivo* (**Figure 7E**). Nevertheless, further studies are necessary to clarify these possibilities.

ECs are exposed to various stimuli, including blood flow, inflammation, and metabolites, which can influence their phenotypes and functions. While the plasticity and heterogeneity of ECs can allow them to adapt to these alterations (65), certain stimuli can lead to diseases. For instance, inflammation accompanied by increased TGFβ expression can trigger reactivation of endoMT (65, 66), resulting in fibrotic disorders and cardiac fibrosis (29, 67–72). Additionally, D-flow can activate endoMT, contributing to the development of atherosclerosis (31, 73–75). Our RNA-seq analysis revealed that SENP2 S344 phosphorylation plays a negatively regulatory role in pulmonary fibrosis idiopathic signaling and hepatic fibrosis/hepatic stella cell activation pathways, suggesting its involvement in regulating fibrotic changes. However, unlike endoMT, we observed an upregulation of both mesenchymal and EC-specific markers in SENP2 S344A KI MLECs compared to WT MLECs after L-flow. This pattern has also been reported in ECs of glaucomatous Schlemm's canal (76). We propose that the fibrotic changes observed in SENP2 S344 KI MLECs, without overt endoMT phenotypes, represent a unique type of EC response to pathophysiological stress.

The role of DDR in blood flow-regulated EC function is not yet established. ATR, which responds to single-stranded DNA breaks by activating the DNA damage checkpoint through phosphorylation of CHK1 S345, can be activated by mechanosensitive ion channel Piezo and NO signaling independently of DNA damage (77). In ous study, we observed that neither L-flow nor d-flow increased CHK1 S345 phosphorylation. However, L-flow did increase CHK1 S280 phosphorylation, which facilitates CHK1 translocation from the cytoplasm to the nucleus and activates downstream CHK1 signaling in response to serum stimulation (55). These findings suggest that ATR activation may not be involved in CHK1 function. Since L-flow induced SENP2 S344 phosphorylation without affecting CHK1 S345 phosphorylation, it is possible that L-flow-induced CHK1 nuclear translocation plays a crucial role in promoting nuclear SENP2 S344 phosphorylation. The mechanism underlying L-flow-induced CHK1 S280 phosphorylation remains unknown and requires further investigation.

We made an unexpected observation that radiation downregulates CHK1 expression in ECs. To the best of our knowledge, this is the first study to demonstrate a reduction in CHK1 protein expression following radiation exposure. While it is known that p53 and RB1/E2F1 can upregulate CHK1 promoter activity (78) and CHK1 ubiquitination has been reported (79), the specific mechanism by which radiation inhibits CHK1 expression in ECs remains unclear. Given that we have established the role of CHK1-mediated SENP2 S344 phosphorylation in EC fibrotic changes, but not in endoMT, it is possible that radiation induces EC fibrotic changes without triggering endoMT, thereby contributing to the formation of vulnerable plaques. Although radiation-induced endoMT associated with radioresistance in cancer has been reported (80), the role of EC fibrotic changes in radioresistance has not been explored. Therefore, it is crucial to investigate the CHK1-SENP2 S344 phosphorylation axis to understand radiation-induced cardiovascular events and resistance against tumorigenesis. Our findings shed light on a novel aspect of CHK1 biology and its potential implications in how blood flow influences atherogenesis. This knowledge informs current preclinical and clinical interest in CHK1 inhibitors.

While epidemiological and experimental studies have demonstrated the detrimental cardiovascular effects of high doses of IR, the impact of low-dose IR remains unclear (81, 82). A study by Schöllnberger et al. (83, 84) did not definitively establish a risk of heart disease for individuals exposed to doses below 2.6 Gy, while Azizova et al. (85) indicated an increased risk of developing ischemic heart disease for cumulative external doses above 1 Gy. However, there is a lack of epidemiological data on the impact of radiation on cardiovascular diseases after exposure to low to moderate doses, particularly below 500 mGy (86–93). Several experimental studies have focused on investigating the effects of low-dose radiation using mouse models of atherosclerosis, specifically genetically modified ApoE knocked out (KO) mice fed a chow diet. These studies underscore the importance of considering the dose-rate of radiation exposure (94). Mitchel et al. (95, 96) demonstrated that exposure to low-dose IR, especially at a low dose rate, slowed plaque progression in mice. Conversely, Mancuso et al. (97) indicated that acute irradiation at moderate doses (300 mGy) can have detrimental effects on atherosclerosis, whereas chronic exposure to the same dose has a lesser impact. Additionally, both Le Gallic et al. (98) and Ebrahimian et al. (99) found that chronic internal low-dose IR enhances plaque stability in ApoE KO mice. Furthermore, these studies (98, 99) showed a decrease in inflammatory parameters following exposure to low-dose IR, such as reduced plaque content of CD68+ foam cells and a shift in aortic mRNA expression favoring anti-inflammatory cytokines over pro-inflammatory ones (98, 99). These findings support the notion that IR affects the immune system, with high doses promoting inflammation (100) and pro-inflammatory macrophages (101), while lower doses lead to decreased inflammation (102). In a study by Rey et al., the immunomodulatory response to different doses of low-dose IR was investigated. The study utilized ApoE KO mice and examined cumulative doses ranging from 50 to 1,000 mGy, with dose-rates of γ rays set at very low (1.4 mGy h^{-1}) or low (50 mGy h^{-1}) levels. The results revealed a significant decrease in pro-inflammatory Ly6CHi monocytes at all cumulative doses when exposed to low dose-rate radiation. However, at very low dose-rates, reductions in Ly6CHi cells were observed only at doses of 50, 100, and 750 mGy. Conversely, the proportions of Ly6CLo monocytes were not affected by low-dose IR. Additionally, the proportions of CD4+ T cell subsets in the spleen showed no differences between irradiated mice and non-irradiated controls, whether assessing CD25+FoxP3+ regulatory or CD69+ activated lymphocytes. Within the aorta, the gene expression of cytokines such as IL-1 and TGF-β, as well as adhesion molecules including E-Selectin, ICAM-1, and VCAM-1, were reduced at an intermediate dose of 200 mGy. These findings suggest that low-dose IR may decrease the formation of

atherosclerotic plaques by selectively reducing pro-inflammatory monocytes in the bloodstream and impairing adhesion molecule expression and inflammatory processes in the vessel wall. In contrast, the splenic T lymphocytes showed no significant effects from low-dose IR. Notably, some responses to irradiation exhibited nonlinear behavior, as reductions in aortic gene expression were significant at intermediate doses but not at the highest or lowest doses. This study contributes to our understanding of how low-dose IR with different dose-rates impacts the immune system response in the context of atherosclerosis (103). Furthermore, in smooth muscle cell lineage-tracing mice (Myh11-ERT2Cre ROSA-STOP-eYFP) on the ApoE KO background, total body γ-irradiation of 12 Gy and subsequent bone marrow reconstitution led to the loss of smooth muscle cell investment in lesions induced by an 18-week Western diet. This effect was observed in the brachiocephalic artery, carotid arteries, and the aortic arch, but not in the aortic root or abdominal aorta (104). Ikeda et al. reported that IR has a suppressive effect on the initiation of atherogenesis in the aortic arch by inhibiting the accumulation of LDL in the intima. However, as time progresses, the growth of lesions is influenced by delayed accumulation of neutral lipid and myeloid cells in the intima, as well as reduced coalescence of small foam cell clusters into larger lesions. Notably, the lateral expansion of lesions, as measured by the lesion outline area, appears to be minimally affected. This suggests that the lateral expansion of lesions may primarily depend on d-flow or other factors that are not influenced by irradiation. Additionally, other mechanisms may contribute to the phenotype observed after BMT, particularly at later stages when the height of lesions is significantly reduced. Single-cell transcriptomic analysis indicates that IR diverts LDL uptake by ECs towards lysosomal degradation and reverse cholesterol transport pathways. This diversion leads to a reduction in intimal lipid accumulation and impacts the initiation and growth of lesions without affecting paracellular leakage (105). These findings demonstrate the complexity of the relationship between radiation and atherosclerosis, which can depend on various factors, including the dose and duration of radiation exposure, the specific tissues or organs affected, and individual susceptibility. While some studies suggest that radiation exposure may contribute to the development or progression of atherosclerosis, other research findings are inconclusive or even indicate potential protective effects. It is important to acknowledge that radiation is employed in medical treatments like radiation therapy, which can have both therapeutic benefits and potential side effects. The impact of radiation on atherosclerosis may vary depending on the context in which it is applied, such as therapeutic radiation versus accidental exposure. Therefore, further research is required to gain a comprehensive understanding of the association between radiation and atherosclerosis. However, the findings from the study by Ikeda et al. provide intriguing insights. According to their research, the lesions observed in our BMT model appear to rely on hemodynamics rather than radiation (105). These findings align perfectly with the objectives of our own study.

We observed a downregulation of CHK1 protein expression in ECs following radiation exposure; however, the specific mechanisms involved remain unclear and require further research. Our findings suggest a potential association between radiation-induced EC fibrotic changes and vulnerable plaque formation, but a comprehensive investigation of the relationship between radiation, endoMT, and atherosclerosis is still needed. Furthermore, it is important to acknowledge that *in vitro* experiments and animal models may not fully capture the intricacies of human physiology and disease. Hence, additional studies utilizing human samples and clinical research are necessary to validate these findings and determine their relevance to human cardiovascular health. Moreover, it should be noted that this study does not focus on the clinical implications or long-term outcomes of radiation-induced cardiovascular events or resistance against tumorigenesis, as they lie beyond the scope of our research. Consequently, future investigations should aim to address these aspects and provide a more comprehensive understanding of the potential impact of the CHK1-SENP2 S344 phosphorylation axis and radiation exposure on human health.

Data availability statement

The datasets presented in this study can be found in online repositories. The names of the repository/repositories and accession number(s) can be found below: https://www.ncbi.nlm.nih.gov/genbank/, GSE222511.

Ethics statement

The animal study was reviewed and approved by Texas A&M Institute of Biosciences and Technology.

Author contributions

MN, MI, SI, KC performed experiments, interpreted the data, and wrote the manuscript. PB, LV, KK, RA, EM, performed the experiments and analyzed the data. VS and YG, L-LL, ET maintained mouse colony. AD, JH, NP, RD, KF, MB, EO, SK, JC, GW and JA, contributed to the interpretation of the data. GW, JA, and N-TL planned and generated the study design, obtained funding, interpreted data, and wrote the manuscript. All authors contributed to the article and approved the submitted version.

Funding

This study received partial funding from the National Institutes of Health (NIH) to JA, N-TL, and JC (HL149303 and HL163857), JA (AI156921), JC (HL148338 and HL157790), and N-TL (HL-134740, HL157790).

Acknowledgment

The authors would like to thank Dr. James M. Kasper (Houston Methodist Research Institute) for a critical reading of this manuscript.

Conflict of interest

The authors declare that the research was conducted in the absence of any commercial or financial relationships that could be construed as a potential conflict of interest.

Publisher's note

All claims expressed in this article are solely those of the authors and do not necessarily represent those of their affiliated organizations, or those of the publisher, the editors and the reviewers. Any product that may be evaluated in this article, or claim that may be made by its manufacturer, is not guaranteed or endorsed by the publisher.

Supplementary material

The Supplementary Material for this article can be found online at: https://www.frontiersin.org/articles/10.3389/fcvm.2023.1187490/full#supplementary-material

SUPPLEMENTARY FIGURE S1
(A,C) Body weight and (B,D) cholesterol levels in HC-induced (A,B) and BMT (C,D) atherosclerosis. Mice with LDL cholesterol level <250 mg/dl were excluded from the HC-induced atherosclerosis analysis (B), and mice with LDL cholesterol level <200 mg/dl were excluded from the BMT atherosclerosis analysis (D). N.S, non-significant.

References

1. Abe J, Berk BC. Novel mechanisms of endothelial mechanotransduction. *Arterioscler Thromb Vasc Biol.* (2014) 34:2378–86. doi: 10.1161/ATVBAHA.114.303428

2. Le NT, Sandhu UG, Quintana-Quezada RA, Hoang NM, Fujiwara K, Abe JI. Flow signaling and atherosclerosis. *Cell Mol Life Sci.* (2017) 74:1835–58. doi: 10.1007/s00018-016-2442-4

3. Shishido T, Woo CH, Ding B, McClain C, Molina CA, Yan C, et al. Effects of MEK5/ERK5 association on small ubiquitin-related modification of ERK5: implications for diabetic ventricular dysfunction after myocardial infarction. *Circ Res.* (2008) 102:1416–25. doi: 10.1161/CIRCRESAHA.107.168138

4. Heo KS, Le NT, Cushman HJ, Giancursio CJ, Chang E, Woo CH, et al. Disturbed flow-activated p90RSK kinase accelerates atherosclerosis by inhibiting SENP2 function. *J Clin Invest.* (2015) 125:1299–310. doi: 10.1172/JCI76453

5. Abe JI, Ko KA, Kotla S, Wang Y, Paez-Mayorga J, Shin IJ, et al. MAGI1 as a link between endothelial activation and ER stress drives atherosclerosis. *JCI Insight.* (2019) 4:e125570. doi: 10.1172/jci.insight.125570

6. Zhou J, Yi Q, Tang L. The roles of nuclear focal adhesion kinase (FAK) on cancer: a focused review. *J Exp Clin Cancer Res.* (2019) 38:250. doi: 10.1186/s13046-019-1265-1

7. Velatooru LR, Abe RJ, Imanishi M, Gi YJ, Ko KA, Heo KS, et al. Disturbed flow-induced FAK K152 SUMOylation initiates the formation of pro-inflammation positive feedback loop by inducing reactive oxygen species production in endothelial cells. *Free Radic Biol Med.* (2021) 177:404–18. doi: 10.1016/j.freeradbiomed.2021.09.023

8. Itahana Y, Yeh ET, Zhang Y. Nucleocytoplasmic shuttling modulates activity and ubiquitination-dependent turnover of SUMO-specific protease 2. *Mol Cell Biol.* (2006) 26:4675–89. doi: 10.1128/MCB.01830-05

9. Heo KS, Chang E, Le NT, Cushman H, Yeh ET, Fujiwara K, et al. De-SUMOylation enzyme of sentrin/SUMO-specific protease 2 regulates disturbed flow-induced SUMOylation of ERK5 and p53 that leads to endothelial dysfunction and atherosclerosis. *Circ Res.* (2013) 112:911–23. doi: 10.1161/CIRCRESAHA.111.300179

10. Heo KS, Berk BC, Abe J. Disturbed flow-induced endothelial proatherogenic signaling via regulating post-translational modifications and epigenetic events. *Antioxid Redox Signal.* (2016) 25:435–50. doi: 10.1089/ars.2015.6556

11. Minamino T, Miyauchi H, Yoshida T, Ishida Y, Yoshida H, Komuro I. Endothelial cell senescence in human atherosclerosis: role of telomere in endothelial dysfunction. *Circulation.* (2002) 105:1541–4. doi: 10.1161/01.cir.0000013836.85741.17

12. Vanhoutte PM. Endothelial dysfunction: the first step toward coronary arteriosclerosis. *Circ J.* (2009) 73:595–601. doi: 10.1253/circj.cj-08-1169

13. Cervelli T, Borghini A, Galli A, Andreassi MG. DNA damage and repair in atherosclerosis: current insights and future perspectives. *Int J Mol Sci.* (2012) 13:16929–44. doi: 10.3390/ijms131216929

14. Mahmoudi M, Mercer J, Bennett M. DNA damage and repair in atherosclerosis. *Cardiovasc Res.* (2006) 71:259–68. doi: 10.1016/j.cardiores.2006.03.002

15. Martinet W, Knaapen MW, De Meyer GR, Herman AG, Kockx MM. Oxidative DNA damage and repair in experimental atherosclerosis are reversed by dietary lipid lowering. *Circ Res.* (2001) 88:733–9. doi: 10.1161/hh0701.088684

16. Rallis KS, Lai Yau TH, Sideris M. Chemoradiotherapy in cancer treatment: rationale and clinical applications. *Anticancer Res.* (2021) 41:1–7. doi: 10.21873/anticanres.14746

17. Uryga A, Gray K, Bennett M. DNA damage and repair in vascular disease. *Annu Rev Physiol.* (2016) 78:45–66. doi: 10.1146/annurev-physiol-021115-105127

18. Blasius M, Forment JV, Thakkar N, Wagner SA, Choudhary C, Jackson SP. A phospho-proteomic screen identifies substrates of the checkpoint kinase Chk1. *Genome Biol.* (2011) 12:R78. doi: 10.1186/gb-2011-12-8-r78

19. Peng Z, Shu B, Zhang Y, Wang M. Endothelial response to pathophysiological stress. *Arterioscler Thromb Vasc Biol.* (2019) 39:e233–e43. doi: 10.1161/ATVBAHA.119.312580

20. Clere N, Renault S, Corre I. Endothelial-to-mesenchymal transition in cancer. *Front Cell Dev Biol.* (2020) 8:747. doi: 10.3389/fcell.2020.00747

21. Cho JG, Lee A, Chang W, Lee MS, Kim J. Endothelial to mesenchymal transition represents a key link in the interaction between inflammation and endothelial dysfunction. *Front Immunol.* (2018) 9:294. doi: 10.3389/fimmu.2018.00294

22. Piera-Velazquez S, Jimenez SA. Endothelial to mesenchymal transition: role in physiology and in the pathogenesis of human diseases. *Physiol Rev.* (2019) 99:1281–324. doi: 10.1152/physrev.00021.2018

23. Huang Q, Gan Y, Yu Z, Wu H, Zhong Z. Endothelial to mesenchymal transition: an insight in atherosclerosis. *Front Cardiovasc Med.* (2021) 8:734550. doi: 10.3389/fcvm.2021.734550

24. Kovacic JC, Dimmeler S, Harvey RP, Finkel T, Aikawa E, Krenning G, et al. Endothelial to mesenchymal transition in cardiovascular disease. *J Am Coll Cardiol.* (2019) 73:190–209. doi: 10.1016/j.jacc.2018.09.089

25. Markwald RR, Fitzharris TP, Smith WN. Sturctural analysis of endocardial cytodifferentiation. *Dev Biol.* (1975) 42:160–80. doi: 10.1016/0012-1606(75)90321-8

26. Markwald RR, Fitzharris TP, Manasek FJ. Structural development of endocardial cushions. *Am J Anat.* (1977) 148:85–119. doi: 10.1002/aja.1001480108

27. Su H, Gorodny N, Gomez LF, Gangadharmath U, Mu F, Chen G, et al. Noninvasive molecular imaging of apoptosis in a mouse model of anthracycline-induced cardiotoxicity. *Circ Cardiovasc Imaging.* (2015) 8:e001952. doi: 10.1161/CIRCIMAGING.114.001952

28. Evrard SM, Lecce L, Michelis KC, Nomura-Kitabayashi A, Pandey G, Purushothaman KR, et al. Endothelial to mesenchymal transition is common in atherosclerotic lesions and is associated with plaque instability. *Nat Commun.* (2016) 7:11853. doi: 10.1038/ncomms11853

29. Bostrom KI, Yao J, Guihard PJ, Blazquez-Medela AM, Yao Y. Endothelial-mesenchymal transition in atherosclerotic lesion calcification. *Atherosclerosis.* (2016) 253:124–7. doi: 10.1016/j.atherosclerosis.2016.08.046

30. Moonen JR, Lee ES, Schmidt M, Maleszewska M, Koerts JA, Brouwer LA, et al. Endothelial-to-mesenchymal transition contributes to fibro-proliferative vascular disease and is modulated by fluid shear stress. *Cardiovasc Res.* (2015) 108:377–86. doi: 10.1093/cvr/cvv175

31. Hooning MJ, Botma A, Aleman BM, Baaijens MH, Bartelink H, Klijn JG, et al. Long-term risk of cardiovascular disease in 10-year survivors of breast cancer. *J Natl Cancer Inst*. (2007) 99:365–75. doi: 10.1093/jnci/djk064

32. Swerdlow AJ, Higgins CD, Smith P, Cunningham D, Hancock BW, Horwich A, et al. Myocardial infarction mortality risk after treatment for Hodgkin disease: a collaborative British cohort study. *J Natl Cancer Inst*. (2007) 99:206–14. doi: 10.1093/jnci/djk029

33. Singal PK, Iliskovic N. Doxorubicin-induced cardiomyopathy. *N Engl J Med*. (1998) 339:900–5. doi: 10.1056/nejm199809243391307

34. Armenian SH, Xu L, Ky B, Sun C, Farol LT, Pal SK, et al. Cardiovascular disease among survivors of adult-onset cancer: a community-based retrospective cohort study. *J Clin Oncol*. (2016) 34:1122–30. doi: 10.1200/JCO.2015.64.0409

35. Lally BE, Detterbeck FC, Geiger AM, Thomas CR Jr., Machtay M, Miller AA, et al. The risk of death from heart disease in patients with nonsmall cell lung cancer who receive postoperative radiotherapy: analysis of the surveillance, epidemiology, and end results database. *Cancer*. (2007) 110:911–7. doi: 10.1002/cncr.22845

36. Darby SC, Ewertz M, McGale P, Bennet AM, Blom-Goldman U, Bronnum D, et al. Risk of ischemic heart disease in women after radiotherapy for breast cancer. *N Engl J Med*. (2013) 368:987–98. doi: 10.1056/NEJMoa1209825

37. Zhou H, Di Palma S, Preisinger C, Peng M, Polat AN, Heck AJ, et al. Toward a comprehensive characterization of a human cancer cell phosphoproteome. *J Proteome Res*. (2013) 12:260–71. doi: 10.1021/pr300630k

38. Bian Y, Song C, Cheng K, Dong M, Wang F, Huang J, et al. An enzyme assisted RP-RPLC approach for in-depth analysis of human liver phosphoproteome. *J Proteomics*. (2014) 96:253–62. doi: 10.1016/j.jprot.2013.11.014

39. Kang X, Qi Y, Zuo Y, Wang Q, Zou Y, Schwartz RJ, et al. SUMO-specific protease 2 is essential for suppression of polycomb group protein-mediated gene silencing during embryonic development. *Mol Cell*. (2010) 38:191–201. doi: 10.1016/j.molcel.2010.03.005

40. Bjorklund MM, Hollensen AK, Hagensen MK, Dagnaes-Hansen F, Christoffersen C, Mikkelsen JG, et al. Induction of atherosclerosis in mice and hamsters without germline genetic engineering. *Circ Res*. (2014) 114:1684–9. doi: 10.1161/CIRCRESAHA.114.302937

41. Ko KA, Wang Y, Kotla S, Fujii Y, Vu HT, Venkatesulu BP, et al. Developing a reliable mouse model for cancer therapy-induced cardiovascular toxicity in cancer patients and survivors. *Front Cardiovasc Med*. (2018) 5:26. doi: 10.3389/fcvm.2018.00026

42. Singh MV, Kotla S, Le NT, Ae Ko K, Heo KS, Wang Y, et al. Senescent phenotype induced by p90RSK-NRF2 signaling sensitizes monocytes and macrophages to oxidative stress in HIV-positive individuals. *Circulation*. (2019) 139:1199–216. doi: 10.1161/CIRCULATIONAHA.118.036232

43. Le NT, Heo KS, Takei Y, Lee H, Woo CH, Chang E, et al. A crucial role for p90RSK-mediated reduction of ERK5 transcriptional activity in endothelial dysfunction and atherosclerosis. *Circulation*. (2013) 127:486–99. doi: 10.1161/CIRCULATIONAHA.112.116988

44. Tian H, Faje AT, Lee SL, Jorgensen TJ. Radiation-induced phosphorylation of Chk1 at S345 is associated with p53-dependent cell cycle arrest pathways. *Neoplasia*. (2002) 4:171–80. doi: 10.1038/sj.neo.7900219

45. Kotla S, Zhang A, Imanishi M, Ko KA, Lin SH, Gi YJ, et al. Nucleus-mitochondria positive feedback loop formed by ERK5 S496 phosphorylation-mediated poly (ADP-ribose) polymerase activation provokes persistent pro-inflammatory senescent phenotype and accelerates coronary atherosclerosis after chemo-radiation. *Redox Biol*. (2021) 47:102132. doi: 10.1016/j.redox.2021.102132

46. Inui M, Miyado M, Igarashi M, Tamano M, Kubo A, Yamashita S, et al. Rapid generation of mouse models with defined point mutations by the CRISPR/Cas9 system. *Sci Rep*. (2014) 4:5396. doi: 10.1038/srep05396

47. Baradaran-Heravi A, Niesser J, Balgi AD, Choi K, Zimmerman C, South AP, et al. Gentamicin B1 is a minor gentamicin component with major nonsense mutation suppression activity. *PNAS*. (2017) 114(13):3479–84. doi: 10.1073/pnas.1620982114

48. Paez-Mayorga J, Chen AL, Kotla S, Tao Y, Abe RJ, He ED, et al. Ponatinib activates an inflammatory response in endothelial cells via ERK5 SUMOylation. *Front Cardiovasc Med*. (2018) 5:125. doi: 10.3389/fcvm.2018.00125

49. Heo KS, Lee H, Nigro P, Thomas T, Le NT, Chang E, et al. PKCzeta mediates disturbed flow-induced endothelial apoptosis via p53 SUMOylation. *J Cell Biol*. (2011) 193:867–84. doi: 10.1083/jcb.201010051

50. Reinhart-King CA, Fujiwara K, Berk BC. Physiologic stress-mediated signaling in the endothelium. *Methods Enzymol*. (2008) 443:25–44. doi: 10.1016/S0076-6879(08)02002-8

51. Akaike M, Che W, Marmarosh NL, Ohta S, Osawa M, Ding B, et al. The hinge-helix 1 region of peroxisome proliferator-activated receptor gamma1 (PPARgamma1) mediates interaction with extracellular signal-regulated kinase 5 and PPARgamma1 transcriptional activation: involvement in flow-induced PPARgamma activation in endothelial cells. *Mol Cell Biol*. (2004) 24:8691–704. doi: 10.1128/MCB.24.19.8691-8704.2004

52. Italiano A, Infante JR, Shapiro GI, Moore KN, LoRusso PM, Hamilton E, et al. Phase I study of the checkpoint kinase 1 inhibitor GDC-0575 in combination with gemcitabine in patients with refractory solid tumors. *Ann Oncol*. (2018) 29:1304–11. doi: 10.1093/annonc/mdy076

53. Leung-Pineda V, Ryan CE, Piwnica-Worms H. Phosphorylation of Chk1 by ATR is antagonized by a Chk1-regulated protein phosphatase 2A circuit. *Mol Cell Biol*. (2006) 26:7529–38. doi: 10.1128/MCB.00447-06

54. Li P, Goto H, Kasahara K, Matsuyama M, Wang Z, Yatabe Y, et al. P90 RSK arranges Chk1 in the nucleus for monitoring of genomic integrity during cell proliferation. *Mol Biol Cell*. (2012) 23:1582–92. doi: 10.1091/mbc.E11-10-0883

55. Capasso H, Palermo C, Wan S, Rao H, John UP, O'Connell MJ, et al. Phosphorylation activates Chk1 and is required for checkpoint-mediated cell cycle arrest. *J Cell Sci*. (2002) 115:4555–64. doi: 10.1242/jcs.00133

56. Hendriks IA, Lyon D, Young C, Jensen LJ, Vertegaal AC, Nielsen ML. Site-specific mapping of the human SUMO proteome reveals co-modification with phosphorylation. *Nat Struct Mol Biol*. (2017) 24:325–36. doi: 10.1038/nsmb.3366

57. Duran-Struuck R, Dysko RC. Principles of bone marrow transplantation (BMT): providing optimal veterinary and husbandry care to irradiated mice in BMT studies. *J Am Assoc Lab Anim Sci*. (2009) 48:11–22.

58. Komaravolu RK, Adam C, Moonen JR, Harmsen MC, Goebeler M, Schmidt M. Erk5 inhibits endothelial migration via KLF2-dependent down-regulation of PAK1. *Cardiovasc Res*. (2015) 105:86–95. doi: 10.1093/cvr/cvu236

59. Biernacka A, Dobaczewski M, Frangogiannis NG. TGF-beta signaling in fibrosis. *Growth Factors*. (2011) 29:196–202. doi: 10.3109/08977194.2011.595714

60. Bikdeli B, Madhavan MV, Jimenez D, Chuich T, Dreyfus I, Driggin E, et al. COVID-19 and thrombotic or thromboembolic disease: implications for prevention, antithrombotic therapy, and follow-up. *J Am Coll Cardiol*. (2020) 75:2950–73. doi: 10.1016/j.jacc.2020.04.031

61. Abdel-Rahman O, Lamarca A. Development of sorafenib-related side effects in patients diagnosed with advanced hepatocellular carcinoma treated with sorafenib: a systematic-review and meta-analysis of the impact on survival. *Expert Rev Gastroenterol Hepatol*. (2017) 11:75–83. doi: 10.1080/17474124.2017.1264874

62. Vu HT, Kotla S, Ko KA, Fujii Y, Tao Y, Medina J, et al. Ionizing radiation induces endothelial inflammation and apoptosis via p90RSK-mediated ERK5 S496 phosphorylation. *Front Cardiovasc Med*. (2018) 5:23. doi: 10.3389/fcvm.2018.00023

63. Imanishi M, Cheng H, Kotla S, Deswal A, Le NT, Chini E, et al. Radiation therapy induces immunosenescence mediated by p90RSK. *Front Cardiovasc Med*. (2022) 9:988713. doi: 10.3389/fcvm.2022.988713

64. Dejana E, Hirschi KK, Simons M. The molecular basis of endothelial cell plasticity. *Nat Commun*. (2017) 8:14361. doi: 10.1038/ncomms14361

65. Rohlenova K, Goveia J, Garcia-Caballero M, Subramanian A, Kalucka J, Treps L, et al. Single-cell RNA sequencing maps endothelial metabolic plasticity in pathological angiogenesis. *Cell Metab*. (2020) 31:862–77 e14. doi: 10.1016/j.cmet.2020.03.009

66. Fu X, Khalil H, Kanisicak O, Boyer JG, Vagnozzi RJ, Maliken BD, et al. Specialized fibroblast differentiated states underlie scar formation in the infarcted mouse heart. *J Clin Invest*. (2018) 128:2127–43. doi: 10.1172/JCI98215

67. Gourdie RG, Dimmeler S, Kohl P. Novel therapeutic strategies targeting fibroblasts and fibrosis in heart disease. *Nat Rev Drug Discov*. (2016) 15:620–38. doi: 10.1038/nrd.2016.89

68. Zhang Y, Wu X, Li Y, Zhang H, Li Z, Zhang Y, et al. Endothelial to mesenchymal transition contributes to arsenic-trioxide-induced cardiac fibrosis. *Sci Rep*. (2016) 6:33787. doi: 10.1038/srep33787

69. Zeisberg EM, Tarnavski O, Zeisberg M, Dorfman AL, McMullen JR, Gustafsson E, et al. Endothelial-to-mesenchymal transition contributes to cardiac fibrosis. *Nat Med*. (2007) 13:952–61. doi: 10.1038/nm1613

70. Moore-Morris T, Guimaraes-Camboa N, Banerjee I, Zambon AC, Kisseleva T, Velayoudon A, et al. Resident fibroblast lineages mediate pressure overload-induced cardiac fibrosis. *J Clin Invest*. (2014) 124:2921–34. doi: 10.1172/JCI74783

71. Chen PY, Qin L, Baeyens N, Li G, Afolabi T, Budatha M, et al. Endothelial-to-mesenchymal transition drives atherosclerosis progression. *J Clin Invest*. (2015) 125:4514–28. doi: 10.1172/JCI82719

72. Straub AC, Zeigler AC, Isakson BE. The myoendothelial junction: connections that deliver the message. *Physiology (Bethesda)*. (2014) 29:242–9. doi: 10.1152/physiol.00042.2013

73. Xiao L, Dudley AC. Fine-tuning vascular fate during endothelial-mesenchymal transition. *J Pathol*. (2017) 241:25–35. doi: 10.1002/path.4814

74. Huang J, Pu Y, Zhang H, Xie L, He L, Zhang CL, et al. KLF2 mediates the suppressive effect of laminar flow on vascular calcification by inhibiting endothelial BMP/SMAD1/5 signaling. *Circ Res*. (2021) 129:e87–e100. doi: 10.1161/CIRCRESAHA.120.318690

75. de Las Fuentes L, Sung YJ, Noordam R, Winkler T, Feitosa MF, Schwander K, et al. Gene-educational attainment interactions in a multi-ancestry genome-wide meta-analysis identify novel blood pressure loci. *Mol Psychiatry*. (2021) 26:2111–25. doi: 10.1038/s41380-020-0719-3

76. Li F, Lo TY, Miles L, Wang Q, Noristani HN, Li D, et al. The ATR-CHEK1 pathway inhibits axon regeneration in response to Piezo-dependent mechanosensation. *Nat Commun*. (2021) 12:3845. doi: 10.1038/s41467-021-24131-7

77. Bargiela-Iparraguirre J, Prado-Marchal L, Fernandez-Fuente M, Gutierrez-Gonzalez A, Moreno-Rubio J, Munoz-Fernandez M, et al. CHK1 expression in gastric cancer is modulated by p53 and RB1/E2F1: implications in chemo/radiotherapy response. *Sci Rep*. (2016) 6:21519. doi: 10.1038/srep21519

78. Puc J, Parsons R. PTEN loss inhibits CHK1 to cause double stranded-DNA breaks in cells. *Cell Cycle*. (2005) 4:927–9. doi: 10.4161/cc.4.7.1795

79. Choi KJ, Nam JK, Kim JH, Choi SH, Lee YJ. Endothelial-to-mesenchymal transition in anticancer therapy and normal tissue damage. *Exp Mol Med*. (2020) 52:781–92. doi: 10.1038/s12276-020-0439-4

80. Yuan R, Sun Z, Cai J, Yang X, Zhang W, Wu C, et al. A novel anticancer therapeutic strategy to target autophagy accelerates radiation-associated atherosclerosis. *Int J Radiat Oncol Biol Phys*. (2021) 109:540–52. doi: 10.1016/j.ijrobp.2020.09.007

81. Hoving S, Heeneman S, Gijbels MJ, te Poele JA, Russell NS, Daemen MJ, et al. Single-dose and fractionated irradiation promote initiation and progression of atherosclerosis and induce an inflammatory plaque phenotype in ApoE(-/-) mice. *Int J Radiat Oncol Biol Phys*. (2008) 71:848–57. doi: 10.1016/j.ijrobp.2008.02.031

82. Schollnberger H, Eidemuller M, Cullings HM, Simonetto C, Neff F, Kaiser JC. Correction to: dose-responses for mortality from cerebrovascular and heart diseases in atomic bomb survivors: 1950-2003. *Radiat Environ Biophys*. (2019) 58:303. doi: 10.1007/s00411-019-00779-0

83. Schollnberger H, Eidemuller M, Cullings HM, Simonetto C, Neff F, Kaiser JC. Dose-responses for mortality from cerebrovascular and heart diseases in atomic bomb survivors: 1950-2003. *Radiat Environ Biophys*. (2018) 57:17–29. doi: 10.1007/s00411-017-0722-5

84. Azizova TV, Muirhead CR, Druzhinina MB, Grigoryeva ES, Vlasenko EV, Sumina MV, et al. Cardiovascular diseases in the cohort of workers first employed at Mayak PA in 1948–1958. *Radiat Res*. (2010) 174:155–68. doi: 10.1667/RR1789.1

85. Little MP, Azizova TV, Richardson DB, Tapio S, Bernier MO, Kreuzer M, et al. Ionising radiation and cardiovascular disease: systematic review and meta-analysis. *Br Med J*. (2023) 380:e072924. doi: 10.1136/bmj-2022-072924

86. Azimzadeh O, Moertl S, Ramadan R, Baselet B, Laiakis EC, Sebastian S, et al. Application of radiation omics in the development of adverse outcome pathway networks: an example of radiation-induced cardiovascular disease. *Int J Radiat Biol*. (2022) 98:1722–51. doi: 10.1080/09553002.2022.2110325

87. Nagane M, Yasui H, Kuppusamy P, Yamashita T, Inanami O. DNA Damage response in vascular endothelial senescence: implication for radiation-induced cardiovascular diseases. *J Radiat Res*. (2021) 62:564–73. doi: 10.1093/jrr/rrab032

88. Little MP, Azizova TV, Hamada N. Low- and moderate-dose non-cancer effects of ionizing radiation in directly exposed individuals, especially circulatory and ocular diseases: a review of the epidemiology. *Int J Radiat Biol*. (2021) 97:782–803. doi: 10.1080/09553002.2021.1876955

89. Baselet B, Rombouts C, Benotmane AM, Baatout S, Aerts A. Cardiovascular diseases related to ionizing radiation: the risk of low-dose exposure (review). *Int J Mol Med*. (2016) 38:1623–41. doi: 10.3892/ijmm.2016.2777

90. Kreuzer M, Auvinen A, Cardis E, Hall J, Jourdain JR, Laurier D, et al. Low-dose ionising radiation and cardiovascular diseases–strategies for molecular epidemiological studies in Europe. *Mutat Res Rev Mutat Res*. (2015) 764:90–100. doi: 10.1016/j.mrrev.2015.03.002

91. Little MP, Azizova TV, Bazyka D, Bouffler SD, Cardis E, Chekin S, et al. Systematic review and meta-analysis of circulatory disease from exposure to low-level ionizing radiation and estimates of potential population mortality risks. *Environ Health Perspect*. (2012) 120:1503–11. doi: 10.1289/ehp.1204982

92. Little MP. Do non-targeted effects increase or decrease low dose risk in relation to the linear-non-threshold (LNT) model? *Mutat Res*. (2010) 687:17–27. doi: 10.1016/j.mrfmmm.2010.01.008

93. Joven J, Rull A, Ferre N, Escola-Gil JC, Marsillach J, Coll B, et al. The results in rodent models of atherosclerosis are not interchangeable: the influence of diet and strain. *Atherosclerosis*. (2007) 195:e85–92. doi: 10.1016/j.atherosclerosis.2007.06.012

94. Mitchel RE, Hasu M, Bugden M, Wyatt H, Hildebrandt G, Chen YX, et al. Low-dose radiation exposure and protection against atherosclerosis in ApoE(-/-) mice: the influence of P53 heterozygosity. *Radiat Res*. (2013) 179:190–9. doi: 10.1667/RR3140.1

95. Mitchel RE, Hasu M, Bugden M, Wyatt H, Little MP, Gola A, et al. Low-dose radiation exposure and atherosclerosis in ApoE(-)/(-) mice. *Radiat Res*. (2011) 175:665–76. doi: 10.1667/RR2176.1

96. Mancuso M, Pasquali E, Braga-Tanaka I 3rd, Tanaka S, Pannicelli A, Giardullo P, et al. Acceleration of atherogenesis in ApoE-/- mice exposed to acute or low-dose-rate ionizing radiation. *Oncotarget*. (2015) 6:31263–71. doi: 10.18632/oncotarget.5075

97. Le Gallic C, Phalente Y, Manens L, Dublineau I, Benderitter M, Gueguen Y, et al. Chronic internal exposure to low dose 137Cs induces positive impact on the stability of atherosclerotic plaques by reducing inflammation in ApoE-/- mice. *PLoS One*. (2015) 10:e0128539. doi: 10.1371/journal.pone.0128539

98. Ebrahimian TG, Beugnies L, Surette J, Priest N, Gueguen Y, Gloaguen C, et al. Chronic exposure to external low-dose gamma radiation induces an increase in anti-inflammatory and anti-oxidative parameters resulting in atherosclerotic plaque size reduction in ApoE(-/-) mice. *Radiat Res*. (2018) 189:187–96. doi: 10.1667/RR14823.1

99. Williams J, Chen Y, Rubin P, Finkelstein J, Okunieff P. The biological basis of a comprehensive grading system for the adverse effects of cancer treatment. *Semin Radiat Oncol*. (2003) 13:182–8. doi: 10.1016/S1053-4296(03)00045-6

100. Gabriels K, Hoving S, Gijbels MJ, Pol JF, te Poele JA, Biessen EA, et al. Irradiation of existing atherosclerotic lesions increased inflammation by favoring pro-inflammatory macrophages. *Radiother Oncol*. (2014) 110:455–60. doi: 10.1016/j.radonc.2014.01.006

101. Rodel F, Frey B, Gaipl U, Keilholz L, Fournier C, Manda K, et al. Modulation of inflammatory immune reactions by low-dose ionizing radiation: molecular mechanisms and clinical application. *Curr Med Chem*. (2012) 19:1741–50. doi: 10.2174/092986712800099866

102. Rey N, Ebrahimian T, Gloaguen C, Kereselidze D, Magneron V, Bontemps CA, et al. Exposure to low to moderate doses of ionizing radiation induces a reduction of pro-inflammatory Ly6chigh monocytes and a U-curved response of T cells in ApoE -/- mice. *Dose Response*. (2021) 19:15593258211016237. doi: 10.1177/15593258211016237

103. Newman AA, Baylis RA, Hess DL, Griffith SD, Shankman LS, Cherepanova OA, et al. Irradiation abolishes smooth muscle investment into vascular lesions in specific vascular beds. *JCI Insight*. (2018) 3:e121017. doi: 10.1172/jci.insight.121017

104. Ikeda J, Scipione CA, Hyduk SJ, Althagafi MG, Atif J, Dick SA, et al. Radiation impacts early atherosclerosis by suppressing intimal LDL accumulation. *Circ Res*. (2021) 128:530–43. doi: 10.1161/CIRCRESAHA.119.316539

105. Ko KA, Fujiwara K, Krishnan S, Abe JI. En face preparation of mouse blood vessels. *J Vis Exp*. (2017) 123:55460. doi: 10.3791/55460

frontiers | Frontiers in Cardiovascular Medicine

TYPE Original Research
PUBLISHED 06 September 2023
DOI 10.3389/fcvm.2023.1224462

OPEN ACCESS

EDITED BY
Silvio Antoniak,
University of North Carolina at Chapel Hill, United States

REVIEWED BY
István Kiss,
University of Pécs, Hungary
Zhenguo Zhai,
China-Japan Friendship Hospital, China

*CORRESPONDENCE
Szilvia Fiatal
✉ fiatal.szilvia@med.unideb.hu

RECEIVED 17 May 2023
ACCEPTED 03 August 2023
PUBLISHED 06 September 2023

CITATION
Natae SF, Merzah MA, Sándor J, Ádány R, Bereczky Z and Fiatal S (2023) A combination of strongly associated prothrombotic single nucleotide polymorphisms could efficiently predict venous thrombosis risk.
Front. Cardiovasc. Med. 10:1224462.
doi: 10.3389/fcvm.2023.1224462

A combination of strongly associated prothrombotic single nucleotide polymorphisms could efficiently predict venous thrombosis risk

Shewaye Fituma Natae[1,2], Mohammed Abdulridha Merzah[1,2], János Sándor[1,3], Róza Ádány[1], Zsuzsanna Bereczky[4] and Szilvia Fiatal[1]*

[1]Department of Public Health and Epidemiology, Faculty of Medicine, University of Debrecen, Debrecen, Hungary, [2]Doctoral School of Health Sciences, University of Debrecen, Debrecen, Hungary, [3]ELKH-DE Public Health Research Group, Department of Public Health and Epidemiology, Faculty of Medicine, University of Debrecen, Debrecen, Hungary, [4]Division of Clinical Laboratory Science, Department of Laboratory Medicine, Faculty of Medicine, University of Debrecen, Debrecen, Hungary

Background: Venous thrombosis (VT) is multifactorial trait that contributes to the global burden of cardiovascular diseases. Although abundant single nucleotide polymorphisms (SNPs) provoke the susceptibility of an individual to VT, research has found that the five most strongly associated SNPs, namely, rs6025 (*F5* Leiden), rs2066865 (*FGG*), rs2036914 (*F11*), rs8176719 (*ABO*), and rs1799963 (*F2*), play the greatest role. Association and risk prediction models are rarely established by using merely the five strongly associated SNPs. This study aims to explore the combined VT risk predictability of the five SNPs and well-known non-genetic VT risk factors such as aging and obesity in the Hungarian population.
Methods: SNPs were genotyped in the VT group (n = 298) and control group (n = 400). Associations were established using standard genetic models. Genetic risk scores (GRS) [unweighted GRS (unGRS), weighted GRS (wGRS)] were also computed. Correspondingly, the areas under the receiver operating characteristic curves (AUCs) for genetic and non-genetic risk factors were estimated to explore their VT risk predictability in the study population.
Results: rs6025 was the most prevalent VT risk allele in the Hungarian population. Its risk allele frequency was 3.52-fold higher in the VT group than that in the control group [adjusted odds ratio (AOR) = 3.52, 95% CI: 2.50–4.95]. Using all genetic models, we found that rs6025 and rs2036914 remained significantly associated with VT risk after multiple correction testing was performed. However, rs8176719 remained statistically significant only in the multiplicative (AOR = 1.33, 95% CI: 1.07–1.64) and genotypic models (AOR = 1.77, 95% CI: 1.14–2.73). In addition, rs2066865 lost its significant association with VT risk after multiple correction testing was performed. Conversely, the prothrombin mutation (rs1799963) did not show any significant association. The AUC of Leiden mutation (rs6025) showed better discriminative accuracy than that of other SNPs (AUC = 0.62, 95% CI: 0.57–0.66). The wGRS was a better predictor for VT than the unGRS (AUC = 0.67 vs. 0.65). Furthermore, combining genetic and non-genetic VT risk factors significantly increased the AUC to 0.89 with statistically significant differences (Z = 3.924, $p < 0.0001$).

Conclusions: Our study revealed that the five strongly associated SNPs combined with non-genetic factors could efficiently predict individual VT risk susceptibility. The combined model was the best predictor of VT risk, so stratifying high-risk individuals based on their genetic profiling and well-known non-modifiable VT risk factors was important for the effective and efficient utilization of VT risk preventive and control measures. Furthermore, we urged further study that compares the VT risk predictability in the Hungarian population using the formerly discovered VT SNPs with the novel strongly associated VT SNPs.

KEYWORDS

venous thrombosis, risk prediction, single nucleotide polymorphisms (SNPs), cardiovascular risk (CVD), Hungarian population

Introduction

Venous thrombosis (VT) is one of the three leading causes of cardiovascular disease (CVD)-related mortality with a significant genetic predisposition (1–3). It is a multifactorial trait that contributes to the global burden of CVD (4–7). In Europe, although overall CVD-related morbidity is decreasing, mortality remains substantially high. CVD is the leading cause of mortality in Europe, accounting for over 3.9 million deaths annually (8–10). Furthermore, approximately 60 million CVD premature deaths (death < 70 years) have been reported in Europe (10).

VT is a major health problem with a significant annual incidence (7.62/100,000) and mortality (3.70/100,000) (11). A higher burden of CVD-related mortality has been reported in Central and Eastern Europe (8, 12). Hungary shares the highest proportion of this mortality (8, 13). CVDs remain the most prominent cause of death in Hungary (13). As of 2014, approximately 35,000 women and 27,000 men have died from CVDs annually, accounting for 55% and 45% of all deaths for women and men, respectively (13). The age-standardized CVD death rate in Hungary is more than double the European Union (EU) average reported in 2014 (13). The availability of prophylaxis could significantly avert this burden by targeting high-risk individuals for treatment (11, 14). According to Rudolf Virchow's triad explanation (15), thrombosis is the result of three major factors, namely, blood flow stasis (16, 17), endothelial injury (18–20), and hypercoagulability (21). The inheritable prothrombotic factors influence VT risk via the coagulation process (21, 22), whereas the non-inheritable risk factors influence VT risk either via stasis or endothelial injury (23, 24).

Various studies have established the impact of heritable factors on VT risk (25–27). The incidence of repeated hospitalization due to VT is twofold higher in people with affected families than that in the general population (1–3). Although abundant single nucleotide polymorphisms (SNPs) provoke the susceptibility of an individual to VT (28–31), research has found that the five most strongly associated SNPs, namely, rs6025 (Leiden mutation) in the *F5* gene, rs1799963 (prothrombin G20210A) in the coagulation factor 2 gene (*F2*), rs8176719 (non-O blood type) in the *ABO* gene, rs2036914 in the coagulation factor eleven gene (*F11*), and rs2066865 in the fibrinogen gamma gene (*FGG*), play the greatest role in determining VT incidence and recurrence in genetically vulnerable individuals (29, 32, 33).

The Leiden mutation is one of the most dominant inheritable VT risk factors that increase the burden of VT in genetically vulnerable individuals (34–36). The Leiden mutation/*F5* prevalence is unevenly distributed across Europe with an average prevalence of 4% in the general population. The highest frequency is reported in Southeastern Europe and Northern Europe, whereas the lowest frequency is reported in Eastern and Western Europe (37, 38). The Leiden mutation prevalence is highest in European descent populations (3%–8%) (34, 39), followed by Caucasian Americans (5%). However, it is highly rare in African Americans (1.2%) and Asian-Americans (0.45%) (34) and absent in Africans (40, 41). Similarly, the prothrombin gene mutation/*F2*, often known as the G20210A mutation, is the second most prevalent inheritable VT risk in Caucasians (2%–4%) (39), particularly those of European ancestry (4%) and Caucasian Americans (2%). However, it is less prevalent in African Americans, accounting for approximately 0.4% (one in 250), and highly rare in Africans and Asians (39, 42).

Often, due to their coexistence and possible gene–gene interaction, the prothrombin gene mutation (rs1799963) and Leiden mutation (rs6025) SNPs were studied together (43). Furthermore, studies showed that the ancestral distribution of coagulation factor 11 (rs2036914) is similar in both Caucasians and African Americans (44, 45). Studies indicated that O blood-type individuals are at lower risk of VT than non-O blood-type individuals (46, 47), who are at a higher risk of VT (48–51). In addition, Kinsella et al. reported that the risk of venous thromboembolism (VTE) is higher in African Americans and non-O blood-type individuals than that in Caucasians and O blood-type individuals (52).

An individual who is a carrier of multiple variants is more vulnerable to VT. Studies have indicated that the combination of strongly associated VT SNPs [rs6025 (*F5*), rs1799963 (*F2*), rs8176719 (*ABO*), rs2036914 (*F11*), and rs2066865 (*FGG*)] poses a greater VT risk than that risk occurring by an individual SNP (29, 53). The genetic risk score (GRS) of strongly associated VT variants results in the greatest risk compared with a larger number of SNP combinations. De Haan et al. (29) showed that the VT risk prediction of the 5-SNP risk score is equivalent to that of the 31-SNP risk score.

In addition, studies have indicated that dual exposure to VT risk factors (genetic and non-genetic) increases the susceptibility of an individual to VT (4, 29). Aging and obesity are well-known non-inheritable VT risk factors that hasten the onset of VT (29). As a result of multiple anatomical and pathophysiological changes, the elderly are prone to age-related cardiovascular morbidity and

mortality (54–56). Aging plays a major role in the higher incidence of VT risk (1%) in elderly individuals (19, 54–57). The diminished efficiency of the calf muscle pump due to aging could lead to peripheral blood reflux and stasis resulting in thrombosis formation (54). Furthermore, age-related endothelial dysfunction is also a contributing factor to the higher incidence of VT in elderly individuals compared with that in younger individuals (19). Valve thickness, muscle fiber atrophy, and reduced endothelial anticoagulant properties are some pathophysiological changes that increase the VT risk among elderly individuals (54, 55). Correspondingly, obese individuals are at higher VT risk than normal-weight individuals. Previously conducted studies showed that the VT risk was two- to sixfold higher in obese individuals than that in normal-weight individuals [body mass index (BMI) = 20–24.9 kg/m^2] (58–62). A study indicated that the VT risk was higher among aged (>50 years old) and obese individuals [61].

Stratifying higher-risk individuals based on their genetic profiling for thromboprophylaxis is important for efficient utilization of the available resources (29). Furthermore, the possibility of reducing unexpected consequences of massive supplementation of prophylactic treatment would be high (63). Although the 5-SNP impact on VT risk is huge, association and risk prediction models are rarely established by using merely five strongly associated SNPs. No study has yet been conducted to explore the VT risk predictability of the combined five strongly associated prothrombotic SNPs in the VT subjects from the Hungarian population. Consequently, this study aims to explore the VT risk predictability of the combined five SNPs [rs6025 (*F5* Leiden), rs2066865 (*FGG*), rs2036914 (*F11*), rs8176719 (*ABO*), and rs1799963 (*F2*)] in the Hungarian population.

Methods and materials

Study population

A total of 698 subjects were involved in the case–control study, of which 298 were VT patients and 400 were healthy controls. The VT patients were recruited consecutively by the Division of Clinical Laboratory Science, Department of Laboratory Medicine, Faculty of Medicine, University of Debrecen during a 1-year period. VT diagnosis was established by standard diagnostic modalities, such as color Doppler ultrasound and phlebography at the Department of Internal Medicine. The controls were selected from the general population via a comprehensive health survey (see survey details and the created database elsewhere) and were free from VT according to a self-report questionnaire conducted 12 months prior to the survey (64).

DNA isolation

DNA was extracted from the peripheral blood using a MagNA Pure LC system (Roche Diagnostics, Basel, Switzerland) with a MagNA Pure LC DNA Isolation Kit–Large Volume according to the manufacturer's instructions. The extracted DNA was eluted in a 200 µl MagNA Pure LC DNA Isolation Kit–Large Volume elution buffer.

SNP selection and genotyping

Based on the genome-wide association study (GWAS) results (30, 65, 66) and our previously conducted studies (4, 67), we identified and considered the five strongly associated prothrombotic SNPs, namely, rs6025 (*F5*), rs2066865 (*FGG*), rs2036914 (*F11*), rs8176719 (*ABO*), and rs1799963 (*F2*), in our current study. We considered them due to their confirmed large effect size and potential predictability of inheritable VT risk (29, 67). The assay design and genotyping were performed by the Karolinska University Hospital, Stockholm, Sweden, Mutation Analysis Core Facility (MAF). A MassARRAY platform (Sequenom, CA, USA) with iPLEX Gold chemistry was used for genotyping. Quality control, validation, and concordance analysis were conducted by the MAF.

Genetic risk score

The weighted GRS (wGRS) and unweighted GRS (unGRS) were computed to identify the combined effect of the included SNPs on VT risk. In the GRS, the individuals were assigned based on the total number of risk-increasing alleles. Consequently, "0," "1," and "2" codes were given for the absence, heterozygosity, and homozygosity of risk alleles, respectively. When the risk allele was found to be protective, the coding for the homozygous risk allele became "0" and "2" for the other homozygous allele (67). Accordingly, the unGRS was simply calculated by adding all risk alleles in a given locus with the assumption that all alleles had the same effect. To comprehend the stronger relationship of some SNPs with VT, we also calculated the wGRS by assigning weights to the risk allele of each SNP corresponding to the logarithm of the average risk estimates reported in the previously conducted genetic association study (29).

Moreover, to determine which SNP is more influential in its discriminatory accuracy of the area under the receiver operating characteristic curve (AUC), we added each SNP one by one into a model. Therefore, we started with the SNP with the highest odds ratio (OR), i.e., the Leiden mutation (rs6025) in the *F5* gene, and assessed whether adding more SNPs in a model could improve the AUC. We continued adding all other SNPs into a model until we verified that adding more SNPs into a model could not reveal any significant discriminatory accuracy.

Non-genetic VT risk factors

We considered age (≥60 years), sex, and obesity (BMI ≥ 30 kg/m^2) as non-genetic VT risk factors. We included each non-genetic risk factor and their combination with genetic VT risk factors into a model to verify the difference in the AUC and their VT risk predictability in the study population. A logistic regression model was used to generate a combined risk score of genetic and non-genetic VT risk factors.

Statistical analysis

Statistical tests were computed using the PLINK (version 1.9) and IBM SPSS (version 26.0) statistical software. The Mann–Whitney *U*-test was used to compare the age, BMI, and GRS distribution in the study population. The Shapiro–Wilk normality test was used to test the distribution of quantitative variables. The Hardy–Weinberg equilibrium (HWE) and risk allele frequency differences between the VT group and control group were estimated using the X^2 test. The association between the five SNPs and VT risk was assessed by the OR with their respective 95% confidence interval (CI) under all genetic models, namely, the multiplicative, additive, dominant, recessive, and genotypic models. Likewise, a logistic regression analysis was also used to compute the OR with 95% of individual SNPs and genetic, non-genetic, and combined VT risk factors.

In addition, the area under the receiver operating characteristic (ROC) curve was determined to assess how well its score classifies the VT group and control group. In general, the AUC ranged from 0.5 (no discrimination between the VT group and control group) to 1.0 (perfect discrimination). We compared the AUCs of the genetic, non-genetic, and combined risk models. The SPSS IBM version 26.0 was used to calculate the ROC curves and AUCs. The Bonferroni multiple testing correction was employed to prevent multiple comparison problems (0.05/5, $p < 0.01$). Statistically significant variables were declared at a conventional *p*-value of 0.05.

Ethical approval

The Hungarian Scientific Council on Health Research committee approved the protocol (61327-2017/EKU). All participants provided written consent before their participation.

Results

Characteristics of the study participants

In total, 698 subjects were enrolled in the case–control study, of which 298 were VT patients and 400 were healthy controls. All subjects with complete genotypic and covariate data were considered for the analyses. The proportion of male participants (51%) in the VT group was higher than that in the control group (44%). The age distribution of the VT group was shifted toward the elderly group, and their mean age was significantly higher than that of the control group (63.4 ± 16.4 vs. 43.8 ± 12.6 years, $p < 0.001$) (**Supplementary Figure S1**). However, the distribution of BMI values (kg/m^2) did not differ significantly (28.2 ± 8.2 vs. 27.2 ± 5.5, $p = 0.76$). The marker check and detailed information of each SNP, including rs (SNP identifier), base pair position (BP), chromosome number (CHR), and major and minor alleles, are listed in **Table 1**.

Risk allele frequency comparison in the study population

The genotypic results were available for 698 subjects: VT patients ($n = 298$) and healthy controls ($n = 400$). All SNPs were tested to determine whether the observed allele frequencies were in accordance with the HWE; no significant deviation from the HWE was detected in the study population (**Table 1**). The risk allele frequencies of the five prothrombotic SNPs analyzed in the study are listed in **Table 2**. The risk allele frequencies of rs6025 (*F5*), rs2036914 (*F11*), and rs8176719 (*ABO*) were higher in the VT group than those in the control group, and the differences remained statistically significant after multiple testing correction was performed ($p < 0.01$) (**Table 2**).

In addition, we also computed the protective allele frequency of the *ABO* gene (DEL); its frequency was higher in the control group than that in the VT group (**Supplementary Table S1**).

Association between SNPs and VT risk in the study population using genetic association models

The association strengths regarding VT risk using complete genetic association models (multiplicative, additive, dominant, recessive, and genotypic models) were estimated. Only the Leiden mutation (rs6025) and *F11* (rs2036914) remained significant after adjustment for multiple testing correction ($p < 0.01$). In particular, the Leiden mutation variant strongly influenced the VT risk in the Hungarian population ($p < 0.001$): among the patients with VT due to the Leiden mutation, the OR of VT risk

TABLE 1 Marker check of the selected SNPs in the study.

Gene	*F5*	*FGG*	*F11*	*ABO*	*F2*
rs ID	rs6025	rs2066865	rs2036914	rs8176719	rs1799963
BP	169549811	154604124	186271327	133257521	46739505
CHR	1	4	4	9	11
Alleles (major: minor)	C:T	G:A	T:C	C:DEL	G:A
Genotype %	100%	100%	100%	100%	100%
MAF	0.1254	0.2536	0.5745	0.4441	0.02436
O(HET)	0.2077	0.3954	0.4957	0.4814	0.04871
E(HET)	0.2193	0.3786	0.4889	0.4938	0.04752
HWE *p*-value	*0.1665*	*0.2716*	*0.7569*	*0.5396*	*1*

MAF, minor allele frequency; O(HET), observed heterozygosity; E(HET), expected heterozygosity.

TABLE 2 Risk allele frequency comparison of the VT group and control group in the Hungarian population.

Gene	SNP	A1	Cases ($n = 298$)	Controls ($n = 400$)	A2	X^2	OR (95% CI)	*p*-value
F5	rs6025	T	0.203	0.0675	C	57.21	3.52 (2.50–4.95)	<0.001*
FGG	rs2066865	A	0.2836	0.2312	G	4.94	1.32 (1.03–1.68)	0.026
F11	rs2036914	C	0.6191	0.5412	T	8.47	1.38 (1.11–1.71)	0.003*
ABO	rs8176719	C	0.5956	0.5262	DEL	6.66	1.33 (1.07–1.64)	0.001*
F2	rs1799963	A	0.0302	0.02	G	1.50	1.53 (0.77–3.02)	0.221

A1, risk allele; A2, reference allele; X^2, chi-square.
*$p < 0.01$ considered significant after multiple correction testing.

ranged from 3.25 (heterozygous genotypic for risk variant; OR = 3.25, 95% CI: 2.22–4.76) to 19.67 (OR = 19.6, 95% CI: 2.57–150.4) in the recessive model/ those who were homozygous for risk variant.

The rs8176719 (*ABO*) remained statistically significant only in the multiplicative (OR = 1.33, 95% CI: 1.07–1.64) and genotypic models (OR = 1.77, 95% CI: 1.14–2.73); nevertheless, it lost its significance in other models after adjustment for multiple testing correction. Similarly, the rs8176719 (*ABO*) protective variant remained statistically significant only in the multiplicative model (OR = 0.75, 95% CI: 0.61–0.93) (**Supplementary Table S2**). In addition, the *FGG* (rs2066865) expressed a significant association with VT risk in the multiplicative, additive, and dominant models before multiple testing correction; however, it lost its significance after adjustment was performed. Conversely, the *F2* (rs1799963) did not show any statistically significant association with VT directly with any of the used models (**Table 3**).

Comparison of genetic risk scores in the study population

The unGRS and wGRS of the five SNPs were computed for the 298 VT patients and 400 healthy controls. The unGRS ranged from 0 to 6 (3.46 ± 1.31) and 0 to 7 (2.77 ± 1.28) for the VT and control groups, respectively (**Figure 1A**). The wGRS ranged from 0 to 4.6 (1.93 ± 0.97) and 0 to 4.7 (1.37 ± 0.78) for the VT and control groups (**Figure 1B**).

Association of GRS with VT risk

The distributions of other covariate variables including the wGRS and unGRS were significantly distinct ($p < 0.001$) between the two groups (**Supplementary Table S3**). The test revealed significant differences (case vs. control) in age (median = 65; 44, $p < 0.001$), BMI (median = 28.72; 26.75, $p < 0.001$), unGRS (median = 3; 3, $p < 0.001$), and wGRS (median = 1.79; 1.34, $p < 0.001$). Although the median unGRS values for the VT group and control group were similar, a larger unGRS value was more frequent in the VT group than in the control group.

Table 4 lists the multivariate logistic regression analysis results of covariate variables adjusted for sex and age. Of the well-known non-genetic VT risk factors, age and obesity were significantly associated with VT risk in the study population, which was higher in the VT group than that in the control group (**Table 4**). The VT risk was 12.8 times higher in the elderly subjects aged ≥60 years than that among the subjects aged below 60 years

TABLE 3 Genetic association test results in the VT group and control group of the study population: implication to determine the inheritable VT disease risk factors in the Hungarian population.

Model	Gene	*F5*	*FGG*	*F11*	*ABO*	*F2*
	SNP	rs6025	rs2066865	rs2036914	rs8176719	rs1799963
Multiplicative	X^2	57.21	4.94	8.47	6.66	1.50
	OR (95% CI)	3.52 (2.50–4.95)	1.32 (1.03–1.68)	1.38 (1.11–1.71)	1.33 (1.07–1.64)	1.53 (0.77–3.02)
	p	<0.001	0.026	0.004	0.001	0.221
Additive	X^2	54.35	5.17	8.59	6.50	1.53
	OR (95% CI)	3.52 (2.50–4.95)	1.32 (1.03–1.68)	1.38 (1.11–1.71)	1.33 (1.07–1.64)	1.53 (0.77–3.02)
	p	<0.001	0.02302	0.003	0.011	0.216
Dominant	X^2	49.61	4.32	5.71	4.88	1.53
	OR (95% CI)	3.67 (2.52–5.33)	1.38 (1.02–1.86)	1.64 (1.09–2.47)	1.54 (1.04–2.26)	1.543
	p	<0.001	0.038	0.017	0.03	0.215
Recessive	X^2	16.07	2.1	5.72	3.96	
	OR (95% CI)	19.67 (2.57–150.4)	1.61 (0.84–3.08)	1.47 (1.07–2.03)	1.39 (1.00–1.91)	
	p	<0.001	0.147	0.017	0.047	NA
Genotypic	X^2	54.35	5.18	8.64	6.60	1.534
	OR (95% CI)	3.25 (2.22–4.76)[a]	1.81 (0.94–3.51)	1.96 (1.24–3.08)	1.77 (1.14–2.73)	1.54 (0.77–3.07)
	p	<0.001	0.075	0.013	0.01	0.215

[a]CT (heterozygous for a risk variant), NA = the value of one cell is 0, i.e., <5; hence, the X^2 test is not applicable.

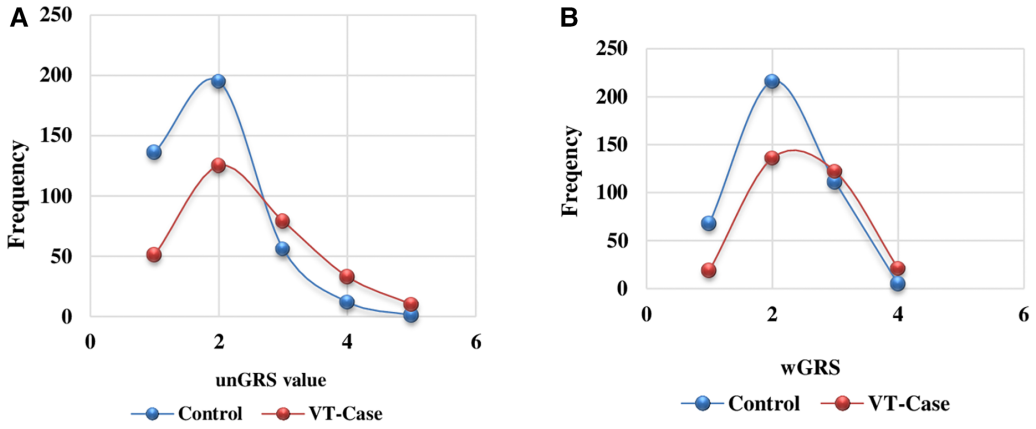

FIGURE 1
Unweighted (A) and weighted (B) GRS distribution comparison among the VT group and the control group of the Hungarian population.

TABLE 4 Association of covariate variables with VT risk in the Hungarian population.

Variables	VT risk[b]			VT risk[c]	
	ß	*p*-value	COR (95% CI)	AOR (95% CI)[d]	AOR (95% CI)[e]
Sex (male)[a]	0.271	0.077	1.31 (0.97–1.77)	—	1.16 (0.84–1.61)
Age ≥ 60 years	2.468	<0.001	11.79 (7.96–17.49)	12.83 (8.38–19.63)*	—
BMI (≥30 kg/m^2)	0.850	<0.001	2.34 (1.59–3.45)	1.41 (0.88–2.26)	2.28 (1.51–3.42)*
unGRS	0.412	<0.001	1.51 (1.34–1.71)	0.88 (0.65–1.18)	0.94 (0.72–1.21)
wGRS	0.729	<0.001	2.07 (1.72–2.50)	2.69 (1.74–4.19)*	2.24 (1.51–3.32)*

[a]Female is a reference.
[b]Crude odds ratio (COR).
[c]Adjusted odds ratio (AOR).
[d]Adjusted for sex.
[e]Adjusted for age.
*p-value < 0.0001.

(AOR = 12.83, 95% CI: 8.38–19.63). Similarly, the VT risk was 2.3 times higher in the obese subjects (BMI > 30 kg/m^2) than that in the normal-weight subjects (AOR = 2.28, 95% CI: 1.51–3.42). Furthermore, the wGRS remained statistically significant after we adjusted for both sex and age (AOR = 2.69, 95% CI: 1.74–4.19 and AOR = 2.24, 95% CI: 1.51–3.32, respectively). However, the unGRS lost its statistical significance (AOR = 0.88, 95% CI: 0.65–1.18) in the multivariate regression analysis model (Table 4).

VT risk prediction in the study population

We calculated the ROC curve to assess how well the score classified VT in the case and control groups. The AUC of the SNPs ranged from 0.51 (95% CI: 0.47–0.55, $p = 0.64$) for rs1799963 in *F2* to 0.62 (95% CI: 0.57; 0.66, $p < 0.001$) for rs6025 in *F5*. The discriminative accuracy of the model improved by adding each SNP (Figure 2). We started with the Leiden mutation (rs6025) with the highest effect size and ended with rs2036914 (*F11*) with the lowest effect size among the five SNPs. The addition of each SNP increased the AUC after *F2* (rs1799963).

The AUC of the 5-SNP risk score was 0.68 (95% CI: 0.64; 0.72). The variability proportion explained by the Leiden mutation (rs6025) was higher than that of the 5-SNP risk score (8% vs. 7%). Furthermore, approximately 39% of the variability observed was attributed to the combination of genetic and non-genetic risk factors, which is higher than that of those factors

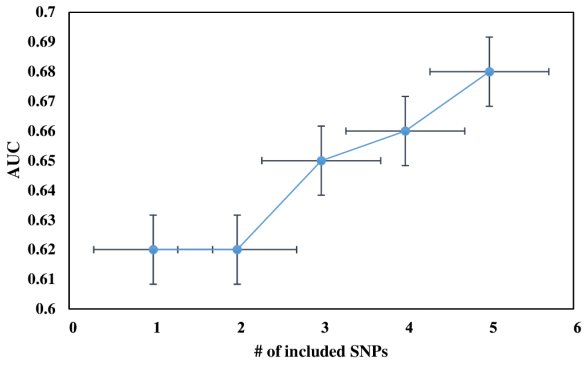

FIGURE 2
The change in the discriminatory accuracy of the AUC of the genetic risk score after adding each SNP into a model; we started with the Leiden mutation (rs6025) with the highest effect size and ended with rs2036914 (*F11*) with the lowest effect size of the five SNPs. The addition of each SNP increases the AUC value after *F2* (rs1799963).

TABLE 5 Venous thrombosis risk predictability of the Leiden mutation, genetic risk, non-genetic risk, and combined model in the Hungarian population.

Variables	r^2	$N = 698$	
		AUC (95% CI)	*p*-value
Leiden mutation risk model[a]	0.08	0.62 (0.57–0.66)	<0.0001
Genetic risk model[b]	0.09	0.68 (0.64–0.72)	<0.0001
Non-genetic risk model[c]	0.31	0.85 (0.82–0.88)	<0.0001
Combined model[d]	0.39	0.89 (0.86–0.91)	<0.0001
Difference[e]	—	0.039 (0.02–0.059)	<0.0001

r^2: variability explained by each variable.
A total of 298 VT patients and 400 healthy controls with complete genotypic and covariate data were considered during the analysis.
[a]Leiden mutation, the most prevalent inheritable VT risk variant in the study population.
[b]**Genetic risk model**: weighted GRS computed from the five SNPs (rs6025, rs2066865, rs2036914, rs8176719, and rs1799963).
[c]**Non-genetic risk model:** age [5-year interval, sex, and BMI (<25, 25–30, and ≥30 kg/m^2)].
[d]**Combined risk model**: genetic risk model plus non-genetic risk model.
[e]Difference between the combined and non-genetic risk models.

independently (Table 5). Similarly, the ROC curve for the weighted 5-SNP risk score had an AUC of 0.68 (95% CI: 0.64–0.72), i.e., there was a 68% probability that a randomly selected VT patient will have a higher score than that of a randomly selected control subject. The wGRS was a better predictor for VT than the unGRS (AUC = 0.65, 95% CI: 0.60–0.69).

There was a difference between the discriminative accuracy of the 5-SNP risk score in men (AUC = 0.68, 95% CI: 0.62–0.74, $p < 0.001$) and women (AUC = 0.61: 95% CI: 0.55–0.67, $p < 0.001$). Moreover, the AUC of the wGRS of the 5-SNPs was significantly higher in men (AUC = 0.71, 95% CI: 0.65–0.76, $p < 0.001$) than that in women (AUC = 0.63, 95% CI: 0.57–0.69, $p < 0.001$).

Risk prediction based on a combination of genetic and non-genetic risk factors

We also evaluated the discriminative accuracy of well-known non-genetic VT risk factors such as age, sex, and obesity to explore their independent and combined VT risk predictability in the study population. The independent AUCs of age and obesity were 0.84, $p < 0.0001$, and 0.59, $p < 0.001$, respectively. The combination of all well-known VT risk factors changed the discriminative accuracy of the AUC to 0.85, $p < 0.000$. Similarly, when we added the non-genetic risk factors into the genetic risk factors, the AUC significantly projected to 0.89 (95% CI: 0.86–0.91) compared to that in the genetic (AUC = 0.68) or non-genetic risk factor predictability (AUC = 0.85; $p < 0.0001$) (Figure 3). The AUC difference in the combined and non-genetic risk factors was statistically significant (AUC = 0.039, 95% CI: 0.02–0.059, $p < 0.0001$). There was no significant AUC difference between men and women in the non-genetic (men: AUC = 0.81, 95% CI: 0.76–0.86 vs. women: AUC = 0.82, 95% CI: 0.78–0.87) and combined risk score (men: AUC = 0.87, 95% CI: 0.83–0.91 vs. women: AUC = 0.86, 95% CI: 0.82–0.90) models.

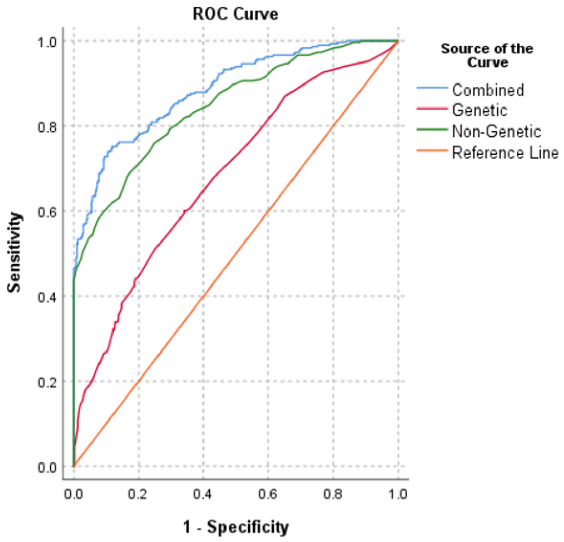

FIGURE 3
ROC curves for combined (genetic and non-genetic), genetic (five prothrombotic SNPs), and non-genetic (age, sex, BMI) risk models.

Discussion

Although there are abundant SNPs that provoke VT events in genetically vulnerable individuals, the contributions of the five strongly associated SNPs, namely, rs6025 (*F5*), rs2066865 (*FGG*), rs2036914 (*F11*), rs8176719 (*ABO*), and rs1799963 (*F2*), to VT risk is immensely high (29, 32, 33). Moreover, previously conducted studies demonstrated the importance of these five prothrombotic SNPs in the relapse of inheritable VT (29, 32, 33). Consequently, we aimed to explore the combined genetic risk predictability of strongly associated VT SNPs and well-known non-genetic VT risk factors in the Hungarian population. Thus, stratifying high-risk individuals based on their genetic profiling might help for the efficient utilization of scarcely available thromboprophylaxis, which might reduce the premature death attributed to VT and CVDs.

In our present study, we considered five VT-associated SNPs to explore the genetic background of VT risk in the Hungarian population. Only the three SNPs, namely, rs6025 (*F5*), rs2036914 (*F11*), and rs8176719 (*ABO*), remained statistically significant after adjustment for multiple testing correction ($p < 0.01$). The highest VT risk was detected among the Leiden mutation carriers/rs6025 (OR = 3.52, 95% CI: 2.50–4.95). Its allele frequency was approximately threefold higher in the VT group (20%) than that in the control group (6.8%). Our findings were consistent with the finding of the previously conducted studies showing that the odds of VT risk are 3.5 (28) and 4.38 times higher for rs6025 (*F5*) variant carriers than those of non-carriers (68).

Moreover, numerous studies suggest that the Leiden mutation is vastly prevalent in Caucasians, particularly those of European descent. It is one of the most influential inheritable VT risk factors that increase the burden of VT in genetically vulnerable individuals (34–36). These findings support our study's result that

F5 is highly prevalent in the case group (20%). Furthermore, it was strongly associated with the trait in all genetic association models. This highlights the fact that the Leiden mutation is an independent predictor of VT risk (28, 35, 69) and its contribution to the burden of VT is remarkable (69), particularly for genetically susceptible individuals and Caucasians (34). Likewise, the risk allele frequency and VT risk for rs2036914 (*F11*) and rs8176719 (*ABO*) were higher in the case group even after adjustment for multiple testing correction. A previously conducted study revealed that *F11* (rs2036914) is an independent predictor of VT (70), which is supported by our result that the risk was 1.38 times higher in the case group than that in the control group. Studies showed that VT risk distribution due to *F11* (rs2036914) is similar in Caucasians and African Americans (44, 45).

The allele frequency of the *ABO* SNP (rs8176719) was more prevalent in the control group (47.4% vs. 40.4%). In addition, it was revealed that the VT risk was lower (OR = 0.75, 95% CI: 0.61–0.93) among the subjects with the rs8176719 variant. Furthermore, the VT risk was 1.33 times higher in the risk variant carriers. Studies indicated that the O blood-type individuals are at a lower VT risk compared with the non-O blood-type individuals (46, 47). On the other hand, several studies showed that non-O blood-type individuals (A, AB, and B) were at a higher VT risk compared with non-O blood-type individuals (48–51). Our findings were also consistent with those of the previously conducted studies. Fang et al. reported that the VTE risk is higher in African Americans and non-O blood-type individuals than that in Caucasians and O blood-type individuals (52).

Although the risk allele frequencies and VT risk were not distinct in the case of prothrombin mutation (rs1799963), it was the second most prevalent risk variant in the Hungarian population. The reason for the lack of statistical significance despite the large OR might be attributed to the limited number of our VT patients. Our findings were also in line with those of the previously conducted studies showing that rs1799963 is more prevalent in European descent populations than in others (Americans, African Americans, Asians, and Africans) (23). Several studies showed that approximately two- to fourfold VT risk was attributed to a hypercoagulability state that resulted from a mutation in the prothrombin gene/rs1799963 (35, 71, 72).

Studies indicated that pooled variants have more impact on VT risk determination than a single variant (29, 53); consequently, we computed the wGRS and unGRS to determine the VT risk in the study population. Our findings showed that the wGRS is an independent predictor of VT risk in the study population, and its value was 2.37 times higher in the VT group than in the control group. Previously conducted studies also supported our findings (29, 53).

The impact of non-genetic risk factors on VT risk is also appreciable. Our study showed that VT was more prevalent in elderly (≥ 60 years) subjects (58.1% vs. 10.5%; $p < 0.0001$). Likewise, the odds of VT risk for elderly subjects were 12-fold higher than that of those aged <60 years. The VT risk increases with age due to different factors, such as anatomical (54), pathophysiological (54–57), and hormonal derangement (73). Consequently, it hastens and increases the vulnerability of elderly subjects to VT risk and other CVDs (19, 55–57). Furthermore, our findings showed that the VT risk is 2.28 times higher in the obese subjects than that in the normal-weight subjects. This finding is in line with those of the previously conducted studies that showed that obesity is an independent predictor of VT risk (58–62).

The ability to predict the risk of a certain event before its occurrence is important in clinical epidemiology. Precise risk prediction helps control an event at as early a stage as possible (74–77) and offers to use the available resources effectively and efficiently (74–77). We used the ROC curves to establish individual and combined VT risk predictability of the SNPs and non-inheritable VT risk factors to develop a risk stratification tool.

In our study, the highest AUC was obtained for the Leiden mutation (AUC = 0.62), whereas the lowest AUC was obtained for the prothrombin mutation/*F2* (0.52). The addition of each SNP into the model after *F5* increased the AUC in general. Our finding is in line with that of the studies showing that adding more SNPs into the model increases the AUC to a certain extent, but after a certain level, the AUC does not change, despite adding more explanatory variables into the model (29, 78).

We also found that the wGRS is a better predictor of VT risk than individual SNPs (0.68 vs. 0.62) and their combination with non-genetic risk factors yields a larger AUC with higher discriminatory accuracy (AUC = 0.89). This finding is consistent with that of the previous studies showing that the combination of clinical and genetic risk factors increases the VT risk eight times more than either the genetic or the clinical model alone (79, 80).

Strengths and limitations of our study

Our study tried to verify the VT risk predictability in the Hungarian population only by using strongly associated VT SNPs [rs6025 (*F5*), rs1799963 (*F2*), rs8176719 (*ABO*), rs2036914 (*F11*), and rs2066865 (*FGG*)] mainly relating to the recurrence and higher incidence of VT risk and well-known non-genetic VT risk factors (age, obesity, and sex), which helped distinguish the higher-risk individuals for the prevention and control of VT in the study population. Furthermore, our study indicated the possibility of efficiently and effectively utilizing the available resource for risk prediction in the given population. However, our study lacked the comparison of formerly identified strongly associated VT SNPs with the novel loci, which are strongly associated with VT risk as well (66, 81–83). As a result, we urged further study that considers the novel and strongly associated VT SNPs and the formerly identified SNPs and their comparison on the VT risk predictability in the Hungarian population.

Altogether, the Leiden mutation, *F11*, and *ABO* risk alleles are highly prevalent and strongly determine the VT risk in the Hungarian population. The pooled genetic risk variants are more influential than a single variant alone. The combined model is the best predictor of VT risk, so stratifying high-risk individuals based on their genetic profiling and well-known non-modifiable VT risk factors is important for the effective and efficient utilization of VT risk preventive and control measures. Furthermore, our study lacks the comparison of formerly identified VT SNPs with the novel SNPs, which are strongly

associated with VT risk. This might provide new insight into the VT risk and its determinants in the Hungarian population. As a result, we urged further study that considers the novel and strongly associated VT SNPs and the formerly identified SNPs and their comparison on the VT risk predictability in the Hungarian population.

Data availability statement

The original contributions presented in the study are included in the article/**Supplementary Material**, further inquiries can be directed to the corresponding author.

Ethics statement

The studies involving humans were approved by the Ethical Committee of the University of Debrecen. The studies were conducted in accordance with the local legislation and institutional requirements. The participants provided their written informed consent to participate in this study.

Author contributions

SN: data handling, writing and interpreting the results, and preparing statistical analysis. MM: participation in the statistical analyses. ZB: review, editing, and finalizing the manuscript. JS and RÁ: institutional background and funding framework. SF: guiding the data analyses, developing the methodology, and writing of the manuscript. All authors contributed to the article and approved the submitted version.

Funding

This work was supported by the Stipendium Hungaricum Scholarship Programme of the Tempus Public Foundation, the European Union under the European Regional Development Fund (GINOP-2.3.2-15-2016-00005), and the National Research, Development and Innovation Office, Hungarian Ministry of Innovation and Technology (Grant No. OTKA K139293).

Conflict of interest

The authors declare that the research was conducted in the absence of any commercial or financial relationships that could be construed as a potential conflict of interest.

Publisher's note

Supplementary material

The Supplementary Material for this article can be found online at: https://www.frontiersin.org/articles/10.3389/fcvm.2023.1224462/full#supplementary-material

References

1. Zöller B, Pirouzifard M, Svensson PJ, Holmquist B, Stenman E, Elston RC, et al. Familial segregation of venous thromboembolism in Sweden: a nationwide family study of heritability and complex segregation analysis. *J Am Heart Assoc.* (2021) 10:24. doi: 10.1161/JAHA.120.020323

2. Zöller B, Li X, Ohlsson H, Ji J, Sundquist J, Sundquist K. Family history of venous thromboembolism as a risk factor and genetic research tool. *Thromb Haemost.* (2015) 114(5):890–900. doi: 10.1160/TH15-04-0306

3. Zöller B, Ohlsson H, Sundquist J, Sundquist K. Family history of venous thromboembolism (VTE) and risk of recurrent hospitalization for VTE: a nationwide family study in Sweden. *J Thromb Haemost.* (2014) 12(3):306–12. doi: 10.1111/jth.12499

4. Natae SF, Kósa Z, Sándor J, Merzah MA, Bereczky Z, Pikó P, et al. The higher prevalence of venous thromboembolism in the Hungarian Roma population could be due to elevated genetic risk and stronger gene-environmental interactions. *Front Cardiovasc Med.* (2021) 8:647416. doi: 10.3389/fcvm.2021.647416

5. Heit JA, Spencer FA, White RH. The epidemiology of venous thromboembolism. *J Thromb Thrombolysis.* (2016) 41(1):3–14. doi: 10.1007/s11239-015-1311-6

6. Morange PE, Suchon P, Trégouët DA. Genetics of venous thrombosis: update in 2015. *Thromb Haemost.* (2015) 114(5):910–9. doi: 10.1160/TH15-05-0410

7. Raskob GE, Angchaisuksiri P, Blanco AN, Buller H, Gallus A, Hunt BJ, et al. Thrombosis: a major contributor to global disease burden. *Arterioscler Thromb Vasc Biol.* (2014) 34(11):2363–71. doi: 10.1111/jth.12698

8. Nichols M, Townsend N, Scarborough P, Rayner M. Cardiovascular disease in Europe: epidemiological update. *J Clin Oncol.* (2014) 32(21):1–192. doi: 10.1200/JCO.2015.61.5757

9. Tadayon S, Wickramasinghe K, Townsend N. Examining trends in cardiovascular disease mortality across Europe: how does the introduction of a new European standard population affect the description of the relative burden of cardiovascular disease? *Popul Health Metr.* (2019) 17(1):1–17. doi: 10.1186/s12963-019-0187-7

10. Townsend N, Kazakiewicz D, Lucy WF, Timmis A, Huculeci R, Torbica A, et al. Epidemiology of cardiovascular disease in Europe. *Nat Rev Cardiol.* (2022) 19 (2):133–43. doi: 10.1038/s41569-021-00607-3

11. Cohen AT, Agnelli G, Anderson FA, Arcelus JI, Bergqvist D, Brecht JG, et al. Venous thromboembolism (VTE) in Europe—the number of VTE events and associated morbidity and mortality. *Thromb Haemost.* (2007) 98(4):756–64. doi: 10.1160/TH07-03-0212

12. Movsisyan NK, Vinciguerra M, Medina-Inojosa JR, Lopez-Jimenez F. Cardiovascular diseases in central and Eastern Europe: a call for more surveillance and evidence-based health promotion. *Ann Glob Heal.* (2020) 86(1):1–10. doi: 10.5334/aogh.2713

13. OECD/European Observatory on Health Systems and Policies. *Hungary: Country Health Profile 2017.* Brussels: State of Health in the EU, OECD Publishing, Paris/European Observatory on Health Systems and Policies (2017). 16 p. Available from: http://dx.doi.org/10.1787/9789264283411-en

14. Monreal M, Agnelli G, Chuang LH, Cohen AT, Gumbs PD, Bauersachs R, et al. Deep vein thrombosis in Europe—health-related quality of life and mortality. *Clin Appl Thromb.* (2019) 25:1–12. doi: 10.1177/1076029619883946

15. Kumar DR, Hanlin ER, Glurich I, Mazza JJ, Yale SH. Virchow's contribution to the understanding of thrombosis and cellular biology. *Clin Med Res.* (2010) 8 (3–4):168–72. doi: 10.3121/cmr.2009.866

16. Byrnes JR, Wolberg AS. New findings on venous thrombogenesis. *Hamostaseologie*. (2017) 37(1):25–35. doi: 10.5482/HAMO-16-09-0034

17. Bovill EG, Van Der Vliet A. Venous valvular stasis-associated hypoxia and thrombosis: what is the link? *Annu Rev Physiol*. (2011) 73:527–45. doi: 10.1146/annurev-physiol-012110-142305

18. Hosseinzadegan H, Tafti DK. Prediction of thrombus growth: effect of stenosis and Reynolds number. *Cardiovasc Eng Technol*. (2017) 8(2):164–81. doi: 10.1007/s13239-017-0304-3

19. Poredos P, Jezovnik MK. Endothelial dysfunction and venous thrombosis. *Angiology*. (2018) 69(7):564–7. doi: 10.1177/0003319717732238

20. Motto D. Endothelial cells and thrombotic microangiopathy. *NIH Public Access*. (2012) 32(2):208–14. doi: 10.1016/j.semnephrol.2012.02.007

21. Monie DD, DeLoughery EP. Pathogenesis of thrombosis: cellular and pharmacogenetic contributions. *Cardiovasc Diagn Ther*. (2017) 7(Suppl 3):S291–8. doi: 10.21037/cdt.2017.09.11

22. Previtali E, Bucciarelli P, Passamonti SM, Martinelli I. Risk factors for venous and arterial thrombosis. *Blood Transfus*. (2011) 9(2):120–38. doi: 10.2450/2010.0066-10

23. Huang SS, Liu Y, Jing ZC, Wang XJ, Mao YM. Common genetic risk factors of venous thromboembolism in Western and Asian populations. *Genet Mol Res*. (2016) 15(1):1–11. doi: 10.4238/gmr.15017644

24. Ashrani AA, Silverstein MD, Lahr BD, Petterson TM, Bailey KR, Melton LJ, et al. Risk factors and underlying mechanisms for venous stasis syndrome: a population-based case-control study. *Vasc Med*. (2009) 14(4):339–49. doi: 10.1177/1358863X09104222

25. Crous-Bou M, Harrington LB, Kabrhel C. Environmental and genetic risk factors associated with venous thromboembolism. *Semin Thromb Hemost*. (2016) 42(8):808–20. doi: 10.1055/s-0036-1592333

26. Jaworek T, Xu H, Gaynor BJ, Cole JW, Rannikmae K, Stanne TM, et al. Contribution of common genetic variants to risk of early-onset ischemic stroke. *Neurology*. (2022) 99(16):E1738–54. doi: 10.1212/WNL.0000000000201006

27. Zöller B, Svensson PJ, Dahlbäck B, Lind-Hallden C, Hallden C, Elf J. Genetic risk factors for venous thromboembolism. *Expert Rev Hematol*. (2020) 13(9):971–81. doi: 10.1080/17474086.2020.1804354

28. Klarin D, Emdin CA, Natarajan P, Conrad MF, Kathiresan S. Genetic analysis of venous thromboembolism in UK Biobank identifies the ZFPM2 locus and implicates obesity as a causal risk factor. *Circ Cardiovasc Genet*. (2017) 10(2):1–17. doi: 10.1161/CIRCGENETICS.116.001643

29. De Haan HG, Bezemer ID, Doggen CJ, Cessie SL, Reitsma PH, Arellano AR, et al. Multiple SNP testing improves risk prediction of first venous thrombosis. *Blood*. (2012) 120(3):656–63. doi: 10.1182/blood-2011-12-397752

30. Klarin D, Busenkell E, Judy R, Lynch J, Levin M, Haessler J, et al. Genome-wide association analysis of venous thromboembolism identifies new risk loci and genetic overlap with arterial vascular disease. *Nat Genet*. (2019) 51(11):1574–9. doi: 10.1038/s41588-019-0519-3

31. Rinde LB, Morelli VM, Småbrekke B, Mathiesen EB, Løchen ML, Njølstad I, et al. Effect of prothrombotic genotypes on the risk of venous thromboembolism in patients with and without ischemic stroke. The Tromsø Study. *J Thromb Haemost*. (2019) 17(5):749–58. doi: 10.1111/jth.14410

32. Van Hylckama Vlieg A, Flinterman LE, Bare LA, Cannegieter SC, Reitsma PH, Arellano AR, et al. Genetic variations associated with recurrent venous thrombosis. *Circ Cardiovasc Genet*. (2014) 7(6):806–13. doi: 10.1161/CIRCGENETICS.114.000682

33. Brotman DJ, Necochea AJ, Wilson LM, Crim MT, Bass EB. Predictive value of factor V Leiden and prothrombin G20210A in adults with venous thromboembolism and in family members of those with a mutation. *JAMA*. (2009) 301(23):2472–85. doi: 10.1001/jama.2009.853

34. Kujovich JL. Factor v Leiden thrombophilia. *Genet Med*. (2011) 13(1):1–16. doi: 10.1097/GIM.0b013e3181faa0f2

35. Simone JEB, De Stefano V, Leoncini E, Zacho J, Martinelli I. Risk of venous thromboembolism associated with single and combined effects of factor V Leiden, prothrombin 20210A and methylenetetrahydrofolate reductase C677T: a meta-analysis involving over 11,000 cases and 21,000 controls. *Eur J Epidemiol*. (2013) 28(8):621–47. doi: 10.1007/s10654-013-9825-8

36. Hosseini S, Kalantar E, Hosseini MS, Tabibian S, Shamsizadeh M, Dorgalaleh A. Genetic risk factors in patients with deep venous thrombosis, a retrospective case–control study on Iranian population. *Thromb J*. (2015) 13(1):4–9. doi: 10.1186/s12959-015-0064-y

37. Simka M, Latacz P. Factor V Leiden distribution—could it shed some light on the pre-history of Europe and the near east? *Phlebol Rev*. (2016) 2–3:40–5. doi: 10.5114/pr.2016.65518

38. Clark JSC, Adler G, Salkic NN, Ciechanowicz A. Allele frequency distribution of 1691G>A F5 (which confers factor V Leiden) across Europe, including Slavic populations. *J Appl Genet*. (2013) 54(4):441–6. doi: 10.1007/s13353-013-0166-9

39. Varga E. The genetics of Thrombophilia. *The National Alliance for Thrombosis and Thrombophilia (NATT)*. (2013). p. 1–9.

40. Fall AOT, Proulle V, Sall A, Mbaye A, Ba PS, Diao M, et al. Risk factors for thrombosis in an African population. *Clin Med Insights Blood Disord*. (2014) 7:1–6. doi: 10.4137/CMBD.S13401

41. Abdi AA, Osman A. Prevalence of common hereditary risk factors for thrombophilia in Somalia and identification of a novel Gln544Arg mutation in coagulation factor V. *J Thromb Thrombolysis*. (2017) 44(4):536–43. doi: 10.1007/s11239-017-1543-8

42. Jadaon MM. Epidemiology of prothrombin G20210A mutation in the Mediterranean region. *Mediterr J Hematol Infect Dis*. (2011) 3(1). doi: 10.4084/MJHID.2011.054

43. Shafia S, Zargar MH, Khan N, Ahmad R, Shah ZA, Asimi R. High prevalence of factor V Leiden and prothrombin G20101A mutations in Kashmiri patients with venous thromboembolism. *Gene*. (2018) 654:1–9. doi: 10.1016/j.gene.2018.02.031

44. Austin H, De Staercke C, Lally C, Bezemer ID, Rosendaal FR, Hooper WC. New gene variants associated with venous thrombosis : a replication study in white and black Americans. *J Thromb Haemost*. (2011) 9:489–95. doi: 10.1111/j.1538-7836.2011.04185.x

45. Cushman M, Pankow JS. Prospective study of circulating factor XI and incident venous thromboembolism: the longitudinal investigation of thromboembolism etiology (LITE). *Am J Hematol*. (2015) 90(11):1047–51. doi: 10.1002/ajh.24168. Prospective

46. Vasan SK, Rostgaard K, Majeed A, Ullum H, Titlestad KE, Pedersen OB, et al. ABO blood group and risk of thromboembolic and arterial disease: a study of 1.5 million blood donors. *Circulation*. (2016) 133:1449–57. doi: 10.1161/CIRCULATIONAHA.115.017563

47. Dentali F, Sironi A, Ageno W, Turato S, Bonfanti C, Frattini F, et al. Non-O blood type is the commonest genetic risk factor for VTE: results from a meta-analysis of the literature. *Semin Thromb Hemost*. (2012) 38(5):535–47. doi: 10.1055/s-0032-1315758

48. Sun X, Feng J, Wu W, Peng M, Shi J. ABO blood types associated with the risk of venous thromboembolism in Han Chinese people: a hospital-based study of 200,000 patients. *Sci Rep*. (2017) 7:42925. doi: 10.1038/srep42925

49. Yu M, Wang C, Chen T, Hu S, Yi K, Tan X. ABO blood groups and risk of deep venous thromboembolism in Chinese Han population from Chaoshan region in south China. *Saudi Med J*. (2017) 38(4):396–9. doi: 10.15537/smj.2017.4.16349

50. Massimo Franchini MM. Non-O blood group: an important genetic risk factor for venous thromboembolism. *Blood Transfus*. (2013) 11(2):164–5. doi: 10.2450/2012.0087-12

51. Miñano A, Ordóñez A, España F, González-porras JR, Lecumberri R, Fontcuberta J, et al. AB0 blood group and risk of venous or arterial thrombosis in carriers of factor V Leiden or prothrombin G20210A polymorphisms. *Haematologica*. (2008) 93(5):729–34. doi: 10.3324/haematol.12271

52. Kinsella M, Monk C. Race, ABO blood type and VTE risk: not black and white. *Transfusion*. (2012) 23(1):1–7. doi: 10.1111/j.1537-2995.2012.03665.x

53. Skille H, Paulsen B, Hveem K, E. Gabrielsen M, Brumpton B, Hindberg K, et al. Combined effects of five prothrombotic genotypes and cancer on the risk of a first venous thromboembolic event. *J Thromb Haemost*. (2020) 18(11):2861–9. doi: 10.1111/jth.15011

54. Van Langevelde K, Šrámek A, Rosendaal FR. The effect of aging on venous valves. *Arterioscler Thromb Vasc Biol*. (2010) 30(10):2075–80. doi: 10.1161/ATVBAHA.110.209049

55. Engbers MJ, van Hylckama Vlieg A, Rosendaal FR. Venous thrombosis in the elderly: incidence, risk factors and risk groups. *J Thromb Haemost*. (2010) 8(10):2105–12. doi: 10.1111/j.1538-7836.2010.03986.x

56. Donato AJ, Machin DR, Lesniewski LA. Mechanisms of dysfunction in the aging vasculature and role in age-related disease. *Circ Res*. (2018) 123(7):825–48. doi: 10.1161/CIRCRESAHA.118.312563

57. Karasu A, Šrámek A, Rosendaal FR, van der Geest RJ, van Hylckama Vlieg A. Aging of the venous valves as a new risk factor for venous thrombosis in the elderly: the BATAVIA study. *J Thromb Haemost*. (2018) 16(1):96–103. doi: 10.1111/jth.13880

58. Genyan Yang WCH, De Staercke C. The effects of obesity on venous thromboembolism: a review. *Open J Prev Med*. (2012) 2(4):499–509. doi: 10.4236/ojpm.2012.24069

59. Morgan ES, Wilson E, Watkins T, Gao F, Hunt BJ. Maternal obesity and venous thromboembolism. *Int J Obstet Anesth*. (2012) 21(3):253–63. doi: 10.1016/j.ijoa.2012.01.002

60. Horvei LD, Brækkan SK, Mathiesen EB, Njølstad I, Wilsgaard T, Hansen JB. Obesity measures and risk of venous thromboembolism and myocardial infarction. *Eur J Epidemiol*. (2014) 29:821–30. doi: 10.1007/s10654-014-9950-z

61. Hotoleanu C. Association between obesity and venous thromboembolism. *Med Pharm Reports*. (2020) 93(2):162–8. doi: 10.15386/mpr-1372

62. Kabrhel C, Varraso R, Goldhaber SZ, Rimm EB, Camargo CA. Prospective study of BMI and the risk of pulmonary embolism in women. *Obesity*. (2009) 17(11):2040–6. doi: 10.1038/oby.2009.92

63. Kahn SR, Lim W, Dunn AS, Cushman M, Dentali F, Akl EA, et al. Prevention of VTE in nonsurgical patients. Antithrombotic therapy and prevention of thrombosis,

9th ed: American College of Chest Physicians evidence-based clinical practice guidelines. *Chest*. (2012) 141(2 Suppl):e195S–226S. doi: 10.1378/chest.11-2296

64. Ádány R, Pikó P, Fiatal S, Kósa Z, Sándor J, Bíró E, et al. Prevalence of insulin resistance in the Hungarian general and Roma populations as defined by using data generated in a complex health (interview and examination) survey. *Int J Environ Res Public Health*. (2020) 17(13):1–22. doi: 10.3390/ijerph17134833

65. Ghouse J, Tragante V, Ahlberg G, Rand SA, Jespersen JB, Leinøe EB, et al. Genome-wide meta-analysis identifies 93 risk loci and enables risk prediction equivalent to monogenic forms of venous thromboembolism. *Nat Genet*. (2023) 55:399–409. doi: 10.1038/s41588-022-01286-7

66. Zhang Z, et al. Genome-wide association analyses identified novel susceptibility loci for pulmonary embolism among Han Chinese population. *BMC Med*. (2023) 21 (1):1–13. doi: 10.1186/s12916-023-02844-4

67. Fiatal S, Pikó P, Kósa Z, Sándor J, Ádány R. Genetic profiling revealed an increased risk of venous thrombosis in the Hungarian Roma population. *Thromb Res*. (2019) 179:37–44. doi: 10.1016/j.thromres.2019.04.031

68. Eppenberger D, Nilius H, Anagnostelis B, Huber CA, Nagler M. Current knowledge on factor V leiden mutation as a risk factor for recurrent venous thromboembolism: A Systematic Review and meta-analysis. *Front Cardiovasc Med*. (2022) 9:883986. doi: 10.3389/fcvm.2022.883986

69. Eppenberger D, Nilius H, Anagnostelis B, Huber CA, Nagler M. Current knowledge on factor V Leiden mutation as a risk factor for recurrent venous thromboembolism: a systematic review and meta-analysis. *Front Cardiovasc Med*. (2022) 9:1–13. doi: 10.3389/fcvm.2022.883986

70. Li Y, Bezemer ID, Rowland CM, Tong CH, Arellano AR, Catanese JJ, et al. Genetic variants associated with deep vein thrombosis : the F11 locus. *J Thromb Haemost*. (2009) 7:1802–8. doi: 10.1111/j.1538-7836.2009.03544.x

71. Bucciarelli P, De Stefano V, M. Passamont S, Tormene D, Legnani C, Rossi E, et al. Influence of proband's characteristics on the risk for venous thromboembolism in relatives with factor V Leiden or prothrombin. *Blood*. (2016) 122(15):2555–62. doi: 10.1182/blood-2013-05-503649

72. Bezgin T, Kaymaz C, Tokgo HC. Thrombophilic gene mutations in relation to different manifestations of venous thromboembolism a single tertiary center study. *Clin Appl Thromb Hemost*. (2018) 24(1):100–6. doi: 10.1177/1076029616672585

73. Karppinen JE, Törmäkangas T, Kujala UM, Sipilä S, Laukkanen J, Aukee P, et al. Menopause modulates the circulating metabolome: evidence from a prospective cohort study. *Eur J Prev Cardiol*. (2022) 29(10):1448–59. doi: 10.1093/eurjpc/zwac060

74. Pate A, Emsley R, Ashcroft DM, Brown B, Van Staa T. Correction: the uncertainty with using risk prediction models for individual decision making: an exemplar cohort study examining the prediction of cardiovascular disease in English primary care (BMC Medicine). *BMC Med*. (2019) 17(1):1–16. doi: 10.1186/s12916-019-1404-8

75. Kamal SA, Yin C, Qian B, Zhang P. An interpretable risk prediction model for healthcare with pattern attention. *BMC Med Inform Decis Mak*. (2020) 20(11):1–11. doi: 10.1186/s12911-020-01331-7

76. Chapman BP, Lin F, Roy Sh, Ralph HB, Benedict RHB, Lyness JM. Health risk prediction models incorporating personality data: motivation, challenges, and illustration. *Personal Disord*. (2019) 10(1):46–58. doi: 10.1037/per0000300

77. Sharma V, Ali I, Van Der Veer S, Martin G, Ainsworth J, Augustine T. Adoption of clinical risk prediction tools is limited by a lack of integration with electronic health records. *BMJ Health Care Inform*. (2021) 28(1):2020–2. doi: 10.1136/bmjhci-2020-100253

78. Ahmad A, Sundquist K, Palmér K, Svensson PJ, Sundquist J, Memon AA. Risk prediction of recurrent venous thromboembolism: a multiple genetic risk model. *J Thromb Thrombolysis*. (2019) 47(2):216–26. doi: 10.1007/s11239-018-1762-7

79. Kolin DA, Kulm S, Elemento O. Prediction of primary venous thromboembolism based on clinical and genetic factors within the U.K. Biobank. *Sci Rep*. (2021) 11(1):1–9. doi: 10.1038/s41598-021-00796-4

80. Hodeib H, Youssef A, Allam AA, Selim A, Tawfik MA, Abosamak MF, et al. Genetic risk profiling associated with recurrent unprovoked venous thromboembolism. *Genes (Basel)*. (2021) 12(6):1–11. doi: 10.3390/genes12060874

81. Lindström S, Wang L, Smith EN, Gordon W, Van Hylckama VA, De Andrade M, et al. Genomic and transcriptomic association studies identify 16 novel susceptibility loci for venous thromboembolism. *Blood*. (2019) 134(19):1645–57. doi: 10.1182/blood.2019000435

82. Thibord F, Klarin D, Brody JA, Chen MH, Levin MG, Chasman DI, et al. Cross-ancestry investigation of venous thromboembolism genomic predictors. *Circulation*. (2022) 146(16):1225–42. doi: 10.1161/CIRCULATIONAHA.122.059675

83. Langley J, Huddleston DE, Merritt M, Chen X, Silver M, Factor SA, et al. Genome-wide association analysis of venous thromboembolism identifies new risk loci and genetic overlap with arterial vascular disease. *Hum Brain Mapp*. (2017) 37 (7):2547–56. doi: 10.1038/s41588-019-0519-3

Frontiers in
Cardiovascular Medicine

Innovations and improvements in cardiovascular treatment and practice

Focuses on research that challenges the status quo of cardiovascular care, or facilitates the translation of advances into new therapies and diagnostic tools.

Discover the latest Research Topics

See more →

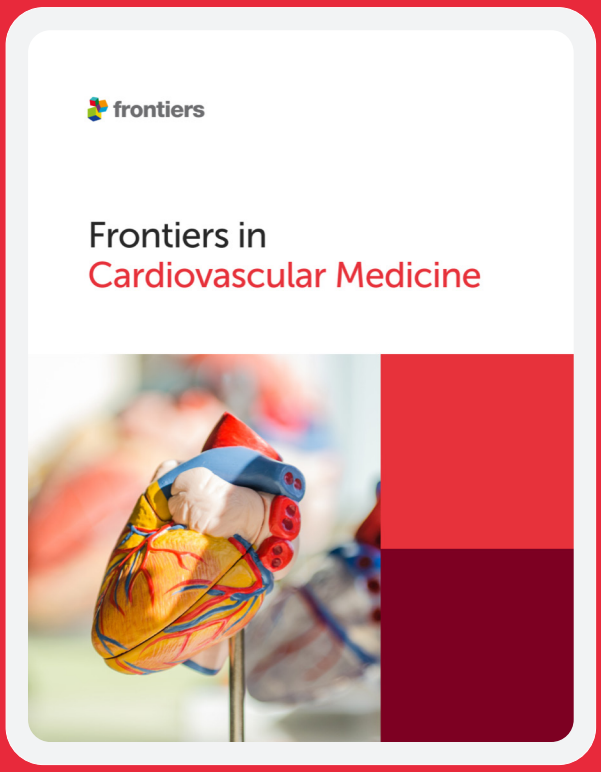

Frontiers

Avenue du Tribunal-Fédéral 34
1005 Lausanne, Switzerland
frontiersin.org

Contact us

+41 (0)21 510 17 00
frontiersin.org/about/contact